

Republic of Iraq  
Ministry of Higher Education and Scientific Research  
University of Misan/Collage of Engineering  
Department of Civil Engineering



**NUMERICAL ANALYSIS FOR SHEAR STRENGTH OF  
COMPOSITE BOX STEEL-CONCRETE BEAMS OF  
TRANSVERSE OPENINGS**

By

Ali Mohsin Oudah

B.Sc. civil engineering, 2012

A Thesis

Submitted in Partial Fulfillment of the

Requirements for the Degree of

Master of Science/Master of Structural Engineering

(in Civil Engineering)

Advisor Name: Assist. Prof. Dr. Nasser Hakeem Tu'ma

بِسْمِ اللَّهِ الرَّحْمَنِ الرَّحِيمِ

﴿أَمَّنْ هُوَ قَانَتْ أُنَاءَ اللَّيْلِ سَاجِدًا وَقَائِمًا يَحْذَرُ الْآخِرَةَ وَيَرْجُو رَحْمَةَ رَبِّهِ ۗ قُلْ هَلْ

يَسْتَوِي الَّذِينَ يَعْلَمُونَ وَالَّذِينَ لَا يَعْلَمُونَ ۗ إِنَّمَا يَتَذَكَّرُ أُولُو الْأَلْبَابِ ﴿﴾

صدق الله العلي العظيم

**سورة الزمزم الآية (9)**

**Numerical Analysis for Shear Strength of Composite Box Steel-Concrete Beams of  
Transverse Openings**

By Ali Mohsin Oudah

Thesis Advisor: Assist. Prof. Dr. Nasser Hakeem Tu'ma

An Abstract of the Thesis Presented  
in Partial Fulfillment of the Requirements for the  
Degree of Master of Science/Master of Structural Engineering  
(in Civil Engineering)

November/ 2024

## ABSTRACT

This thesis investigates the structural performance of composite box steel-concrete beams with transverse openings, focusing on how variations in opening size, shape, and location impact shear strength and deflection. This research provides valuable insights into optimizing composite beam designs by adjusting opening size, shape, location, (a/d) ratio, concrete strength, and reinforcement to enhance shear strength and structural flexibility. The study analyzes beams with square and circular openings of sizes 50×50 mm, 70×70 mm, 90×90 mm, 110×110 mm, and 136×136 mm and examines the effects of different shear span-to-depth ratios (a/d), concrete compressive strengths, and longitudinal reinforcement configurations.

The results indicate that increasing the size of transverse openings significantly decreases shear strength and increases deflection. Changing the opening size from 50×50 mm to 136×136 mm reduces the shear strength by up to 47.7%. Additionally, circular openings reduce shear strength compared to square openings for smaller sizes ( $\emptyset 50$ ,  $\emptyset 70$ ,  $\emptyset 90$ ,  $\emptyset 110$ ), but for larger openings (136×136 mm), circular opening ( $\emptyset 136$ ) increases the shear strength by 13.25% compared with square opening. The study also found that beams with openings near the supports perform better in terms of shear strength than those with openings near the applied load, particularly for larger openings, where the shear strength decreased by up to 15.9% for openings near the applied load comparing with openings near the supports.

Shear span-to-depth ratios also significantly affect shear strength, with a decrease in the (a/d) ratio leading to increased shear strength. For example, reducing the (a/d) ratio from 2.8 to 2 increased the shear strength by up to 20% for smaller openings. Conversely, the shear strength of beams with large openings was less sensitive to changes in the (a/d) ratio. Furthermore, increasing the concrete compressive strength from 23.5 MPa to 37.5 MPa increases shear strength of up to 11.71% for openings of 50\*50 mm dimensions, with slightly improved shear strength for other dimensions openings.

Lastly, the study shows that the diameter of reinforcing bars plays a role in shear strength. Beams with larger reinforcement areas, such as those with (2Ø25 & 2Ø16,  $A_s=1384 \text{ mm}^2$ ) reinforcement, demonstrated increased shear strength compared to beams with (3Ø16,  $A_s=603 \text{ mm}^2$ ) reinforcement. However, the influence of reinforcement was less pronounced for large openings, where the behavior remained largely unaffected by changes in reinforcement.

## **SUPERVISOR CERTIFICATION**

I certify that the preparation of this thesis entitled "**Numerical Analysis for Shear Strength of Composite Box Steel-Concrete Beams of Transverse Openings**" was presented by "**Ali Mohsin Oudah**" and prepared under my supervision at The University of Misan, Department of Civil Engineering, College of Engineering, as a partial fulfillment of the requirements for the degree of Master of Science in Civil Engineering (Structural Engineering).

Signature:

**Assist. Prof. Dr. Nasser Hakeem Tu'ma**

Date:

In view of the available recommendations, I forward this thesis for discussion by the examining committee.

Signature:

**Assist. Prof. Dr. Murtada Abass A. Alrubaie**

(Head of Civil Eng. Department)

Date:

## EXAMINING COMMITTEE'S REPORT

We certify that we, the examining committee, have read the thesis titled **(Numerical Analysis for Shear Strength of Composite Box Steel-Concrete Beams of Transverse Openings)** which is being submitted by **Ali Mohsin Oudah**, and examined the student in its content and in what is concerned with it, and that in our opinion, it meets the standard of a thesis for the degree of Master of Science in Civil Engineering (Structures).

Signature:

Name: **Assist. Prof. Dr. Nasser Hakeem Tu'ma**

(Supervisor)

Date: / /2024

Signature:

Name: **Prof. Dr. Sa'ad Fahad Resan**

(Chairman)

Date: / /2024

Signature:

Name: **Assist. Prof. Dr. HayderAl-Khazraji**

(Member)

Date: / /2024

Signature:

Name: **Assist. Prof. Dr. Wisam Hulail Sultan**

(Member)

Date: / /2024

Approval of the College of Engineering:

Signature:

Name: **Prof. Dr. Abbas Oda Dawood**

Dean, College of Engineering

Date: / /2024

## DEDICATION

I dedicate this thesis to Allah Almighty, the Giver and the Guide, who granted me the success and assistance to complete this thesis. O Allah, accept this work from me and make it solely for Your sake, by Your mercy, O Most Merciful of the merciful.

To the Messenger of Allah, Muhammad (peace be upon him and his family), and to his pure household (peace be upon them), the beacons of guidance and the Ark of Salvation, who are the example and light on the path of knowledge and faith.

To my master, the Imam of the Age, Al-Mahdi (may Allah hasten his reappearance), for whom we pray to be among his supporters and helpers, and for whom we hope to serve under his banner.

To my family, whose unwavering support and encouragement have been the foundation of my journey. To my parents, who instilled in me the values of perseverance and hard work, and to my siblings, who have been my constant source of inspiration.

To my mentors and professors, whose guidance has shaped my academic path and whose belief in my abilities has driven me to achieve my goals.

Finally, to my friends, who have been my pillars of strength throughout this process. Your laughter, understanding, and companionship have made this journey not only bearable but also memorable.

Thank you all for being part of this journey with me.



## ACKNOWLEDGEMENTS

I would like to express my deepest gratitude to all those who have supported me throughout the process of completing this thesis.

First and foremost, I would like to thank my supervisor, [Assist. Prof. Dr. Nasser Hakeem Tu'ma], for his invaluable guidance, insightful advice, and unwavering patience. Your expertise and feedback have been instrumental in shaping this work.

I am also immensely grateful to my committee members for their time, suggestions, and encouragement. Your constructive criticisms have greatly improved the quality of this thesis.

Special thanks to my colleagues and friends, whose camaraderie and support have been a source of motivation during the challenging moments. Your insights and shared experiences have enriched my research journey.

To the faculty and staff of [Department of Civil Engineering/ University of Misan], thank you for providing a conducive environment for research and learning. Your assistance and resources were essential in the completion of this work.

Finally, I extend my heartfelt thanks to my family. Your love, encouragement, and understanding have been my driving force. This achievement would not have been possible without your constant support.

Thank you all.

# TABLE OF CONTENTS

<b>ABSTRACT .....</b>	<b>IV</b>
<b>SUPERVISOR CERTIFICATION .....</b>	<b>VI</b>
<b>EXAMINING COMMITTEE’S REPORT .....</b>	<b>VII</b>
<b>DEDICATION.....</b>	<b>VIII</b>
<b>ACKNOWLEDGEMENTS .....</b>	<b>IX</b>
<b>TABLE OF CONTENTS .....</b>	<b>X</b>
<b>LIST OF TABLES.....</b>	<b>XV</b>
<b>LIST OF FIGURES .....</b>	<b>XI</b>
<b>LIST OF SYMBOLES .....</b>	<b>XII</b>
<b>LIST OF ABBREVIATIONS .....</b>	<b>XIII</b>
<b>CHAPTER ONE :INTRODUCTION .....</b>	<b>1</b>
1.1 General.....	1
1.2 Composite Members.....	2
1.3 Composite Box Steel-Concrete Beams .....	2
1.4 Shear Connector.....	3
1.5 Beams With Openings .....	4
1.6 Reinforced Concrete Beams Behavior with Web Openings .....	6
1.7 Categorization of Openings .....	7
1.7.1 Categorization of Openings based on the Shape .....	7
1.7.2 Categorization of Openings based on the Size .....	7

1.7.2.1 Small Openings.....	8
1.7.2.2 Large Openings.....	9
1.7.3 Categorization of Openings based on Type of Failure .....	10
1.7.3.1 Pure Bending.....	10
1.7.3.2 Combined Bending and Shear .....	11
1.7.3.3 Beam-kind failure .....	12
1.7.3.4 Frame-kind failure .....	13
1.8 Composite beams Benefits : .....	15
1.9 Purposes of Study The main goals of this research are:.....	15
1.10 Thesis Outline .....	16
<b>CHAPTER TWO: LITRATURE REVIEW.....</b>	<b>17</b>
2.1 Introduction .....	17
2.2 Literature Reviews .....	18
2.2.1 Beam with Opening .....	20
2.2.2 Beam Improvements .....	31
2.3 Summery of Literature Review .....	34
<b>CHAPTER THREE: NUMERICAL FORMULATION AND MODELINGN..</b>	<b>37</b>
3.1 Introduction .....	37
3.2 ABAQUS Finite Element Analysis .....	38
3.3 ABAQUS Finite Element Procedure.....	39
3.3.1 Material and Geometry Modeling .....	42
3.3.1.1 Part Modeling .....	42

3.3.1.2 Properties of Materials Modeling .....	45
3.3.1.3 Assembly of Modeling .....	62
3.3.1.4 Meshing of Modeling .....	63
3.3.2 Boundary and Constraint Conditions .....	70
3.3.2.1 Boundary Conditions .....	70
3.3.2.2 Constraint and Interaction Conditions.....	72
3.3.3 Output Analysis .....	75
3.3.3.1 Step Field .....	75
3.3.3.2 Load Field .....	75
3.3.3.3 Output Field and History .....	76
3.3.3.4 Job Field.....	77
3.3.4 Results Post Processing .....	78
<b>CHAPTER FOUR: RESULTS AND DISCUSSIONS .....</b>	<b>79</b>
4.1 Introduction .....	79
4.2 Modelling Verification.....	79
4.2.1 Modelling Details.....	80
4.2.1.2 The Second Group.....	81
4.2.1.3 The Third Group.....	82
4.2.2 Convergence Details .....	83
4.2.2.1 Dilation Angle.....	84
4.2.2.2 Viscosity Parameter .....	88
4.3 Validation of Finite Element Models.....	92

4.4 Parametric Study .....	97
4.5 Ductility.....	99
4.6 Ultimate Shear Load and Ultimate Deflection .....	100
4.8 Energy Absorption Capacity.....	101
4.9 Openings Size Parameter .....	102
4.9.1 Effect of Openings Size on Ultimate Shear Strength .....	102
4.9.2 Effect of Opening Size on Initial stiffness.....	107
4.8.1 Effect of Opening Location on Energy Absorption Capacity .	108
4.9 Opening Shape Parameter .....	109
4.9.1 Effect Opening Shape on Ultimate Shear Strength .....	109
4.9.2 Effect of Opening Shape on Initial stiffness.....	113
4.9.3 Effect of Opening Shape on Energy Absorption Capacity .....	114
4.10 Opening Location Parameter .....	115
4.10.1 Effect Opening Location on Ultimate Shear Strength.....	115
4.10.2 Effect of Opening Location on Initial stiffness .....	119
4.8.3 Effect of Opening Location on Energy Absorption Capacity .	120
4.11 Shear Span-to-Depth Ratio (a/d) Parameter .....	121
4.11.1 Effect of (a/d) Ratio on Ultimate Shear Strength .....	121
4.11.2 Effect of Shear Span to Effective Depth on Initial stiffness..	125
4.8.4 Effect of Shear Span to Depth Ratio on Energy Absorption Capacity .....	126
4.12 Compressive Strength of Concrete Parameter .....	128

4.12.1 Effect of Compressive Strength of Concrete on Ultimate Shear Strength.....	128
4.12.2 Effect of Compressive Strength of Concrete on Initial stiffness .....	132
4.12.3 Effect of Compressive Strength of Concrete on Energy Absorption Capacity .....	133
4.13 Tensile Reinforcement Parameter.....	134
4.13.1 Effect of Tensile Reinforcement on Ultimate Shear Strength.....	134
4.13.2 Effect of Tensile Reinforcement on Initial stiffness.....	137
4.13.3 Effect of Tensile Reinforcement on Energy Absorption Capacity .....	138
<b>CHAPTER FIVE: CONCLUSIONS AND RECOMENDATIONS .....</b>	<b>140</b>
<b>REFERENCES .....</b>	<b>144</b>
<b>APPENDIX A.....</b>	<b>I</b>

## LIST OF TABLES

<b>Table (3-1):</b> Elastic Properties Of Concrete. ....	46
<b>Table (3-2):</b> Default Parameter Of CDP Model Under Compound Stress.....	51
<b>Table (3-3):</b> Concrete Compressive Behavior For 23.5 Mpa .....	54
<b>Table (3-4):</b> Concrete Compressive Behavior For 30 Mpa.....	54
<b>Table (3-5):</b> Concrete Compressive Behavior For 37.5 Mpa .....	55
<b>Table (3-6):</b> Concrete Tensile Behavior Displacement Type.....	57
<b>Table (3-7):</b> Elastic Material Properties For Steel.....	60
<b>Table (3-8):</b> Plastic Material Properties For Steel.....	61
<b>Table (4-1):</b> The Ultimate Load And Deflection Of The Verification Results. ....	92
<b>Table (4-2):</b> Model's Details For The Composite Beams. ....	98
<b>Table (4-3):</b> Model's Results For Group 1 Of The Composite Beams. ....	103
<b>Table (4-4):</b> Model's Results For Group 2 Of The Composite Beams. ....	109
<b>Table (4-5):</b> Model's Results For Group 3 Of The Composite Beams. ....	116
<b>Table (4-6):</b> Model's Results For Group 4 Of The Composite Beams. ....	122
<b>Table (4-7):</b> Model's Results For Group 5 Of The Composite Beams. ....	128
<b>Table (4-8):</b> Model's Results For Group 6 Of The Composite Beams. ....	135
<b>Table (A-1):</b> Information The Composite Beams. ....	I

## LIST OF FIGURES

<b>figure 1.1</b> Examples Explain The Openings in Beams [3].	1
<b>Figure 1.2</b> Examples Explain The Types Of Composite Encased Beams [6].	3
<b>Figure 1.3:</b> Service Ducts and Pipes in Beams.	4
<b>Figure 1.4:</b> Service Ducts and Pipes in Beams.	5
<b>Figure 1.5:</b> Opening Shapes Considered.	7
<b>Figure 1.6:</b> Description of Small Openings Based on Openings' Dimensions.	8
<b>Figure 1.7:</b> Description of Large And Small Openings (Assessment of The Validity of Bernoulli's Hypothesis of Plane Strain Distribution).	9
<b>Figure 1.8:</b> Large Openings Description Based on Structural Reaction.	10
<b>Figure 1.9:</b> The Two Shear Failure Modes at Small Openings.	11
<b>Figure 1.10:</b> Shear Resistance, $V_s$ , Provided by Shear Reinforcement at An Opening.	13
<b>Figure 1.11:</b> Free-Body Diagram at Beam Opening.	14
<b>Figure 2.1:</b> Composite Beam Overview.	17
<b>Figure 2.2:</b> Typical Composite Beam Shapes.	18
<b>Figure 2.3:</b> Composite Beam Model's Geometry.	20
<b>Figure 2.4:</b> Tested Beams Reinforcement Arrangement, Cross-Sectional, and Geometry: (A) Solid One, (B) Opening Beam.	22
<b>Figure 2.5:</b> Numerical Finite Element Model Of Concrete Beam With Meshing Details and The Vertical Circular Shape Opening Details.	23
<b>Figure 2.6:</b> Beam Details and Test Setting Up Used in	25
<b>Figure 2.7:</b> Modelling of The Utilized Composite Beam By	26



<b>Figure 2.8:</b> Details of Tested Beams With Web Openings. ....	27
<b>Figure 2.9:</b> Beam Details and Testing Sketch. ....	29
<b>Figure 2.10:</b> Localized A) Two-Face Steel Plates; B) One Face Steel Plates. ....	31
<b>Figure 3.1:</b> Abaqus Finite Element Procedure. ....	40
<b>Figure 3.2:</b> Details of Geometry And Specifications of The First Sample CB Beam.....	43
<b>Figure 3.3:</b> Geometry Creation.....	43
<b>Figure 3.4:</b> Concrete Beam Geometry in CBModel.....	43
<b>Figure 3.5:</b> Concrete Beam Geometry in BW1 Model. ....	44
<b>Figure 3.6:</b> Concrete Beam Geometry in BW2 Model. ....	44
<b>Figure 3.7:</b> Reinforcement and Steel Geometry in CB Model.....	44
<b>Figure 3.8:</b> Hyperbolic Surface of Plastic Potential In Meridional Plane.....	48
<b>Figure 3.9:</b> Strength of Concrete Under Biaxial Stress in The CDP Model. ....	49
<b>Figure 3.10:</b> Deviatoric Cross Section of Failure Surface in Cdp Model.....	50
<b>Figure 3.11:</b> Response of Concrete to Uniaxial Loading in Compression.....	53
<b>Figure 3.12:</b> Response of Concrete to Uniaxial Loading in Tension.....	56
<b>Figure 3.13:</b> Definition of Elastic Properties in Abaqus Software. ....	57
<b>Figure 3.14:</b> Definition of Elastic Properties in Abaqus Software. ....	58
<b>Figure 3.15:</b> Selection of The CDP Model To Define The Plastic Properties of Concrete.....	58
<b>Figure 3.16:</b> Homogeneous Distribution of Concrete Properties.....	59
<b>Figure 3.17:</b> Perfectly Plastic Behavior.....	61
<b>Figure 3.18:</b> Material Properties Definition Menu In Abaqus Software.....	61

<b>Figure 3.19:</b> Determining The Distribution of Material Properties For Reinforcements In The Form of Trusses.....	62
<b>Figure 3.20:</b> Homogeneous Distribution of Concrete Properties.....	62
<b>Figure 3.23:</b> Illustration of Chosen Elements For The Solid Model.....	66
<b>Figure 3.24:</b> Illustration of First- And Second-Order Interpolation Function of Solid Elements.....	67
<b>Figure 3.25:</b> Example of Truss Element Randomly Oriented In A 3d Space.....	68
<b>Figure 3.26:</b> Meshing of The Concrete Section. ....	68
<b>Figure 3.27:</b> Meshing of The Steel Box Section. ....	69
<b>Figure 3.28:</b> Meshing of The Rebar Reinforcement Section. ....	69
<b>Figure 3.29:</b> Type of Meshing In The Rebar Reinforcement Section.....	70
<b>Figure 3.30:</b> Boundary Conditions of The Lower Parts of The Model.....	71
<b>Figure 3.31:</b> Boundary Conditions of Model. ....	71
<b>Figure 3.32:</b> Load Applied to The Upper Part of The Model. ....	72
<b>Figure 3.33:</b> Using The Embedded Region Constraint Between Rebars And Concrete.....	73
<b>Figure 3.34:</b> Using The Tie Constraint Between Upper Surface of Concrete And Load Plates, And Between Bottom Surface And Support Plats. ....	73
<b>Figure 3.35:</b> Input of Contact Properties Interaction Between Inside Surface of Concrete And Steel Box.....	74
<b>Figure 3.36:</b> Using The Contact Interaction Between Inside Surface of Concrete And Steel Box. ....	74
<b>Figure 3.37:</b> Determine The Solution Type Static. ....	76
<b>Figure 4.1:</b> Details of Experimental Encased Composite Beams Group 1. ....	81
<b>Figure 4.2:</b> Details of Experimental Encased Composite Beams, Group 2. ....	82
<b>Figure 4.3:</b> Details of Experimental Encased Composite Beams Group 3. ....	83

<b>Figure 4.13:</b> Load Deflection Curves of BW2 Model In Change of Viscosity Parameter.....	90
<b>Figure 4.14:</b> Load Deflection Curves of C1s1 Model In Change of Viscosity Parameter.....	90
<b>Figure 4.18:</b> Load-Deflection Curves Theoretical and Experimental Comparisons of Encased Composite Beams Group 1.....	93
<b>Figure 4.19:</b> Load-Deflection Curves Theoretical and Experimental Comparisons of Encased Composite Beams Group 2.....	94
<b>Figure 4.20:</b> Load-Deflection Curves Theoretical and Experimental Comparisons of Encased Composite Beams Group 3.....	94
<b>Figure 4.21:</b> Theoretical And Experimental Comparisons of Mode Failure in Encased Composite Beams Group 1.....	95
<b>Figure 4.22:</b> Theoretical And Experimental Comparisons of Mode Failure in Encased Composite Beams Group 2.....	96
<b>Figure 4.23:</b> Theoretical And Experimental Comparisons of Mode Failure in Encased Composite Beams Group 3.....	97
<b>Figure 4.24:</b> Definition of Displacement–Ductility Ratio.....	100
<b>Figure 4.25:</b> Load Deflection Curve of Opening Size Parameter in Group 1.....	103
<b>Figure 4.26:</b> Details of Beams of Opening Size Parameter in Group 1.....	104
<b>Figure 4.27:</b> Mode Failure of Opening Size Parameter in Group 1.....	105
<b>Figure 4.28:</b> Initial Stiffness of Opening Size Parameter in Group 1.....	107
<b>Figure 4.29:</b> Energy Absorption of Opening Size Parameter in Group 1.....	108
<b>Figure 4.30:</b> Details of Beams of Opening Shape Parameter in Group 2.....	110
<b>Figure 4.31:</b> Mode Failure of Opening Shape Parameter in Group 2.....	111
<b>Figure 4.32:</b> Load Deflection Curve Of Opening Shape Parameter in Group 2.....	112
<b>Figure 4.33:</b> Initial Stiffness Of Opening Shape Parameter in Group 2.....	114

**Figure 4.34:** Energy Absorption of Opening Shape Parameter in Group 2.....115

**Figure 4.35:** Load Deflection Curve of Opening Shape Parameter in Group 3.....117

**Figure 4.36:** Initial Stiffness of Opening Location Parameter in Group 2.....120

**Figure 4.37:** Energy Absorption of Opening Location Parameter in Group 3.....121

**Figure 4.38:** Load Deflection Curve of Opening Shape Parameter in Group 4.....124

**Figure 4.39:** Initial Stiffness of Shear Span To Effective Depth Parameter in Group 4  
.....126

**Figure 4.40:** Energy Absorption of Shear Span To Effective Depth Ratio  
Parameter in Group 4. ....127

**Figure 4.41:** Load Deflection Curve of Opening Shape Parameter in Group 5.....130

**Figure 4.42:** Initial Stiffness of Compressive Strength of Concrete Parameter In  
Group 5.....132

**Figure 4.43:** Energy Absorption of Compressive Strength of Concrete Parameter  
In Group 5. ....134

**Figure 4.44:** Load Deflection Curve of Opening Shape Parameter in Group 6.....136

**Figure 4.45:** Initial Stiffness of Tensile Reinforcement Parameter in Group 6. ....138

**Figure 4.46:** Energy Absorption of Tensile Reinforcement Parameter in Group 6.139

## LIST OF SYMBOLES

Symbol	Description	Unit
$\sigma^{th}$	Ambient hydrostatic stress state	MPa
$P$ and $V$	Any applied force on the structure	kN
$f_c'$	Compressive strength of concrete cylinder	MPa
$f_t$	Concrete strength in tension	MPa
$f_c'$	Concrete ultimate uniaxial compressive strength	MPa
[D]	Constitutive matrix	
$f_{cr}$ , $\varepsilon_{cr}$	Cracking stress and strain	MPa
[L]	Differential operator matrix	
$u$ , $v$ , $w$	Displacement components in x,y and z coordinates	mm
{U}	Displacement vector	
$D.I$	Ductility index	None
$Me$	Elastic moment strength	MPa
$[K]_e$	Element stiffness matrix	
$\psi$	Energy dissipation	None
$W_{ext}$ , $W_{int}$	External and internal work	kN
$I_1$	First stress invariant	MPa
F	Function of principal state ( $\sigma_{xp}$ , $\sigma_{yp}$ , $\sigma_{zp}$ )	MPa
$x$ , $y$ , $z$	Global coordinate	None
$\alpha$	Haunch angle with horizontal line	Degree
$\sigma_h$	Hydrostatic stress	MPa
[J]	Jacobian matrix	
{f}	Load vector	
$\zeta$ , $\eta$	Local coordinates	None
[N]	Matrix of shape functions	
$L_f$	Middle uniform region	mm
E	Modulus of elasticity	MPa

$E_c$	Modulus of elasticity of concrete	MPa
$E_s$	Modulus of elasticity of reinforcing bars	MPa
$f_r$	Modulus of rupture of concrete	MPa
{a}	Nodal displacement vector	
E	Normal strain	mm/mm
( $\sigma$ )	Normal stress	MPa
$B_t, \beta_c$	Opened and closed shear transfer coefficient	None
[K]	Overall stiffness matrix	
$\nu$	Poisson's ratio	
$\sigma_{xp}$	Principal stress in the x – direction.	MPa
$\sigma_{yp}$	Principal stress in the y – direction.	MPa
$\sigma_{zp}$	Principal stress in the z – direction.	MPa
$J_2$	Second deviatoric stress invariant	MPa
$\gamma$	Shear strain	mm/mm
$\tau$	Shear stress	MPa
$\beta$	Shear transfer coefficient	None
L	Span length of the beam	mm
$f_u$	Steel ultimate tensile strength	MPa
$\epsilon_o$	Strain at ultimate compressive stress $f_c'$	mm/mm
{ $\epsilon$ }	Strain vector	
[B]	Strain-displacement matrix	
$R_s$	Strength rating	None
{ $\sigma$ }	Stress vector	

[T]	Transformation matrix	
[A] <sup>T</sup>	Transpose of matrix [A]	
$F_{cb}$	Ultimate biaxial compressive strength	MPa
$f_1$	Ultimate compression superimposed on hydrostatic stress state compressive strength for a state of biaxial.	MPa
$f_2$	Ultimate compressive strength for a state of uniaxial compression superimposed on hydrostatic stress state.	MPa
$P_u$	Ultimate load	kN
$M_u$	Ultimate moment strength	MPa
$\varepsilon_u$	Ultimate strain	mm/mm
$f_t$	Ultimate uniaxial tensile strength of concrete	MPa
$F^a$	Vector of applied loads	
$f_y$	Yielding stress of steel reinforcement	MPa
a	Shear span	mm
d	Effective depth	mm

## LIST OF ABBREVIATIONS

AASHTO	American Association of State Highway and Transportation Officials.
ACI	American Concrete Institute
CFRP	Carbon Fiber Reinforced Polymer
EC2	Euro Code2
FE	Finite Element
FEA	Finite Element Analysis
FRP	Fiber-Reinforced polymer
FRPRC	Fiber-Reinforced polymer Reinforced Concrete
GFRP	Glass Fiber Reinforced Polymer
HPC	High Performance Concrete
HPFRCC	High Performance Fiber Reinforced Cement Composite.
HRWRA	High-Range Water Reducers Admixture.
HSC	High Strength Concrete.
JSCE	Japan Society of Civil Engineers.
N. A	Neutral Axis
PVC	Poly vinyl Chloride.
RC	Reinforced Concrete
RCC	Reinforced Cement Concrete
RPC	Reactive Powder Concrete
RTS	Residual Tensile Stress
SCC	Self-Compacting Concrete
SF	Silica Fume.
UHPC	Ultra-high-performance concrete



# CHAPTER ONE :INTRODUCTION

## 2.1 General

Composite beams, combining steel and concrete, are commonly employed in building and bridge construction. To ensure the composite behavior of these beams, mechanical shear connectors are utilized [1]. Holes in concrete beams weaken them and make them bend easier when loaded. The strength of beams around openings can be enhanced by adding additional steel reinforcement bars. This method aims to reduce the stresses that build up around the holes, which would improve the beam's ability to carry loads and reduce bending [2]. Modern buildings require numerous pipes and ducts for air conditioning, electricity, communication, and data networks that can be seen in Fig. (1.1)[3]. These services are accommodated through openings in concrete beams. In general, these openings can weaken the beam. Web openings in reinforced concrete beams affect the beam's performance in several ways:

- Reduced stiffness, leading to increased beam deflection.
- Increased cracking, potentially compromising beam integrity.
- Reduced beam shear capacity, limiting the weight of the beam can support[4].



**Figure 1.1** Examples explain the openings in beams [3].

## 2.2 Composite Members

Structural elements combining reinforced concrete and steel (rolled or fabricated) create composite structural members; this combination illustrates the concept of composite materials; Composite beams combine different materials, like when beams are encased in concrete. In contrast to conventional steel design, which only considers steel strength, composite design relies on the combined strength of steel and concrete. Including concrete in the design helps save costs by reducing the amount of steel needed. The concrete also protects the steel from fire and corrosion, making the beam less likely to buckle [5].

## 2.3 Composite Box Steel-Concrete Beams

As seen in Figure 1.2 a, the most common composite member in structural engineering is usually a concrete slab stiffened by a steel I-beam. However, recent studies have been investigating an approach that uses a composite member (composite-encased beam) having an embedded steel I-section in the center of the concrete section, increasing this bond and causing them to act as one entity, as depicted in Figure 1.2 b. Hollow concrete beams are frequently employed in tall reinforced concrete structures for the purpose of reducing member weight. However, there is a concern that these hollow members may not have enough flexibility to absorb applied energy. Hence, extensive research is essential to ensure the safety of these components. Considering this, a unique type of composite section has been developed for the present investigation, which significantly differs from the sections studied in the past. This section incorporates a hollow steel structure within the concrete section, offering additional advantages apart from its structural integrity. The hollow core in this new design provides a secure pathway for service conduits, such as electrical and plumbing lines. Figure 1.2 c illustrates these innovative encased composite beams, also referred to as hollow composite beams. One of the

main advantages of this section is the cost savings from using less concrete due to the hollow core, resulting in a lighter structural element. The study employs an ultra-high-performance concrete (UHPC) mixture, renowned for its superior quality, though it comes with a relatively high cost [6].

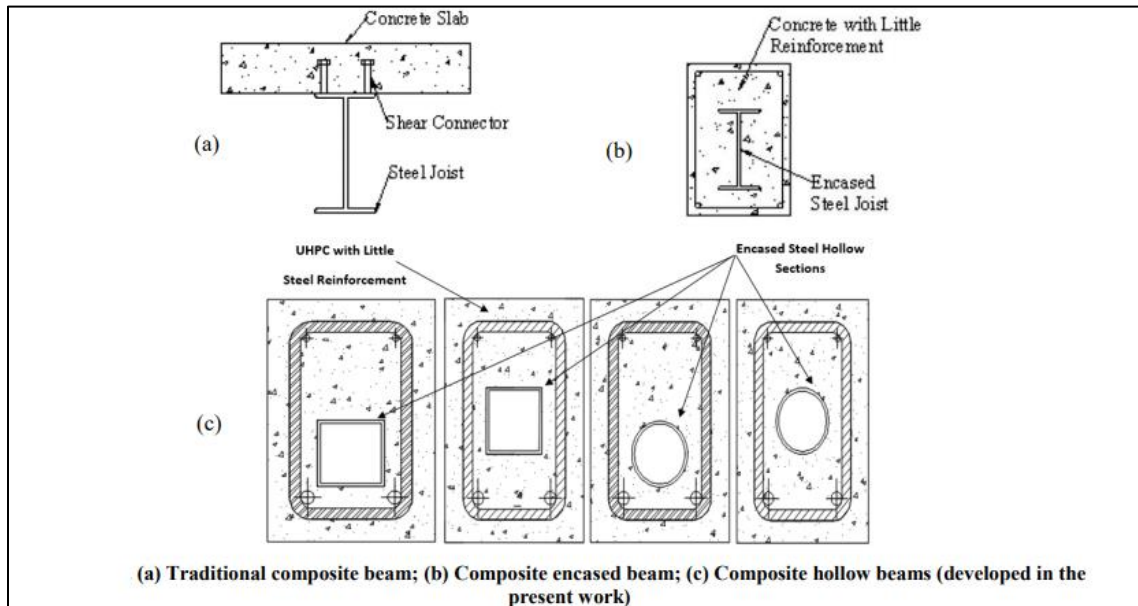


**Figure 1.2** Examples explain the types of composite encased beams [6].

## 2.4 Shear Connector

To work effectively as one cohesive entity, composite action is employed in connecting prefabricated units like prestressed or precast reinforced concrete, steel beams, and cast in place concrete. Although there may be an initial dependence between the steel beam and concrete slab, this relationship does not last forever because it continuously deteriorates because of repeated use or heavy weights. The mechanical shear connectors are designed to enhance the composite behavior of the steel and concrete elements by disregarding the contribution of the natural bond between them. Shear connectors help distribute horizontal shear forces between the steel beam and concrete slab, as well as prevent horizontal movement between the two components. They are also used to prevent the slab from separating vertically from the steel girder at the contact surface.

## 2.5 Beams With Openings

In recent years, the demand for buildings with high ceilings has been steadily increasing. However, installing ducts and apertures for electro-mechanical systems within the clear heights underneath reinforced concrete beams is necessary. Most building systems use ceiling under beams to cover these ducts and pipes; this covering takes from floor height and creates dead space on each floor, as shown in Figure 1.3. The height of this area can contribute to the total building height by the pipes and ducts that pass-through beams, as shown in Figure 1.4. Thus, several investigators exerted great efforts to study the behavior of such beams and introduce reliable techniques for analyzing and designing such beams.



**Figure 1.1:** Service ducts and pipes in beams.



**Figure 1.4:** Service ducts and pipes in beams.

Openings that are square, circular, or nearly square can be considered small if their depth (or diameter) is less than 40% of the total beam depth[7]. If such a situation occurs, beam activity will likely dominate. Hence, the analysis and design of a beam with small openings can be approached in a manner like that of a solid beam. However, openings create interruptions or disruptions in the regular distribution of forces, resulting in the accumulation of stress and the formation of cracks in the vicinity of the opening. To avoid potential early failure of the beam, it is necessary to provide an adequate amount of specific reinforcement around the opening's perimeter to regulate crack widths, as with any discontinuity [8].

The position and size of any apertures present often influence the deformation and strength of a beam. By carefully selecting the location, it is possible to create relatively big gaps in reinforced concrete beam constructions without compromising their final load-bearing capacity [9]. Nevertheless, even little apertures situated in an

undesirable location might result in a significant reduction in the intensity of the beam. Therefore, it is essential to meticulously strategize the dimensions and positioning of the apertures [10]. Nevertheless, the presence of the apertures leads to interruptions or disruptions in the regular passage of stress, leading to a buildup of stress and the occurrence of cracks in the opening at an early stage. Hence, it is necessary to ensure sufficient reinforcement is placed in the opening area to effectively manage the breadth of cracks and prevent any potential early beam failure [11]. Vertical apertures in reinforced concrete beams are utilized as an alternative to tiny holes in slabs, particularly in modest structures in both height and size (low-rise buildings). Frequently, because the forces can be rearranged in the structure, little openings have no influence on how concrete slabs with their reinforcement behave [12]. Nevertheless, installing it will occupy valuable space and make the services more noticeable, which might not be aesthetically convenient. To address this, a suspended ceiling or specific decorating may be required to make it visually acceptable. However, to conceal most pipes and ducts, they are often routed via vertical apertures in beams and remain concealed behind the partitions until they reach the designated position. This is why vertical openings in reinforced concrete (RC) beams have been widely utilized [13].

## **2.6 Reinforced Concrete Beams Behavior with Web Openings**

Web holes in beams are often used in practical applications to allow for the simple passage of environmental services [14]. Consequently, reducing the height of stories in structures and somewhat decreasing the weight of concrete beams would enhance the stress on the supporting frame during gravity loading and seismic excitation, leading to significant cost savings [15]. The apertures may vary in form and size and are often positioned near the supports where shear forces are most significant. In concrete beams, openings must be properly located to allow the chords

have enough area made of concrete that will form the maximum compression block and deep enough to hold shear reinforcement effectively in case of bending motion.

## 2.7 Categorization of Openings

### 2.7.1 Categorization of Openings based on the Shape

Beams may have many forms for transverse apertures, such as irregular, trapezoidal, triangular, diamond, rectangular, and circular shapes [16], as seen in Figure 1.5. Circular and rectangular openings are the most prevalent, and many different forms of apertures exist. Service pipes, including those for electrical supply, need circular holes. On the other hand, air-conditioning ducts are usually rectangular and are placed in rectangular slots that go through beams. In some cases, a rectangular hole's sharp corners are smoothed down to minimize stress concentration. This helps to enhance the beam's durability by lowering the likelihood of cracks forming at these corners. This concept is discussed in references [17], [18].

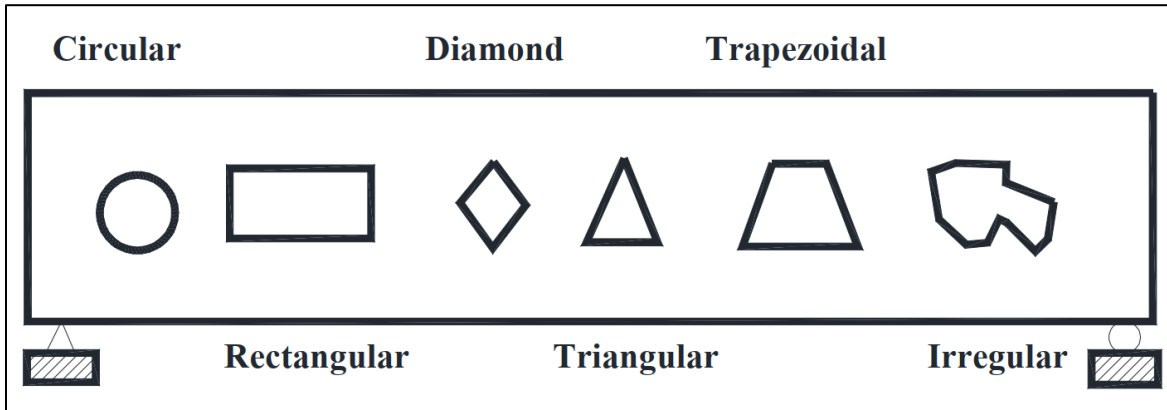


**Figure 1.5:** Opening shapes considered [19].

### 2.7.2 Categorization of Openings based on the Size

When considering the size of openings, it is necessary to clearly identify small and big holes. The strength of the beam greatly depends on how big the aperture is. A web with a square entrance that is one-quarter of the web depth or a circular aperture that is three-eighths of the web depth does not weaken the strength of the

sample. This is considered a modest opening, while it is classified as a big opening in other cases [20].

Another criterion for circular apertures is that they are considered tiny if the diameter of the opening is less than 48% of the depth of the beam web. If such a situation occurs, beam activity will likely dominate. Therefore, the analysis and design process for a beam with small openings can be approached similarly to that of a solid beam[21].

### 2.7.2.1 Small Openings

Based on Somes and Corley [22] an aperture is deemed small if its depth ( $d$ ) or diameter ( $D$ ) is less than or equal to 0.25 times the beam's depth ( $h$ ), and its width does not exceed its depth ( $d$ ), as shown in Figure 1.6. In such cases, as illustrated in Figure 1.5, beam action is likely to prevail. Consequently, the analysis and design of a beam with small apertures can be handled in a manner like that of a solid beam. Small apertures are defined as those that are sufficiently small and strategically positioned so that a strut-and-tie model (STM) can span over them without the need for additional horizontal or vertical reinforcement in the chords above and below the openings[23].

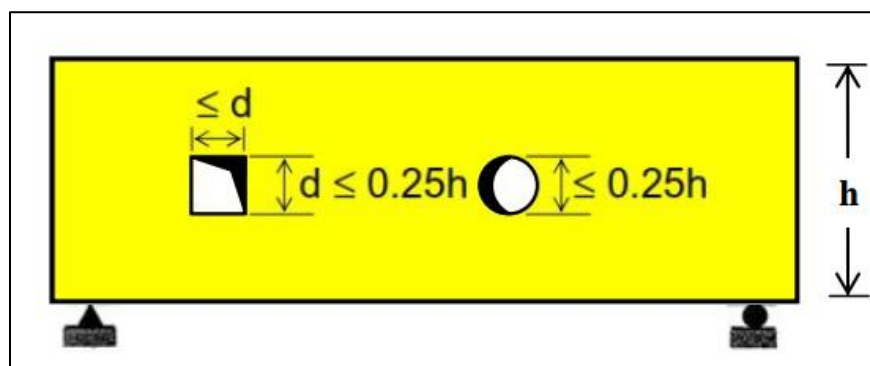


**Figure 1.6:** Description of small openings based on openings' dimensions.

In this scenario, the notion that a strut-and-tie model can pass through apertures without needing additional struts or ties in the top or bottom chords implies that



strain distribution across the opening's cross-section is nearly linear, as shown in 1.7a [24]. Nevertheless, openings create interruptions or disruptions in the regular flow of stresses, resulting in the accumulation of stress and the formation of cracks in the vicinity of the opening. To regulate fracture widths and avoid early failure of the beam, it is necessary to provide an adequate amount of specific reinforcement around the opening's perimeter, like any other kind of discontinuity.

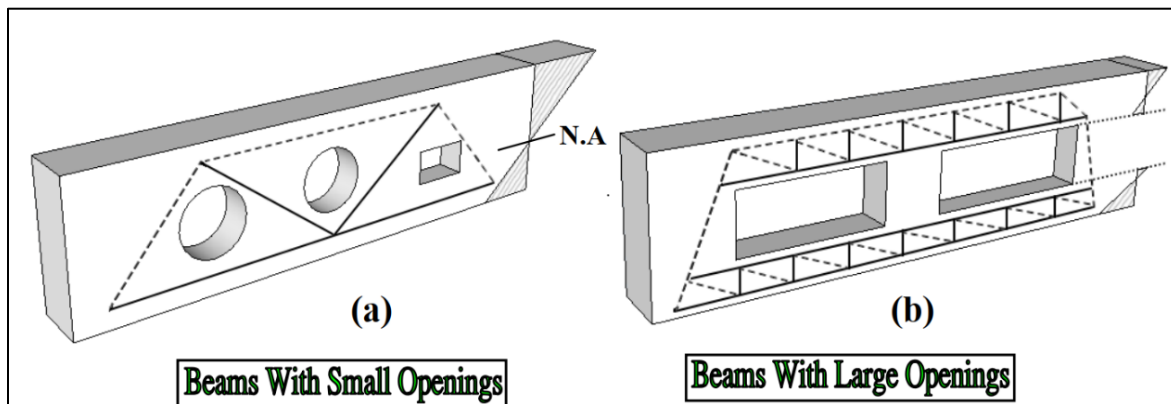


**Figure 1.7:** Description of large and small openings (Assessment of the validity of Bernoulli's hypothesis of plane strain distribution) [23].

### 2.7.2.2 Large Openings

Like a beam with tiny apertures, big openings may be described as openings that need more horizontal and vertical supports in the upper and lower sections of the beam [23]. The validity of Bernoulli's concept about the distribution of plane strain over the whole cross-section of a big aperture, as shown in 1.7b [23], is questionable. An opening is considered large if its depth ( $d$ ) or diameter ( $D$ ) is greater than 0.25 times the beam's depth ( $h$ ), and its length ( $\ell$ ) exceeds its depth ( $d$ ). Such openings reduce the beam's strength, resulting in the behavior shown in Figure 1.8, as described by Somes and Corley[22].

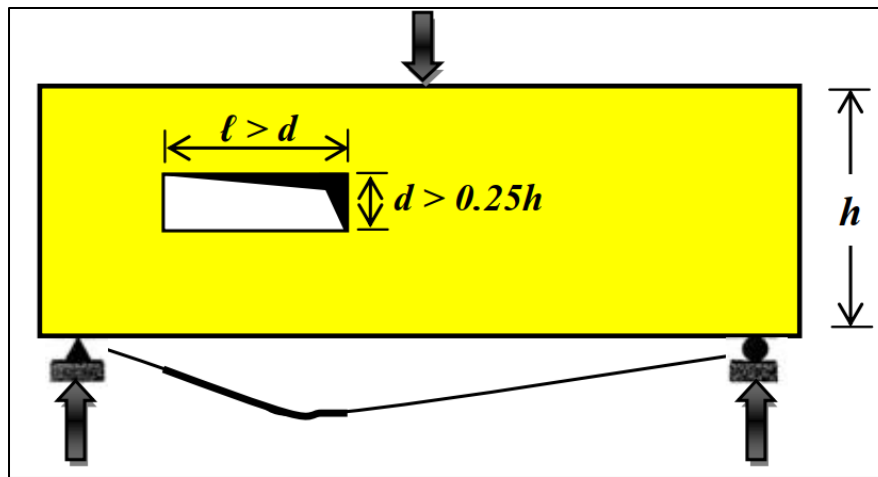


Figure 1.8: large openings description based on structural reaction.

### 2.7.3 Categorization of Openings based on Type of Failure

#### 2.7.3.1 Pure Bending

When it comes to pure bending, if an aperture is placed entirely inside the tension zone of a beam, it does not alter how the beam carries the load. This is because the concrete in that area would have cracked due to bending stress at its maximum capacity, regardless of the presence of the opening. Mansur and Tan [17] have shown this concept by providing detailed instances and supporting their findings with test data. It follows that a beam can withstand maximum moment unaffected by an opening as long as its minimum compression chord depth  $h_c$  is equal to or exceeds a certain limit corresponding to ultimate compressive stress block depth, occurring when:

$$h_c \leq \frac{A_s f_y}{0.85 f'_c b} \quad (1.1)$$

where  $A_s$  = tensile reinforcing area;

$f_y$  = tensile reinforcing yield strength;

$f'_c$  = cylindrical concrete compressive strength;

$b$  = the compression area width.

Although the moment of inertia is reduced at a section with an aperture, leading to earlier onset of fractures, the impact on maximum fracture widths and deflection under service loads is minimal and can generally be considered negligible in the design process.

### 2.7.3.2 Combined Bending and Shear

Shear and bending moments are continuously interconnected in a beam, except at the inflection point. When a small aperture is introduced in a region subjected to significant shear and is surrounded by reinforcement (as shown by the solid lines in Figure 1.9, experimental results documented by [22],[25],[26] The beam may fail in two distinct ways. The first type of failure resembles that of solid beams, except the failure plane intersects the center of the aperture (see Figure 1.9a). The second type occurs when two diagonal cracks develop, with one fracture in each member connecting the two solid segments of the beam (as illustrated in Figure 1.9b). These failure modes are referred to as beam-type and frame-type failures, respectively. [27], must be treated separately.

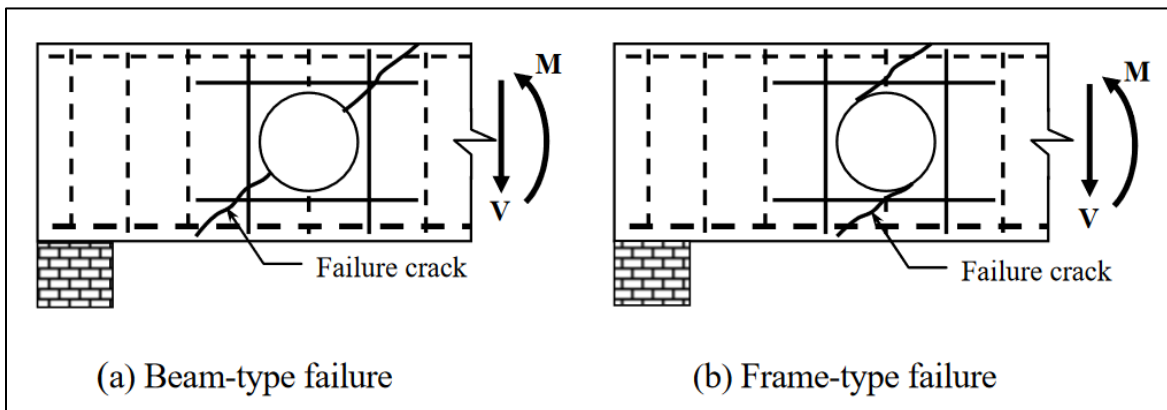


**Figure 1.9:** The two shear failure modes at small openings.

Both in the standard shear design technique and in these circumstances, it might be assumed that the nominal shear resistance,  $V_n$ , is contributed by both the concrete,  $V_c$  and the shear reinforcing that crosses the failure plane,  $V_s$ . In other words,

$$V_n = V_c + V_s \quad (1.2)$$

Bending design might be conducted separately using conventional methods and then integrated with shear design solutions.

### 2.7.3.3 Beam-kind failure

When designing for beam-kind failure, it is possible to assume a 45° inclined failure plane comparable to a solid beam. This plane passes through the center of the aperture, as seen in Figure 1.9. According to the ACI Code [28], the shear resistance  $V_c$  of the concrete may be determined by considering the available net concrete area, as stated in [27].

$$V_c = \frac{1}{6} \sqrt{f'_c} b_w (d - d_o) \quad (1.3)$$

Where:  $b_w$  = width of web;  $d$  = effective depth;  $d_o$  = opening diameter.

To determine the shear reinforcement contribution  $V_s$ , refer to Figure 1.10. The stirrups that can resist shear across the failure plane are positioned on the sides of the aperture within the distance  $(d_v - d_o)$ . Here,  $d_v$  represents the distance between the bottom and top longitudinal rebars, while  $d_o$  denotes the depth or diameter of the opening. Therefore,

$$V_s = \frac{A_v f_{yv}}{s} (d_v - d_o) \quad (1.4)$$

Where:  $A_v$  = of vertical legs area of stirrups per spacing  $s$ ;  $f_{yv}$  = stirrups yield strength.

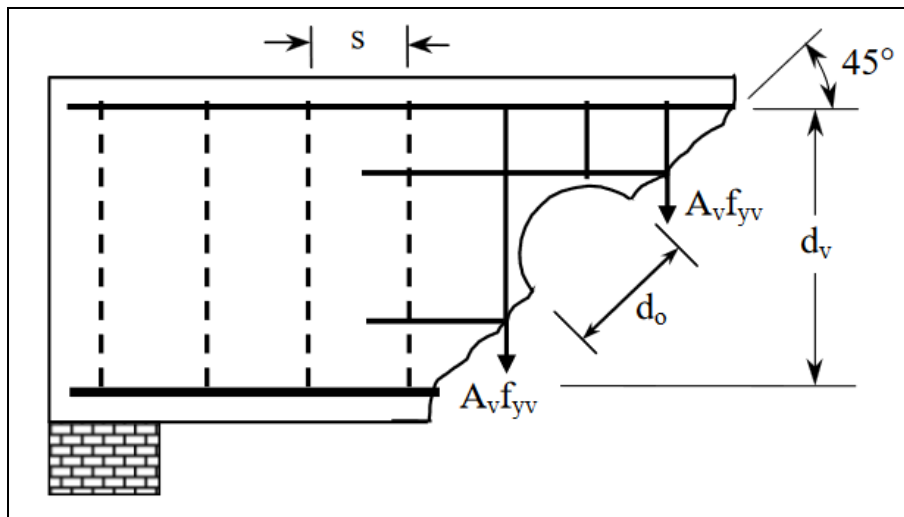


**Figure 1.10:** Shear resistance,  $V_s$ , provided by shear reinforcement at an opening.

To determine the necessary quantity of web reinforcement to support the factored shear through the center of the aperture, one may use the conventional method by considering the values of  $V_c$  and  $V_s$ . The specified quantity should be confined to a range of  $\frac{(d_v - d_o)}{2}$  or, ideally, be consolidated on both sides of the aperture. It is important to properly follow additional limitations that apply to solid beams' typical shear design process.

#### 2.7.3.4 Frame-kind failure

Frame-kind failure is caused by the development of two separate diagonal fractures, one on each chord member located below and above the aperture, as seen in 2.10b. Each structure component exhibits autonomous behavior, much like the members in a framed construction. Thus, it is necessary to provide separate therapy for each chord member, as proposed by [27].

To devise an enhancement against this failure mode, we examine the free-body diagram at the beam opening, as shown in Figure 1.11. The conventional bending mechanism, which entails the couple made up of compressive and tensile stress resultants,  $N_u$ , , in the members above and below the opening, opposes the applied

factored moment,  $M_u$ , locally in the middle of the gap due to global action. By using the following equations one, can get these stress resultants:

$$(N_u)_t = \frac{M_u}{(d-a)} = -(N_u)_b \quad (1.5)$$

subject to the constraints given by equation (2.11). In this equation,  $d$  represents the effective beam depth,  $a$  is the depth of the equivalent rectangular stress block, and the subscripts  $t$  and  $b$  refer to the top and bottom cross members of the opening, respectively.

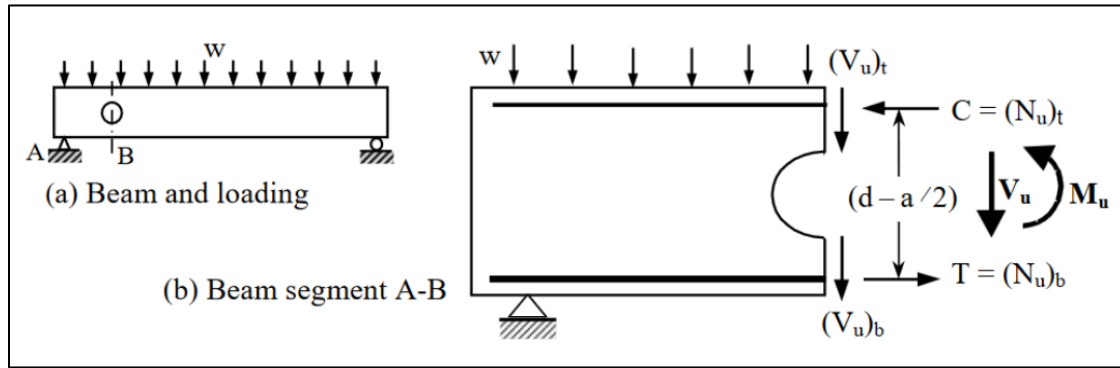


**Figure 1.11:** Free-body diagram at beam opening.

So, because  $V_u$ , (the applied shear) could possibly be proportioned to their cross-sectional areas between two actors[29]. Therefore,

$$(V_u)_t = V_u \left[ \frac{A_t}{A_t + A_b} \right] \quad (1.6)$$

and

$$(V_u)_b = V_u - (V_u)_t \quad (1.7)$$

Given the factored shear and axial forces, each member can be designed independently for shear using the same approach as for traditional solid beams. Axial

compression is applied to the top chord, while axial tension is applied to the bottom chord.

### **2.8 Composite beams Benefits [30]:**

- The steel and concrete are efficiently used.
- Composite buildings utilize a more cost-effective steel section than traditional non-composite buildings while maintaining similar span and loading requirements.
- The necessary weight and depth of the steel beam are decreased. Therefore, reducing the building depth also increases the structure's headroom.
- Composite beams have greater stiffness, resulting in less deflection than steel beams.
- Composite beams can span enormous areas without requiring any additional support columns.
- Composite construction is more efficient than cast-in-situ concrete because it uses prefabricated and rolled steel elements, resulting in speedier construction.
- Encased steel beams have greater corrosion and fire resistance.

### **2.9 Aims of Study**

The main goals of this research are:

1. Numerical Studying how the current square opening in the shear zone impacts the behavior of steel-concrete beams with composite encasement and comparing them with experimental work.
2. Numerical Investigating how the size of the opening affects the shear resistance of composite encased steel-concrete beams and comparing them with experimental work.

3. Numerical exploring methods to strengthen the shear zone in composite encased steel-concrete beams with square web openings and compare them with experimental work.

## 2.10 Thesis Outline

**Chapter 1 (Introduction):** This chapter provides some background on steel-concrete composite structures, particularly box steel-concrete beams. Along with an overview of the study, it describes the use, advantages, and overall performance of the box steel-concrete beam.

**Chapter 2 (Review of Literature):** In this chapter, examine several numerical studies and scientific experiments conducted on horizontal steel-concrete composite beams.

**Chapter 3 (Finite Element Modeling and Formulation):** In this chapter, it's explored the foundational concepts of the finite element theory by discussing the connections and material modeling. And focus on concrete and reinforcing steel, the depiction of steel beams and shear connectors, as well as specimen modeling.

**Chapter 4 (Numerical Application and Results):** This chapter present the results and discussions from the finite element analysis.

**Chapter 5 (Conclusions and Recommendations):** In this chapter, the findings and recommendations have been gathered for further research.



## CHAPTER TWO: LITERATURE REVIEW

### 2.1 Introduction

Steel-concrete composite beams are steel beams covered by a reinforced concrete slab. The slab has been poured with shear connections, as seen in Figure 2.1. In traditional composite buildings, concrete slabs are placed directly on top of steel beams and are supported by them [31]. These two elements function autonomously when subjected to loads since there is no link between the concrete slabs and the steel beam. Any slippage is prevented by including a shear connection between the concrete slab and steel beams, allowing the steel beam and concrete slab to function as a unified composite beam. The behavior of a composite beam seems like that of a Tee beam [32].

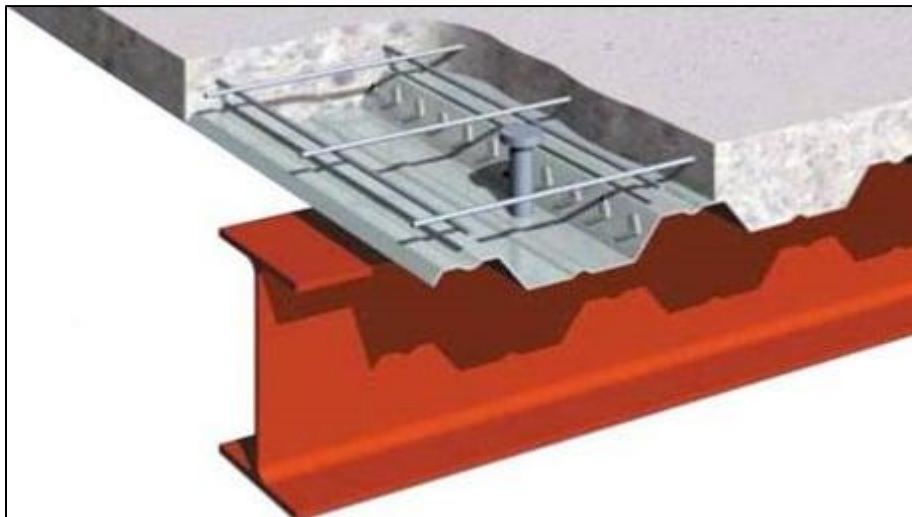


**Figure 2.1:** Composite beam overview [33].

The fundamental principle of a composite beam is because concrete has a higher strength in compression compared to steel, which is prone to buckling when subjected to compression. On the other hand, steel has a higher strength in tension

[34]. The benefits of both materials are fully harnessed by utilizing the combined effect of these two elements, as seen in Figure 2.2.

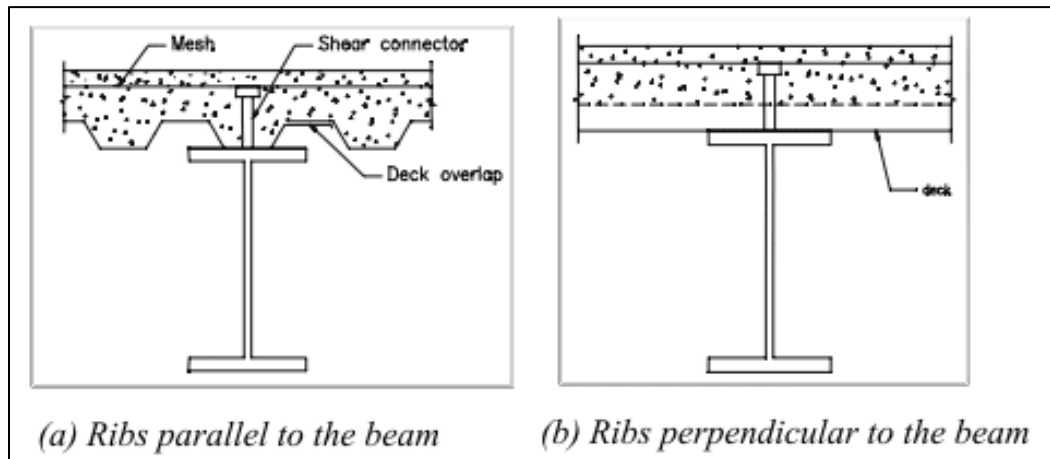


**Figure 2.2:** Typical composite beam shapes [33].

## 2.2 Literature Reviews

There has been a significant focus on steel-concrete composite structures in the past few years owing to their complex characteristics and significant use in engineering projects. Gattesco [35] utilized sophisticated stress-strain constitutive formulas to examine the nonlinear characteristics of the composite beams. Sebastian and Mcconnel [36] developed finite element software that utilizes the layering approach to accurately model composite constructions of steel and concrete reinforced with steel. Bullo and Marco [37] examined the ductile characteristics of stud connections in composite beams, which may avoid local connection shear failure when there is insufficient connection ductility. Many scholars have recognized the significance of integrating experimental and numerical investigations in advanced construction engineering design. Numerical simulation tools, particularly the finite element approach, are crucial in analyzing the mechanical properties of concrete and steel composite structures [38], [39], [40].

Nevertheless, conventional composite beams are joined together using steel shear studs. Unfortunately, these shear studs may occasionally cause stress concentration and cracking in the composite beam, ultimately reducing its lifespan.

Conversely, the collage method has been extensively used across several disciplines. Barnes and Mays [41] studied enhancing the strength of concrete beams made of reinforcement under shear by using externally joined steel plates with adhesive. Serrano [42] investigated the susceptibility of several testing methods for wood-adhesive bonding to variations in geometric defects. Jang and Kishi [43] examined the impact of acid etching on the interface's adhesive strength by modifying the TiNi fiber surface. Nevertheless, there is a need for more study on the use of adhesives for joining steel beams and concrete slabs. The significance of such a study lies in the distinct mechanical characteristics shown by an adhesive junction compared to a steel shear stud. Before using this new approach, it is essential to ascertain its dependability. The research investigates a novel composite beam connected by an adhesive junction between the I-steel and concrete beam. This adhesive connection securely bonds the steel beam and concrete slab, ensuring seamless and consistent stress distribution throughout the composite structure's section. Thus, the stress concentration is absent in the junction of the steel-concrete composite beam. In addition, the novel connecting technique simplifies the manufacture of the composite beam and significantly decreases costs.

Zhao and Li [44] investigated the nonlinear mechanical properties and failure mechanism of a connected steel–concrete composite beam utilizing the finite element modeling approach. In this study, a 3-D FE model was constructed. This work uses the finite element technique to examine the cracking and failure process analysis in steel-concrete composite beams. A model using an advanced 3D finite element has been developed and used to study the non-linear features of steel-

concrete composite beams. The accuracy of the computation model was tested in terms of its predictions and their comparison with the experimental results. Subsequently, an examination and discussion were conducted on the distributions of longitudinal strain and the neutral axis. Subsequently, the concrete slab underwent a cracking process, and the resulting redistributed stresses were then exhibited. The findings suggest that the composite beam's failure may be attributed to three primary factors: localized tensile stress causing concrete cracking, compressive stress leading to concrete crushing, and significant yielding of the steel beam due to the overall bending moment.

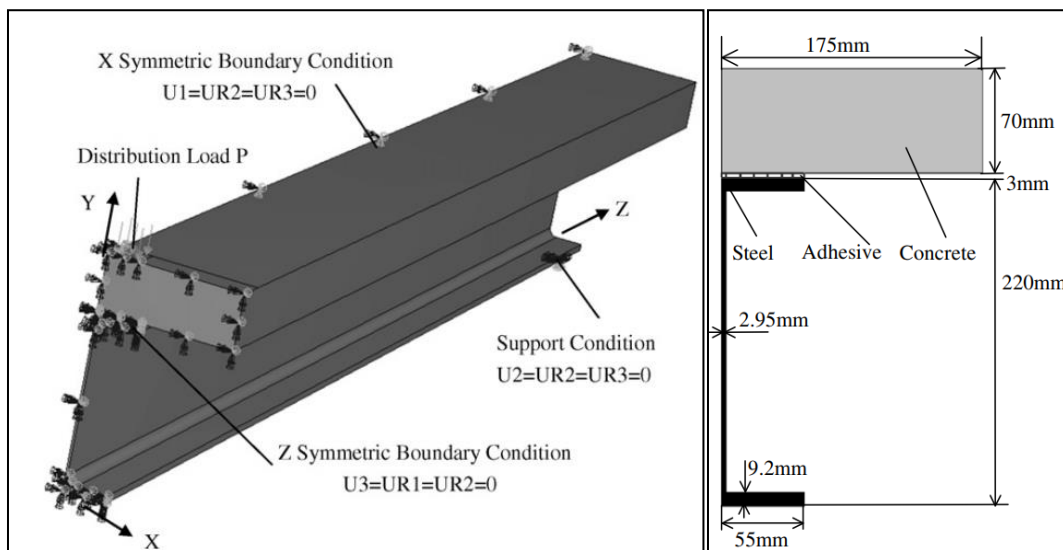


**Figure 2.3:** Composite beam model's geometry [44].

### 2.2.1 Beam with Opening

Multiple investigations were carried out on reinforced concrete beams, including holes in their web. Most of these experiments had commonly used circular and rectangular opening shapes. The prevalence of circular opening geometry may be attributed to the ease of drilling round holes using core drilling equipment [45]. Therefore, much research in the literature has concentrated on examining the impact of the position of openings (specifically, their distance to supports), the size of

openings, and the number of openings on the reinforced concrete beams' behavior that have one or more transverse openings along their span.

In one of their research, Ashour and Rishi [46] conducted experiments on 16 two-span continuous deep reinforced concrete beams with transverse apertures. The test criteria included the dimensions and positioning of the web apertures and the specific specifications for reinforcing the web. The findings of this investigation indicate that the positioning of apertures significantly influences the kinds of failures seen in the beams. Mansur et al. [47] A technique for calculating the maximum capacity of reinforced concrete beams with a single, large, rectangular opening subjected to concentrated loads was developed. This study was carried out by Mansur et al.[47] revealed that the allocation of shear forces between the upper and lower chords and the maximum load at which an RC beam with openings fails mostly relies on the position and dimensions of the opening(s).

Osman et al. [48] utilized experimental and FE methods to examine the shear behavior of reinforced concrete (RC) beams with openings. The main variables studied in this research included the shear span-to-depth ratios ( $a/d$ ), openings sizes and position. The beams were divided into three categories based on their shear span-to-depth ratios. An experimental investigation was conducted on four reinforced concrete beams: three were solid, and one had openings. They were then subjected to two-point loading and served as control specimens to validate the accuracy of the finite element model using ANSYS 14.5 software. ANSYS 14.5 was later used to analyze a total of 31 specimens, taking into consideration all specified parameters such as shear span-to-depth ratios ( $a/d$ ), opening sizes, and positions. During this research, it was observed that premature failure of beam occurred at those points where there were openings created in the areas subjected to high shear forces, especially along the line connecting loading and support point. Besides, a comparison between the results from nonlinear finite element method (NFEM)

analyses and experimental test results indicated very close agreement between them. Consequently, from this information, analytical formula has been derived to spring up a relation for circular void reinforced concrete beams' shearing strength prediction. The resulting data was subsequently compared to that gained from a finite element model. Moreover, the created finite element models may function as a computational framework for forecasting the performance of reinforced concrete beams with various configurations of web openings.

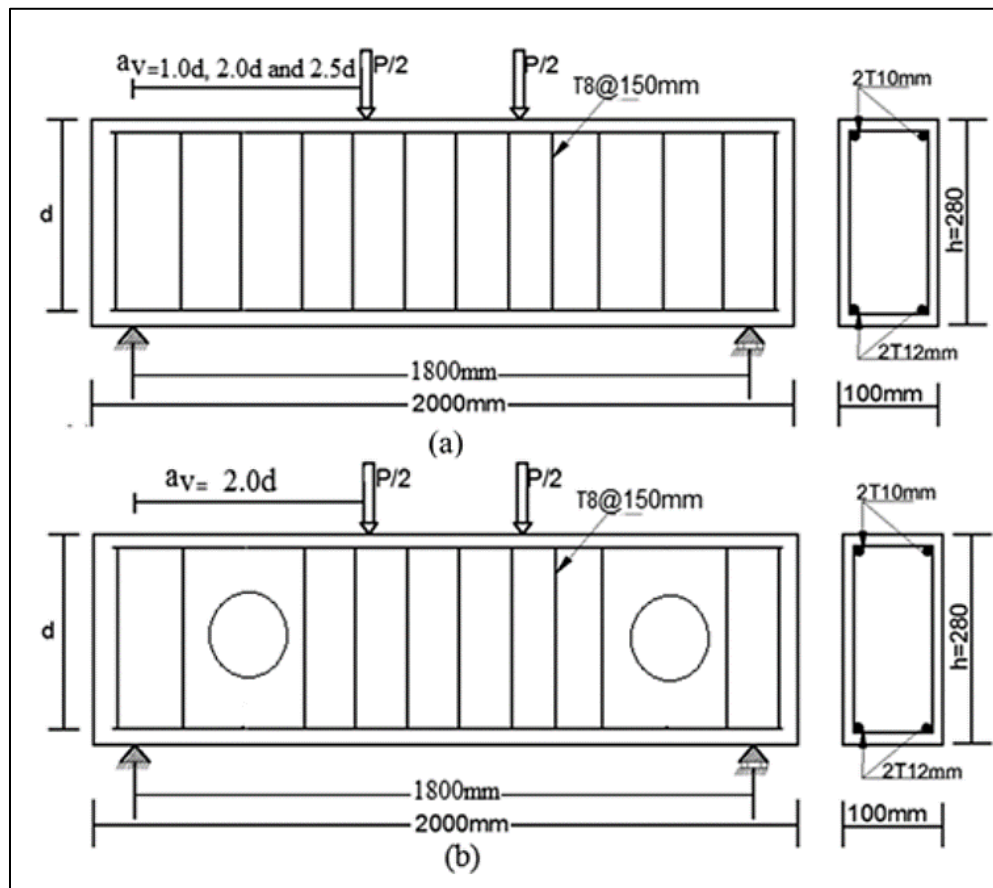


**Figure 2.4:** Tested Beams Reinforcement Arrangement, Cross-Sectional, and Geometry: (a) Solid one, (b) Opening beam [48].

Ahmed [49] The effect of several circular openings on the shear force capacity of reinforced concrete (RC) beams was investigated in this research. Moreover, a three-dimensional finite element model was constructed to analyze such beams. The

results suggested that the aperture size was more influential on beam behavior than the length of shear span. In the same vein, it was found that the number of openings did not have as much impact on the beam's performance as did the size of its aperture. According to the American ACI 318-05 code, it is important to take into consideration the influence of web holes on the shear strength of reinforced concrete beams[50].

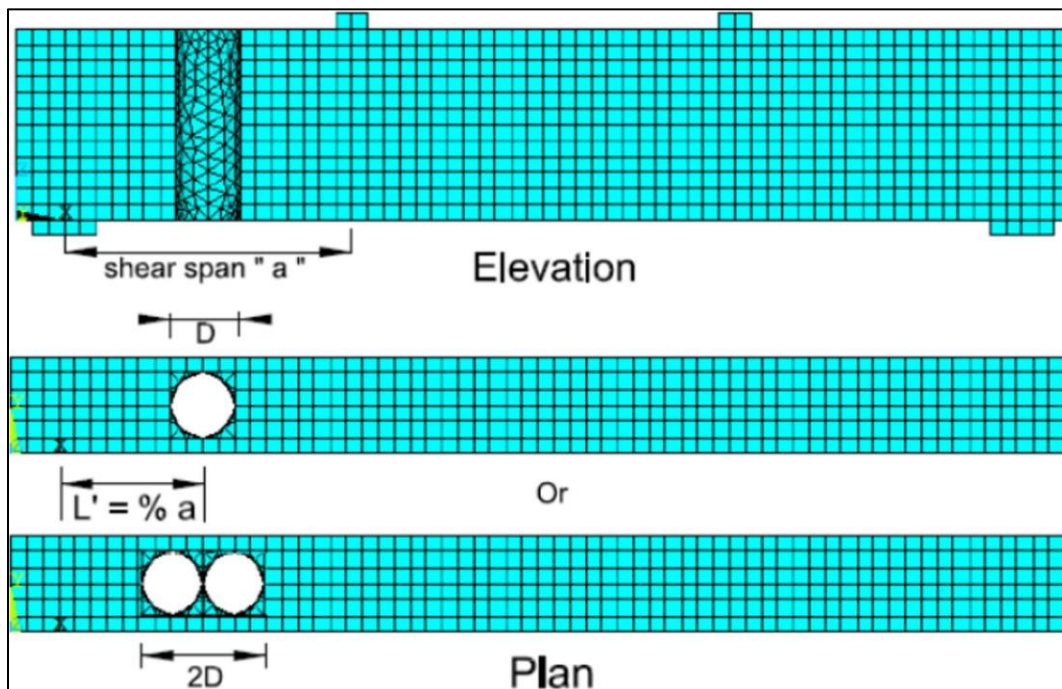


**Figure 2.5:** Numerical Finite element model of concrete beam with meshing details and the vertical circular shape opening details.

Yamada [51], [52], [53] performed FE studies and experiments on reinforced concrete (RC) beams having several apertures in the shear spans. The study examined the effect of longitudinal reinforcement proportions on the beams' failure. The investigations focused on analyzing several factors, such as the position of debonding fractures at the tension-reinforcing level, crack widths, and the opening location. The beams examined and studied had no shear reinforcement, and the openings were present throughout pouring the concrete. This research highlighted that the existence of holes has little impact on the strength of the beam. This is

because the openings enhance the control of the arch mechanism in the beam rather than the beam mechanism.

Torunbalci [54] conducted nonlinear FE simulations to create an analytical approach for estimating the load capabilities of reinforced concrete beams having significant openings. The research examined the effect of web apertures and web strengthening on the load-carrying capacity of reinforced concrete beams with openings. The FE analysis predictions were also compared with the experimental findings, and a high level of concordance between the experimental and numerical findings was achieved.

The research conducted by Özkılıç *et al.* [55] focuses on examining the effect of transverse opening sizes and shear reinforcement proportions on the flexural and shear behavior of reinforced concrete (RC) beams with two web holes. These openings are positioned across distinct spans, with a single opening in each half-span. The research included testing a total of 12 reinforced concrete beams. These beams had varying opening diameter-to-beam depth ratios, namely 0.47, 0.40, 0.33, 0.27, 0.20, and 0.0. Additionally, various shear-strengthening proportions were used. The beams were subjected to four-point bending until failure. A comparison was made between beams' rigidities, ductility, load capacities, and energy dissipation capabilities in both the elastic and plastic behavior ranges.

Additionally, the load capabilities of the beams were compared with the current analytical shear strength formulas found in the literature. The test findings revealed that when the diameter of apertures in an RC beam increases, frame-kind shear failure is much more prominent, regardless of whether the beam has sufficient or insufficient shear reinforcement. The decrease in load capacity and modulus of toughness is more significant as the opening diameter increases, particularly when there is insufficient reinforcement for shear. However, the ductility of shear-



deficient reinforced concrete beams with openings has a smaller impact than those with sufficient shear strengthening.

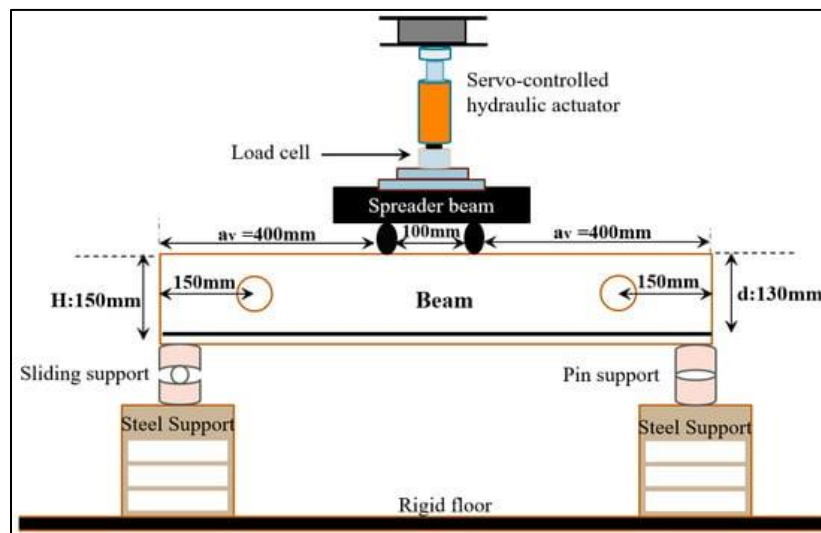
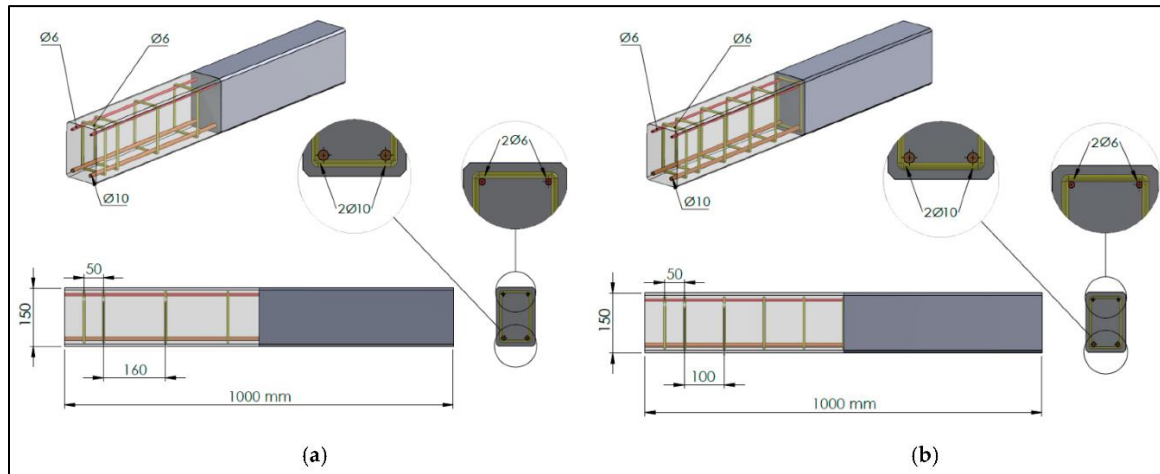


**Figure 2.6:** Beam details and test setting up used in [55].

Mastan et al. [56] adjust the design and location of the aperture to improve its structural performance. The composite steel-concrete beam was studied using ABAQUS v6.14, considering three shapes: triangle, rectangle, and circle. The optimal geometry is positioned at several locations between the span's support end and midpoint. The numerical analysis determined that the circular shape positioned at one-third of the span was useful in reducing stress concentration and maximizing

stress resistance. The beams' load-carrying capacity was estimated utilizing an artificial neural network (ANN) model. The accuracy of the predictions was assessed utilizing multiple mean square error (MSE) and coefficients of determination (R<sup>2</sup>). The MSE and R<sup>2</sup> values for all the models were more than 0.09 and 0.94, respectively. This suggests that artificial neural networks (ANN) are suitable for analyzing numerical data.

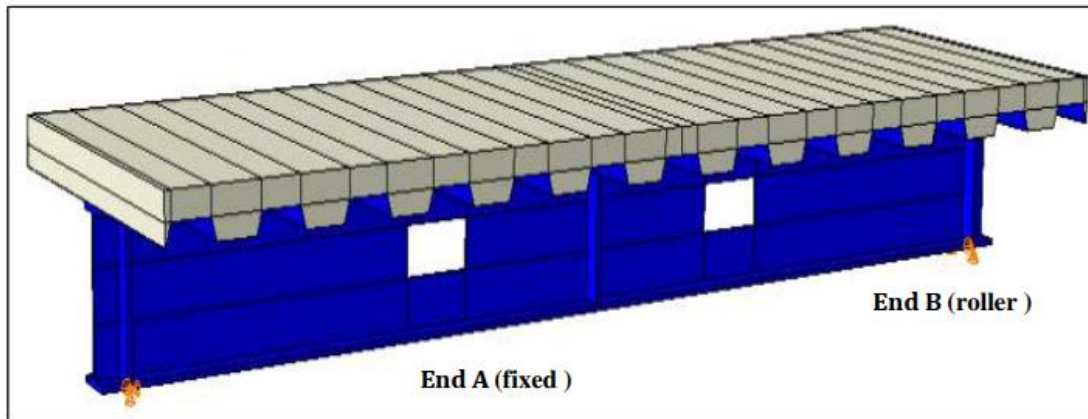


**Figure 2.7:** Modelling of the utilized composite beam by [56].

Abdulridha et al. [57] examine the flexural characteristics of reinforced concrete beams with a circular cross-section hole throughout their length. The beams are supported and subjected to monotonic two-point loads. The commercial finite element software ABAQUS was utilized to simulate and implement the behavior of the samples experimentally evaluated in prior research studies. A total of thirteen RC rectangular beam specimens were examined, with the first being solid and the other having longitudinal circular holes. The perforation samples were categorized into three sets, each with a designated aperture diameter of 2.5 cm, 4 cm, and 5 cm. The distance from the center of the hole to the top section face exhibited variability, with the hole being either entirely inside the stress block, below it, or partly within it. The accuracy of the simulated model was confirmed by comparing the obtainable load deflection data with the implemented data, revealing a strong agreement

between the two. The simulated models may include the maximum load, the initial cracking load, its propagation, and the highest deflection observed. It has been determined that the presence of a longitudinal hole with a diameter-to-beam depth ratio below 20% at various points from the top cross-sectional surface to the hole's center leads to a decrease in the maximum load by no more than 5% in comparison to a solid beam.

Jabbar et al. [58] examined the behavior of four reinforced concrete beams having a square cross-sectional area. These beams were subjected to three-point loads until they failed. Three beams were specifically constructed with tiny web apertures of varying forms: circular, rectangular, and square. The goal of including a beam without any openings (the control beam) was to facilitate a comparison of the results. The load-deflection curves were satisfactorily produced for the samples that were tested. The findings showed that introducing tiny web gaps in reinforced concrete beams resulted in a marginal decrease in their maximum loads, corresponding to an increase in the maximum deflection. Furthermore, it was determined that the beams with circular web holes exhibited superior shear resistance compared to the other chosen designs.

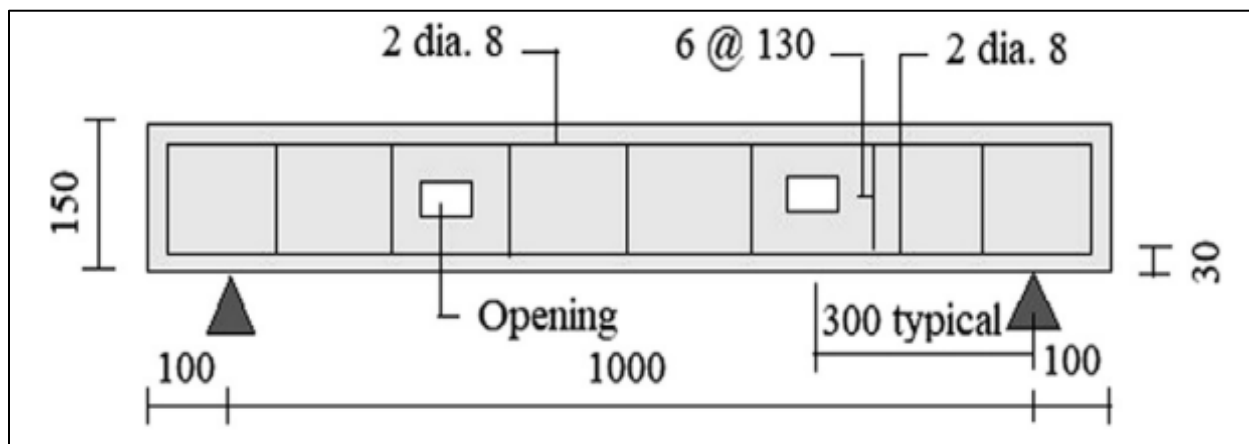


**Figure 2.8:** Details of tested beams with web openings.

Liang et al. [59] employed the FEM for assessing shear and flexural capacity of simple composite beams subject to composite bending and shear. An attempt to develop and validate a finite element model featuring geometric and material nonlinearity for composite beams using experimental data has been made. The time that finite element model has been validated, it can be used to find out how composite action and concrete slab influence shear capacities and moments of composite beams. This research is considering the impact of shear connectors on the vertical shear strength of deep composite beams under shear loadings. The supported composite beam designs that combine with both shear and bending methods should lead to vertical shear strengths. The models are finally considering the effects from concrete slabs, composite action, and moment-shear interaction. The proposed designs offer a systematic and cost-effective design process for simple supported composite beams.

Jen et al. [60] conducted experimental research on reinforced concrete beams that included circular transverse holes. A four-point load test was performed to examine the impact of the opening's size and location on the beam's performance when subjected to shear and flexural stresses. Furthermore, three supplementary techniques for the introduction were examined. The beams were assessed based on their load-displacement responses, mechanical characteristics, deflections, and failure mechanisms. The presence of an aperture with a diameter that does not exceed 0.25 times the height of the beam reduces the beam strength by about 20% when no reinforcements are used at the entrance. The diagonal bar reinforcement technique successfully enhanced the beam's structural integrity when the opening size did not exceed one-third of the beam's height. The formula model suggested accurately predicting the maximum load-bearing capacity of the beam with a transverse aperture using a cautious approach.

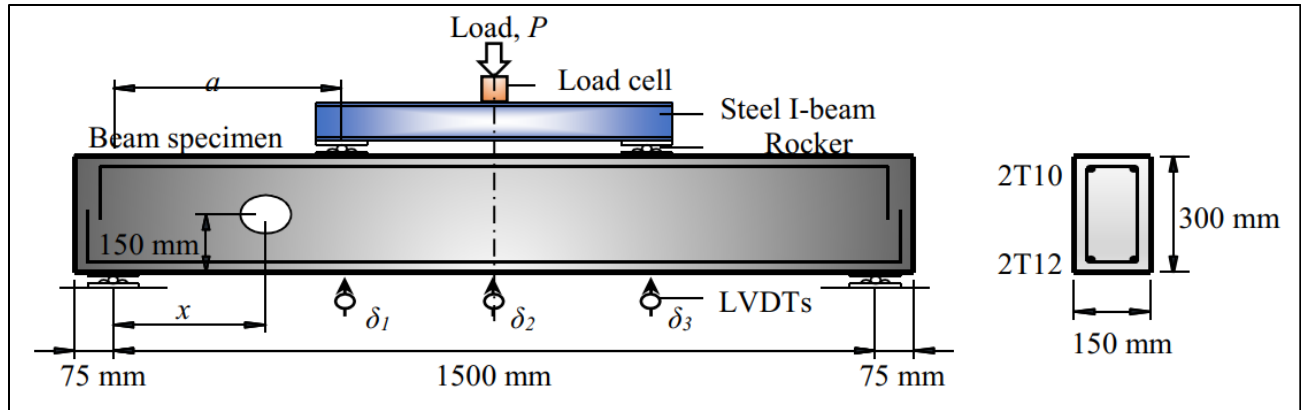


**Figure 2.9:** Beam details and testing sketch.

Altemen et al. [61] conducted experimental research on high-strength concrete (HSC) beams and used the finite element approach for implementation. The experimental findings were validated utilizing ANSYS software, comparing the force-displacement relationship, fracture pattern, maximum displacement, and ultimate load capacity. The program was used to ensure that the same attributes, materials, geometry, and situations were maintained in the analysis. The verification procedure between the theoretical program and experimental work strongly converged the acquired findings. The high level of resemblance in the outputs indicates a strong correlation between the experimental and numerical results, with a matching accuracy of 99% in force and 94% in displacement. The variations were caused by the little disparity between the experimental and theoretical sides, which the numerical analysis deemed the optimum condition. This research investigated the behavior of RC beams with both transverse and longitudinal openings. The primary failure mechanism seen in the beam was flexural failure, despite the existence of shear fractures. However, the flexural cracks predominantly influenced the beam's behavior.

Hamzah and Ali [62] examined how the vertical opening affects the shear strength and behavior of supported reinforced concrete beams. The research included testing five reinforced concrete (RC) beams, with one beam as a reference

without any openings, while the other beams had an opening at their mid-shear span. The factors considered in this study included the orientation of the apertures, the configuration of the holes, and the specific methods used to replace the reinforcement that may impede the penetration of the openings. The experimental findings indicated that a vertical aperture marginally decreased the maximum load-bearing capability. Furthermore, it has a negligible impact on the augmentation of the highest deflection under the service loads. However, it has been shown that square holes have a greater impact on lowering the final load capacity than circular openings. Regarding the techniques utilized to substitute the obstructed rebars, the findings indicate that utilizing a stirrup on both sides of the aperture in the longitudinal direction is sufficient to improve the ductility index and regain the lost strength. Furthermore, it has been shown that the transverse apertures have a substantial impact on the maximum load in comparison to the impact of the vertical opening.

Moatt and Aziz [63] examine the effect of reinforcing self-compacting concrete (SCC) box beams with steel plates in a localized manner on the torsional strength. The study focuses on seven hollow core beam specimens with a transverse opening subjected to pure torsional forces. The seven beam specimens underwent testing and were constructed with the following dimensions: length=1.8m, width=30cm, and depth=30cm. Out of the seven samples, six of them had transverse apertures measuring 10 x10cm. The parameter investigations included examining the effects of having a transverse opening and the location of the transverse opening at either one-fourth or one-half of the clear span length of the beams, from either one side or both sides. The present reinforcing strategy relies on localized steel plates securely attached to the self-compacting concrete (SCC) utilizing bolts acting as shear connectors. The experimental findings indicate that the maximum torque was reduced by 34.7 and 45.3% for the tested samples with transverse apertures located

at  $L/4$  and  $L/2$ , respectively, compared to the reference beam. The torsion moments of the tested samples, which had transverse openings at  $L/4$  and were reinforced by one or two face-specific steel plates, were enhanced by 34 and 55.5%, respectively, compared to the reference samples. The torsional moments increased by approximately 20 and 24% for the tested samples with a transverse opening at  $L/2$ . Compared to the reference beam, they were further reinforced by one and two-face localized steel plates. The study concluded that the presence of the transverse opening decreased torsional capacity, while the approved method contributed to its enhancement.



**Figure 2.10:** Localized a) Two-Face Steel Plates; b) One Face Steel Plates.

### 2.2.2 Beam Strengthening

Renjini and Manasa [64] assessed the efficiency of a beam with reinforced openings utilizing CFRP when subjected to effect loads. For this numerical investigation, a total of 3 beams were simulated. One of the beams had a rectangular post aperture used as a reference beam for comparative purposes. The two remaining beams were reinforced externally using carbon fiber-reinforced polymer (CFRP) sheets. These sheets were applied separately, one around the opening and the other within the opening. The purpose of this reinforcement was to assess the performance

of the reinforced beam when subjected to an impact load in the ANSYS autodyne platform. The numerical findings indicate that the load-bearing capability of beams with apertures is significantly affected by the placement of FRP laminates. Based on the comprehensive analysis, applying CFRP lamination around the aperture is more effective in mitigating the impact.

Abtan and Abdul-Jabbar [65] investigated the behavior of eight RC beams. These beams were divided into two sets. All beams were uniform in size, reinforcing, concrete kind, and hole diameters. The study was conducted to determine the most optimal hollow core section and assess the impact of web openings on a hollow core. The observed load capacity indicated a drop of approximately 2 to 14% in the hollow core location at the bottom and mid sections, compared to the solid portion. Thus, the most optimal configuration for the hollow core part is positioned in the middle of the beam, thereby integrating the beam with both transverse and longitudinal opening portions. The beam's longitudinal and transverse openings provide distinct loading data depending on the location of the web opening. The opening provision decreased by about 20.4% compared to the hollow beam (without transverse opening) and by approximately 22% compared with the solid beam. The most favorable configuration for the beam, with both longitudinal and transverse openings, was achieved once the web opening was positioned in the mid-shear area. However, the most crucial configuration occurred once the web opening was situated in the mid-span and near the supports of a similar beam with transverse and longitudinal openings. The failure modes seen in all beams may be classified into two basic types: abrupt flexural failure in the compressive area due to crushing of the concrete cover and flexural-shear failure.

Suresh and Prabhavathy [66] the study examined the use of steel plates and steel fibers to enhance the opening areas in reinforced concrete beams subjected to two-point loading tests. The test specimens had a cross-section of 15x30 cm and a length



of 2 meters. The experimental program involved testing 14 reinforced concrete beams, including two without openings (one without fibers and one reinforced with fibers), four with openings of varying sizes in the shear zone, four steel fiber-reinforced concrete beams with openings of varying sizes in the shear zone, and four steel fiber-reinforced concrete beams with openings of varying sizes in the shear zone that were further reinforced with steel plates. The control beam was a solid beam with no openings. The investigation focused on analyzing the behavior of concrete beams with and without openings under maximum load, paying particular attention to cracking patterns and deflection. Beams with duct openings in the shear zone experienced a 55% to 70% reduction in load-bearing capacity. The experimental results showed that reinforcing the duct openings with steel fibers improved both the load-bearing capacity and ductility of the beams. Additionally, strengthening the duct openings in steel fiber-reinforced concrete beams with 0.4 cm thick steel plates further enhanced the load-bearing capacity and significantly increased the beam's deflection before failure. Reinforcing the beam with steel plates also delayed crack initiation.

Morsya and Barima [67] a comprehensive experimental study was conducted to investigate the effect of openings on the performance of reinforced concrete beams with and without reinforcement. The total number of samples tested in two series was 24 considering the number of openings in their behavior. The consideration pointed out the orientation, aspect ratio as well as shape of openings which had the same area for both shear and bending zones. The influence of different strengthening techniques applied to these voids on reinforced concrete (RC) beams is also investigated here. These include internal strengthening techniques such as internal steel reinforcement, internally placed fiber-strengthened bars or near surface mounted FRP laminate reinforcement (N.S.M). Externally connected strengthening techniques like FRP strips externally bonded and/or steel boxes were also examined.

All specimens were subjected to three-point loading. The effective beam length was 1.5m.

Additionally, all samples were intended to fail due to flexure before shear. According to the experimental data, the first set of tests revealed that circular apertures had the smallest decrease in the load capacity of the beam in comparison to square and rectangular openings, if all the openings had the same area. The second set of experiments demonstrated the impact of reinforcing the apertures on the beams' behavior. The application of externally connected CFRP enhances the beams' strength and ductility, although to varying degrees compared to other reinforcement methods.

Meleka [68] an experimental test program was conducted on fourteen reinforced concrete (RC) beams with major holes. These beams were reinforced by adding extra layers of externally connected steel plates or CFRP plates through different methods. The beams were then subjected to a four-point bending test. The study explored the behavior of tested samples both with and without reinforcement, to evaluate different techniques and materials for increasing shear and flexural strength of beams with varying opening locations. The study reveals that CFRP plates are more effective than steel plates in terms of reinforcement.

## **2.3 Concluding Remark**

### **2.3.1 Summery of Literature Review**

The review focuses on various studies that investigate the impact of transverse openings on the structural performance of beams, particularly in composite box steel-concrete beams. Multiple strategies for enhancing beam performance with transverse openings are examined, focusing on the shear strength and structural behavior under various loading conditions.

- 1- Reinforcement with CFRP Sheets:** Renjini and Manasa[64] explored the use of Carbon Fiber-Reinforced Polymer (CFRP) sheets to reinforce beams with openings. Their numerical analysis revealed that applying CFRP around the aperture significantly improved load-bearing capacity and mitigated the effects of impact loads. This emphasizes the importance of the positioning of FRP laminates for enhancing beam strength.
- 2- Optimal Configuration of Hollow Core Sections:** Abtan and Abdul-Jabbar[65] examined the influence of web openings in reinforced concrete (RC) beams with hollow cores. They observed a reduction in load capacity, with optimal performance achieved when openings were located in the middle of the beam. Their study also highlights the importance of the position of web openings in minimizing strength loss, with an average reduction of 20.4% for hollow beams compared to solid ones.
- 3- Steel Fibers and Plates for Enhancement:** Suresh and Prabhavathy[66] investigated the use of steel fibers and steel plates to improve the strength of beams with openings under two-point loading. Their findings indicate that using steel plates around the openings increased the load-bearing capacity and delayed crack initiation, while the addition of steel fibers enhanced ductility.
- 4- Impact of Opening Shape and Orientation:** Morsya and Barima[67] conducted an experimental study on RC beams, examining the effects of different opening shapes (circular, square, and rectangular) on shear and flexural behavior. Circular openings were found to have the least impact on load capacity. Various strengthening techniques, such as FRP strips and steel boxes, were also analyzed, with CFRP enhancing strength and ductility.
- 5- CFRP vs. Steel Plates:** Meleka[68] compared the effectiveness of externally connected CFRP plates and steel plates in reinforcing RC beams with major

openings. The study concluded that CFRP plates offered better shear and flexural strength compared to steel plates.

Overall, the literature suggests that the introduction of transverse openings in beams reduces load capacity and affects overall performance. However, the application of reinforcement materials such as CFRP, steel fibers, and plates can mitigate these effects, particularly when strategically placed around or within openings. These findings guide the numerical analysis of composite box steel-concrete beams, focusing on enhancing shear strength through appropriate reinforcement techniques.

### **2.3.2 Current Study Coverage**

The current study aims to numerically analyze the shear strength of steel and concrete composite beams with a hollow steel box along the beam encased with concrete with transverse openings of different dimensions and shapes, as well as studying other variables that were not covered in previous studies, such as the locations of the openings, the ratio of shear length to effective depth, the compressive strength of concrete, and the percentage of reinforcing steel in the tension.

# CHAPTER THREE: NUMERICAL FORMULATION AND MODELING

## 3.1 Introduction

When it comes to numerical formulation and modeling, the key is turning complicated real-world situations into mathematical equations that can work with them. This is essential for modern scientific research and engineering advancements. By using numerical methods, experts can simulate, study, and forecast how things behave in various systems, like fluid dynamics, structural mechanics, economic markets, and biological processes.

Numerical formulation is essentially the process of converting physical laws, empirical data, and governing principles into mathematical equations. The equations are the foundation of computational models, allowing researchers to study how systems behave under different circumstances. By choosing the right numerical techniques and algorithms, these models can offer valuable insights into complex phenomena that are difficult or impossible to analyze using traditional methods.

When numerical models are created, the start is by defining the problem and figuring out the equations that govern it. This usually means we have to simplify things to make the problem easier to solve. Then break down the continuous system into smaller, discrete pieces or nodes. This is important for using numerical methods like finite element techniques, which work on these smaller chunks of the system.

Upon discretizing the equations of the system, the sequenced solving through computational algorithms should be used. The types of algorithms used vary based on the complexity of the problem and the level of accuracy required, ranging from

basic iterative solvers to advanced optimization routines. Validation and verification are crucial during this process to ensure the accuracy of the numerical model by comparing simulated results with experimental data or analytical solutions.

Numerical formulation and modeling are not just for theoretical research; they have many real-world uses across various fields. For example, in engineering, simulations help design structures, improve manufacturing processes, and make mechanical systems more efficient. In the natural sciences, models aid in studying ecosystems, climate patterns, and the behavior of particles. And in finance, numerical methods are essential for assessing risks, optimizing portfolios, and pricing options.

There are many different software programs that can be used for nonlinear analysis, such as ANSYS, ABAQUS, and ADINA. In this study, the shear behavior of composite steel-concrete beams with transverse openings will be examined using ABAQUS/Standard through nonlinear finite element analysis and extended finite element analysis [69].

### **3.2 ABAQUS Finite Element Analysis**

ABAQUS Finite Element Analysis (FEA) is a powerful computational tool that is commonly used in engineering, research, and manufacturing industries to simulate and analyze the behavior of structures and systems in different conditions. Developed by Dassault Systèmes, Abaqus is widely utilized to predict the performance of components or products in real-world situations [70].

ABAQUS (FEA) utilizes the finite element method (FEM) to solve partial differential equations that control the behavior of intricate systems. The FEM breaks down the system into smaller elements, making it easier to approximate the system's behavior using mathematical models for each element. With Abaqus, users can develop detailed finite element models of structures, components, or materials by

considering factors like geometry, material properties, boundary conditions, and loading conditions [71].

After creating a model, ABAQUS enables users to investigate how the system behaves by solving the equations obtained from the finite element discretization. This examination can offer understanding into different mechanical phenomena such as stress distribution, deformation, heat transfer, fluid flow, and structural reaction to dynamic loads [72].

ABAQUS has a diverse set of analysis features, such as linear and nonlinear static analysis, dynamic analysis, thermal analysis, coupled-field analysis, and optimization. Moreover, it has a vast array of post-processing tools for visualizing and interpreting simulation results, which helps users gain a better understanding of the system's behavior [73].

In general, ABAQUS Finite Element Analysis allows engineers and researchers to model and analyze intricate systems accurately and efficiently. This tool helps them make informed design choices, improve performance, and reduce risks [74].

### 3.3 ABAQUS Finite Element Procedure

Performing finite element analysis using the ABAQUS software requires following a series of steps (see the Figure 3.1). Below is a comprehensive explanation of the ABAQUS finite element procedure:

- 1- **Preprocessing:** which includes setting up the model geometry, specifying material properties, adding boundary conditions, and creating a mesh. In ABAQUS, you can build the model using the graphical interface (ABAQUS/CAE) or by scripting with input files (ABAQUS/Standard or ABAQUS/Explicit). Meshing is important as it breaks down the geometry into smaller elements, influencing the accuracy and efficiency of the analysis.

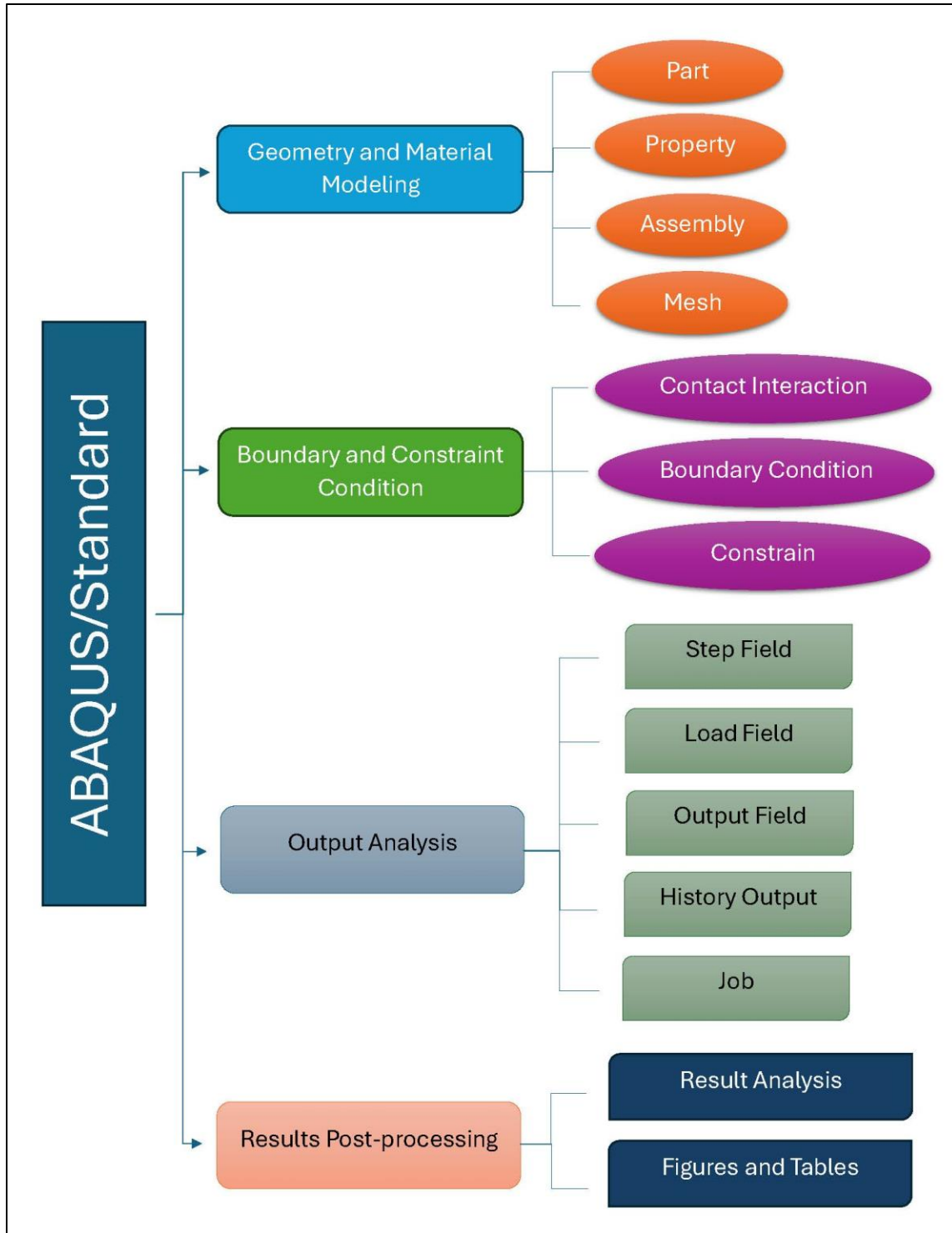


**Figure 3.1:** ABAQUS finite element procedure.

2- **Analysis:** involves determining the type of analysis (such as static, dynamic, nonlinear, etc.), setting up loads and constraints, choosing solution controls,



and specifying output requests. It is important to have a good understanding of the physics of the problem being simulated and what the desired results are.

- 3- **Solution:** With the setup complete, ABAQUS solves the finite element equations to obtain the numerical solution. Depending on the type of analysis and complexity of the model, this step may involve solving linear or nonlinear equations iteratively using numerical methods like the finite element method.
- 4- **Postprocessing:** After obtaining the solution, postprocessing involves analyzing and interpreting the results. ABAQUS provides various tools for visualizing results, such as contour plots, graphs, animations, and reports. Engineers can evaluate the performance of the model, assess the response of the structure to applied loads, and extract useful engineering data.
- 5- **Iterative Analysis:** In many cases, the analysis may not converge or may yield unexpected results. In such situations, iterative analysis becomes necessary. Engineers revisit the preprocessing, analysis setup, or material properties to refine the model and improve convergence.
- 6- **Verification and Validation:** Before drawing conclusions from the analysis, it's essential to verify and validate the results. Verification ensures that the numerical solution accurately represents the mathematical model, while validation confirms that the model accurately represents the physical system being simulated.

Overall, the ABAQUS finite element procedure is a systematic approach to simulating the behavior of engineering structures under various conditions, enabling engineers to optimize designs, predict performance, and make informed decisions.

### 3.3.1 Material and Geometry Modeling

Material and geometry modeling in ABAQUS are critical steps in creating accurate simulations of engineering structures. Here's an overview of both aspects:

#### 3.3.1.1 Part Modeling

Part modeling in ABAQUS involves creating or importing the geometric representation of the individual components or parts that make up the entire structure to be analyzed. Here's an overview of the part modeling process in ABAQUS:

##### 1- Geometry Creation:

- ABAQUS provides tools within its graphical user interface (ABAQUS/CAE) for creating geometric models directly. Users can define basic geometric entities such as points, lines, curves, surfaces, and volumes to construct the desired part geometry as shown in Figures(3.2,3.3,3.4,3.5 and 3.6).
- Geometric operations like extrusion, sweeping, lofting, and revolve can be used to create complex shapes and features within the part model.

##### 2-Importing Geometry:

- Alternatively, users can import part geometry from CAD software using standard file formats such as IGES, STEP, or Parasolid. This allows for seamless integration of existing CAD models into the ABAQUS environment for analysis.
- Imported geometry can undergo further editing or manipulation within ABAQUS to prepare it for finite element analysis.

##### 3- Geometry Editing:

- ABAQUS offers a range of editing tools to modify imported or created geometry as needed. Users can perform operations such as filleting, chamfering, splitting, and merging to refine the part geometry for analysis.

- Geometry editing capabilities in ABAQUS enable users to adjust and modifications to the part model to accurately represent the physical component being analyzed.

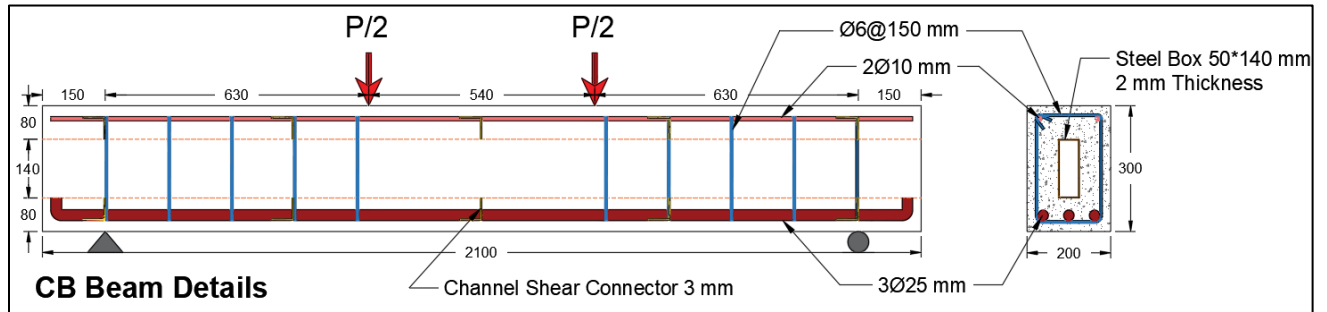


**Figure 3.2:** Details of Geometry and specifications of the first sample CB beam.

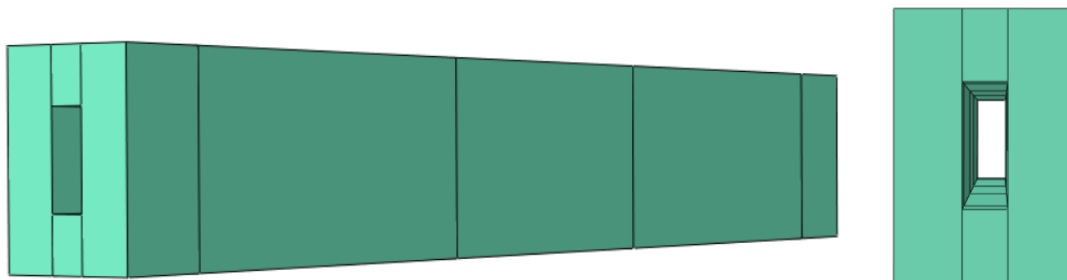
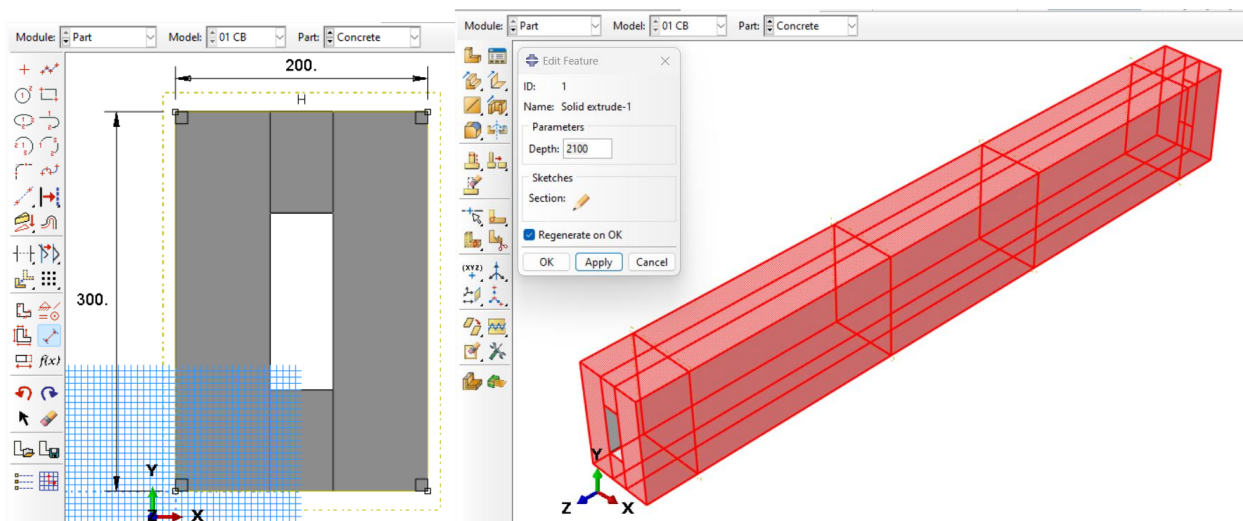


**Figure 3.4:** Concrete beam geometry in CB model.

## Beam with small transverse opening geometry model

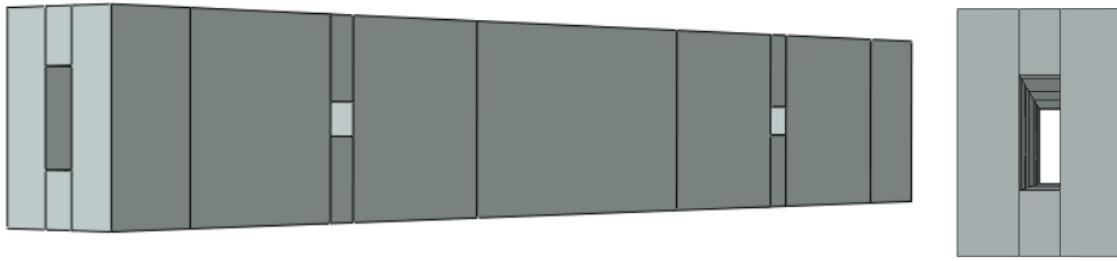


**Figure 3.5:** Concrete beam geometry in BW1 model.

## Beam with large transverse opening geometry model

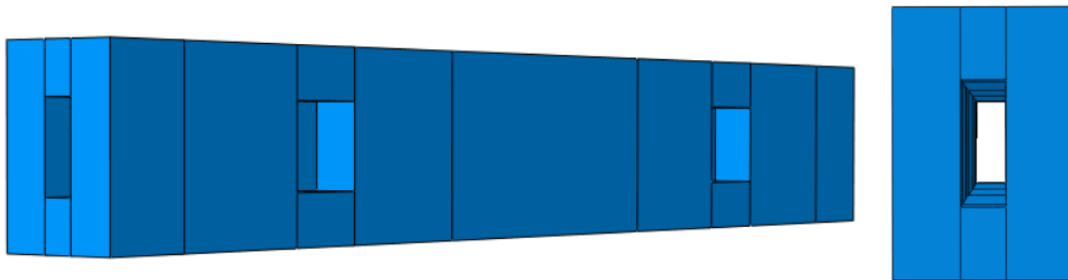


**Figure 3.6:** Concrete beam geometry in BW2 model.

## Reinforcement rebar and steel geometry model

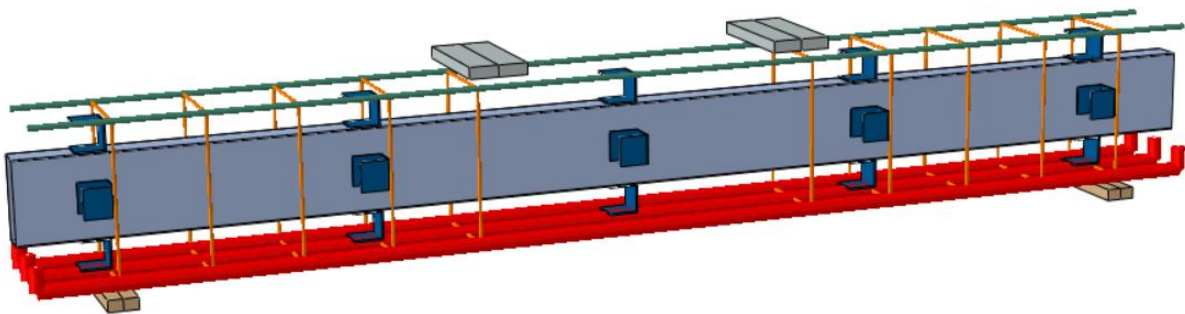


**Figure 3.7:** Reinforcement and steel geometry in CB model.

### 3.3.1.2 Properties of Materials Modeling

Material modeling is important in ABAQUS because it helps engineers simulate how different materials behave when they are under different types of stress. Here are some important properties and features of material modeling in ABAQUS:

#### 1- Concrete Properties

When working with ABAQUS, creating a concrete model requires specifying the material characteristics and choosing appropriate models to accurately replicate its response to different loads. Key concrete properties usually consist of variables like stiffness, Poisson's ratio, mass density, compression resistance, and tensile strength. These attributes may differ depending on factors like the specific mix used and the curing process.

ABAQUS provides a variety of material models that can accurately simulate the behavior of concrete. These models range from simple linear elastic models to more complex nonlinear models that consider concrete's response to stress and strain, as well as factors like cracking and damage. Among these models, the concrete damaged plasticity model is frequently used to study behavior under different loading scenarios. Additionally, models like the concrete smeared crack model are used to simulate concrete cracking and tensile failure.

Concrete behaves in a nonlinear manner because of cracking and crushing, characteristics that ABAQUS material models can represent with stress-strain relationships. Nonlinear models enable the simulation of the intricate behavior of concrete when subjected to both monotonic and cyclic loading. This material is susceptible to cracking, spalling, and ultimately failing when exposed to excessive loads or unfavorable conditions.

With the ABAQUS material models, engineers can accurately simulate concrete damage and failure by including criteria for crack initiation, propagation, and concrete crushing. By specifying concrete properties and choosing the right material models in ABAQUS, engineers can effectively analyze, design, and optimize concrete structures in different engineering scenarios.

### I. Elastic Property of Concrete

The elastic properties of concrete refer to its ability to deform reversibly under applied stress within the linear elastic range. In ABAQUS, these properties are typically characterized by Density and two main parameters shown in Table (3-1):

**Table (3-1):** Elastic properties of concrete.

Type	Density (ton/mm <sup>3</sup> )	Youngs Modulus (MPa)	Poisson's Ratio
Isotropic	2400	23500	0.2

### II. Concrete Damage Plasticity (CDP)

The Concrete Damage Plasticity (CDP) model in ABAQUS is a commonly used method for simulating how concrete structures behave under different types of loads. By incorporating both plasticity and damage mechanisms, this model can accurately represent concrete's non-linear response, which includes that the deformations are not reversible after formation of the cracks. The connections among tension and deformation are given by compulsive mathematical expressions, while the material parameters are established by means of different experiments. The (CDP) model can predict when cracks will start to form and how they will spread under different types of loads, making it a valuable tool for analyzing the stability of buildings, bridges, and other concrete structures. ABAQUS provides resources for checking and confirming the accuracy of this model. In ABAQUS, Concrete Damage Plasticity (CDP) depends on a lot of things that determine how it reacts to different loads. Some of the main parameters that are often used in (CDP) are mentioned below:

## A. Concrete Plasticity Parameters

### a) Dilation angle ( $\psi$ )

The angle of inclination of the failure surface towards the hydrostatic axis, measured in the meridian plane, plays a crucial role in determining the material's behavior. When this angle is small, the material tends to exhibit brittle behavior, whereas higher values of this angle indicate behavior closer to ductile. Experimental observations from four-point loaded beam tests indicate that this parameter typically falls within the range of  $20^\circ$  to  $45^\circ$ , although some researchers suggest values between  $30^\circ$  and  $55^\circ$ . In ABAQUS, the default value for this parameter under compound stress is  $36^\circ$ . This angle is often equated to the dilation angle  $\psi$ , which can be seen as the internal friction angle of concrete. In concrete modeling,  $\psi$  is typically set between  $25^\circ$  to  $40^\circ$  or higher depending on the compressive strength of the concrete. In the context of the thesis, the inclination angle was observed to range between  $31^\circ$  and  $45^\circ$ .

### b) Eccentricity ( $\epsilon$ )

The plastic potential eccentricity is a small positive parameter that indicates how quickly the plastic potential hyperbola approaches its asymptote. Along the hydrostatic axis, it represents the distance between the vertex of the hyperbola and the intersection of the hyperbola's asymptotes (the center of the hyperbola). The eccentricity can also be interpreted as a ratio of tensile strength to compressive strength. In the Concrete Damage Plasticity (CDP) model, a value of  $\epsilon = 0.1$  is commonly recommended [75]. Additionally, in the meridional plane, the surface is represented as a straight line when  $\epsilon = 0$ , following the strength hypothesis of Drucker-Prager. In this thesis, a value of  $\epsilon = 0.1$  was utilized.

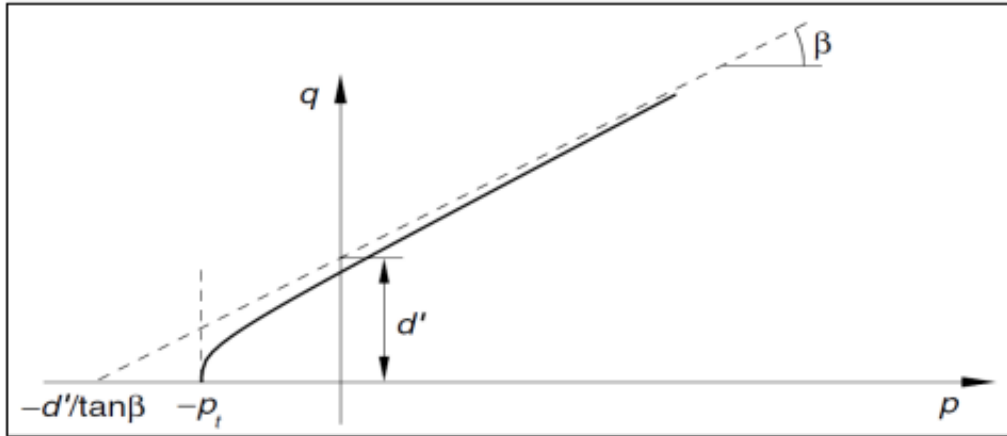


**Figure 3.8:** Hyperbolic surface of plastic potential in meridional plane [75].

### c) $fb_0/fc_0$ Parameter

The parameter  $\sigma_{b0}/\sigma_{c0}$ , or  $fb_0/fc_0$ , represents the ratio of the strength of concrete under biaxial compression to its strength under uniaxial compression. This provides an understanding of how the material performs under different types of loading. In ABAQUS, this ratio is commonly used to describe how the material reacts to biaxial compression. The default value provided in the ABAQUS user manual for this ratio is  $fb_0/fc_0 = 1.16$ , indicating that the concrete's strength under biaxial compression is around 1.16 times greater than its strength under uniaxial compression, as shown in Figure (3.9).

In ABAQUS, the value of  $fb_0/fc_0$  is set to 1.16, which is likely based on empirical correlations. This value is a trusted default for simulating concrete behavior under biaxial compression. Users have the option to tweak this parameter to better match their material properties or experimental data for more precise simulations [76].



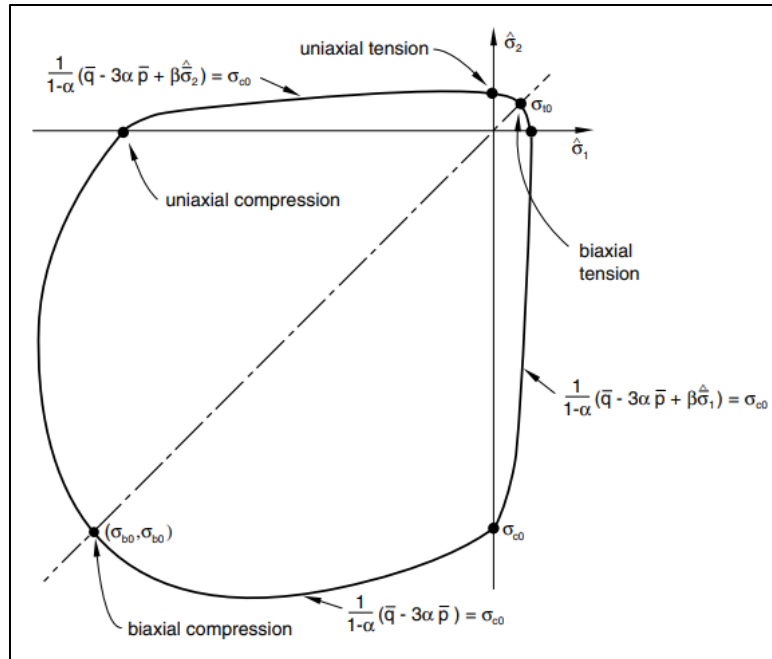


**Figure 3.9:** Strength of concrete under biaxial stress in the CDP model [75].

#### d) $K_c$ Parameter

$K_c$  is a parameter that can be defined as the quotient of distances between the hydrostatic axis and the compression meridian. To that there is a tension meridian lying in the deviatoric cross-section. This Figure (3.9) illustrates how it determines what shape the deviatoric cross-sections of the failure surface will take.

When  $K_c$  is greater than 0.5, it indicates that the compression meridian is closer to the hydrostatic axis than the tension meridian. As  $K_c$  approaches 1, the deviatoric cross-section becomes more circular, resembling the classic Drucker–Prager strength hypothesis where the failure surface is a circle.

Experimental results, as reported by Majewski, indicate that for a mean normal stress of zero,  $K_c$  is approximately 0.6 and tends to increase slightly with decreasing mean stress. However, the Concrete Damage Plasticity (CDP) model recommends assuming  $K_c = 2/3$  as a default value.

The shape described by  $K_c = 2/3$  is like the strength criterion formulated by William and Warnke, which consists of a combination of three mutually tangent ellipses. This criterion is a theoretical-experimental approach based on triaxial stress test results and provides a representation of the failure surface under various stress conditions [76].

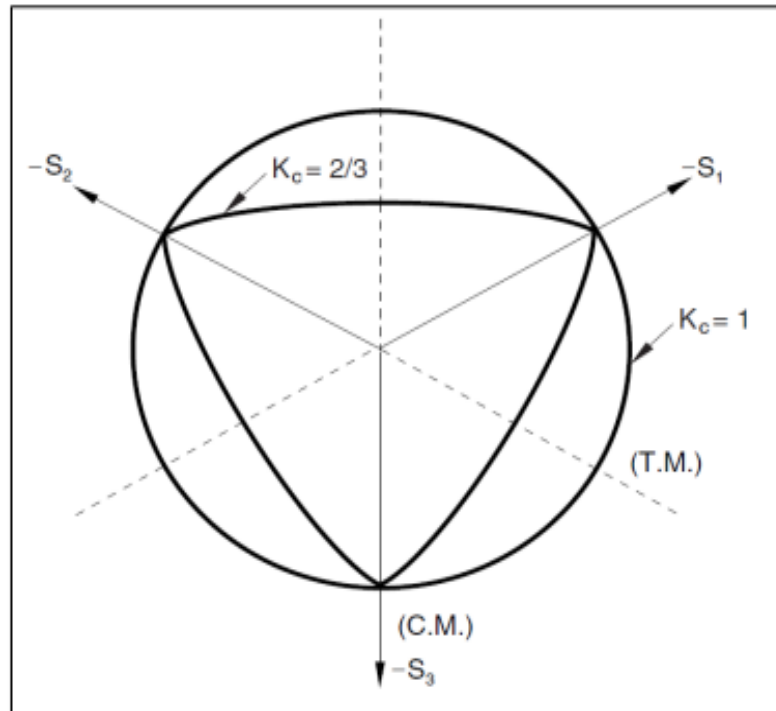


**Figure 3.10:** Deviatoric cross section of failure surface in CDP model [75].

### e) Viscosity Parameter ( $\eta$ )

The viscosity parameter, also known as the relaxation time ( $\eta$ ), is a key factor in complex material models that show stiffness reduction and strain softening. These models can face problems with convergence, especially when modeling materials experiencing significant deformation or damage. One common method to tackle convergence issues is through constitutive equation regularization. This technique involves adjusting the material's tangent stiffness to ensure convergence, particularly

during small time steps. By ensuring the tangent stiffness becomes positive during these small-time increments, the regularization method helps stabilize the solution process. When working with visco-plastic materials, it is common to choose a regularization parameter that is a small fraction of the maximum load values. By using smaller values for this parameter, the rate of convergence in the softening stage of the material model can be improved without greatly affecting the accuracy of the results. In the ABAQUS/Standard software, the viscosity parameter is typically set to zero as the default, which means that no viscoelastic regularization is applied automatically. To improve convergence and stability, it is necessary to assign a non-zero value for the viscosity parameter, usually a small one; a value of  $\eta=0.00023-0.00055$  was selected to aid in convergence and guarantee the reliability of the results. The (CDP) model stands out for its clear physical interpretations of parameters, giving it a definite edge. The ABAQUS manual details the functions of these parameters and the mathematical methods for defining stress boundaries in three-dimensional space. The model also calculates concrete performance under uniaxial stress, with default parameters shown in Table (3-2) for ABAQUS program users to assess its performance under compound stress.

**Table (3-2):** Default parameter of CDP model under compound stress.

Parameter	Default Value	Used in Present Study
<b>Eccentricity</b>	<b>0.1</b>	<b>0.1</b>
<b>Dilation angle</b>	<b>36</b>	<b>31-45</b>
$\frac{fb_0}{fc_0}$	<b>1.16</b>	<b>1.16</b>
$K_c$	<b>0.667</b>	<b>0.667</b>
<b>Viscosity Parameter</b>	<b>0</b>	<b>0.0002-0.00065</b>

## B) Concrete Compressive Behavior

When concrete is under pressure from being squeezed in one direction, it goes through different stages of reaction. First, it bends without permanently changing shape, then it starts to bend more and more easily until it reaches a limit. After that, it starts to act in a way that isn't perfectly predictable, with the resistance increasing quickly as it gets squeezed more. Once it reaches its maximum ability to resist being squished, it starts to show signs of damage like small cracks. If the pressure keeps increasing, the concrete will eventually break apart completely, which can look like it's being crushed, breaking into pieces, or splitting apart.

After a failure occurs, the material might start to soften after reaching its peak, leading to a quick drop in strength because of cracks spreading and the release of elastic energy. It is essential to comprehend these stages to guarantee the longevity and safety of concrete buildings when subjected to different types of loads. The conversion of uniaxial stress-strain curves to stress against plastic strain curves is assumed. (This conversion is performed automatically by ABAQUS from the user-provided stress versus “inelastic” strain data, as explained below.) So,

$$\sigma_c = \sigma_c(\tilde{\epsilon}_c^{pl}, \dot{\tilde{\epsilon}}_c^{pl}, \theta, f_i) \quad (3.1)$$

As depicted in Figure (3.11), whenever the concrete specimen is unloaded from any point on the curve of strain softening, there is a reduction in its reaction when remaining under stress. This suggests that even though unloading is done, still elastic properties have partly been lost or decreased. The decrease in elastic strength depends on two parameters  $d_c$  which are believed to depend upon plastic strains, temperature, as well as other environmental factors:

$$d_c = d_c(\tilde{\epsilon}_c^{pl}, \theta, f_i); \quad 0 \leq d_c \leq 1 \quad (3.2)$$

If  $E_0$  represents the initial (undamaged) elastic stiffness of the material, the stress-strain relationship under uniaxial compression loading can be expressed as:

$$\sigma_c = (1 - d_c)E_0(\varepsilon_c - \tilde{\varepsilon}_c^{pl}) \quad (3.3)$$

It's defined the “effective” compressive cohesion stresses as:

$$\bar{\sigma}_c = \frac{\sigma_c}{(1 - d_c)} = E_0(\varepsilon_c - \tilde{\varepsilon}_c^{pl}) \quad (3.4)$$

The effective cohesion stresses determine the size of the yield (or failure) surface [75].

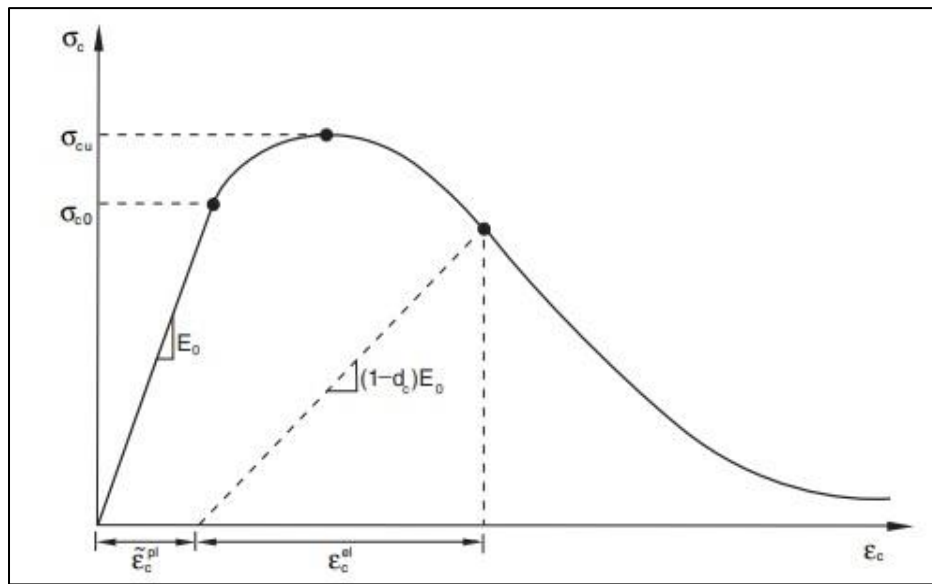


**Figure 3.11:** Response of concrete to uniaxial loading in compression [75].

And used to describe both tensile and compressive response. Writing the Saenz relation in terms of equivalent uniaxial strain (Elwi and Murray, 1979) yields as shown in in Table (3-3) for compressive strength of concrete (23.5 MPa) , Table (3-4) for compressive strength (30 MPa) and Table (3-5) for compressive strength (37.5 MPa).

**Table (3-3):** Concrete compressive behavior for 23.5 MPa

Yield stress (MPa)	Inelastic strain
7.731917764	0
13.32711463	0.000255157
17.43222093	0.000509742
20.31181232	0.000815494
22.17673224	0.001160577
23.21735256	0.001549577
23.53	0.001967921
23.37240335	0.002304833
22.9322917	0.002660137
22.27904039	0.003022791
21.47959747	0.003387856
20.55939882	0.003764218
19.58119093	0.004141124
12.66731646	0.006919383
8.096980003	0.009639848
5.461811629	0.012260433
3.896412156	0.014804094
2.886751573	0.017368381
2.220021489	0.019902625

**Table (3-4):** Concrete compressive behavior for 30 MPa

Yield stress (MPa)	Inelastic strain
10.46904244	0
16.91199884	0.000177776
22.0273261	0.000354356
25.76097949	0.000582373
28.21703659	0.000855552
29.58976003	0.001177515
30	0.001534633
29.64632808	0.001927871
28.70276345	0.002350925
27.37705645	0.002786523
25.8451503	0.00322553
24.1812339	0.003676566
22.51047321	0.004125568
13.68193299	0.006943517
8.579330804	0.009661731
5.771370302	0.012275808
4.127789334	0.014814654
3.070968596	0.017375706
2.372074661	0.019907855

**Table (3-5):** Concrete compressive behavior for 37.5 MPa

Yield stress (MPa)	Inelastic strain
13.9222989	0
21.30534706	0.000107431
27.48596485	0.000225132
32.13639864	0.00039402
35.23961427	0.000612707
36.98074215	0.000884656
37.5	0.00119708
36.84753961	0.001632249
35.18253555	0.002110099
32.96350711	0.002604698
30.53217602	0.003101674
28.02317259	0.003608848
25.62131097	0.004109799
15.03413354	0.006952646
9.383005677	0.009668992
6.338315008	0.012279778
4.560814204	0.014816537
3.414091866	0.017376379
2.651829781	0.019907863

### C) Concrete Tensile Behavior

When concrete is stretched in one direction, it goes through a series of changes. At first, it stretches elastically in a straight line, following Hooke's Law, until it reaches the point where it can no longer hold the stress,  $\sigma_0$  which is when tiny cracks start to form within the material. After this, the relationship between stress and strain weakens, showing a decrease in both stiffness and strength as the cracks spread. This weakening response causes localized strain within the concrete and eventually leads to a complete breakdown. Understanding this process (from stretching without damage to the start of cracks and then to weakening) is essential for assessing how well concrete structures can handle being stretched.

Uniaxial stress-strain curves can be transformed into plastic strain curves against stress. (This automatic conversion is performed by ABAQUS, using user-defined stress versus “inelastic” strain data as described below.) Therefore,

$$\sigma_t = \sigma_t(\tilde{\varepsilon}_t^{pl}, \dot{\varepsilon}_t^{pl}, \theta, f_i) \quad (3.5)$$

It is indicated through Figure (3.12) that unloading a concrete specimen with respect to any point upon the stress-strain curves' strain softening branch results in a weakened unloading response; it is as though the material's elastic stiffness were somehow impaired (or diminished). Two damage variables  $d_c$  define this deterioration process of elastic stiffness depending on plastic strains, temperature, and other field variables:

$$d_t = d_t(\tilde{\varepsilon}_t^{pl}, \theta, f_i); \quad 0 \leq d_t \leq 1 \quad (3.6)$$

If  $E_0$  represents the initial (undamaged) elastic stiffness of the material, the stress-strain relationship under uniaxial compression loading can be expressed as:

$$\sigma_t = (1 - d_t)E_0(\varepsilon_t - \tilde{\varepsilon}_t^{pl}) \quad (3.7)$$

It's defined the "effective" compressive cohesion stresses as:

$$\bar{\sigma}_t = \frac{\sigma_t}{(1 - d_t)} = E_0(\varepsilon_t - \tilde{\varepsilon}_t^{pl}) \quad (3.8)$$

The effective cohesion stresses determine the size of the yield (or failure) surface [75].

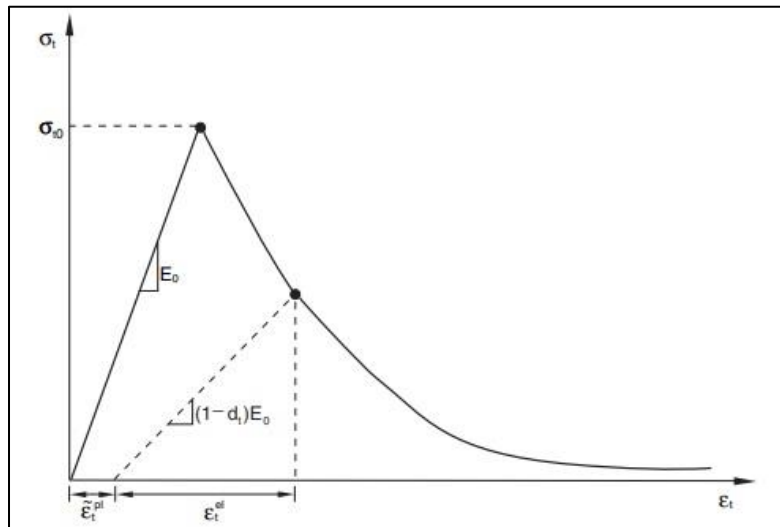


**Figure 3.12:** Response of concrete to uniaxial loading in tension [75].



And to describe tensile behavior used The Hordijk's model (Hordijk 1991) as shown in Table (3-5).

**Table (3-6):** Concrete tensile behavior displacement type

Yield stress (MPa)	Displacement
0.8	0
0.65759257	0.066
0.482602261	0.173
0.423992592	0.22
0.33792481	0.308
0.305810165	0.35
0.279619784	0.39
0.257107662	0.43
0.233328396	0.48

Concrete properties of elastic and concrete damage plasticity (CDP) parameters and for compressive and tension behavior can be entered into the ABAQUS to simulate concrete behavior as shown in the figures (3.13, 3.14, 3.15 and 3.16 ).

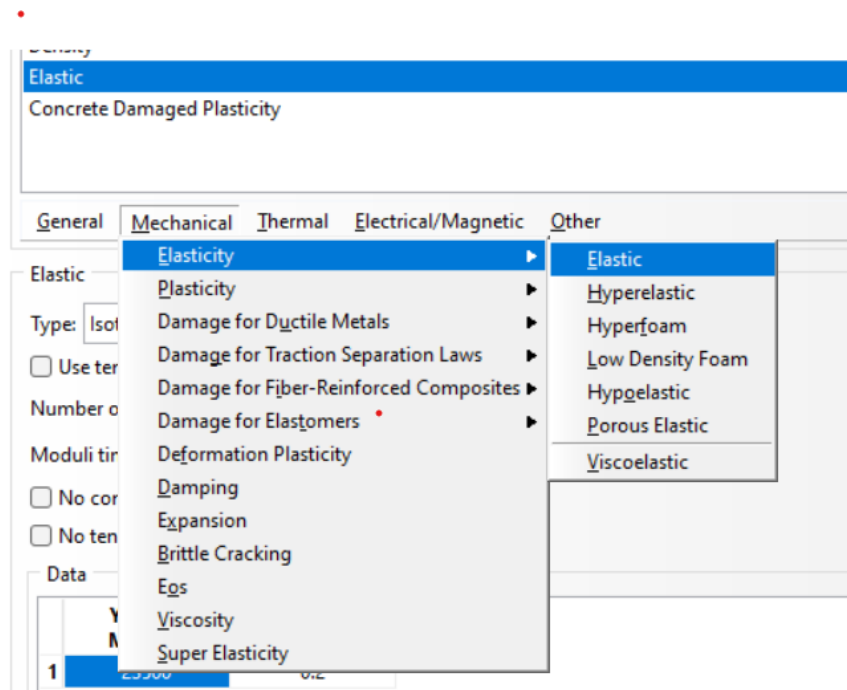


**Figure 3.13:** Definition of elastic properties in Abaqus software.

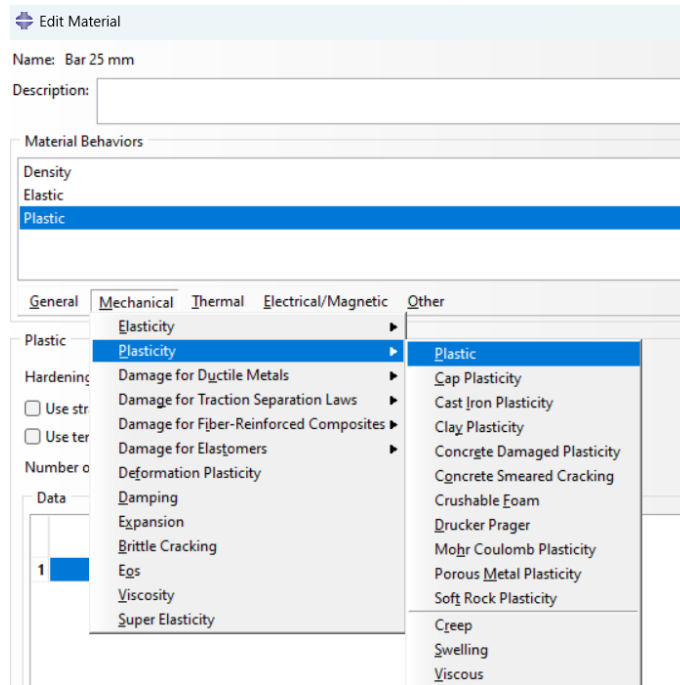


Figure 3.14: Definition of elastic properties in Abaqus software.

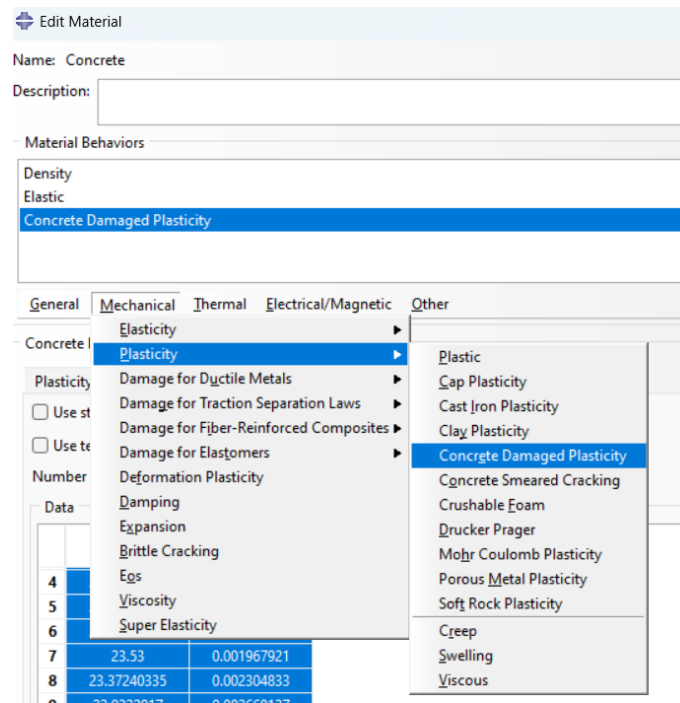
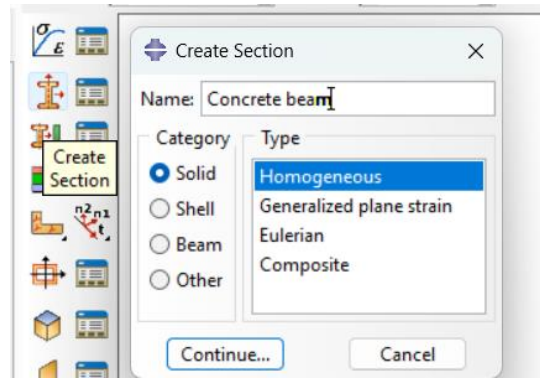


Figure 3.15: Selection of the CDP model to define the plastic properties of concrete.



**Figure 3.16:** Homogeneous distribution of concrete properties.

## 2-Steel Properties

When running simulations in ABAQUS, it is crucial to accurately input steel properties to predict how steel structures will respond to different types of stress. These properties include the elastic modulus, which dictates how stiff the material is, and the yield strength, which shows when the material starts to deform plastically. The ultimate tensile strength shows the maximum stress the steel can handle before breaking, while the yield stress ratio reveals how the material behaves under tension versus compression. Steel also undergoes strain hardening in the plastic zone, with the plastic strain hardening modulus playing a key role. Ductility indicates how much a material can deform before breaking, measuring its ability to withstand plastic deformation.

In predicting how steel will respond to changes in temperature, it is important to consider its thermal properties, such as thermal expansion coefficient and conductivity. These properties are determined through material testing and specifications and are essential for accurately simulating the behavior of steel in ABAQUS. By incorporating these inputs, engineers can ensure the reliability and effectiveness of steel structures in various engineering scenarios as shown in Figures ( 3.14, 3.15 and 3.16 ).

## I. Elastic Property of Steel

In ABAQUS, the elastic properties of steel are essential for accurately modeling its mechanical behavior in finite element analysis (FEA). These properties describe how steel deforms elastically under applied loads and are crucial for predicting the response of steel structures and components. The primary elastic properties of steel typically defined in ABAQUS include:

These elastic properties are fundamental inputs for defining the material behavior of steel in ABAQUS simulations. They are often derived from material testing data or specified based on standard material properties for common steel grades as shown in Table (3-7).

**Table (3-7):** Elastic material properties for Steel

Material	Type	Density (ton/mm <sup>3</sup> )	Youngs Modulus (MPa)	Poisson's Ratio	Position
Ø6 rebar	Isotropic	7800	200000	0.3	diagonal reinforcement and stirrups
Ø10 rebar	Isotropic	7800	200000	0.3	longitudinal reinforcement for top
Ø25 rebar	Isotropic	7800	200000	0.3	longitudinal reinforcement for bottom
steel box	Isotropic	7800	210000	Isotropic	longitudinal incased beam

## II. Plastic Property of Steel

In ABAQUS simulations, accurately representing the plastic behavior of steel is crucial for predicting how structures deform under mechanical loads. Important plastic properties include the yield strength, which indicates when plastic deformation begins, and the plastic strain hardening modulus, which shows how steel hardens as it deforms. Other parameters like strain at failure and ductility are

also important for understanding how steel deforms before failing. These properties are essential for accurate nonlinear analyses in ABAQUS, allowing engineers to simulate the behavior of steel structures in different conditions as shown in Figure (3.17) and Table (3-8).

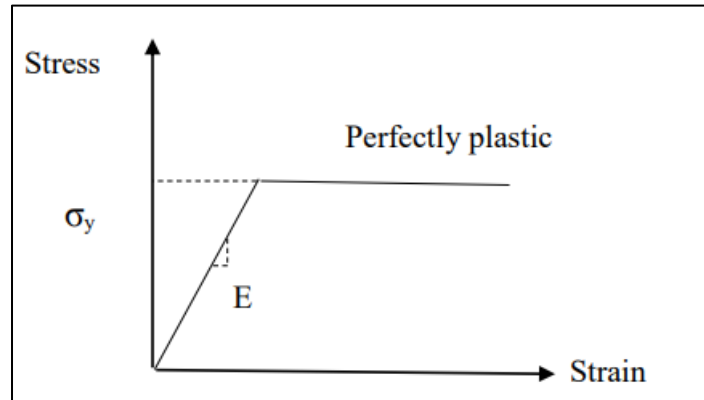


**Figure 3.17:** Perfectly plastic behavior [77].

**Table (3-8):** Plastic material properties for Steel

Material	Yield stress (MPa)	Plastic strain
Ø6 rebar	379	0
Ø10 rebar	416	0
Ø25 rebar	585	0
steel box	280	0

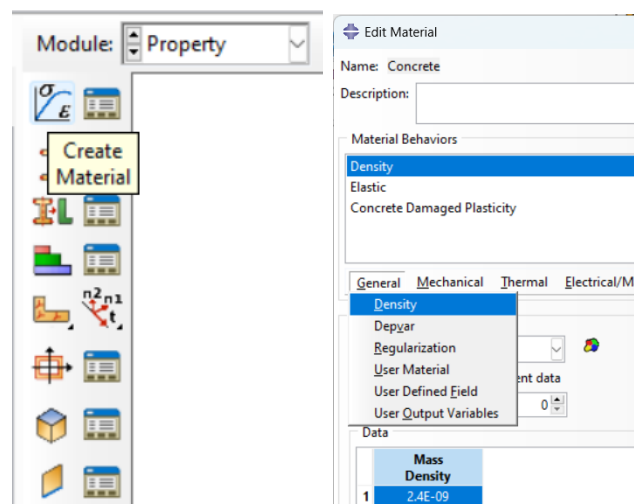


**Figure 3.18:** Material properties definition menu in Abaqus software.

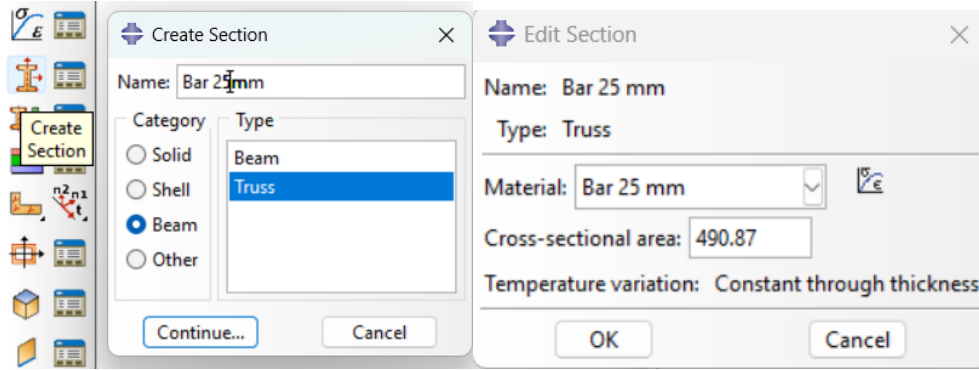


**Figure 3.19:** Determining the distribution of material properties for reinforcements in the form of trusses.

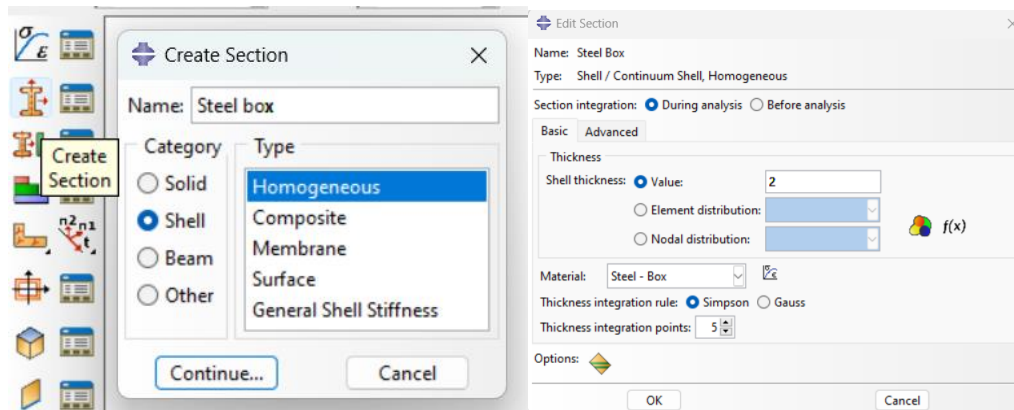


**Figure 3.20:** Homogeneous distribution of concrete properties.

### 3.3.1.3 Assembly of Modeling

When working in ABAQUS, assembling models requires putting together different parts to create complex structures. To start, parts need to be formed, which can be achieved using ABAQUS's tools or by importing designs from CAD software. Each part embodies a specific element of the assembly and may vary in materials, characteristics, and shapes as shown in the figure 3.9. After creating the part geometries, they are then arranged and adjusted in relation to one another to create the final assembly. ABAQUS offers a range of tools and capabilities to simplify this assembly process, enabling users to accurately specify connections,

interfaces, and interactions between the parts. These can involve constraints such as contact, coupling, or tie constraints to simulate the interactions between the parts.

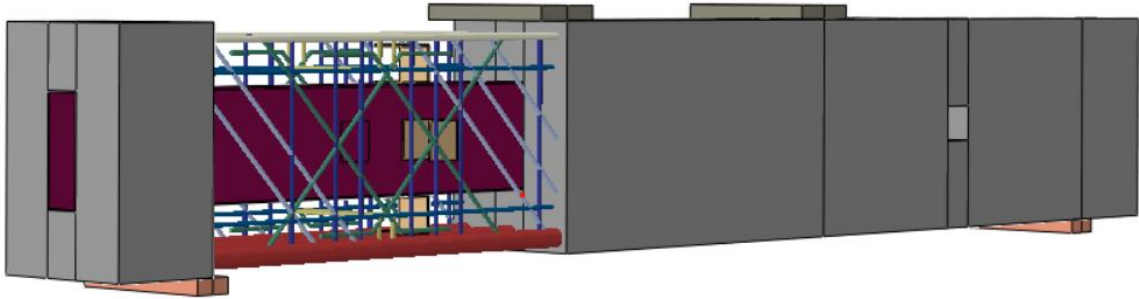


**Figure 3.21:** Assembly of modeling parts.

### 3.3.1.4 Meshing of Modeling

Meshing in ABAQUS is a key step in finite element analysis (FEA) that is essential for accurately representing complex geometries and predicting structural behavior under different loads. The mesh generation process then takes place, offering automatic, manual, and controlled meshing options to divide the geometry into finite elements. Quality checks are important after mesh generation to ensure that elements meet specific criteria for accuracy and reliability. Mesh refinement may be needed for complex models to improve solution accuracy. ABAQUS also offers visualization tools for users to examine and assess mesh quality and distribution.

For engineers to achieve accurate and reliable analysis results for their designs, it is crucial that they have a deep understanding and effectively use meshing techniques.

#### I. Shell Elements

Shell components have a thickness that is far less than both their length and width. Thin or thick shell FE analysis can be performed on shell structures. Classical Kirchhoff theory describes thin shells while Reissner-Mindlin theory regulates kinematics of thick shells.

As of now, for the purpose of modelling, the preferred type of element to use is a thick one for the RC beam. This is because it is approximated by employing a shell model and using a non-zero thickness. By doing so, it can represent physical attributes of the beam more accurately. The chosen section is homogeneous along the length of the beam and described in terms of shell thickness, Poisson's ratio, layers of rebar, and material models for steel and concrete. The thicknesses of these elements are variable according to Poisson's ratio  $\nu$  that have been established, and thus also changeable according to finite element analysis results. The conventional shell model can be constructed using either triangular or quadrilateral elements, but quadrilateral shell elements are preferred because they better reflect bending behavior. Figure 3.22 shows an example of the selected elements for the shell model. Moreover, there are two kinds of interpolation functions that can be utilized in shell elements: linear and quadratic, resulting in S4 and S8 elements, respectively, having four and eight nodes. These analyses make use of the quadratic elements because, in essence, the RC beam is mainly subject to bending. Such behavior can be better portrayed using the quadratic element thereby making them yield more precise results than the linear ones.

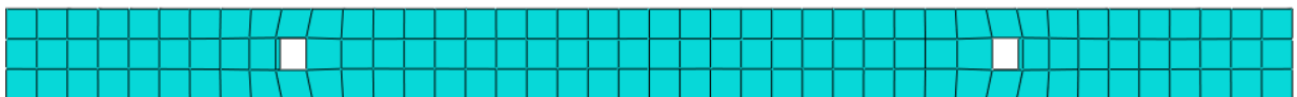
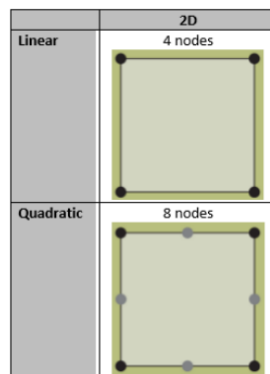


**Figure 3.22:** Illustration of chosen elements for the shell [78].



## II. Solid Elements

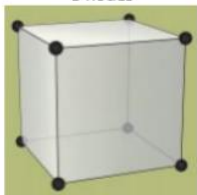
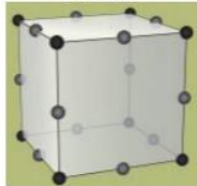
It seems like you're talking about choosing solid elements for building a 3D finite elements (FE) model, particularly with ABAQUS/CAE. Solid elements like C3D8 and C3D20 are often selected because they are cost-effective when modeling intricate structures.

When choosing between linear (C3D8) and quadratic (C3D20) interpolation functions, it all comes down to what you need for your analysis. Linear interpolation elements are easier to work with and faster to compute, but they may struggle to accurately represent more complex deformations or strain fields. This could be a problem, especially when dealing with coarse mesh or intricate deformation patterns.

Quadratic interpolation elements (C3D20) provide more accurate results, especially in capturing linear strain fields, and are highly useful for bending-related issues. Nonetheless, they require more computational resources because of their added complexity.

When choosing between these options, it's important to think about the trade-off between speed and precision. Linear interpolation elements might be enough for basic calculations or when resources are scarce. But for intricate problems requiring high accuracy, quadratic interpolation elements could be needed even though they require more computational power.

Furthermore, techniques for refining meshes can address certain restrictions of using linear interpolation elements by enhancing the accuracy of the model's geometry representation. Nonetheless, this method also leads to higher computational costs. It is crucial to find a suitable equilibrium that considers the needs and limitations of the analysis as shown in Figure 3.23.

3D	
Linear	8 nodes 
Quadratic	20 nodes 

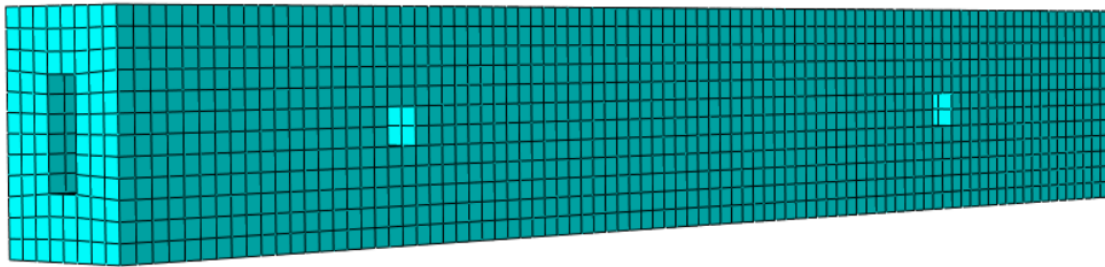


**Figure 3.23:** Illustration of chosen elements for the solid model [78].

When dealing with bending issues, first-order iso-parametric elements tend to face shear locking too. They cannot give an appropriate solution for bending because the linear interpolation function doesn't show it well, in this way making them stiff. Using reduced integration, however, helps to avoid such problems, though it enables fake singular modes. In contrast, second order iso-parametric elements are free from shear locking, as has already been indicated their linear strain field can accurately depict thin finite-element buildings being bent in any manner around a point. The distinction between what is represented by linearity and parabolic forms is exemplified in Fig. (3.24)[78].

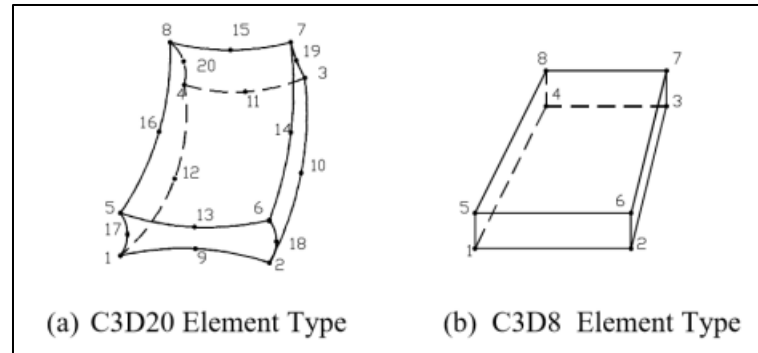


**Figure 3.24:** Illustration of first- and second-order interpolation function of solid elements [78].

### III. Truss Elements

In a 3D finite element (FE) model of reinforced concrete (RC) structures, solid elements are commonly used to represent the concrete areas. Truss elements are also included to simulate the presence of reinforcing bars (rebars). Truss elements are one-dimensional (1D) and can be oriented in any direction in 3D space. Each truss element has one node at each end and can only transmit axial forces. These elements have three translational degrees of freedom (DOF) per node (usually referred to as  $D_x$ ,  $D_y$ , and  $D_z$ ), which represent movement along the  $x$ ,  $y$ , and  $z$  axes, respectively. See Figure 3.25 for a visual representation.

Truss elements in structural modeling are given a cross-sectional area equal to the reinforcing bar they represent, and steel material characteristics are assigned to them based on the properties of the reinforcing steel. In applications involving reinforced concrete, truss elements are often employed to incorporate reinforcement bars into the concrete model. Their performance relies heavily on how the surrounding concrete behaves, as they transfer forces within the concrete structure. This method ensures an accurate depiction of the bond between concrete and reinforcing steel in structural assessments [78].

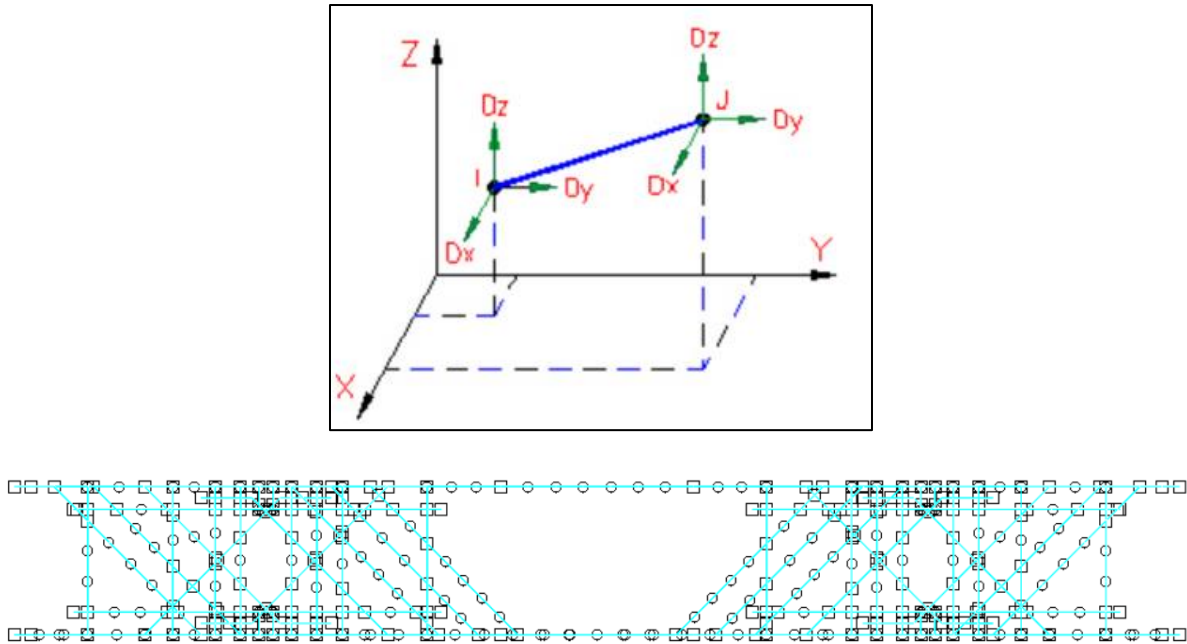


**Figure 3.25:** Example of truss element randomly oriented in a 3D space [78].

The meshes used for the concrete part are 8-node linear brick of C3D8R type, which is a three-dimensional 8-node mesh with a grain size of 2.5 cm as shown in the Figure 3.26, 4-node of S4R type for steel box mesh with a grain size of 2.5 cm according to Figure 3.27 and the meshes used for the reinforcements are truss mesh with a grain size of 5 cm and 2-node linear truss of T3D2 type as shown in Figure 3.28 and 3.29.

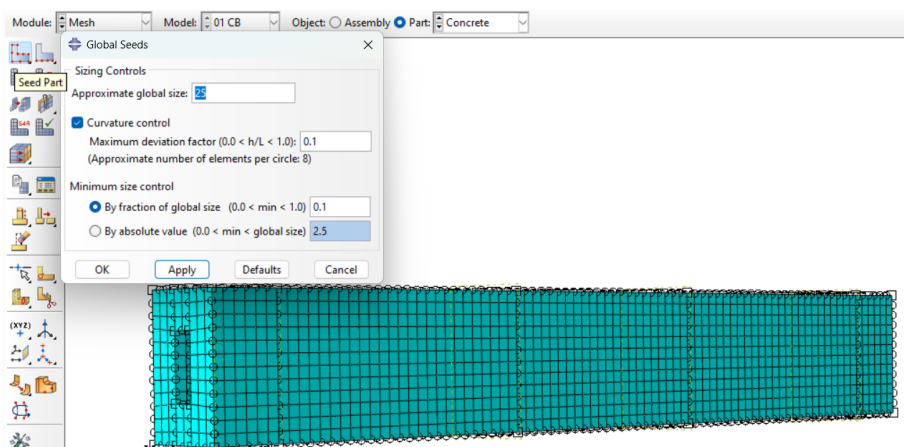


**Figure 3.26:** Meshing of the concrete section.

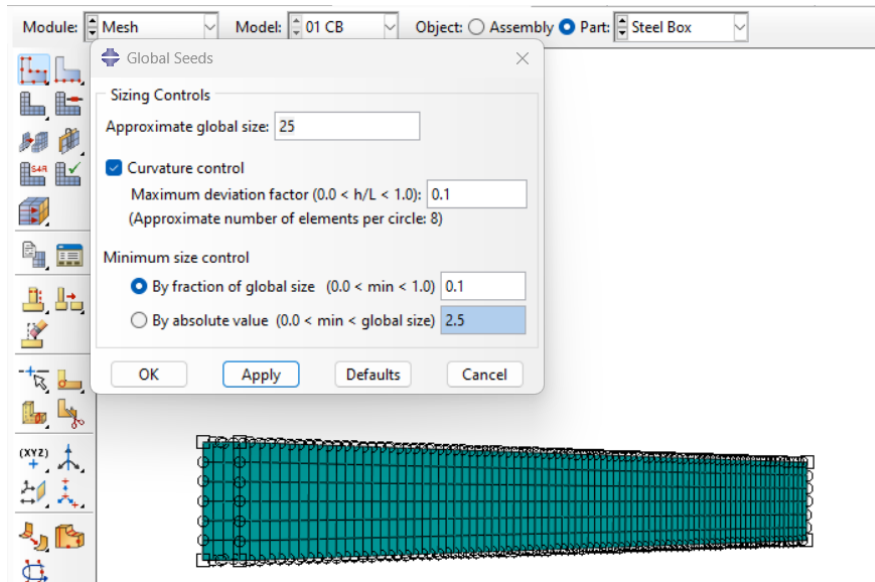


Figure 3.27: Meshing of the steel box section.

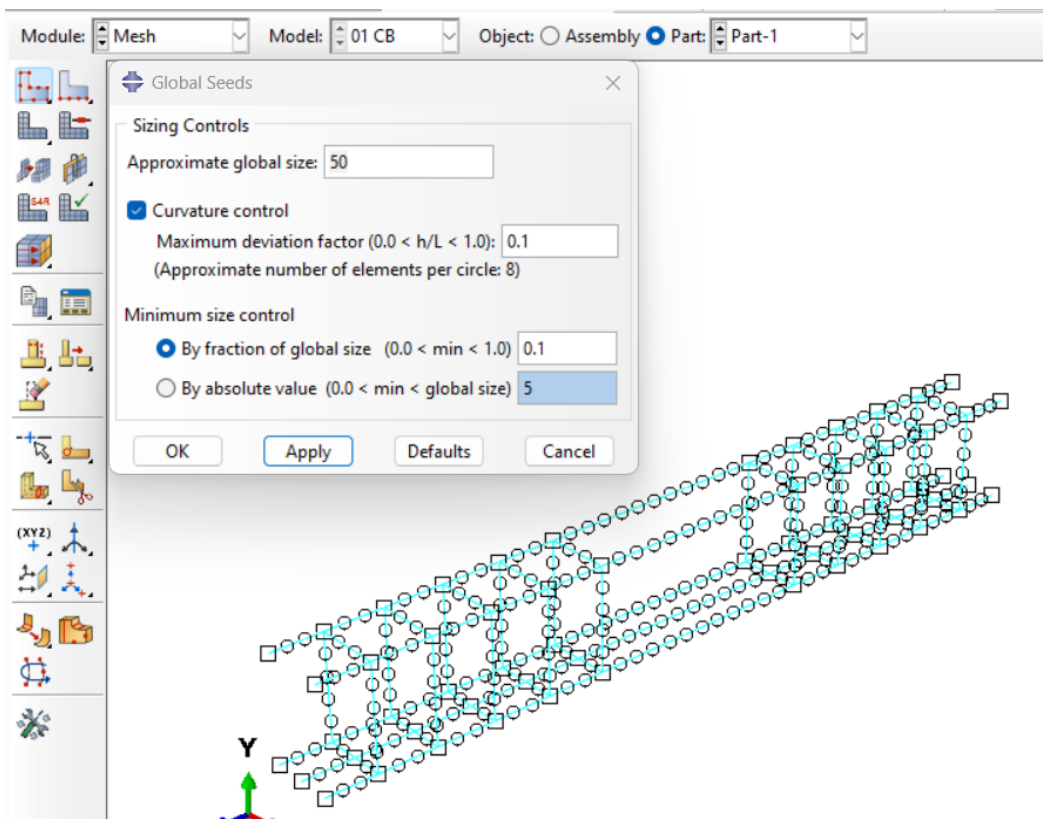
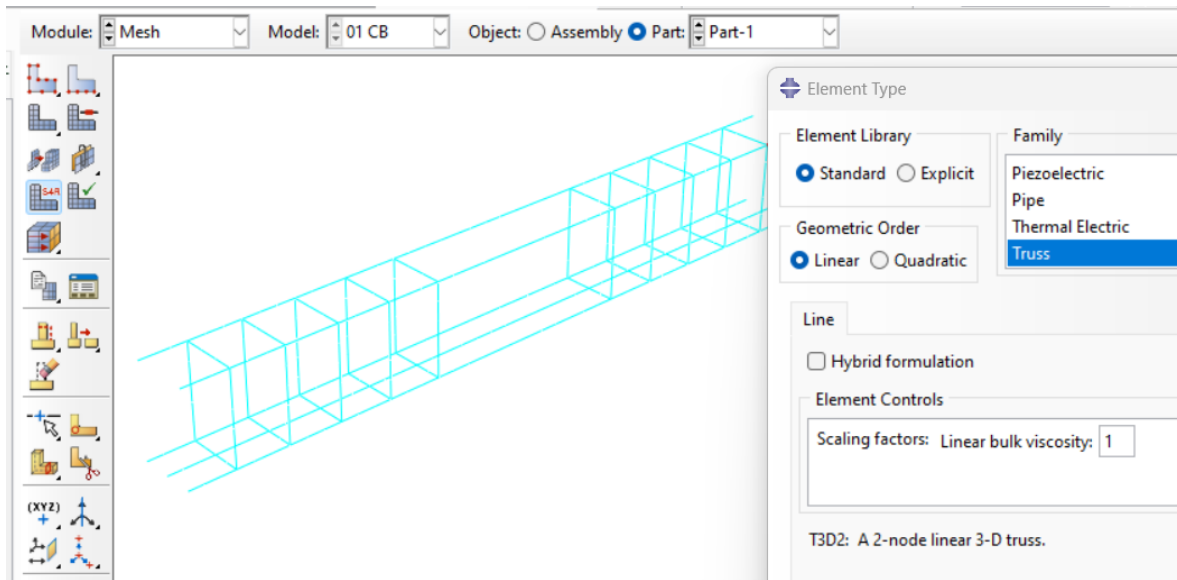


Figure 3.28: Meshing of the rebar reinforcement section.



**Figure 3.29:** Type of meshing in the rebar reinforcement section.

### 3.3.2 Boundary and Constraint Conditions

When ABAQUS is used for finite element analysis, it is important to consider boundary and constraint conditions that affect how structures behave in different environments. Boundary conditions specify how loads or displacements are applied to model surfaces, reflecting actual loading situations. Constraints, on the other hand, limit the movement of nodes or elements within the structure. These conditions are set up using the ABAQUS/CAE interface, where users can select specific regions and define the necessary conditions for an accurate simulation setup and reliable analysis results.

#### 3.3.2.1 Boundary Conditions

Boundary conditions in ABAQUS are crucial specifications that determine how a finite element model interacts with its external environment. They include directives like forces, displacements, velocities, temperatures, or other physical quantities applied to the model's boundaries or surfaces. Engineers use these

conditions to simulate real-world loading scenarios, such as structural loads or environmental effects, to accurately represent the system being analyzed. These boundary conditions are essential in predicting the model's behavior and obtaining valuable insights into structural, thermal, or fluid dynamics within ABAQUS simulations. The loading and boundary conditions used in this research are presented in this section. The two lower parts are completely bound according to Figure 3.30, and the load is applied to the upper two parts of the model according to Figures 3.31 and 3.32.

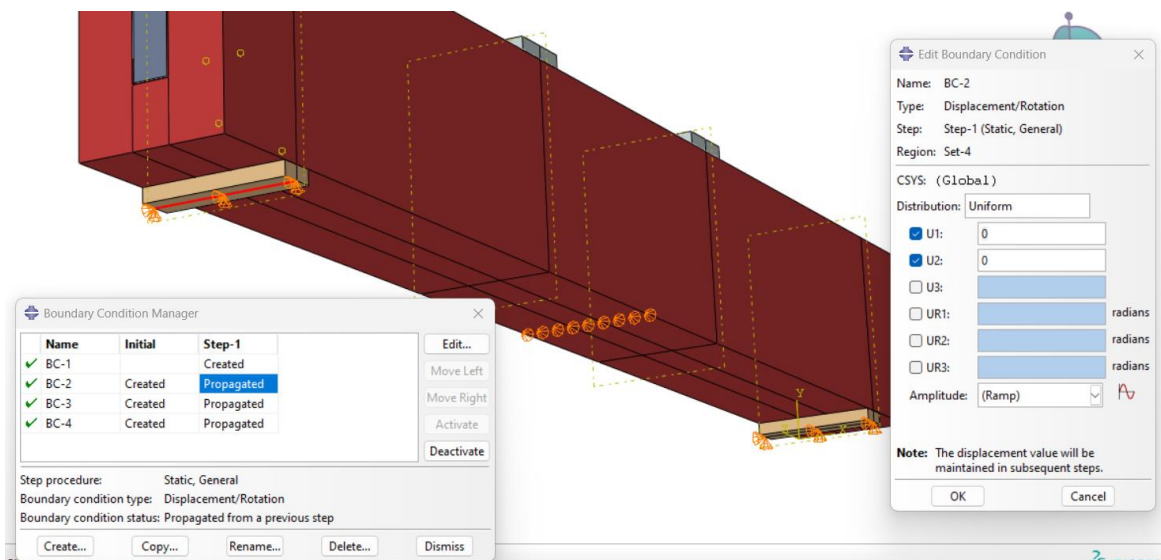


**Figure 3.30:** Boundary conditions of the lower parts of the model.

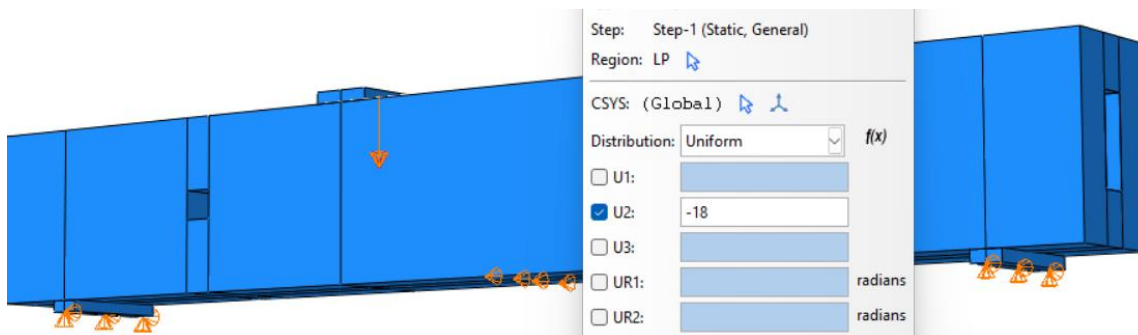


**Figure 3.31:** Boundary conditions of model.

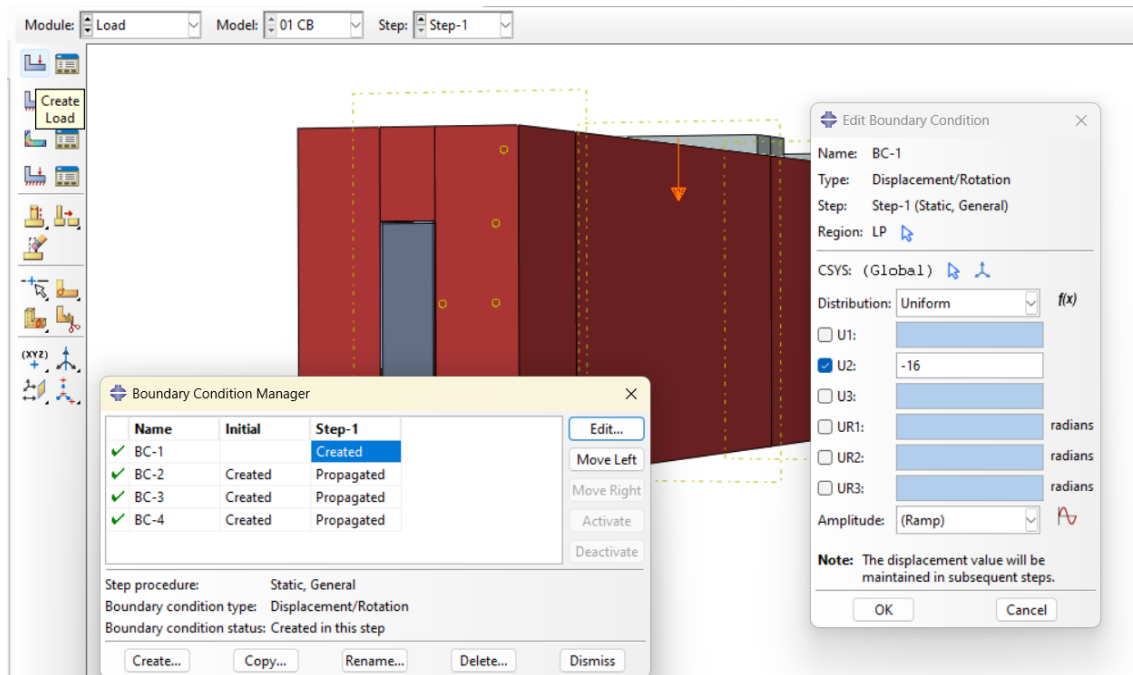


**Figure 3.32:** Load applied to the upper part of the model.

### 3.3.2.2 Constraint and Interaction Conditions

When using ABAQUS, constraints and interactions play essential roles in controlling the behavior and connections in finite element models. Constraints limit the movement of nodes or elements, either by fixing specific areas or by linking components together. These constraints are vital for accurately depicting real-world limitations, like fixed supports or connected interfaces, which help maintain the stability and integrity of the analysis. On the other hand, interaction conditions simulate how different sections of the structure interact with each other or with the environment.

Contact interactions in ABAQUS allow engineers to mimic friction, separation, or adherence between surfaces, as well as enforce tie constraints to ensure displacements between connected regions are compatible. By specifying constraint and interaction conditions, engineers can accurately model complex behaviors and



phenomena, facilitating realistic simulations of mechanical, thermal, or multi-physics systems as shown in Figures ( 3.33, 3.34, 3.35 and 3.36 ).

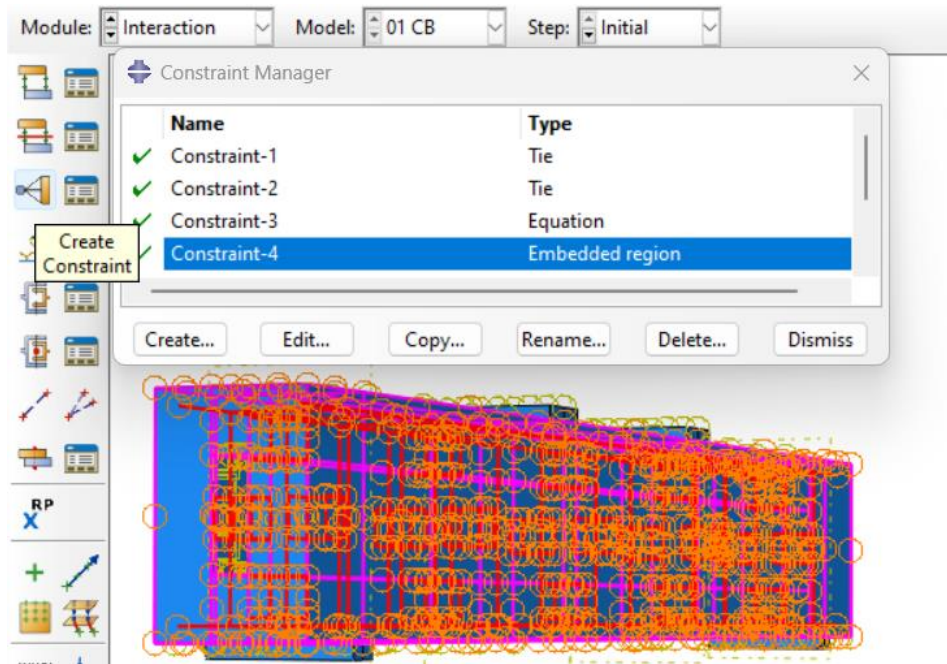


**Figure 3.33:** Using the Embedded Region constraint between rebars and concrete.

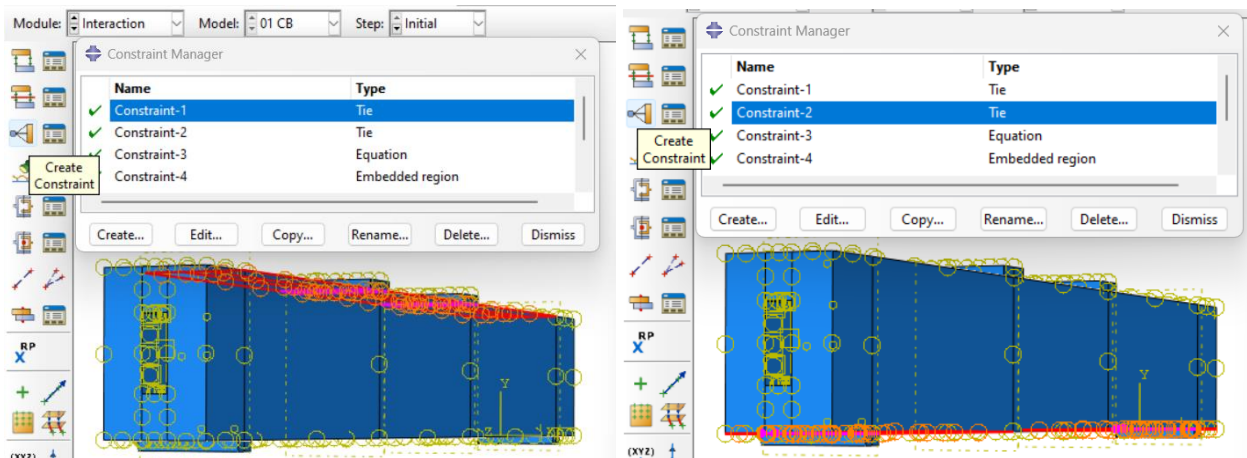


**Figure 3.34:** Using the Tie constraint between upper surface of concrete and load plates, and between bottom surface and support plats.

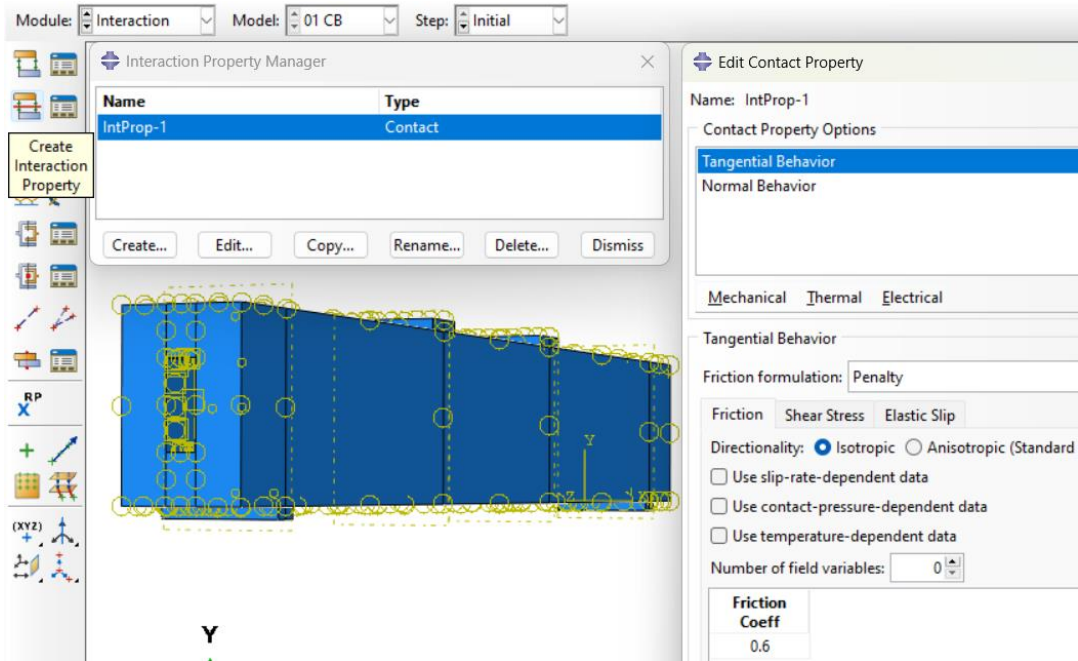


**Figure 3.35:** Input of contact properties interaction between inside surface of concrete and steel box.

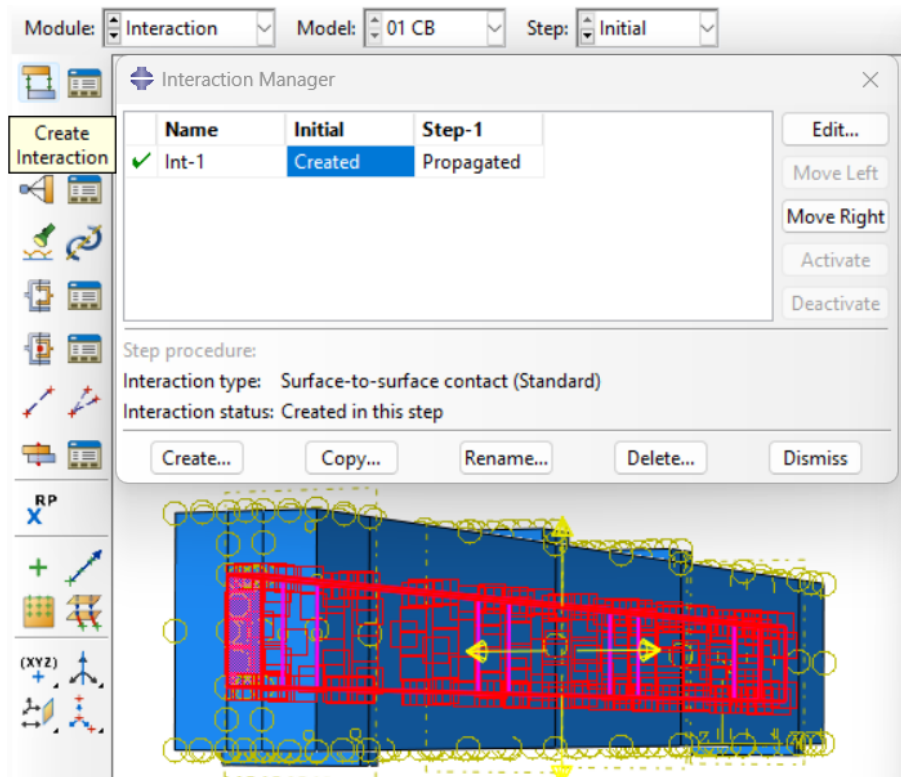


**Figure 3.36:** Using the contact interaction between inside surface of concrete and steel box.

### 3.3.3 Output Analysis

When using ABAQUS, analyzing output involves looking at and making sense of the results from finite element simulations. This includes visualizing the data, finding details like displacements and stresses, and processing the information to draw useful conclusions. Comparing the results to real-world data or theoretical solutions helps ensure they are accurate, and sensitivity analysis shows how the system reacts to changes in parameters. The goal of output analysis in ABAQUS is to gain insights into the behavior of complex systems, which in turn guides decisions and improvements in engineering.

#### 3.3.3.1 Step Field

In ABAQUS, a step represents a unique phase or stage in a finite element analysis. Each step corresponds to a particular loading condition, boundary condition, or material behavior that is applied to the model during the simulation. Steps are defined in order and can involve different actions like applying loads, displacements, temperature changes, or modifying material properties.

Usually, a simulation consists of several stages, each depicting a specific aspect of structural response or material performance. For instance, in a structural examination, the stages could involve an initial phase for setting boundary conditions, followed by subsequent phases where forces or displacements are gradually applied. Similarly, in a material simulation, the stages could indicate various levels of material deformation, like elastic loading, plastic deformation, and eventual failure. The Step module in ABAQUS offers tools for defining, managing, and analyzing each step of the simulation process. Users can choose the type of analysis, set boundary conditions, specify loadings, and adjust other parameters for each step. This organization allows for accurate simulation of complex behaviors

and loading conditions, leading to a thorough understanding of the system's response.

The type of solution is considered statically and considering large deformations as shown in Figure 3.21.

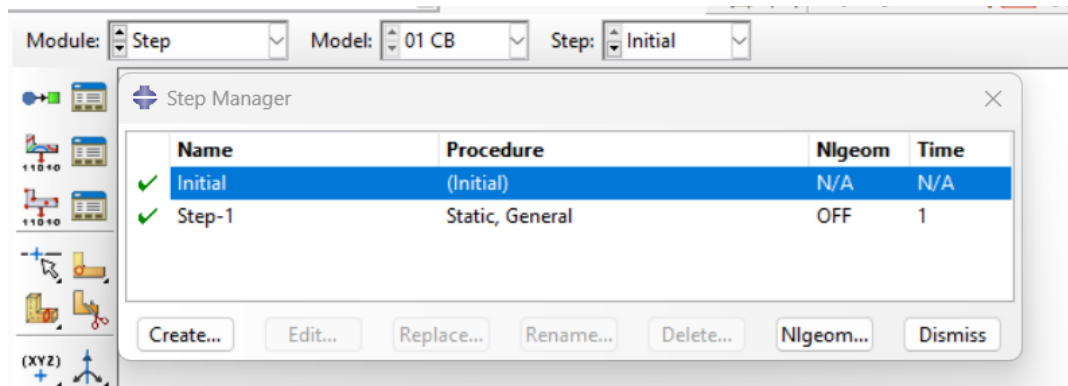


**Figure 3.37:** Determine the solution type static.

### 3.3.3.2 Output Field and History

The output field and history are connected parts of the finite element analysis process, important for extracting and analyzing simulation results over time or specific intervals. The Output field includes tools for visualizing, extracting, and processing data produced during simulations. Users can view different quantities like deformations, stresses, strains, and displacements, understanding the simulated system's behavior. With post-processing methods, users can find more quantities or examine specific parts of the simulation results.

History in the simulation context refers to the changing values of certain parameters over time. For instance, users may want to monitor how stress or displacement changes at nodes or elements throughout the simulation. ABAQUS offers features to specify and keep track of such historical data, enabling users to gather information at set intervals or specific time points. By merging the output field with historical data, users can efficiently study the evolution of different parameters throughout the

simulation duration. This allows for a deeper understanding of temporary behaviors, dynamic reactions, and the development of deformation and stress patterns. Moreover, historical results help in comparing with real data or analytical forecasts, which assist in confirming and checking simulation outcomes. In general, the output section and historical results within ABAQUS are essential for examining and understanding finite element simulations, allowing users to obtain important insights, and understanding the behavior of complicated systems being studied.

### 3.3.3.3 Job Field

The job field encompasses the management and execution of finite element analysis tasks. It serves as the framework for setting up, submitting, monitoring, and post-processing simulation jobs. Key functionalities of the job field include:

1. **Model Setup:** Users define the geometry, material properties, boundary conditions, loads, and other parameters necessary for the simulation within the job environment. This involves creating or importing the finite element model and specifying the analysis type (e.g., static, dynamic, thermal, etc.).
2. **Job Submission:** Once the model setup is complete, users submit the job for analysis. ABAQUS then performs the calculations based on the specified parameters and settings. Users can submit multiple jobs simultaneously for efficient use of computational resources.
3. **Job Monitoring:** During the analysis, users can monitor the progress of the job, including its status, computational progress, and any potential errors or warnings. This allows users to intervene if necessary and ensures the successful completion of the simulation.
4. **Results Post-Processing:** After the job has finished running, users can access and analyze the simulation results within the job environment. This involves

visualizing the results, extracting relevant data, and performing further analysis or interpretation as needed.

5. **Job Management:** The job field also includes features for managing simulation jobs, such as organizing them into projects or folders, renaming, copying, deleting, or archiving completed jobs for future reference.

### 3.3.4 Results Post Processing

Results post-processing involves two main aspects: results analysis and visualization through figures and tables.

1. **Results Analysis:** This aspect entails examining and interpreting the simulation outcomes to gain insights into the behavior of the analyzed system. It involves extracting relevant data from the simulation results, such as displacements, stresses, strains, reaction forces, etc. Users can analyze this data to understand the performance and response of the structure or material under various loading conditions. Analysis may include calculating derived quantities, comparing results against design criteria or standards, identifying critical areas or failure modes, and drawing conclusions about the system's behavior.
2. **Figures and Tables:** ABAQUS provides tools for visualizing simulation results through figures and tables. Figures can display graphical representations of data, such as contour plots, stress-strain curves, displacement plots, and mode shapes. These visualizations help users to intuitively understand the distribution and variation of different quantities across the model. Tables present numerical data in a structured format, allowing for detailed analysis and comparison.

## **CHAPTER FOUR: RESULTS AND DISCUSSIONS**

### **4.1 Introduction**

This chapter compares numerical simulations with test data on composite box steel-concrete beams having transverse openings. Understanding the correct working of such beams requires that you study the load-deflection curves as well as crack patterns.

Additionally, the chapter aims to examine into the analysis of various variables that influence the behavior of such beams. This analysis likely involves investigating factors such as material properties, geometry, loading conditions, and construction techniques. The ultimate goals appear to be determining the yield and ultimate loads of the beams and assessing the deflection at the ultimate load point.

It is necessary to provide detailed descriptions about the methodologies utilized in numerical simulations (those carried out with the usage of ABAQUS / Standard 2019) and in experiments to ensure that there is clarity and rigor. Moreover, for the study to be credible, it would be worthwhile to highlight any shortcomings or uncertainties inherent within any of them.

### **4.2 Modeling Verification**

Modeling verification is a crucial step in the development of reliable computational models, ensuring that the numerical model accurately represents the underlying theoretical formulation. In structural engineering, where simulations are often used to predict the behavior of materials and components under various loading conditions, verification ensures that the model is solving the equations correctly, free from numerical errors.

Verification differs from validation in that it does not focus on comparing numerical results with experimental data but rather on confirming the mathematical and algorithmic accuracy of the simulation. This involves testing the model under controlled conditions, such as simplified loading scenarios or analytical benchmarks, where the expected outcomes are known. Any discrepancies between the numerical results and theoretical expectations can then be attributed to issues like mesh sensitivity, time-stepping errors, or incorrect implementation of material models.

In this study, the process of modeling verification will be conducted by examining key factors such as mesh independence, time step convergence, and algorithmic stability. Various model parameters will be systematically adjusted to ensure that the results are robust and independent of numerical artifacts. This verification process is essential to establish confidence in the model before it can be used for more complex simulations or further validation against experimental results. Through rigorous testing and refinement, the verified model can be relied upon for accurate predictions in structural analysis.

### **4.2.1 Modelling Details**

The study developed in this thesis is adopted to the behavior of Strengthening Techniques for Web Opening Shear Span of Composite Encased Steel-Concrete Beams [79]. The specimens were divided into three groups to make comparisons between these specimens in terms of the type of failure, maximum load failure, deflections, and cracks.

#### **4.2.1.1 The First Group**

Consisted of three beams of composite encased steel-concrete, one of them is a solid beam and two others with square transverse web openings that were fabricated in steel section in the shear zone by embedded cork material. To make comparison



between the solid beam (CB), composite encased steel-concrete beam with small (50×50mm) square openings (BW1) at center of shear zone, and encased steel-concrete beam with large (136×136) square openings (BW2) at center of shear zone, as shown in Figure (4.1).

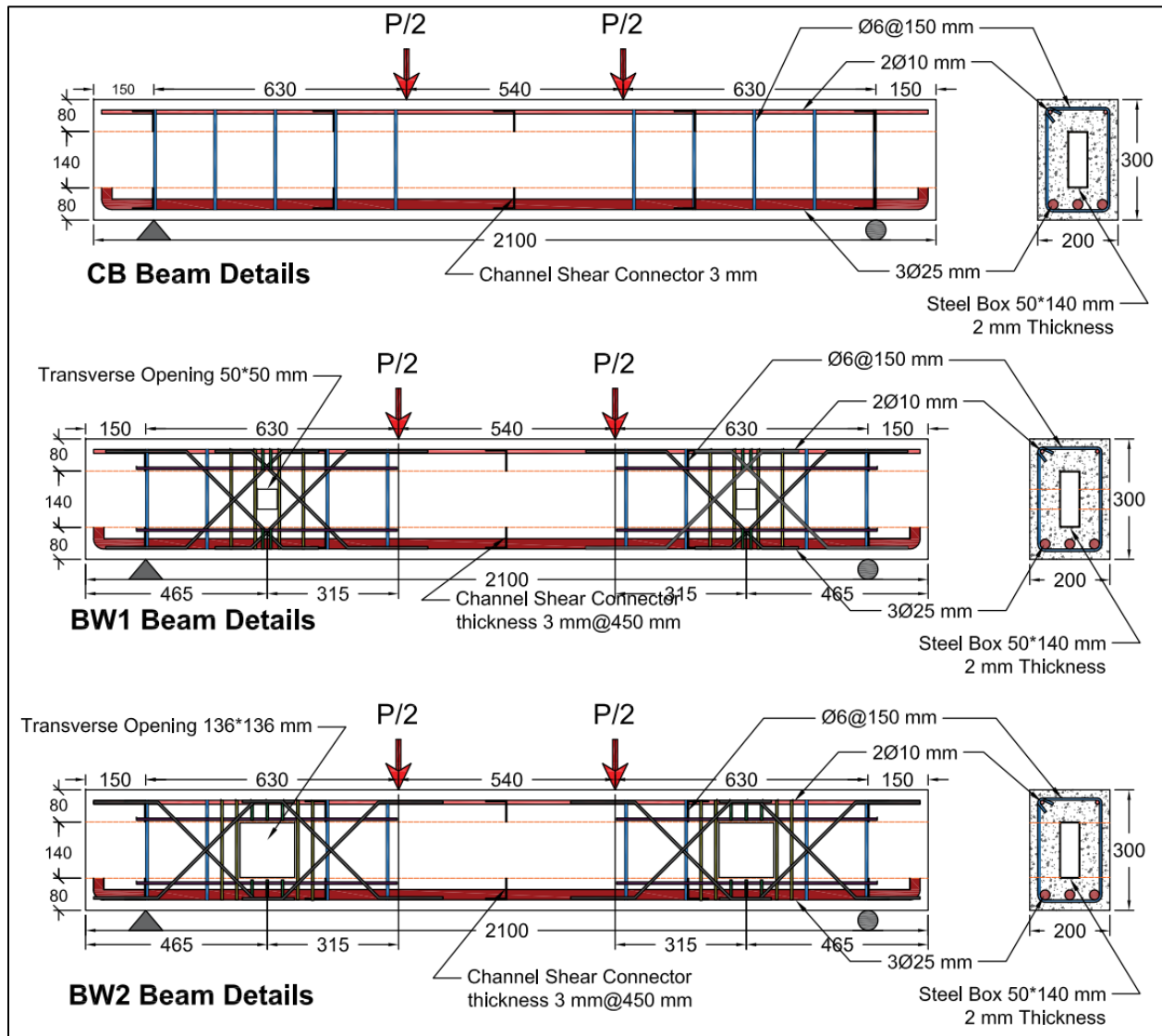
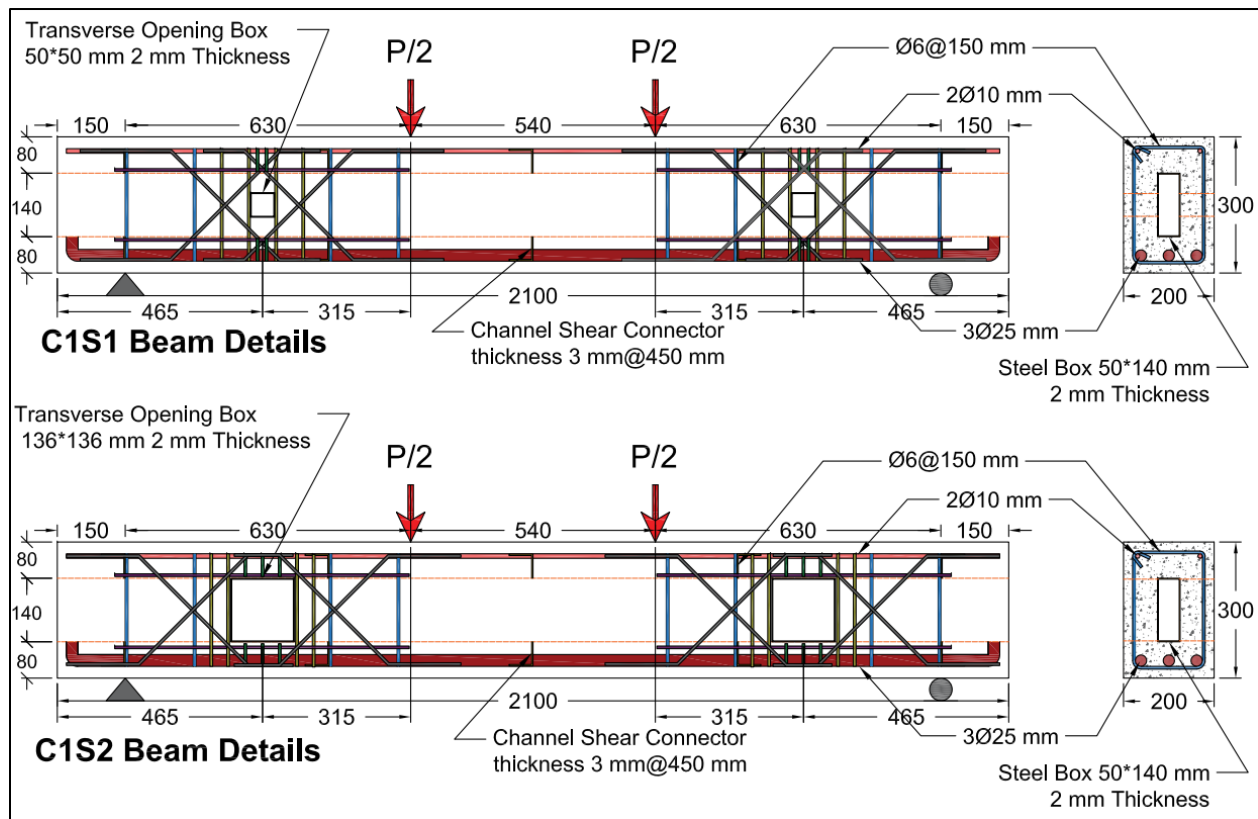


Figure 4.1: Details of experimental encased composite beams group 1.

#### 4.2.1.2 The Second Group

Investigates the effect of the strengthening technique by using the extruded encasing transversely (EET), which consisted of steel sections with a thickness of (2mm)

welded around square opening. The dimensions of the steel section welded depend on the dimensions of the transverse square opening with respect to the small opening dimension of the welded steel section which is (50×50) mm and extends to the end of the beam width (70) mm. On the other hand, with respect to the large opening dimension of the welded steel section, it is (136×136) mm and extends to the end of the beam width (70) mm, as shown in Figure (4.2).



**Figure 4.2:** Details of experimental encased composite beams, group 2.

### 4.2.1.3 The Third Group

Studies the reinforcement arrangement strengthening method, which includes adding diagonal bars at each side of the web opening to increase load-carrying capacity for composite encased steel-concrete beams with small and large square openings, and results comparison between beams strengthened and control beams as shown in Figure (4.3).

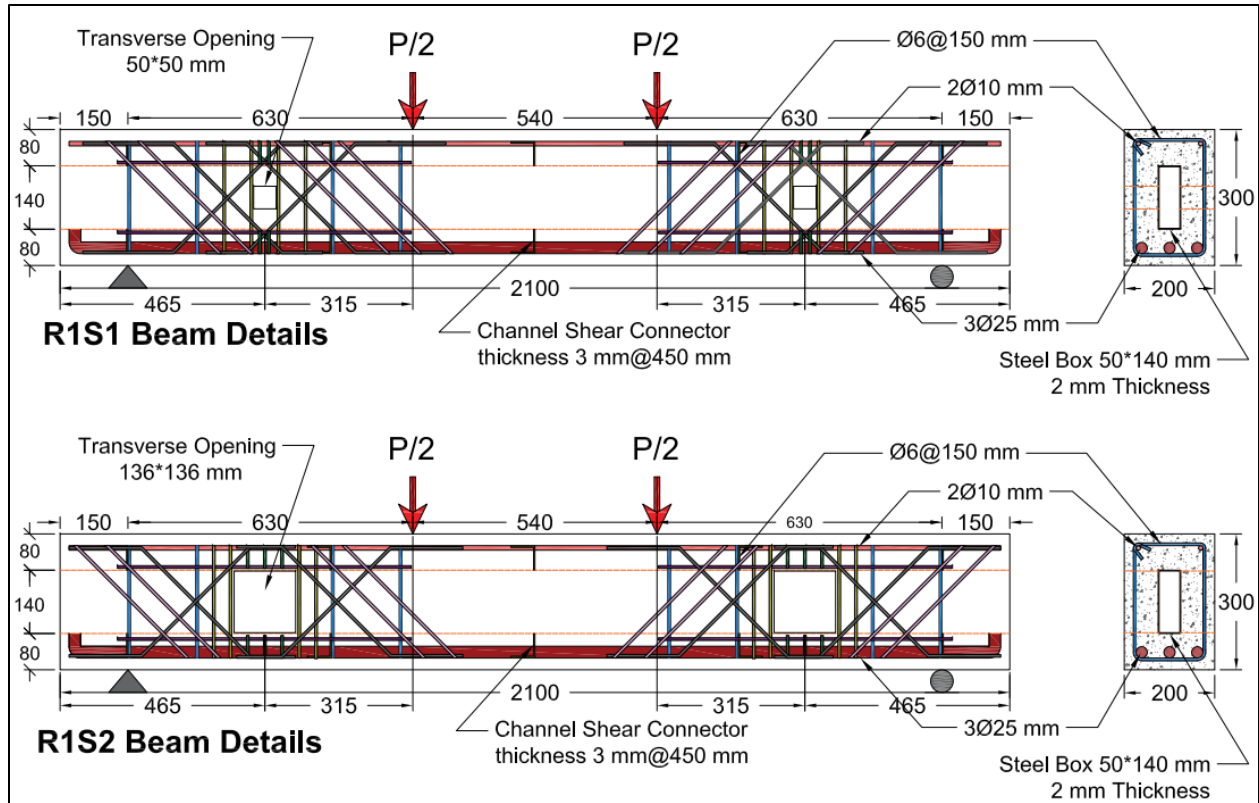


**Figure 4.3:** Details of experimental encased composite beams group 3.

#### 4.2.2 Convergence Details

In structural engineering, the convergence between numerical simulations and experimental results is critical for validating computational models. Numerical methods, such as finite element analysis (FEA), are widely used to simulate the behavior of structural components under various loading conditions. However, the accuracy of these simulations depends significantly on the selection of material and model parameters. Two key parameters influencing the accuracy of numerical simulations, particularly in problems involving plasticity and viscous flow, are the dilation angle and viscosity parameter.

In this convergence study, aims to investigate the effects of varying the dilation angle and viscosity parameter on the accuracy of numerical models compared to experimental results. By systematically adjusting these parameters, we seek to

achieve closer alignment between the simulated load-deformation curves and those obtained experimentally, ensuring that the numerical model accurately captures both material and structural behavior. This study will provide insights into the sensitivity of the model to these parameters and offer guidance for achieving reliable numerical predictions.

#### **4.2.2.1 Dilation Angle**

The dilation angle affects the volume change of a material when subjected to shear deformation, influencing the prediction of failure mechanisms such as cracking and yielding. When simulate the seven models to make comparison (CB, BW1, BW2, C1S1, C1S2, R1S1, R1S2) used deferent dilation angles to converge curves of numerical analysis and experimental work as follows ( for CB beam try dilation angles 31 and 39 and used 45 for more convergence, BW1 and BW2 beams try dilation angles 31 and 39 and used 36 for more convergence, C1S1 beam try dilation angles 31 and 36 and used 33 for more convergence, C1S2 beam try dilation angles 27 and 36 and used 33 for more convergence, R1S1 beam try dilation angles 31 and 36 and used 38 for more convergence and R1S2 beam try dilation angles 27 and 34 and used 31 for more convergence ), as shown in the Figures (4.4, 4.5, 4.6, 4.7, 4.8, 4.9 and 4.10) for try values of dilation angles and Figures (4.18, 4.19 and 4.20) of the used values of dilation angles for more convergence of curves between numerical analysis and experimental work.

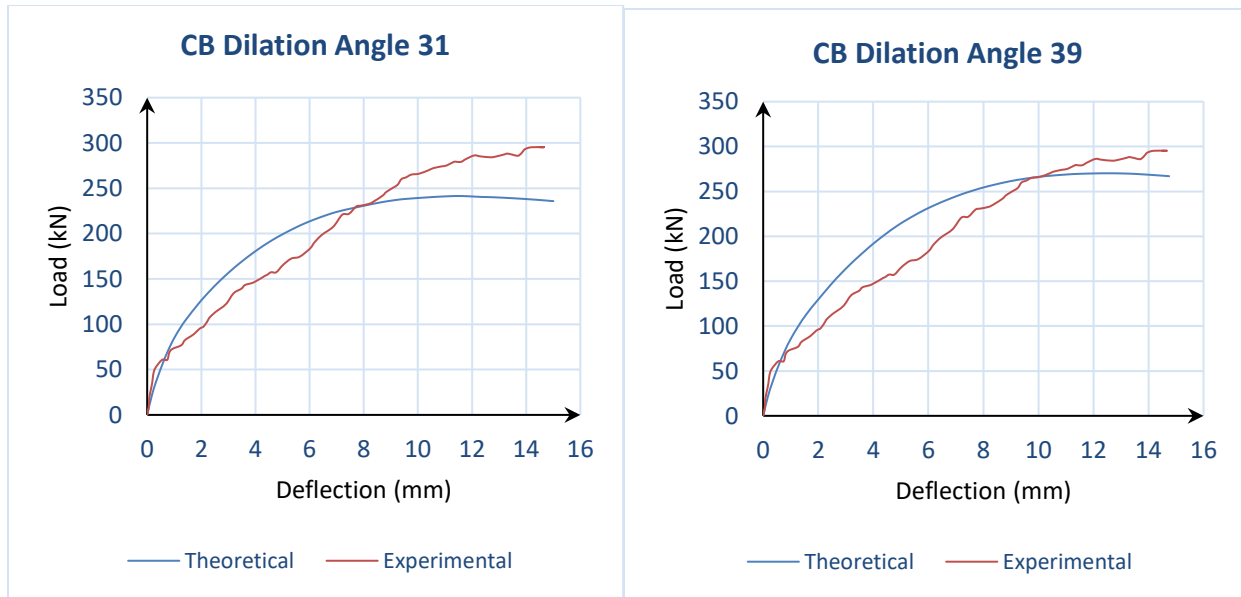


**Figure 4.4:** Load Deflection curves of CB model in change of dilation angle parameter.

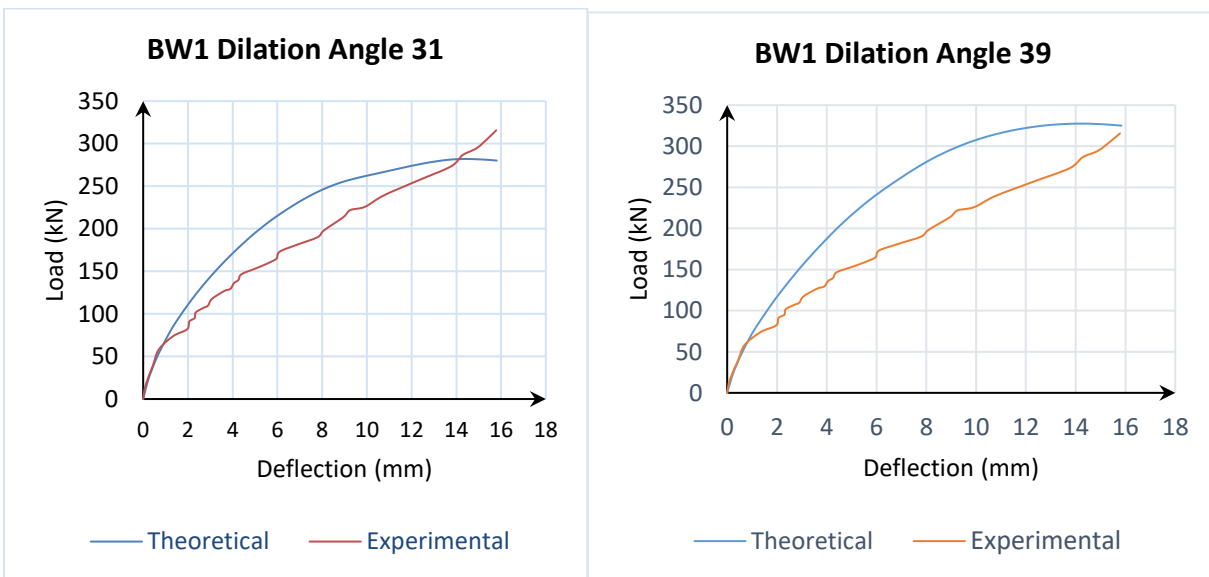


**Figure 4.5:** Load Deflection curves of BW1 model in change of dilation angle parameter.

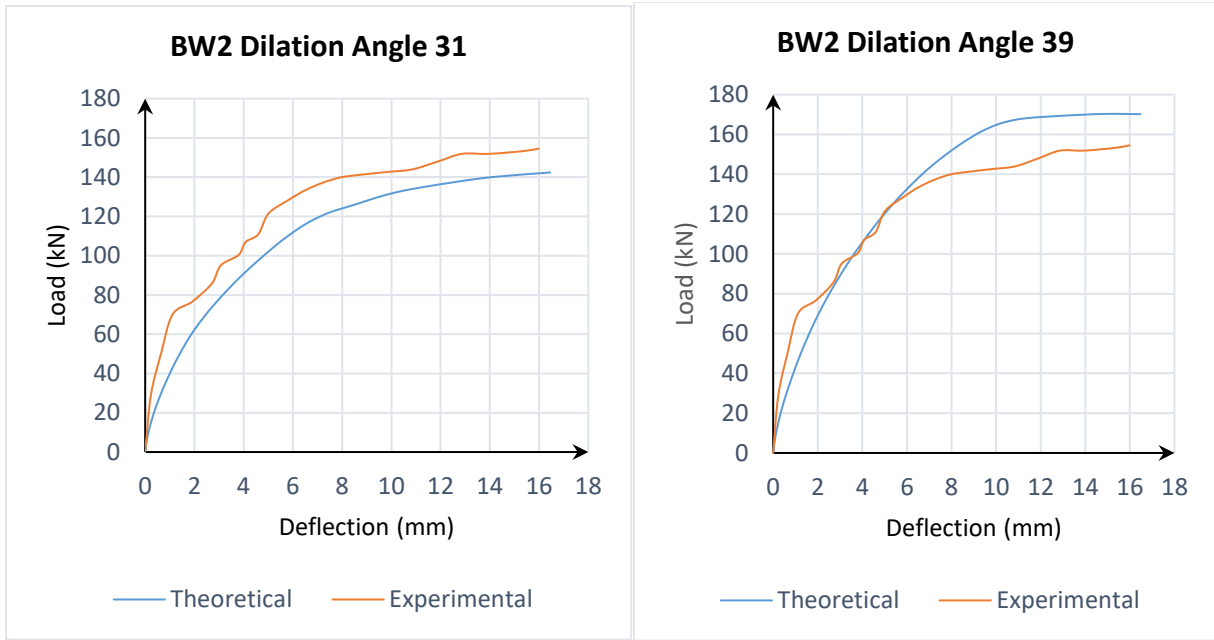


**Figure 4.6:** Load Deflection curves of BW2 model in change of dilation angle parameter.

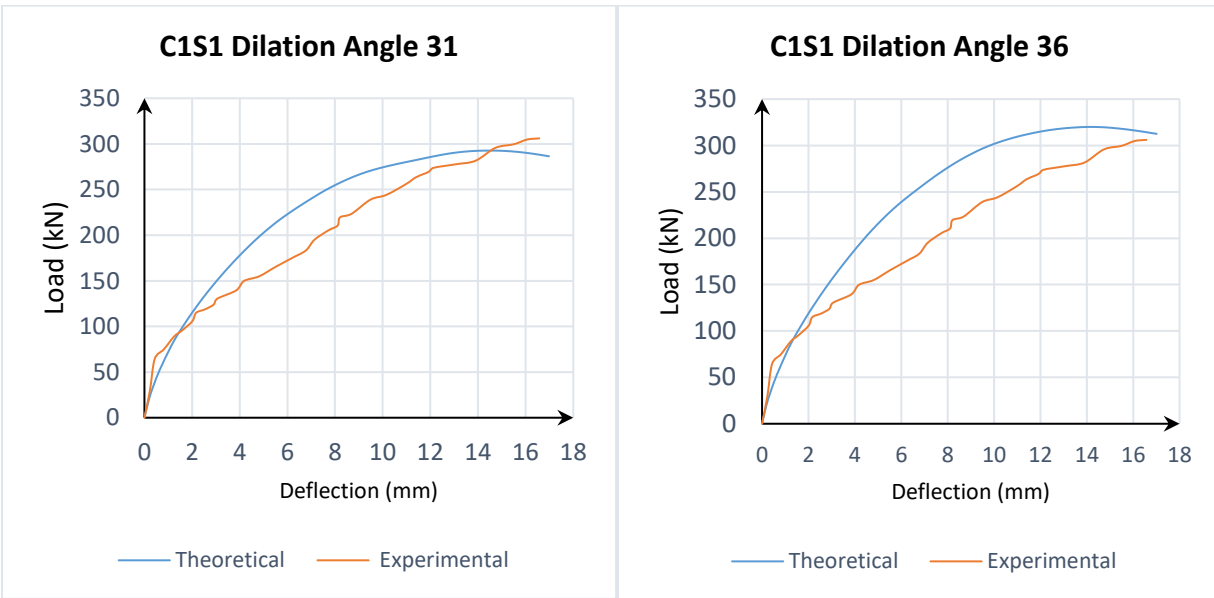


**Figure 4.7:** Load Deflection curves of C1S1 model in change of dilation angle parameter.

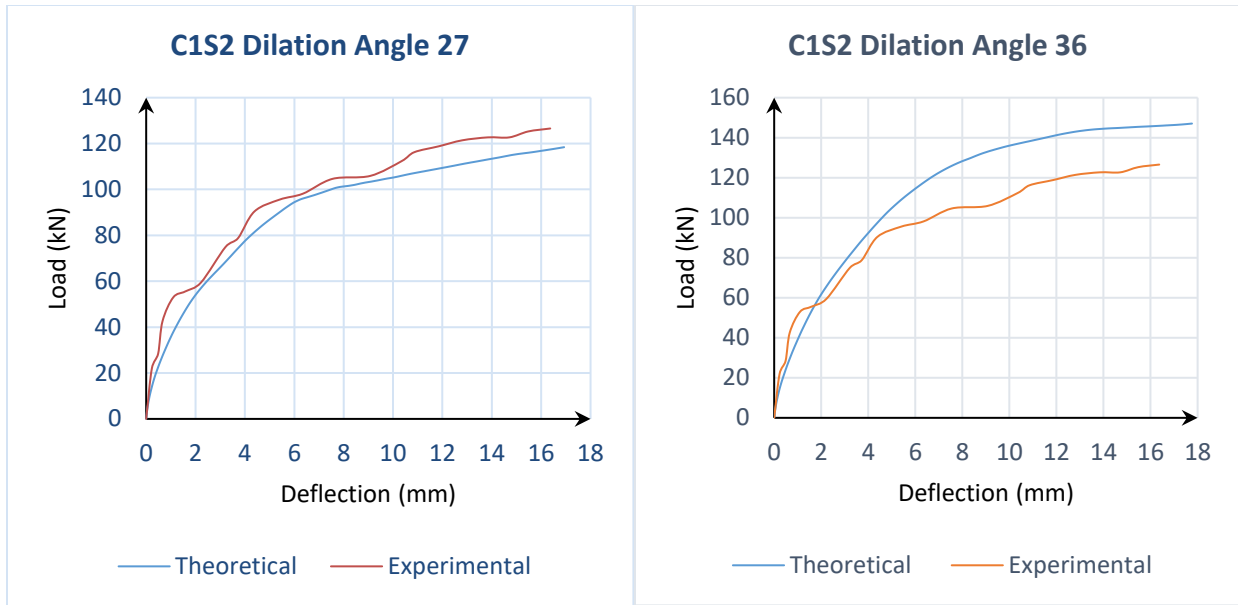


**Figure 4.8:** Load Deflection curves of C1S2 model in change of dilation angle parameter.

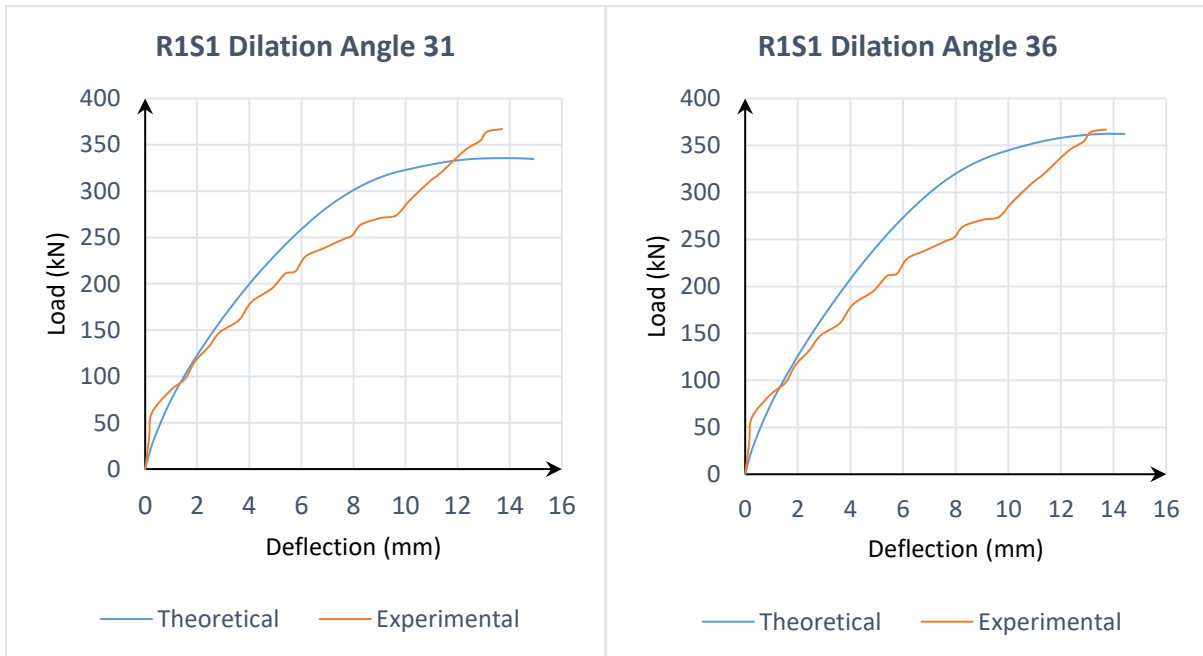


**Figure 4.9:** Load Deflection curves of R1S1 model in change of dilation angle parameter.

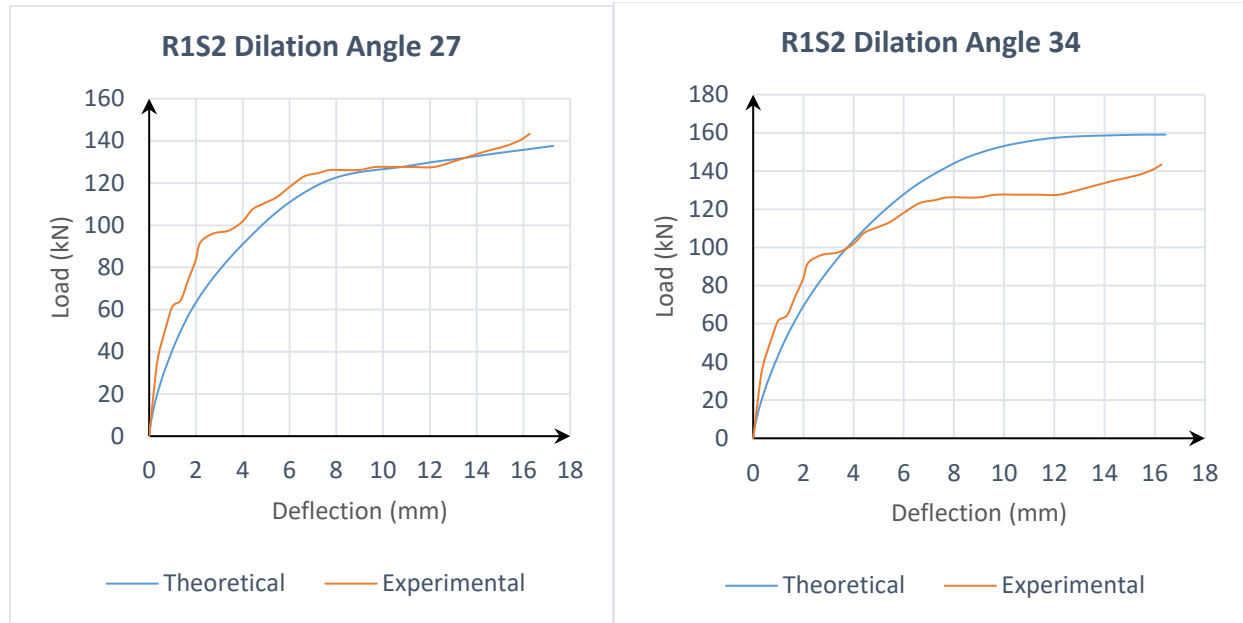


**Figure 4.10:** Load Deflection curves of R1S2 model in change of dilation angle parameter.

#### 4.2.2.2 Viscosity Parameter

The viscosity parameter controls the rate-dependent behavior of materials, particularly in dynamic and high-strain rate analyses, ensuring stability in numerical simulations, in this study try and use deferent viscosity parameters to get more accurate convergence between curve of numerical simulations and experimental work for the specimens (CB, BW1, BW2, C1S1, C1S2, R1S1, R1S2) as follows (for CB beam try viscosity parameters 0.00012 and 0.00055 and used 0.00023 for more convergence, BW1 beam try viscosity parameters 0.00012 and 0.00055 and used 0.00065 for more convergence, BW2 beam try viscosity parameters 0.00012 and 0.00055 and used 0.000375 for more convergence, C1S1 beam try viscosity parameters 0.00012 and 0.00055 and used 0.0007 for more convergence, C1S2 beam try viscosity parameters 0.00009 and 0.00035 and used 0.0002 for more convergence, R1S1 beam try viscosity parameters 0.00012 and 0.00035 and used 0.00055 for more convergence and R1S2 beam try viscosity parameters 0.00012 and 0.00055 and used 0.000375 for more convergence ), as shown in the Figures (4.11,



4.12, 4.13, 4.14, 4.15, 4.16 and 4.17) for try values of viscosity parameters and Figures (4.18, 4.19 and 4.20) of the used values of viscosity parameters for more convergence of curves between numerical analysis and experimental work.

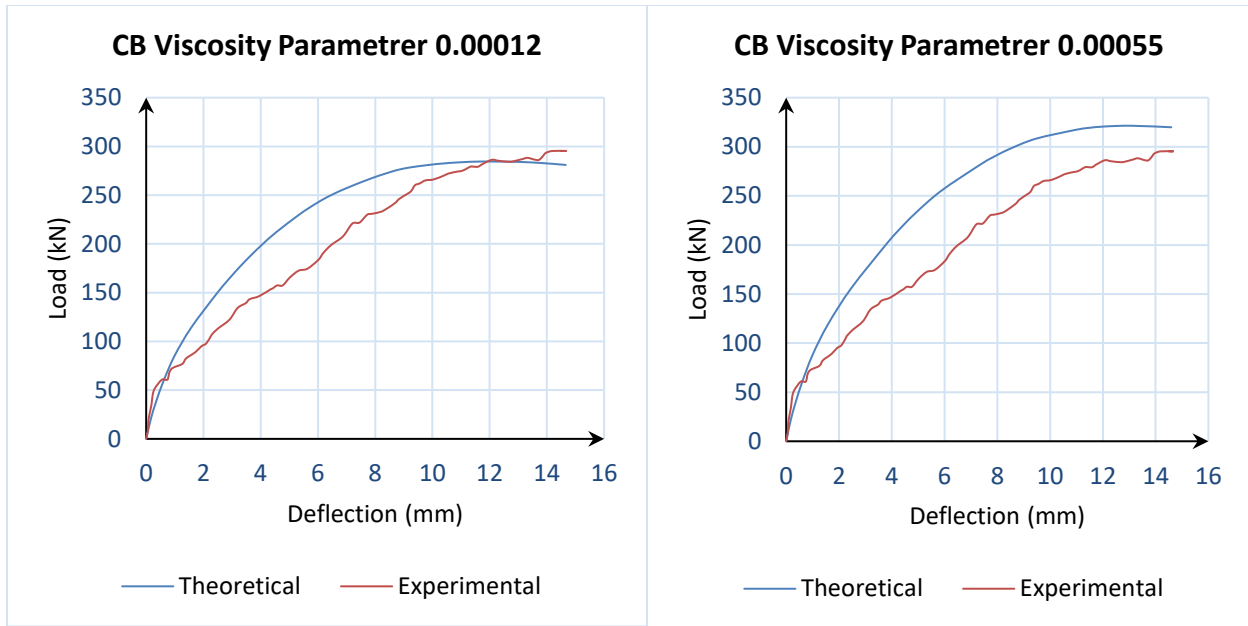


**Figure 4.11:** Load Deflection curves of CB model in change of viscosity parameter.

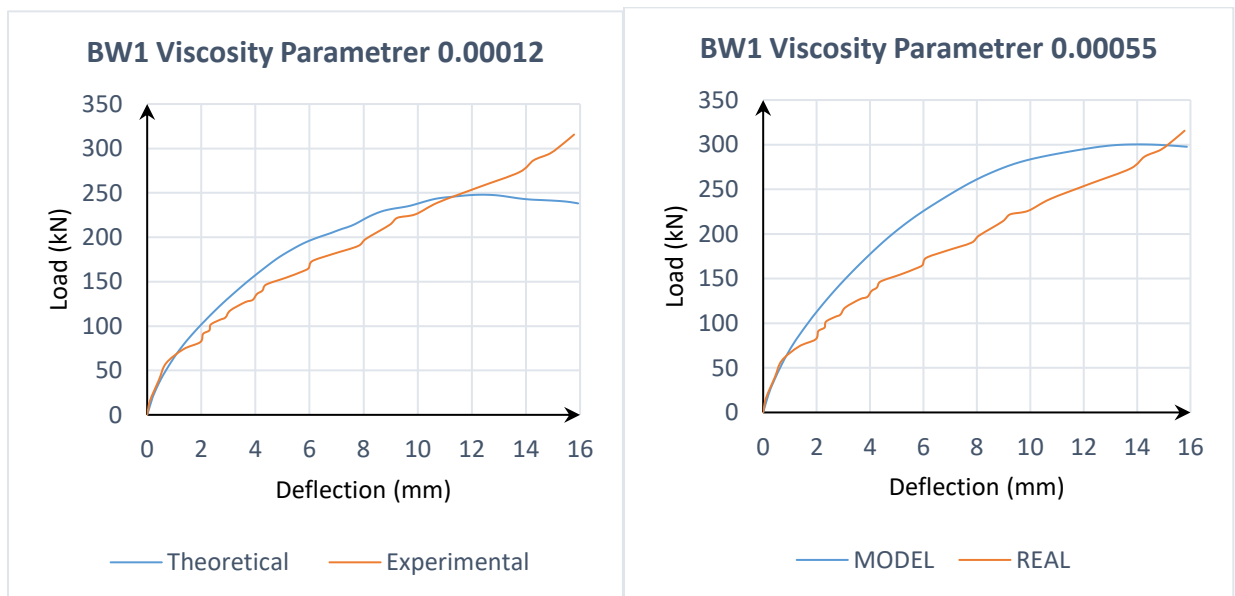


**Figure 4.12:** Load Deflection curves of BW1 model in change of viscosity parameter.

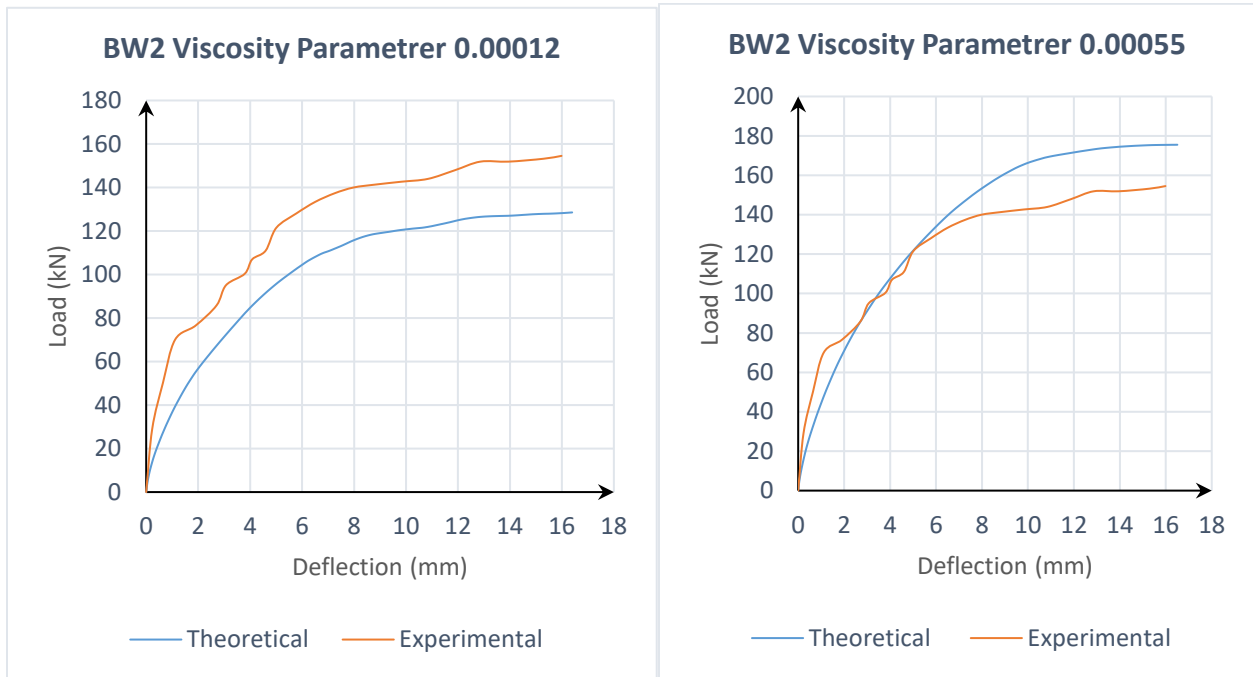


**Figure 4.13:** Load Deflection curves of BW2 model in change of viscosity parameter.

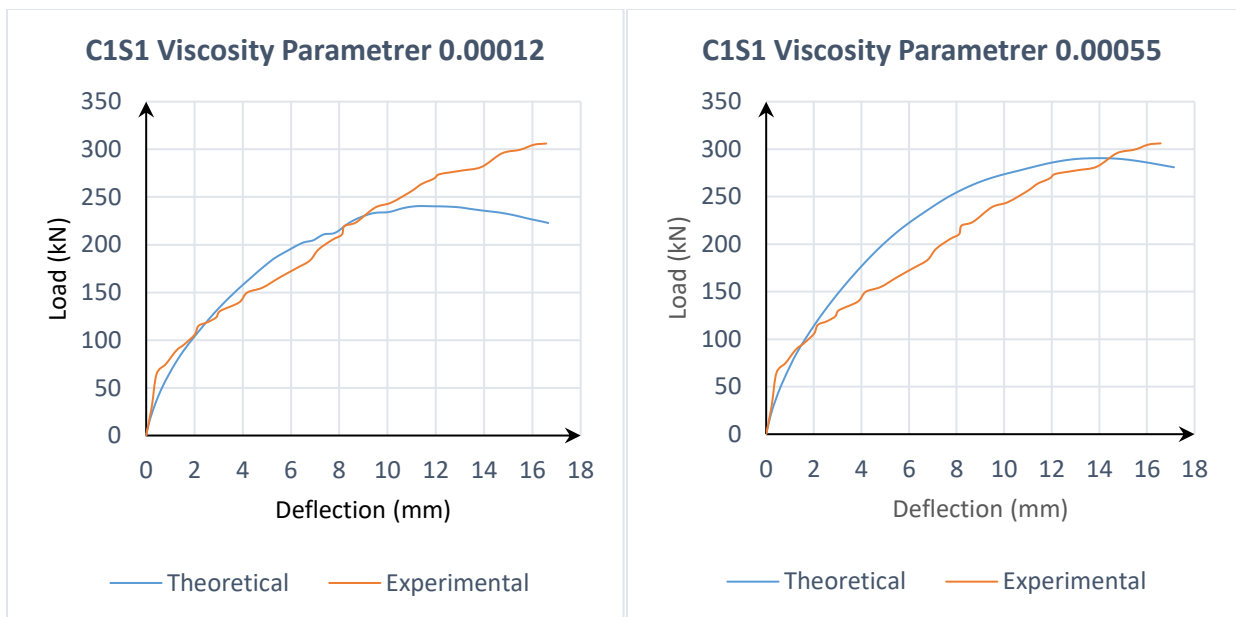


**Figure 4.14:** Load Deflection curves of C1S1 model in change of viscosity parameter.

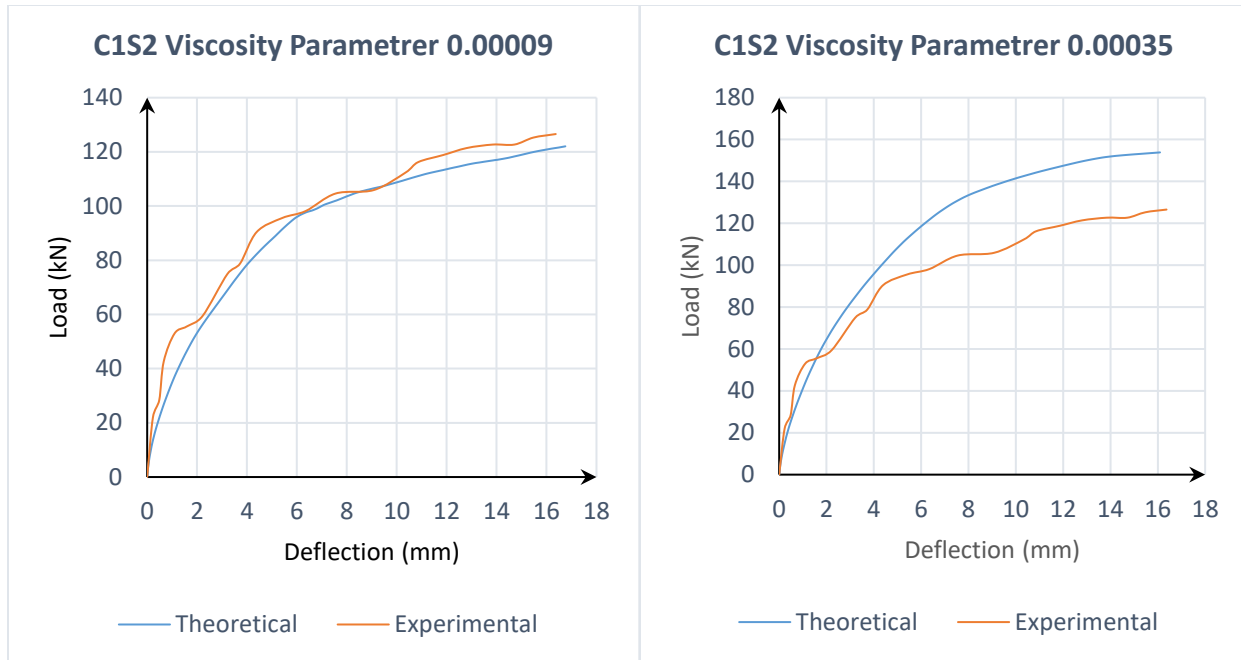


**Figure 4.15:** Load Deflection curves of C1S2 model in change of viscosity parameter.

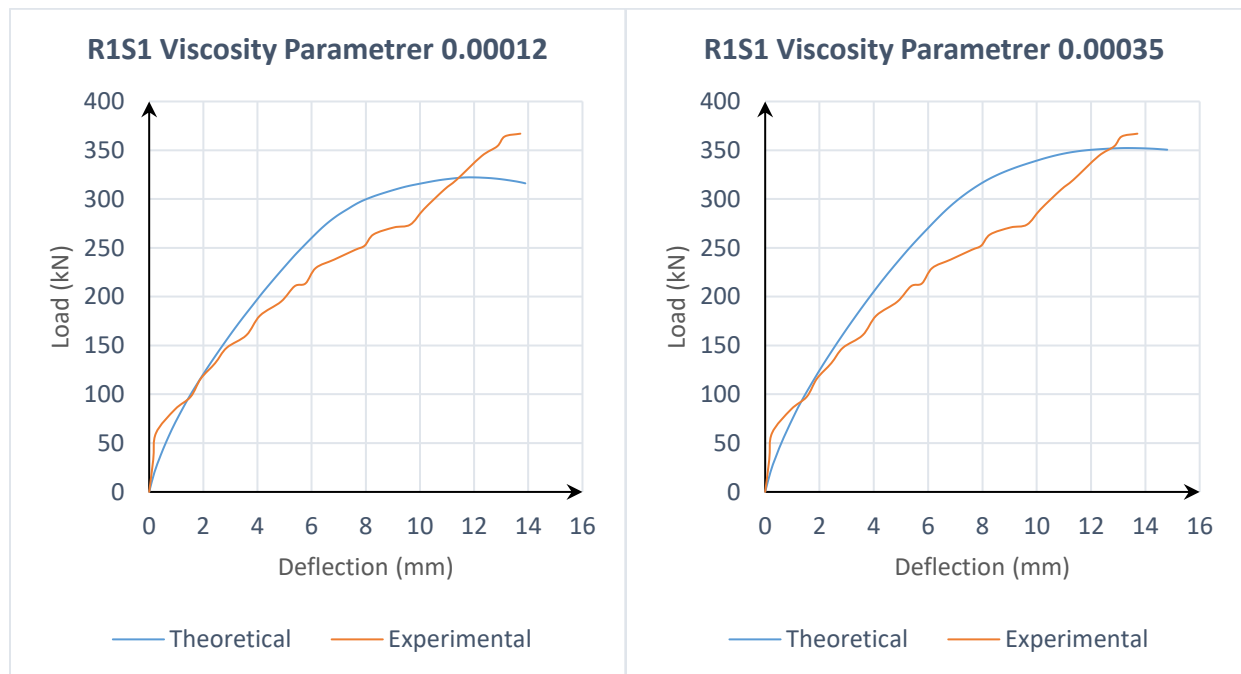


**Figure 4.16:** Load Deflection curves of R1S1 model in change of viscosity parameter.

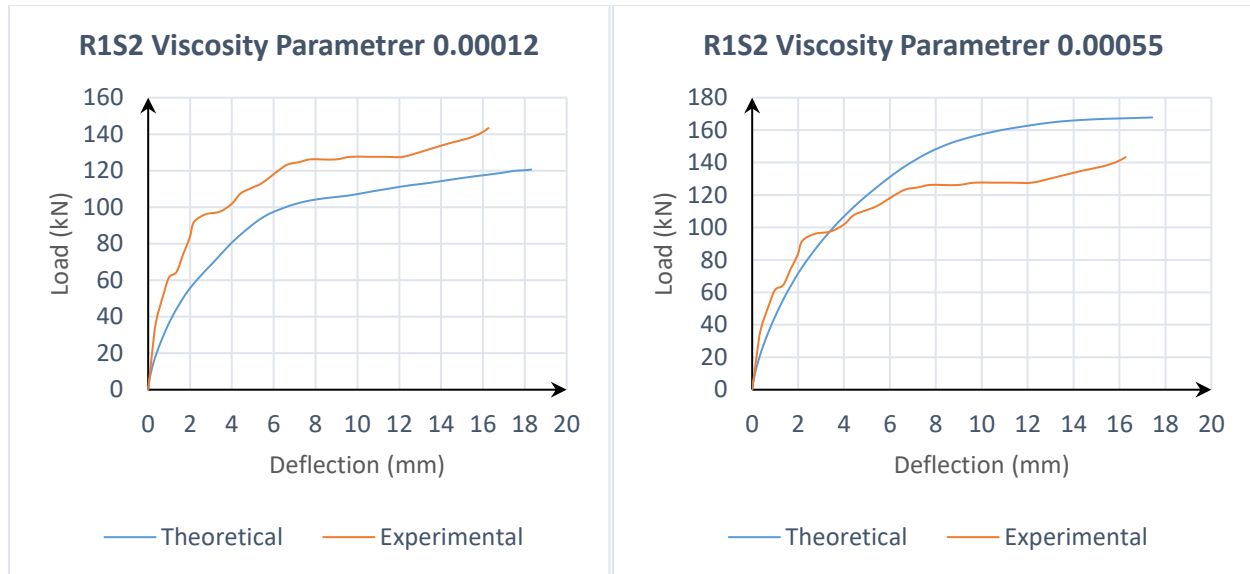


**Figure 4.17:** Load Deflection curves of R1S2 model in change of viscosity parameter.

### 4.3 Verification of Finite Element Models

The experimental and numerical comparison values produced by finite element analysis in this study for 7 specimens divided into three groups are [(G1:CB, CW1, CW2), (G2:C1S1, C1S2), and (G3:R1S1, R1S2)] in terms of maximum deflection and the load capacity of shear are listed in Tables (4-1), load-deflection curve figures (4.4), (4.5), and (4.6), and mode failure in figures (4.7),(4.8), and (4.9).

**Table (4-1):** The ultimate load and deflection of the verification results.

Group	Specimens	$P_{u Exp.}$ (KN)	$P_{u Num.}$ (KN)	$\frac{P_{u Exp.}}{P_{u Num.}}$	$\Delta_{u Exp.}$ (mm)	$\Delta_{u Num.}$ (mm)	$\frac{\Delta_{u Exp.}}{\Delta_{u Num.}}$
Group 1	CB	295.4	295.75	0.998	14.734	12.26	1.201
	BW1	320	309.94	1.032	15.779	14.36	1.098
	BW2	153.9	159.13	0.967	15.98	16.14	0.99
Group 2	C1S1	307	303.311	1.012	16.57	14.255	1.162
	C1S2	127	136.92	0.927	16.36	16.72	0.978
Group 3	R1S1	367	373.55	0.982	13.709	13.96	0.982
	R1S2	143.4	149.96	0.956	16.27	16.83	0.966
Mean				0.982			1.054
Standard Deviation				0.036			0.098

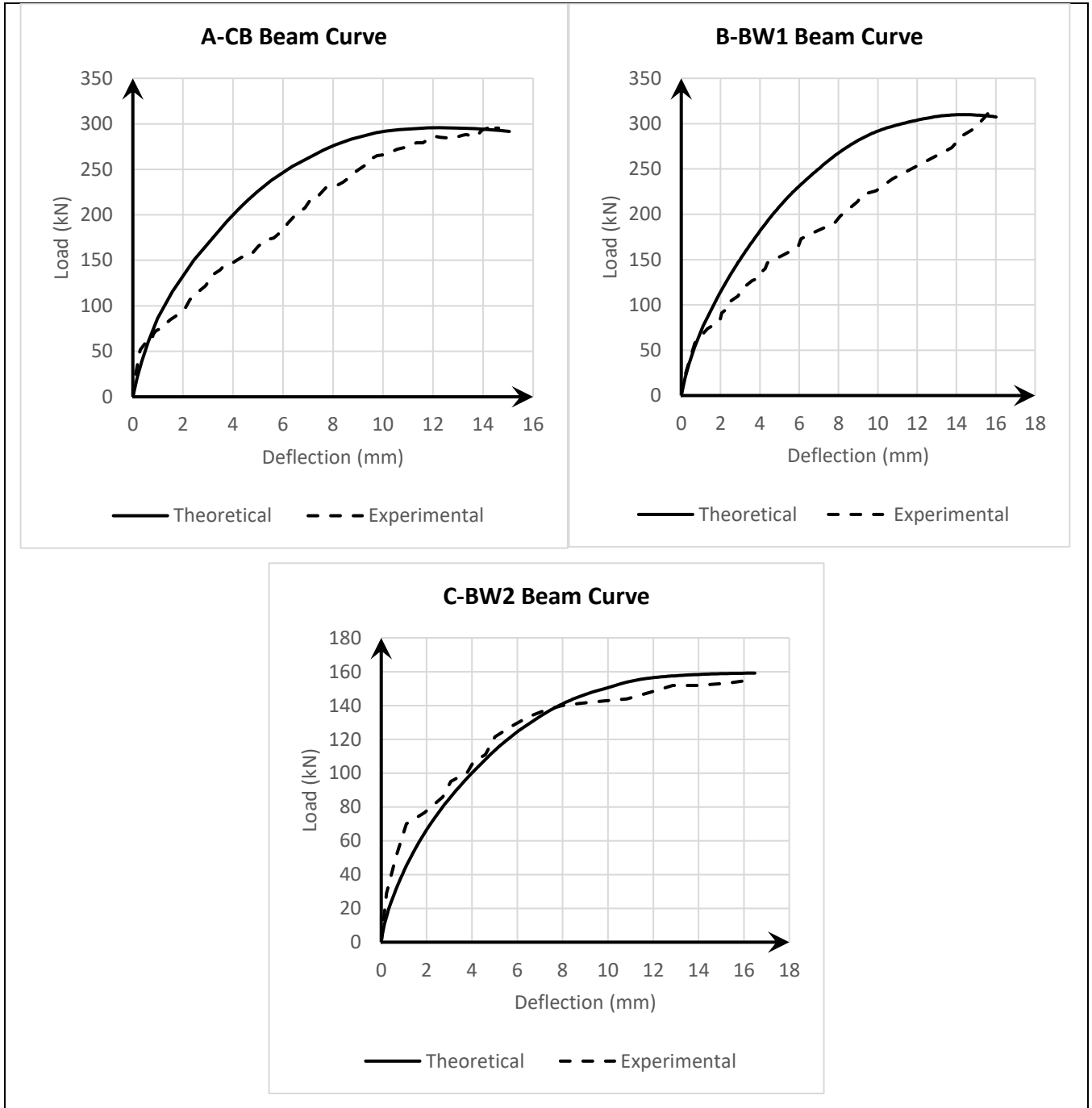


**Figure 4.18:** Load-Deflection curves theoretical and experimental comparisons of encased composite beams group 1.

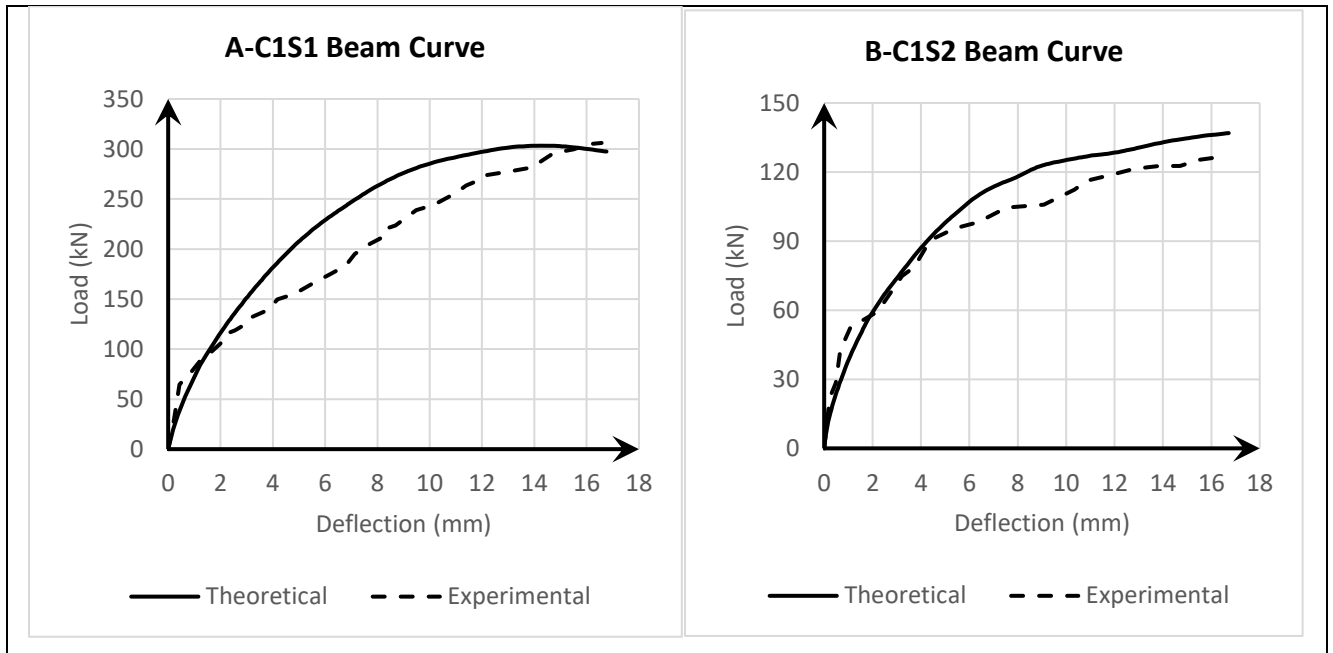


**Figure 4.19:** Load-Deflection curves theoretical and experimental comparisons of encased composite beams group 2.

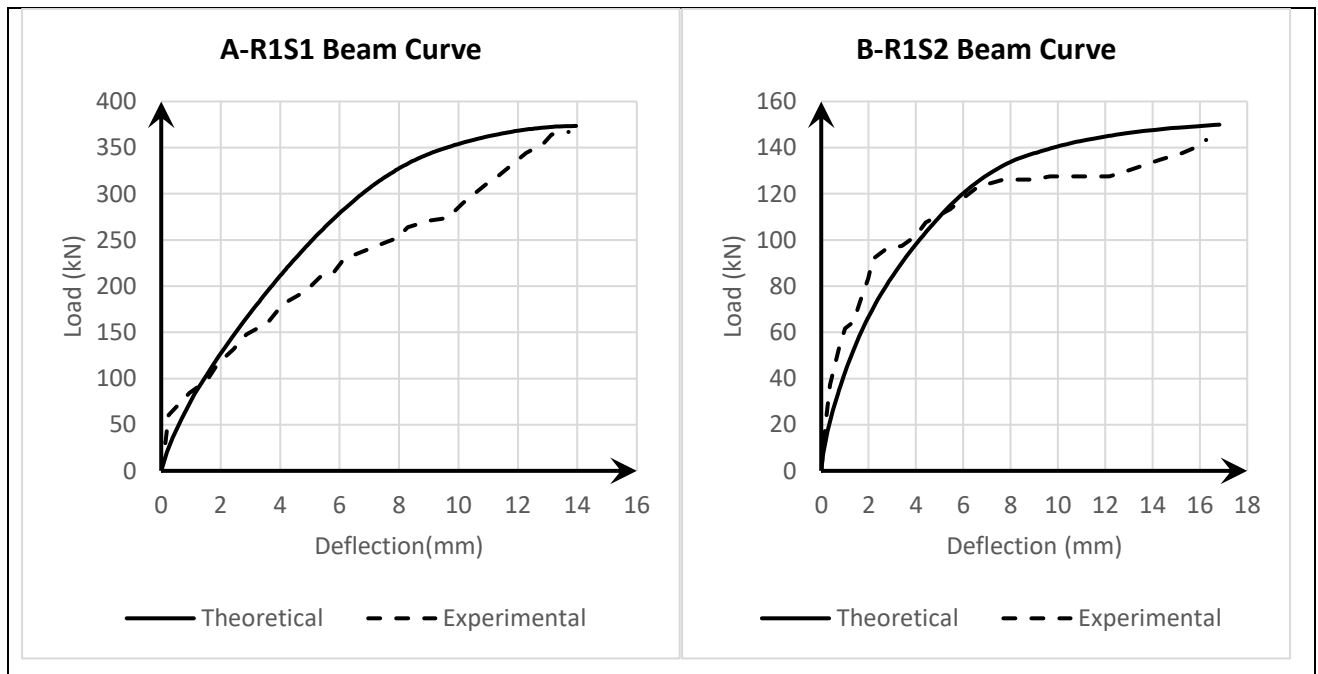


**Figure 4.20:** Load-Deflection curves theoretical and experimental comparisons of encased composite beams group 3.

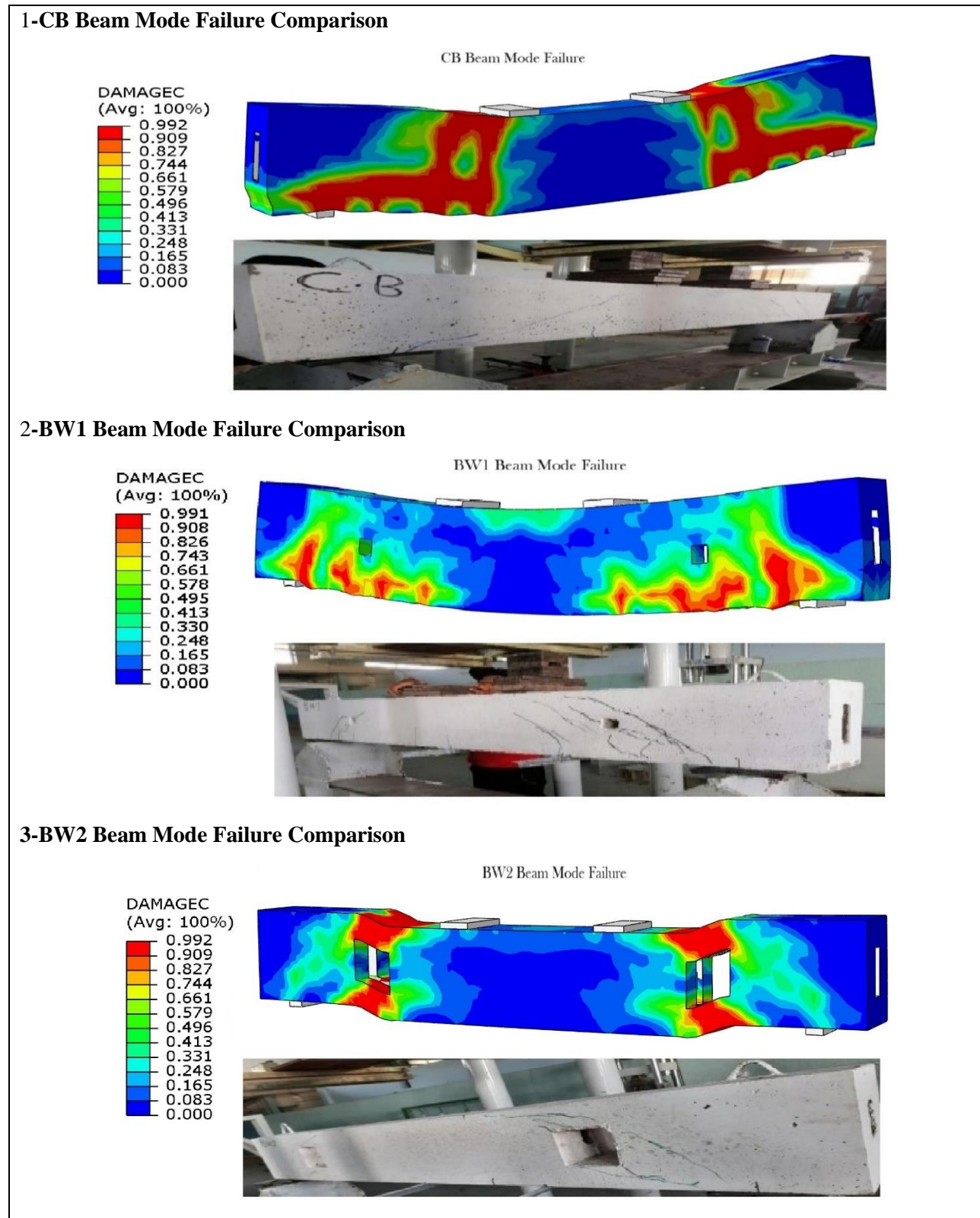
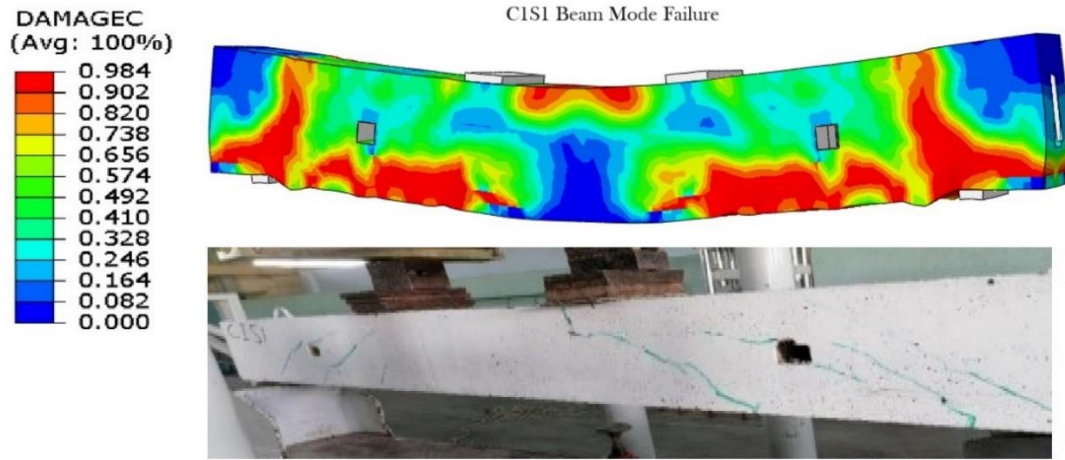
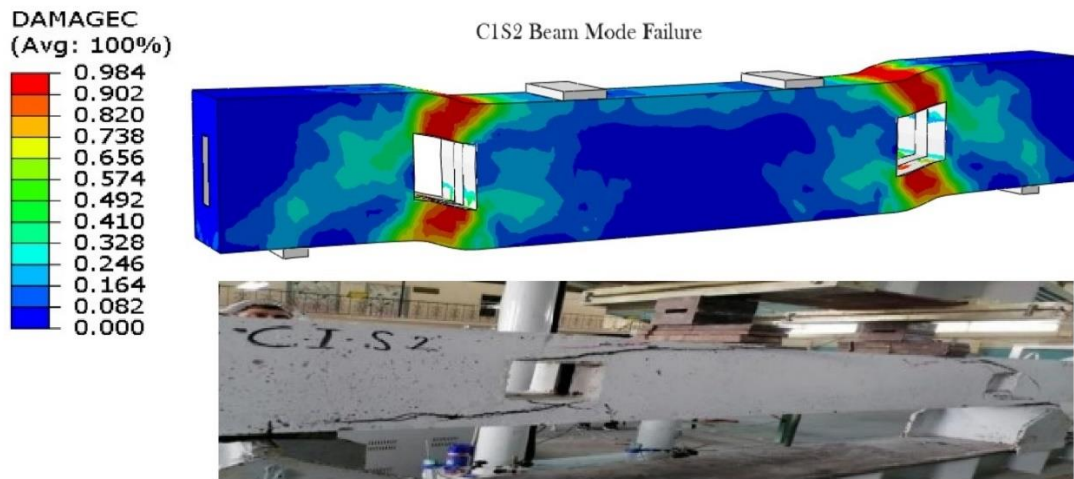


**Figure 4.21:** Theoretical and experimental comparisons of mode failure in encased composite beams group 1.

**1-C1S1 Beam Mode Failure Comparison**

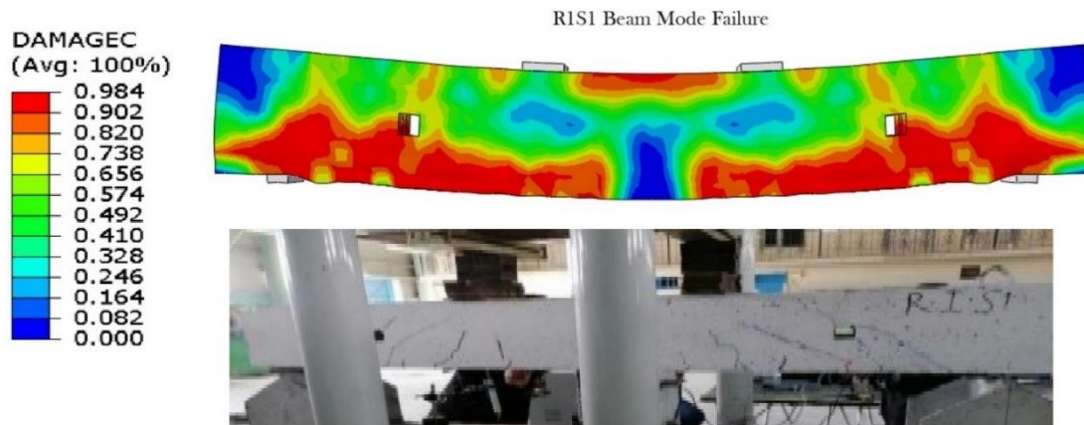


**2-C1S2 Beam Mode Failure Comparison**



**Figure 4.22:** Theoretical and experimental comparisons of mode failure in encased composite beams group 2.

**1-R1S1 Beam Mode Failure Comparison**





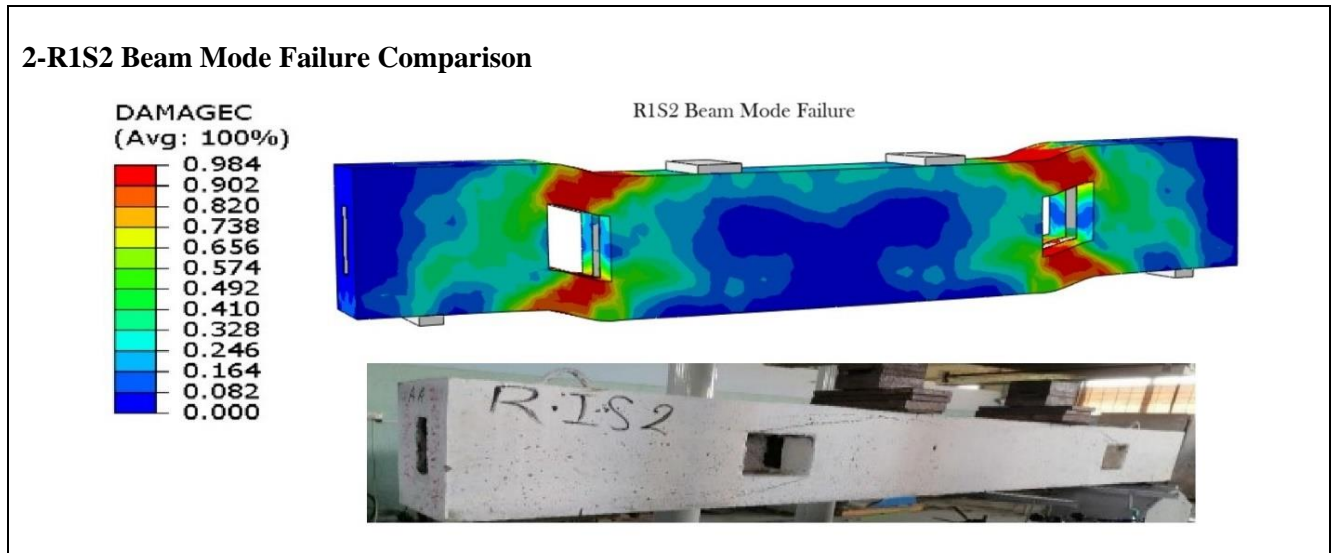


**Figure 4.23:** Theoretical and experimental comparisons of mode failure in encased composite beams group 3.

#### 4.4 Parametric Study

The primary objective of this study is to investigate the effects of several critical parameters that have been insufficiently covered in previous research, or to expand upon those studies, ductility, stiffness, deflection, and shear strength of composite steel box-concrete beams with transverse openings. The parameters considered in this study include the shear span to effective depth ratio, tensile steel rebar diameter, compressive strength of concrete, as well as the location, shape, and dimensions of the openings. The finite element method (FEM) was employed and developed using the general commercial software ABAQUS. The parametric study results obtained by the finite element modeling include the yield load ( $P_y$ ) for the whole composite beam, the ultimate shear load ( $P_u$ ), and the ultimate vertical mid-span deflection ( $\Delta u$ ). Detailed information on the studied can be found in Table (4-2).

The abbreviations refers assigned based on the first word of each parameter, for example, the size of the openings was used as BOS and B refer to Beam used for all abbreviations and the shape of the openings was circular used BOD and D refer to diameter of opening, while the abbreviation BOL is refer to the location of openings,

BAD abbreviation refer to the ratio ( $a/d$ ), BFC abbreviation refer to the compressive strength of concrete ( $f'_c$ ) and the abbreviation BDB refer to diameter of reinforced bars.

**Table (4-2):** Model's details for the composite beams.

Group	Beam ID	Opening Size (mm)	Opening Shape	Opening Location (mm)	a/d	$f'_c$ (MPa)	Reinforced Bars (mm)
Group 1	BW1	50*50	Square	Center of shear span	2.4	23.5	3Ø25
	BOS1	70*70					
	BOS2	90*90					
	BOS3	110*110					
	BW2	136*136					
Group 2	BOD1	Ø50	Circular	Center of shear span	2.4	23.5	3Ø25
	BOD2	Ø70					
	BOD3	Ø90					
	BOD4	Ø110					
	BOD5	Ø136					
Group 3	BOL1	50*50	Square	126(a/5) Near loads	2.4	23.5	3Ø25
	BOL2	70*70					
	BOL3	90*90					
	BOL4	110*110					
	BOL5	136*136					
	BOL6	50*50		126(a/5) Near supports			
	BOL7	70*70					
	BOL8	90*90					
	BOL9	110*110					
	BOL10	136*136					
Group 4	BAD1	50*50	Square	Center of shear span	2	23.5	3Ø25
	BAD2	70*70					
	BAD3	90*90					
	BAD4	110*110					
	BAD5	136*136					
	BAD6	50*50			2.8		
	BAD7	70*70					
	BAD8	90*90					
	BAD9	110*110					
	BAD10	136*136					

Group 5	<b>BFC1</b>	50*50	Square	Center of shear span	2.4	30	3Ø25
	<b>BFC2</b>	70*70					
	<b>BFC3</b>	90*90					
	<b>BFC4</b>	110*110					
	<b>BFC5</b>	136*136					
	<b>BFC6</b>	50*50				37.5	
	<b>BFC7</b>	70*70					
	<b>BFC8</b>	90*90					
	<b>BFC9</b>	110*110					
	<b>BFC10</b>	136*136					
Group 6	<b>BDB1</b>	50*50	Square	Center of shear span	2.4	23.5	3Ø16
	<b>BDB2</b>	70*70					
	<b>BDB3</b>	90*90					
	<b>BDB4</b>	110*110					
	<b>BDB5</b>	136*136					
	<b>BDB6</b>	50*50				2Ø16&2Ø25	
	<b>BDB7</b>	70*70					
	<b>BDB8</b>	90*90					
	<b>BDB9</b>	110*110					
	<b>BDB10</b>	136*136					

#### 4.5 Ductility Index

An index of ductility for the curved composite beam models was estimated as a ductility index ratio. Ductility index  $\mu\Delta$  is defined as the ratio of maximum mid-span displacement over the first yield displacement of beams. The first yield displacement  $\Delta_y$  corresponds to the load-deflection curve and maximum displacement  $\Delta_u$ , Figure (4.24). Thus, it would be more suitable if ductility ratio can also be used as an additional criterion alongside strength criteria for predicting a curved composite steel-concrete beam behavior.[80]

Ductility is a measure of a material's ability to undergo significant plastic deformation before rupture or breaking.

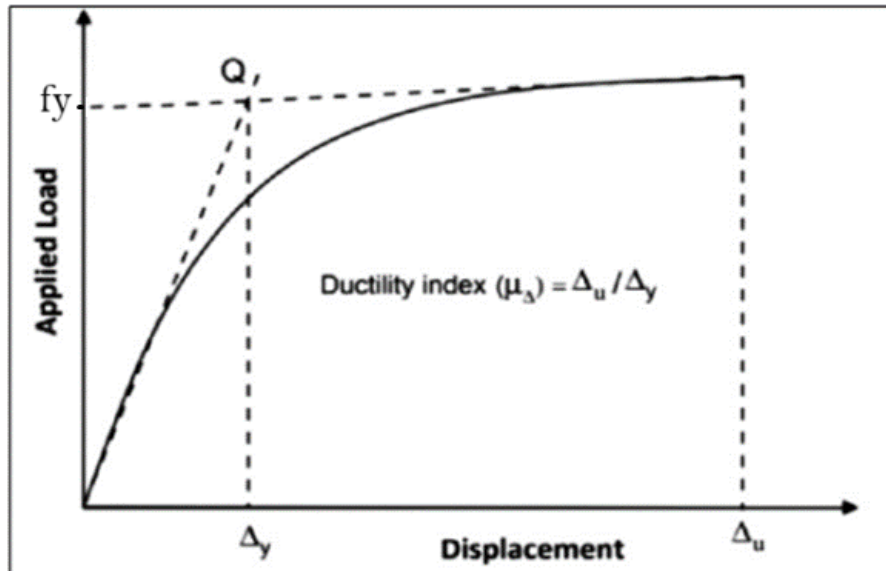


**Figure 4.24:** Definition of displacement–ductility ratio.[80]

#### 4.6 Ultimate Shear Load and Ultimate Deflection

The ultimate shear force that a structural element, for instance, a beam, can withstand before it fails in shear is referred to as the ultimate shear load. This load is essential for maintaining the structural integrity of the element under different loading conditions. The ultimate shear load for a composite simply supported beam involves looking at both the contributions made by steel and concrete sections. Usually, the ultimate shear load equation for a composite simply supported beam incorporates both concrete slab and steel section (like an I-beam or steel box) for composite action considerations.

#### 4.7 Initial stiffness

Initial stiffness was calculated based on the load-deflection curve by dividing the maximum yield load ( $P_y$ ) by the yield deflection ( $\Delta_y$ ) in the case of initial stiffness. The equations used are shown below:

$$\text{Initial stiffness} = \frac{P_y}{\Delta_y} \quad (4.5)$$

Stiffness calculation is carried out according to the N. Priestley study[81].

In the context of composite steel-concrete beams, initial stiffness plays a vital role in determining the structural performance under service loads. The stiffness of such composite beams is influenced by several factors, including the material properties of steel and concrete, the bond between them, and the presence of transverse openings. The introduction of transverse openings, often necessary for mechanical or utility passage, can significantly alter the stiffness by reducing the effective cross-sectional area and increasing stress concentrations around the openings.

Understanding the initial stiffness of beams, particularly those with transverse openings, is essential for predicting their behavior under various loading conditions. It not only impacts the load-deflection relationship but also provides insights into the load-carrying capacity, deflection limits, and potential failure modes. Hence, accurately quantifying the initial stiffness is a key step in the numerical and experimental analysis of composite beams with openings.

#### **4.8 Energy Absorption Capacity**

Energy absorption capacity is a fundamental property of structural elements, reflecting their ability to withstand and dissipate energy during loading, particularly under dynamic or impact conditions. It is crucial for understanding how structures behave when subjected to sudden or high-intensity forces, such as seismic events, blasts, or accidental impacts. A structure's energy absorption capacity can be visualized as the area under its load-deflection curve, representing the amount of energy it can absorb before failure.

In composite steel-concrete beams, energy absorption capacity is of particular interest due to the combined action of materials with different mechanical properties. Steel offers high ductility and tensile strength, while concrete provides compressive

strength. Together, they form a composite system that can distribute loads efficiently, enhancing the structure's ability to absorb and dissipate energy.

However, the presence of transverse openings, often introduced for utility or mechanical services, can significantly influence a beam's energy absorption capacity. These openings create stress concentrations and reduce the overall stiffness and strength of the beam, potentially lowering its ability to absorb energy. Understanding the effect of opening size, shape, and location on energy absorption is critical for ensuring the structural integrity and safety of composite beams under dynamic loading conditions.

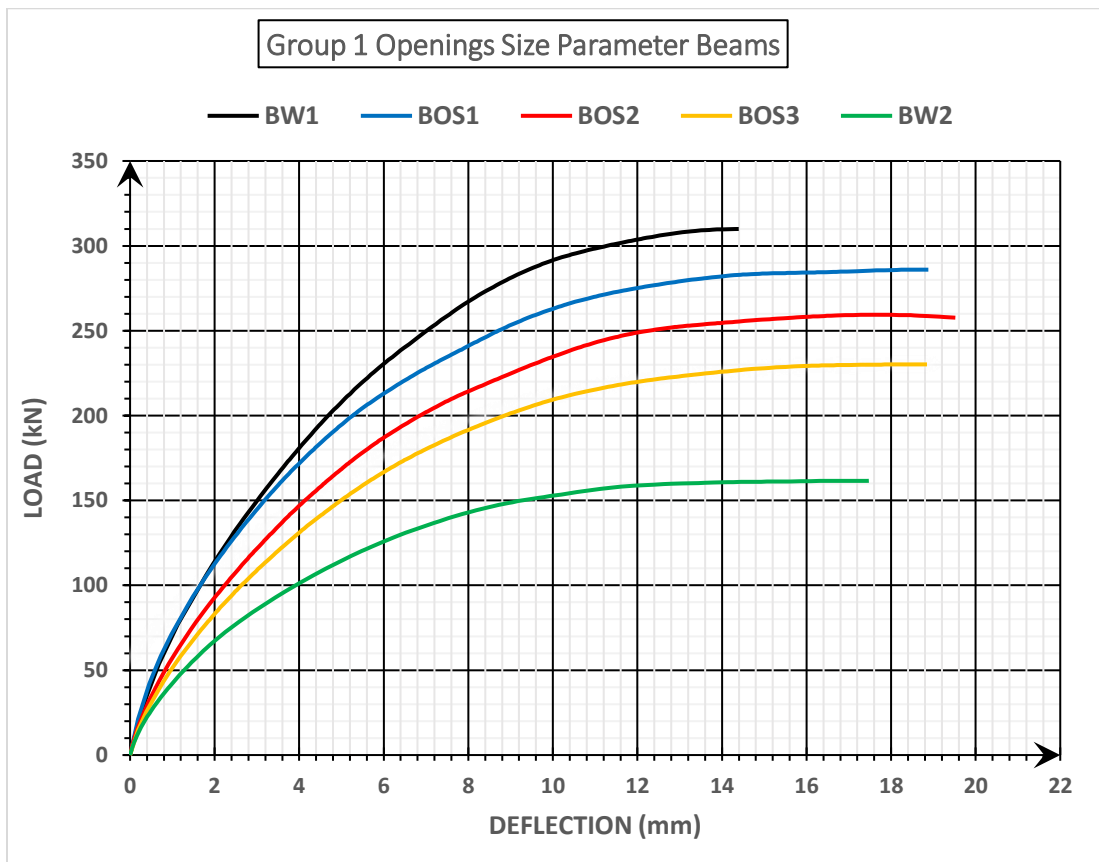
## **4.9 Openings Size Parameter**

### **4.9.1 Effect of Opening Size on Ultimate Shear Strength**

In this investigation, an attempt was made to study the shear strength of composite box steel-concrete beams having a transverse square opening. The simulate of modeling have been determining the shear strength of composite beams that have five (50\*50mm and 70\*70mm, 90×90 mm, 110×110mm, and 136×136mm) dimensions of transverse openings. All details of composite beams are illustrated in Figure 4.26. The dimension, shape, and location of the opening's center were changed. The composite beam's cross section and reinforcement ratio in the beam were kept the same. The constant 23.5 MPa concrete compressive strength was used in all the beams. An increase in the size of the openings resulted in a decrease in the ultimate shear strength, as shown in Table (4-3) and Figure 4.25. All varied distributions of transverse openings with a dimension of 50\*50mm were shown to have a higher ultimate shear strength than other hollow beams. The ultimate shear strength of the composite beam rises as the dimension of the opening is reduced. And Figure 4.27 shows the mode failure of composite beams.

**Table (4-3):** Model's Results for Group 1 of the composite beams.

Beam with opening (mm)	Ultimate Shear Load (kN)	Yild Shear Load (kN)	Ultimate Deflection (mm)	Yild Deflection (mm)	Ductility Index	Initial Stiffness (kN/mm)	Energy Absorption (kN.mm)
<b>BW1 (50x50)</b>	<b>309</b>	<b>190</b>	<b>14.4</b>	<b>4.1</b>	<b>3.5</b>	<b>46</b>	<b>3239</b>
<b>BOS1 (70x70)</b>	<b>286</b>	<b>170</b>	<b>18.9</b>	<b>4</b>	<b>4.7</b>	<b>43</b>	<b>4258</b>
<b>BOS2 (90x90)</b>	<b>259.40</b>	<b>170</b>	<b>17.6</b>	<b>5</b>	<b>3.5</b>	<b>34</b>	<b>3452</b>
<b>BOS3 (110x110)</b>	<b>230.15</b>	<b>150</b>	<b>18.6</b>	<b>5</b>	<b>3.7</b>	<b>30</b>	<b>3306</b>
<b>BW2 (136x136)</b>	<b>161.60</b>	<b>90</b>	<b>17.5</b>	<b>3.1</b>	<b>5.6</b>	<b>29</b>	<b>2238</b>

**Figure 4.25:** Load Deflection Curve of Opening Size Parameter in Group 1.

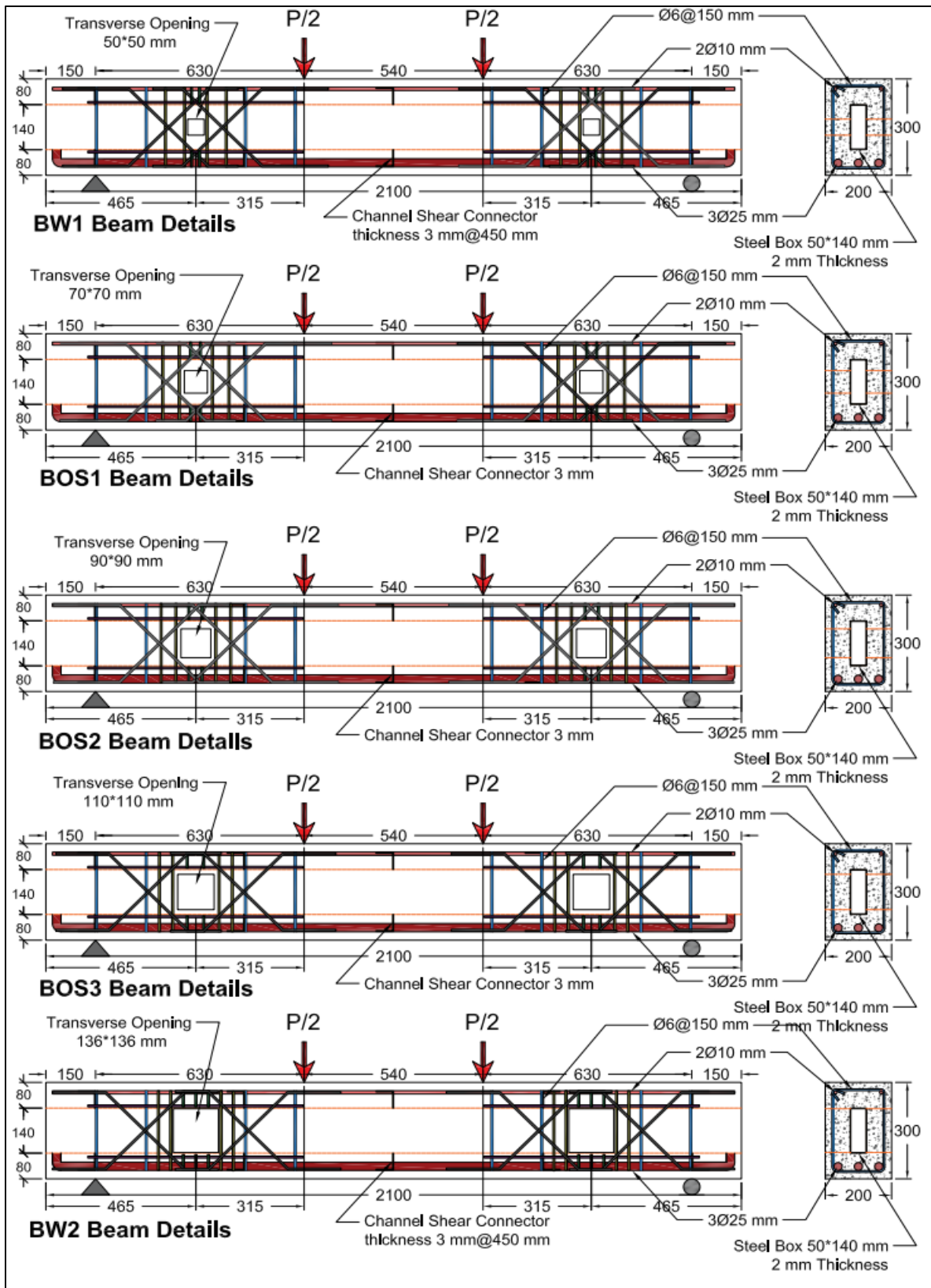


Figure 4.26: Details of Beams of Opening Size Parameter in Group 1



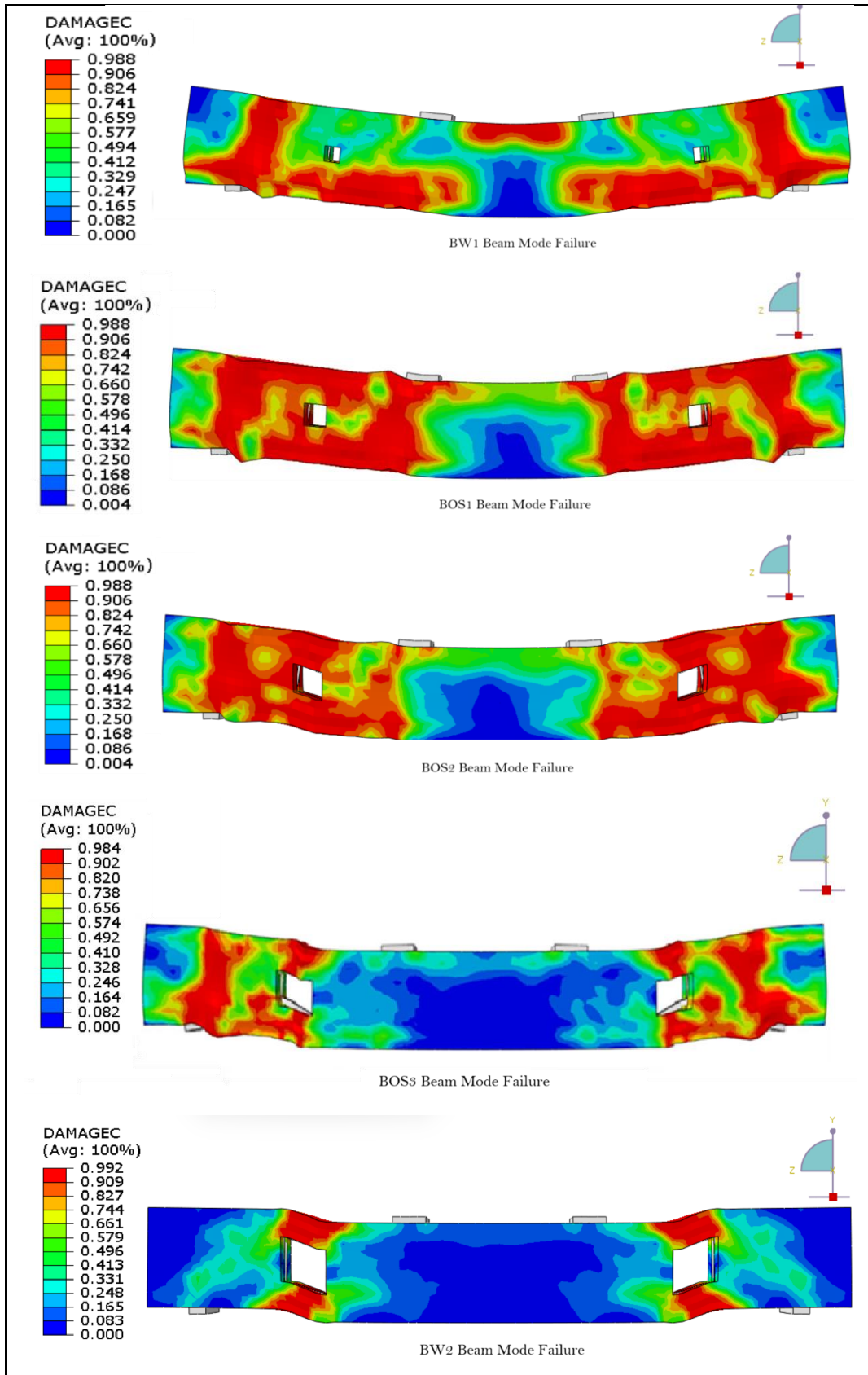


Figure 4.27: Mode Failure of Opening Size Parameter in Group 1.

This study investigates how different sizes of transverse openings affect the structural behavior of composite simply supported beams under shear forces. The research analyzed beams with two transverse openings of size ranging from 50×50 mm to 136×136 mm and measured ultimate shear strength capacities and deflections. Among all the beams that were studied, beam BW1 had the smallest openings but exhibited higher shear load capacity as well as lower deflection, reflecting it has high strength as well as stiffness. However, as for the other beam types that were examined in this study, the trend was just opposite since beam BOS1's shear strength capacity dropped by 7.4% relative to BW1, whose size was much smaller. That trend continued through beam BOS2, whose shear strength capacity was found to be 16.1% lower than BW1, while beam BOS3 recorded a fall off rate of 25.5% based on BW1 data. It is evident from this research that, through its greatest opening size, when compared with BW1, there was much lower support for shear strength in BW2, being about 47.7%. The finding also shows that larger opening sizes result in higher deflection levels. Overall, these findings show how the size of an opening increases with load bearing ability and flexibility of composite beams.

Shear strength carrying capacity reduces significantly as the sizes of openings increase while deflection rises. Several effects come into play: bigger openings minimize an effective cross-sectional area for counteracting shear forces, thus compromising a beam's web, hence leading to an overall decrease in its shear strength. Moreover, the beam's moment of inertia is reduced as more openings are made on it, making it more pliable, hence deflecting is larger under loading. At the same time, greater flexibility along with localized stress concentrations at the openings damages the integrity of beams. Therefore, these observations show that opening size has substantial effects on beam behavior, requiring proper design to optimize load carrying power against deformation.

### 4.9.2 Effect of Opening Size on Initial Stiffness

The present analysis evaluated the influence of different sizes of transverse holes on the initial stiffness of composite beams. The initial stiffness of five beams having (50×50) mm, (70×70) mm, (90×90) mm, (110×110) mm and (136×136) mm size transverse openings was investigated. The results indicated that there was a consistent decrease in the initial stiffness with an increase in the size of the opening. In particular, the initial stiffness reduced by about 6.52% from beam BW1 (50 × 50 mm) to beam BOS1 (70 × 70 mm), as well as 26.09%, 34.78%, and 36.96% from beam BOS1 to beam BOS2 (90 × 90 mm), from beam BOS2 to beam BOS3 (110 × 110 mm), and finally from beam BOS3 to beam BW2 (136 × 136 mm). Such findings have shown that the initial stiffness of a beam may be greatly diminished by larger transverse openings hence revealing how opening sizes affect structural behavior. This study, therefore, highlights the need for opening dimensions consideration in beam design to achieve adequate stiffness and structural safety. Figure 4.28 shows the distribution of initial stiffness between beam models and the effect of the transverse opening size on the initial stiffness.

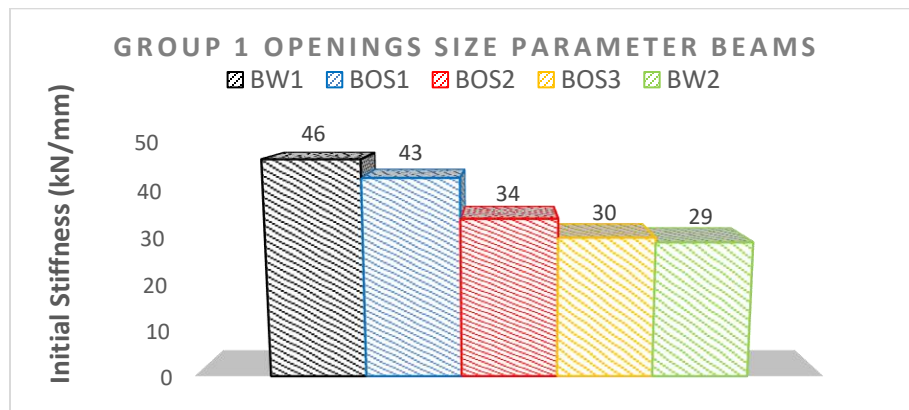


**Figure 4.28:** Initial Stiffness of Opening Size Parameter in Group 1.

### 4.8.1 Effect of Opening Size on Energy Absorption Capacity

This parameter examines characteristics of energy absorption in composite beams of different sizes transverse openings. Five beams were analyzed, each having varying dimensions of openings: BW1 (50×50 mm); BOS1 (70×70 mm); BOS2 (90×90 mm); BOS3 (110×110 mm); and BW2 (136×136 mm). The energy absorption values observed were, respectively, 3239 kN.mm for BW1; 4258 kN.mm for BOS1; 3452 kN.mm for BOS2; 3306 kN.mm for BOS3; and 2238 kN.mm for BW2. The results showed a mixed performance trend: Beam BW1 to BOS1 exhibited a 23.93% increase in energy absorption while there was an 6.17% increase when comparing BW1 to BOS2, followed by a little increase of 2.03% from BW1 to BOS2, whereas from BW1 to BW2 it had its highest decrease of 30.90%. These findings indicate how the increased opening sizes affect the energy absorption capacity of composite beams, suggesting that smaller openings may slightly enhance energy absorption, but large ones tend to cause serious impairment on their structural capability. As shown in Figure 4.29.

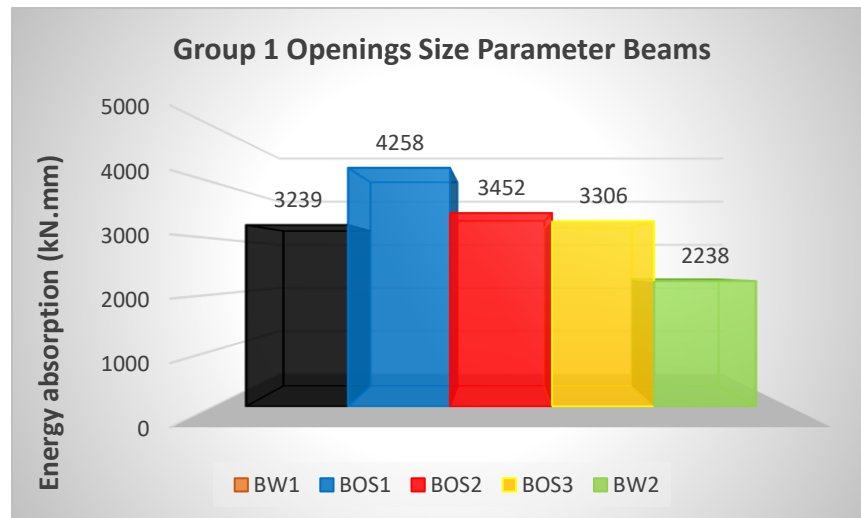


**Figure 4.29:** Energy absorption of Opening Size Parameter in Group 1.

## 4.9 Opening Shape Parameter

### 4.9.1 Effect of Opening Shape on Ultimate Shear Strength

The purpose of this investigation is to evaluate how the size and shape of round holes affect the way beams work by analyzing five different types of models having round openings size that vary. (BOD1, BOD2, BOD3, BOD4, and BOD5) are some of them. The diameter for the circular openings varies from (50 mm) until about (136 mm). The aim herein lies on understanding how an increase in circular opening dimensions influences the shear behavior of beams as well as other structural attributes like deflection at its peak value or respective stiffness. Performance features helped us communicate opening dimensions, which we compared in these models such that strength-flexibility trade-offs used for design improvement were realized within them. Ultimate shear strength, maximum deflection, initial stiffness, and energy absorption have all been evaluated for each beam model included in these results, as presented below in Figure 4.32 and Table (4-4). These analyses throw light on how size and shape of circular openings affect structural performance of beams, thus enhancing our understanding of difficulties tied with designing beams to include openings while providing guidelines for enhancing performance in actual usage.

**Table (4-4):** Model's Results for Group 2 of the composite beams.

Beam with opening (mm)	Ultimate Shear Load (kN)	Yild Shear Load (kN)	Ultimate Deflection (mm)	Yild Deflection (mm)	Ductility Index	Initial Stiffness (kN/mm)	Energy Absorption (kN.mm)
<b>BOD1 (Ø50)</b>	<b>293</b>	<b>165</b>	<b>14.4</b>	<b>3.6</b>	<b>4.0</b>	<b>46</b>	<b>3120</b>
<b>BOD2 (Ø70)</b>	<b>258</b>	<b>150</b>	<b>14.3</b>	<b>3.4</b>	<b>4.2</b>	<b>44</b>	<b>2795</b>
<b>BOD3 (Ø90)</b>	<b>226.10</b>	<b>130</b>	<b>15.65</b>	<b>3.2</b>	<b>4.9</b>	<b>41</b>	<b>2700</b>
<b>BOD4 (Ø110)</b>	<b>201.60</b>	<b>120</b>	<b>14.80</b>	<b>3.2</b>	<b>4.6</b>	<b>38</b>	<b>2321</b>
<b>BOD5 (Ø136)</b>	<b>186.25</b>	<b>95</b>	<b>16</b>	<b>2.8</b>	<b>5.7</b>	<b>34</b>	<b>2423</b>

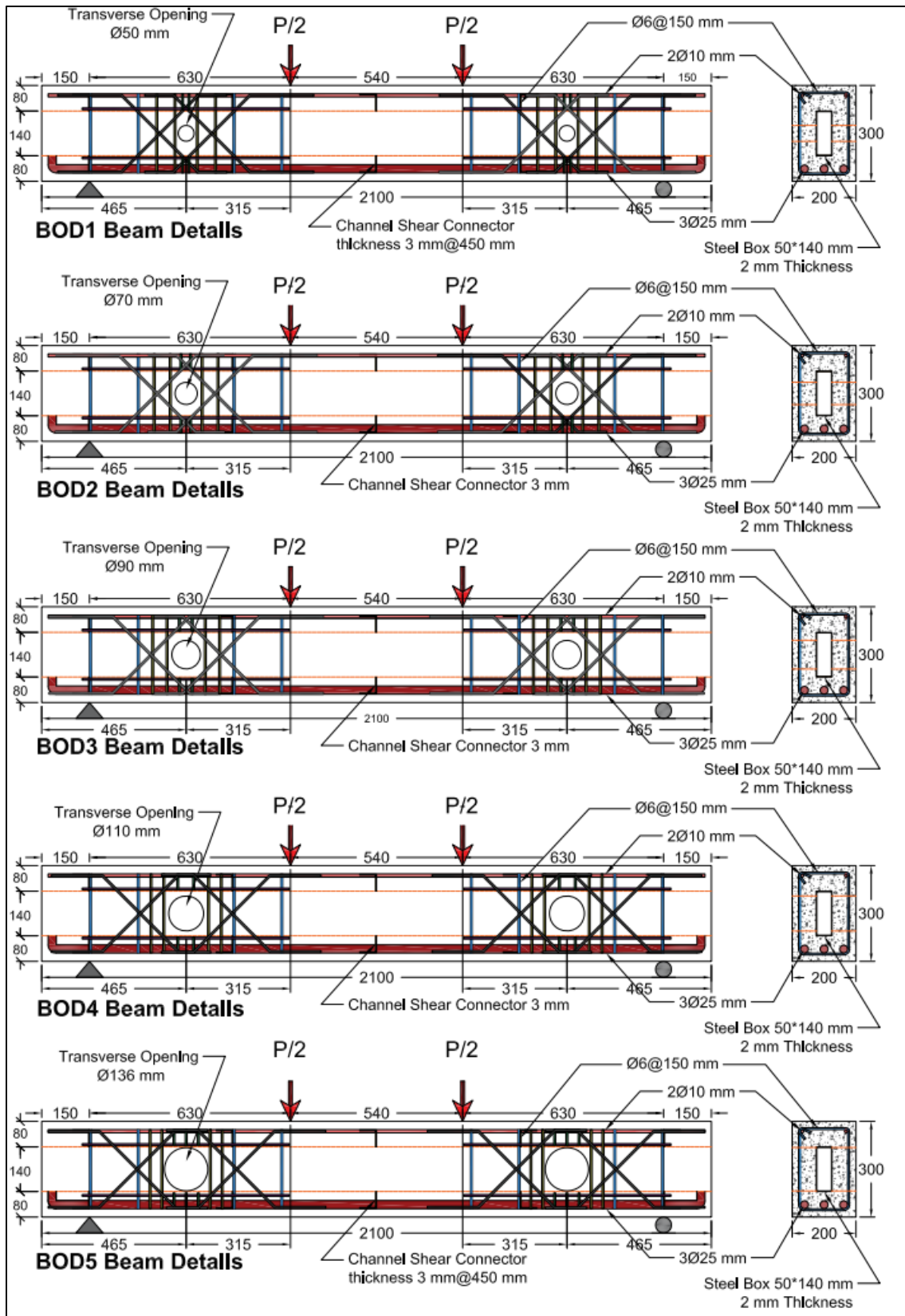
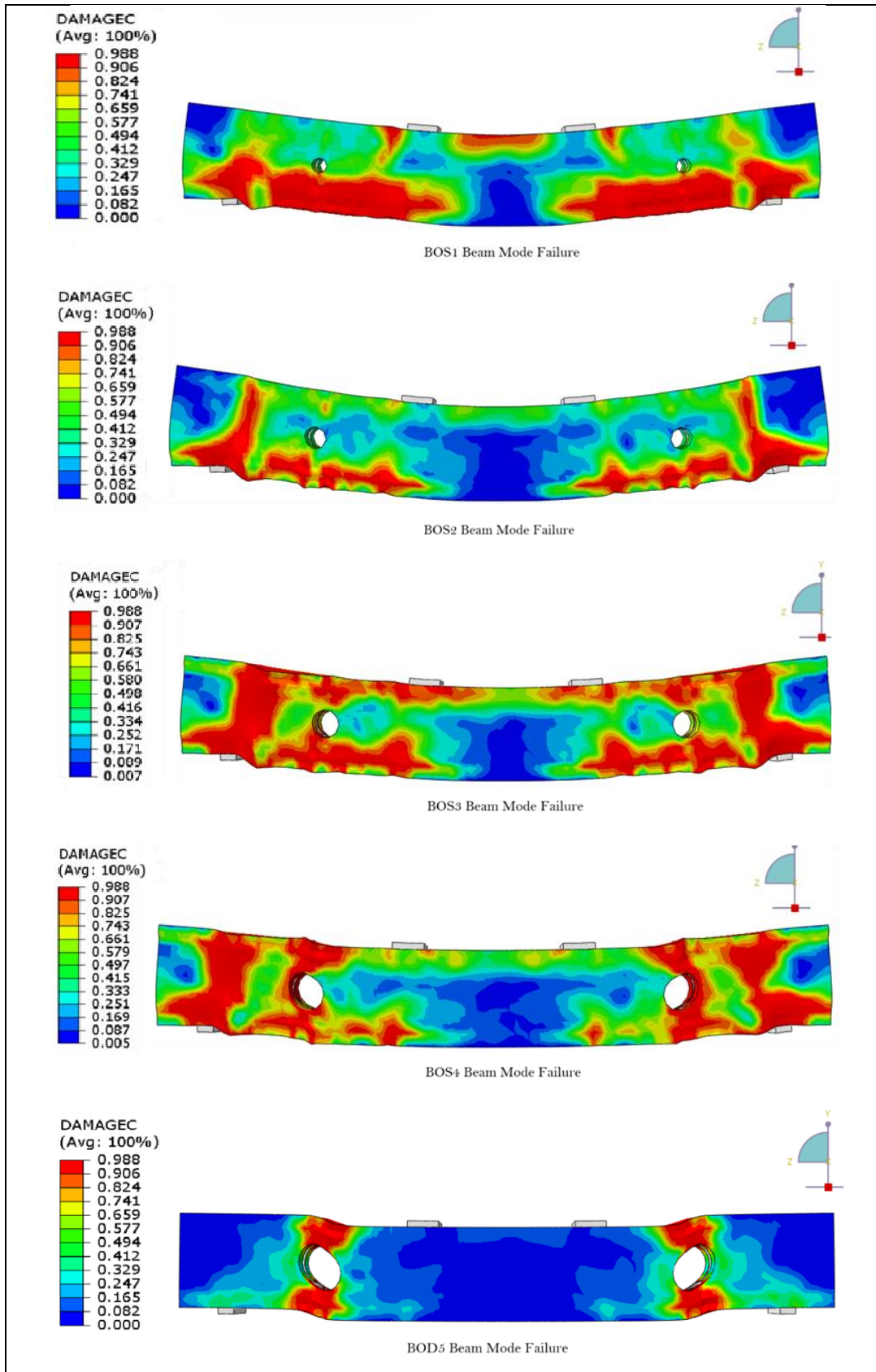
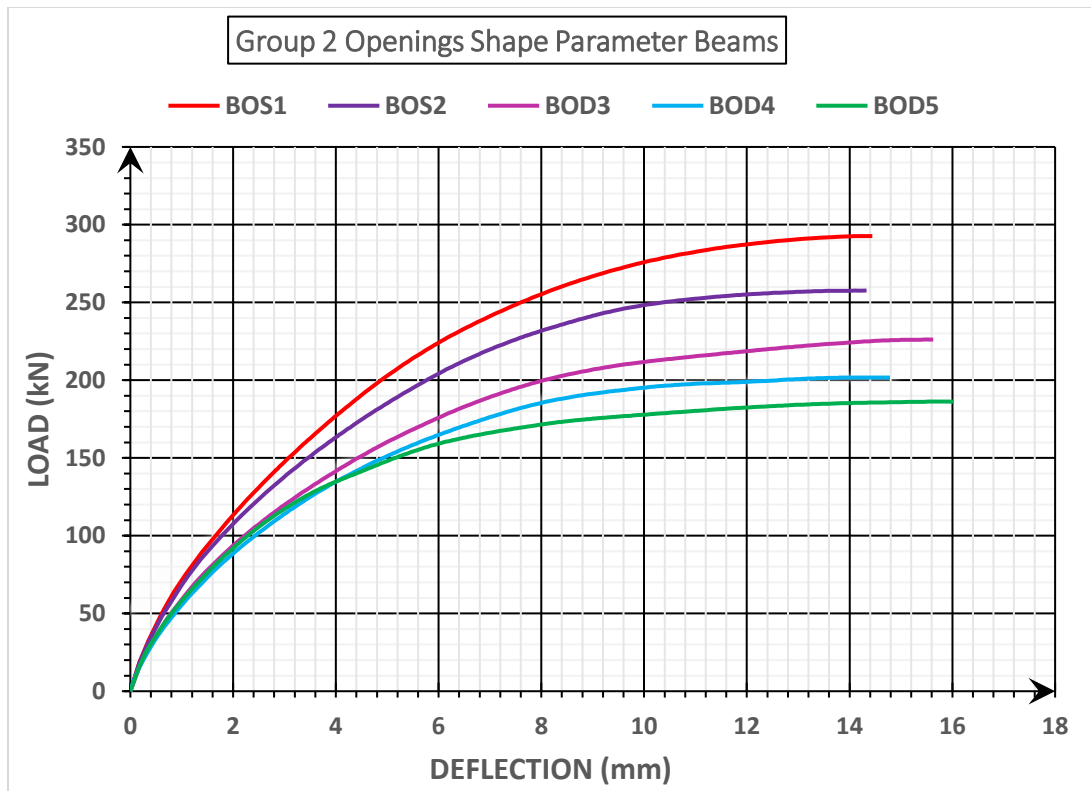


Figure 4.30: Details of Beams of Opening Shape Parameter in Group 2.



**Figure 4.31:** Mode Failure of Opening Shape Parameter in Group 2.



**Figure 4.32:** Load Deflection Curve of Opening Shape Parameter in Group 2.

This parameter investigation examines how the circular transverse openings influence the final shear load and deflection features of composite simple supports beams. With growing diameters in circular punches, shear load capacity trends downward consistently. A 50 mm opening in beam BOD1 provides ultimate shear strength of 293 kN implying less or no effect by smaller openings. However, it is observed that when the diameter is raised to 70 mm on beam BOD2, shearing strength tends to drop by approximately 11.95 percentage points at 258 kN. This behavior continues in beam BOD3 where shearing capacity decreases further to about 22.83 percent reaching 226.1 kN when enlarged up to 90 mm across. On beam BOD4 whose diameter stands at 110 mm shearing force falls again by 17.39 percent at 201.6 kN while on beam BOD5 with the widest opening measuring 136 mm minimum value of shear force recorded was 186.25 kN which is a decreased of around 26.09 percent when compared to the 50mm diameter opening BOD1 beam.



Larger openings are normally associated with greater deflection since there can be seen here the joint action of reducing section strength and stiffness.

In contrast to square openings of similar dimensions, circular openings usually result in smaller shear capacity reductions as well as deflections. Except for the large opening, the circular has a higher shear strength than the square, which is mainly because it causes a uniform stress distribution and less local stress concentration and the presence of the encased steel box inside the beam along its length, which affects the shear strength and stress distribution.

#### **4.9.2 Effect of Opening Shape on Initial stiffness**

The initial stiffness of beams varies depending on the proportion of round holes which have different diameters. For this analysis, five different kinds of beams were used with round holes that had diameters varying between 50 mm and 136 mm. The results indicated a definite trend whereas the size of the holes increased, stiffness decreased in an initial manner. It was observed that for the beam BOD1 (50 mm) to beam BOD2 (60 mm) there was a drop in initial stiffness of about 4.35%, for beam BOD1 (50 mm) to beam BOD3 (75 mm) it was 10.87%, from beam BOD1 (50 mm) to beam BOD4 (90 mm) it was 17.39% and from beam BOD1 (50 mm) to beam BOD5 (136 mm) there was an approximate reduction of 26.09%.

Moreover, beams structural behavior is greatly influenced by the shape of openings on them because stress tends to be unevenly distributed in comparison with rectangular or square openings although they do spur some stress concentrations that diminish stiffness. Since large round openings make these stress concentrations larger; this results into a notable decrease in beams' capability to resist initial loads. Hence, when designing beams, one must focus on both size and shape as such larger more circular openings can really damage their structure functionally. As such, it is

necessary to carefully consider these elements if required stiffness is to be achieved besides keeping structure soundness intact. As shown in the figure 4.33.

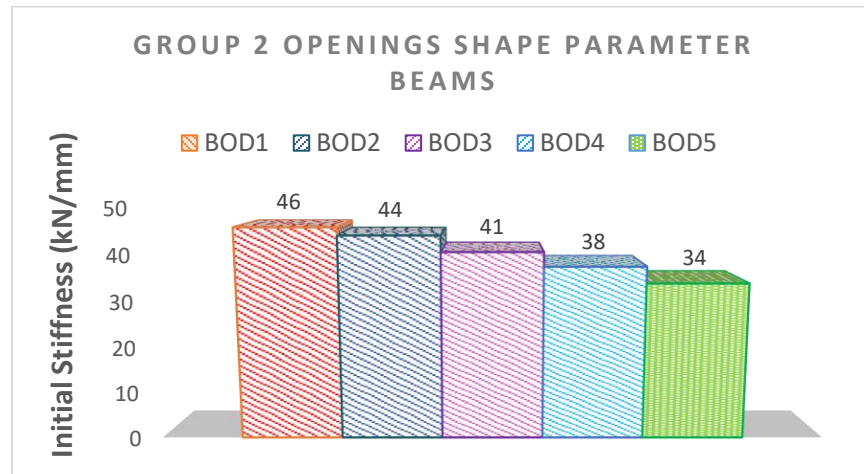


**Figure 4.33:** Initial Stiffness of Opening Shape Parameter in Group 2.

#### 4.9.3 Effect of Opening Shape on Energy Absorption Capacity

This parameter investigates the impact of round hole size and shape on energy absorption of beams by examining five different models with varying hole diameters: BOD1 (50 mm), BOD2 (70 mm), BOD3 (90 mm), BOD4 (110 mm) and BOD5 (136 mm). The recorded energy absorption values were 3120 kN.mm for BOD1, 2795 kN.mm for BOD2, 2700 kN.mm for BOD3, 2321 kN.mm for BOD4 and 2423 kN.mm for BOD5. It is apparent from the results that as the diameter of the round holes increases, so does the decrease in beam energy absorption capacity. Specifically, an energy absorption decreases of 10.43% was observed in BOD2 relative to that of BOD1 whereas BOD3 shows a decrease of 13.48% with respect to BOD1; on its part, BOD4 exhibited an 25.61% drop compared to BOD1 while there was a marginal 22.33% reduction between BOD5 and BOD1 hole sizes.

These findings reveal how hole shape significantly affects beam performance. Increased sized round holes results to diminished energies absorption ability by

beams thus indicating structural integrity loss as hole size increases. It further goes ahead to point out that when designing beams for optimal performance; it is very important to consider both opening sizes and forms since there will be reduced energies' absorption. This study suggests that even though bigger openings can bring down structural strength understanding their effects is helpful in achieving balance between design requirements and structural capabilities. Figure 4.34 show the effect of size and shape of transverse openings on energy absorption of beams.

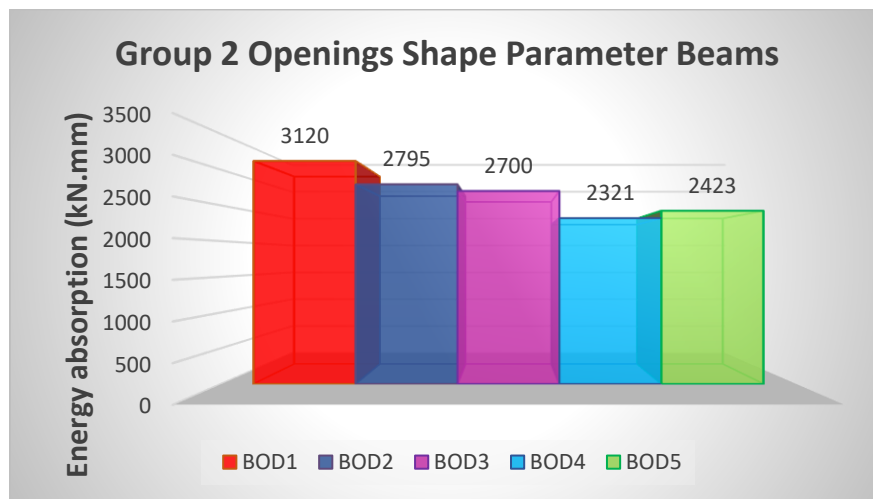


**Figure 4.34:** Energy absorption of Opening Shape Parameter in Group 2.

## 4.10 Opening Location Parameter

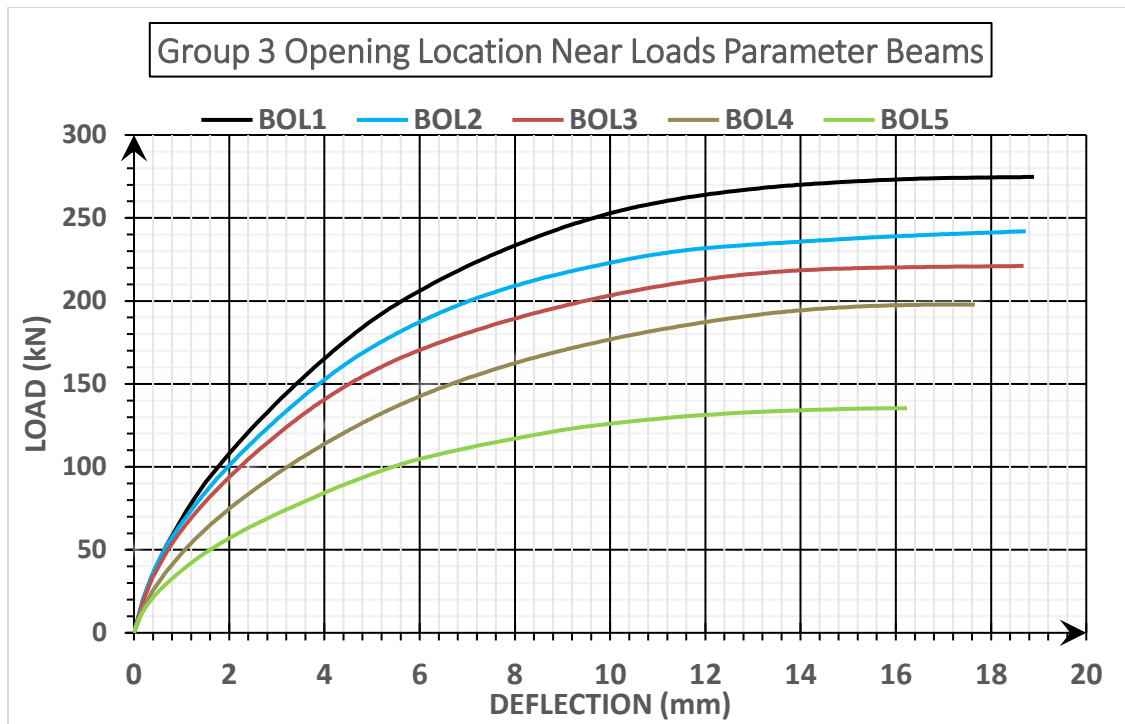
### 4.10.1 Effect Opening Location on Ultimate Shear Strength

The existence of the opening through the beam and in transvers axis in the beam significantly lowers the compression and tensile strengths, which lowers the flexural and shear resistance. This study aims to examine the optimum position that give a better shear force. Ten composite beams; with square two openings (50\*50, 70\*70, 90\*90, 110\*110 and 136\*136mm), near the loads by  $(a/5)$  equal to 126 mm (BOL1, BOL2, BOL3, BOL4 and BOL5), and beams with square two openings (50\*50,

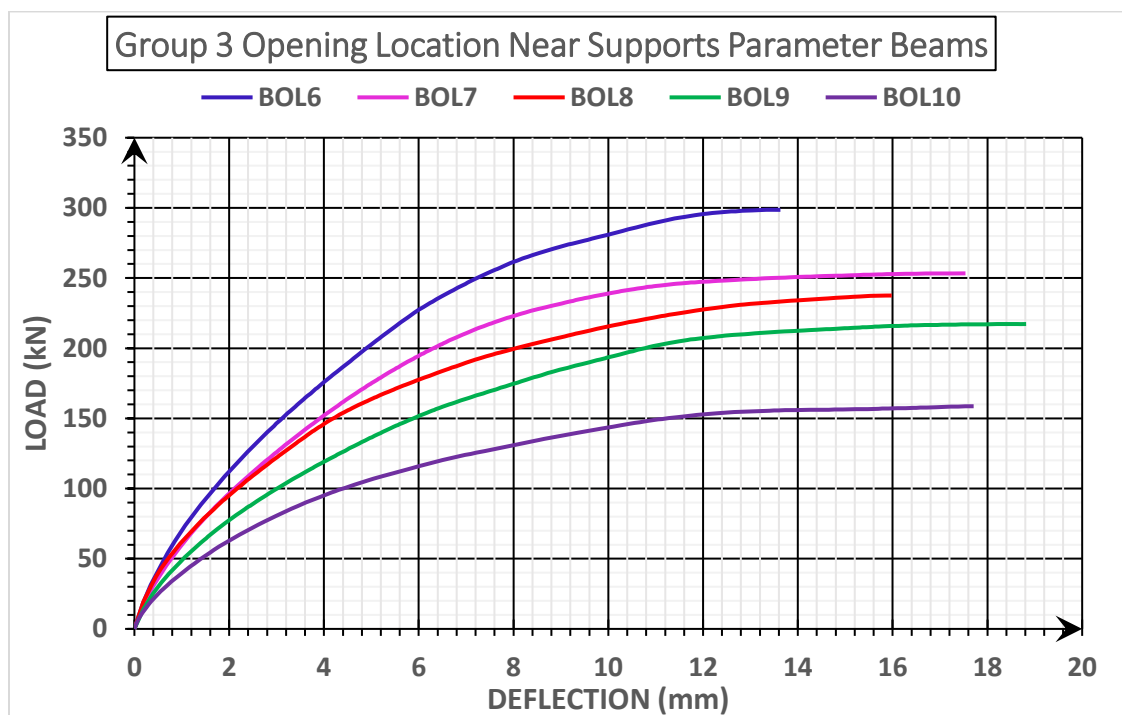
70\*70, 90\*90, 110\*110 and 136\*136mm) near supports by (a/5) equal to 126 mm (BOL6, BOL7, BOL8, BOL9 and BOL10). Results and explanations of the dimension of openings and locations are shown in Table (4-2). And the results presented below Figure 4.35 and Table (4-5).

**Table (4-5):** Model's Results for Group 3 of the composite beams.

Beam with opening (mm)	Ultimate Shear Load (kN)	Yild Shear Load (kN)	Ultimate Deflection (mm)	Yild Deflection (mm)	Ductility Index	Initial Stiffness (kN/mm)	Energy Absorption (kN.mm)
<b>BOL1 (50x50)</b>	<b>275</b>	<b>180</b>	<b>18.9</b>	<b>4.5</b>	<b>4.2</b>	<b>40</b>	<b>4100</b>
<b>BOL2 (70x70)</b>	<b>242</b>	<b>140</b>	<b>18.75</b>	<b>3.6</b>	<b>5.2</b>	<b>39</b>	<b>3608</b>
<b>BOL3 (90x90)</b>	<b>221</b>	<b>100</b>	<b>18.7</b>	<b>2.4</b>	<b>7.8</b>	<b>42</b>	<b>3301</b>
<b>BOL4 (110x110)</b>	<b>198</b>	<b>100</b>	<b>17.65</b>	<b>3.2</b>	<b>5.5</b>	<b>31</b>	<b>2652</b>
<b>BOL5 (136x136)</b>	<b>135</b>	<b>75</b>	<b>16.25</b>	<b>3.2</b>	<b>5.1</b>	<b>23</b>	<b>1695</b>
<b>BOL6 (50x50)</b>	<b>299</b>	<b>190</b>	<b>13.65</b>	<b>4.4</b>	<b>3.7</b>	<b>43</b>	<b>3649</b>
<b>BOL7 (70x70)</b>	<b>253</b>	<b>160</b>	<b>17.5</b>	<b>4.2</b>	<b>4.2</b>	<b>38</b>	<b>3475</b>
<b>BOL8 (90x90)</b>	<b>238</b>	<b>110</b>	<b>16</b>	<b>2.4</b>	<b>6.7</b>	<b>46</b>	<b>2854</b>
<b>BOL9 (110x110)</b>	<b>217</b>	<b>125</b>	<b>18.8</b>	<b>4.2</b>	<b>4.5</b>	<b>30</b>	<b>3121</b>
<b>BOL10 (136x136)</b>	<b>159</b>	<b>88</b>	<b>17.7</b>	<b>3.2</b>	<b>5.5</b>	<b>28</b>	<b>2161</b>



(a) Load-Deflection Curves of Beams Near Loads Location



(b) Load-Deflection Curves of Beams Near Supports Location

**Figure 4.35:** Load Deflection Curve of Opening Shape Parameter in Group 3.

An analysis of ultimate shear load in beams with square transverse openings shows that there is a pattern where placing the openings nearer to the supports increases the ultimate shear load more than when they are positioned nearer to the loads. Shear load in beams with 50×50 mm openings increase by approximately 6.55% when they are located closer to the supports. This trend continues for beams of similar conditions having 70×70 mm openings, where shear load increases by about 4.55%. On the other hand, when the size of opening increased to 90×90 mm, there was a significant increase in shear load of 7.69% if these were close to the support compared with load. In terms of 110×110 mm openings, there are even greater increases since an ultimate shear now rises by about 9.60%. While positioning the openings near supports cause increases most significant changing in ultimate shear loads observed at largest opening cases 136×136 mm would lead to increase in ultimate shear with support side positioning resulting to 17.78%. Hence it can be said that placing openings near supports as opposed to placing them near load enhances beam's ability to resist shear forces depending on their size.

According to the analysis, it was found that beams with openings placed close to the supports bear larger ultimate shear loads than those with openings positioned close to acting loads, especially in terms of increase in shear load which was more pronounced in terms of size of openings from 6.55% for beams having openings sized 50 mm by 50 mm to 17.78% for beams having openings sized 136 mm by 136 mm. Scientifically speaking, these findings relate to shear force distributions within the beam since shear forces are greatest towards its supports. Such regions consequently expectance disruption in load path leading to higher stresses concentration thereby causing significant decreases in shear capacity. When placed near applied loads on the other hand where there are less shear forces more shear strength is retained by beam thereby enabling it to sustain even heavier ultimate

shear loads compared to those having openings located elsewhere. This indicates the need for consideration of where transversal openings are incorporated when designing beams for instance under high amount of shearing stresses-based structures should pay careful attention on their placement too.

#### **4.10.2 Effect of Opening Location on Initial stiffness**

The analysis presented herein evaluates how the location of transverse openings affects the initial stiffness of composite beams. Ten beams with square openings measuring either 50×50 mm, 70×70 mm, 90×90 mm, 110×110 mm or 136×136 mm was considered; in this case, the openings were positioned either closer to the loads or closer to the supports. The results show that beam stiffness is greatly influenced by where they are located. This is evidenced by the fact that beams whose openings were near their supports generally had a higher initial stiffness than those whose openings were located adjacent to their loads. Specifically, increases in stiffness of 6.98% (BOL6 compared to BOL1), 8.70% (BOL8 compared to BOL3), and 17.86% (BOL10 compared to BOL5), were observed for beams whose openings were located close to their supporting ends. In some cases, however, it resulted into slight decrease in stiffness as shown by decline of 2.56% (BOL7 compared with BOL2) and -3.23 % (BOL9 as opposed to BOL4) when they were at support location. Therefore, such information highlights the significance of proper layout planning for maximum structural performance hence opening placement near support sides often results into increased initial beam rigidity. As shown in Figures 4.36, it can be concluded that regardless of the location of the opening, the transverse opening area can be increased by 325% while holding the initial stiffness constant.

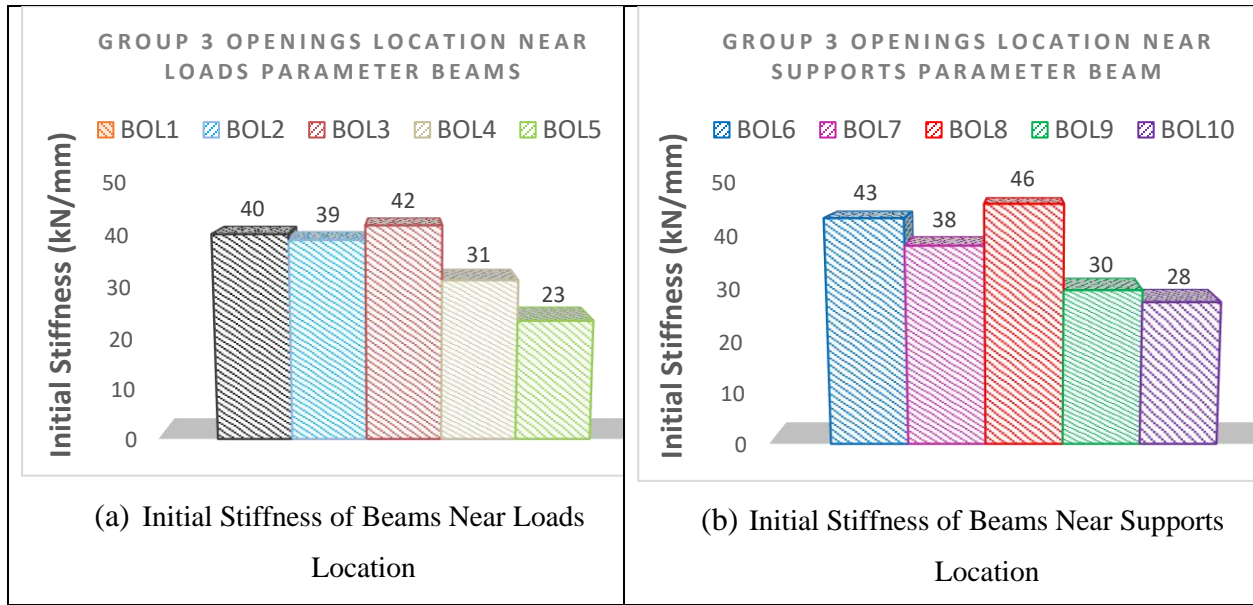


**Figure 4.36:** Initial Stiffness of Opening Location Parameter in Group 2.

### 4.8.3 Effect of Opening Location on Energy Absorption Capacity

These finding studies the effect that location of the opening has on the capacity for energy absorption in composite beams having square traverse spaces. Two different configurations were examined: beams with open ends nearer loads (from BOL1 – BOL5) and those with their ends adjacent to the anchorages (from BOL6 - BOL10). The diameters of the holes were kept constant at either 50mm or 70mm. The recorded energy absorption values ranged from 4100 kN.mm for BOL1 to 1695kN.mm for BOL5 as well as 3649kN.mm for BOL6 up until 2161kN.mm for BOL10. In general, a consistent trend was observed where beams with openings closer to the supports tended to absorb relatively higher energy compared to those with openings closer to the loading points. From BOL1 to BOL6 there was an increase in energy absorption by 11% while it increased by 3.69% from BOL2 to BOL7 and 13.54% when considering BOL3-BOL8; further, we observe a decrease in energy absorption by 15.03% and 21.56% when considering BOL4-BOL9 and BOL5-BOL10 respectively. Therefore, further investigations show that placing openings (holes) closer to the supporting structures enhances the energy absorption



capabilities of these beams for small and medium openings while for large openings, placing them closer to the supports reduces the energy absorption. As shown in Fig. 4.37.

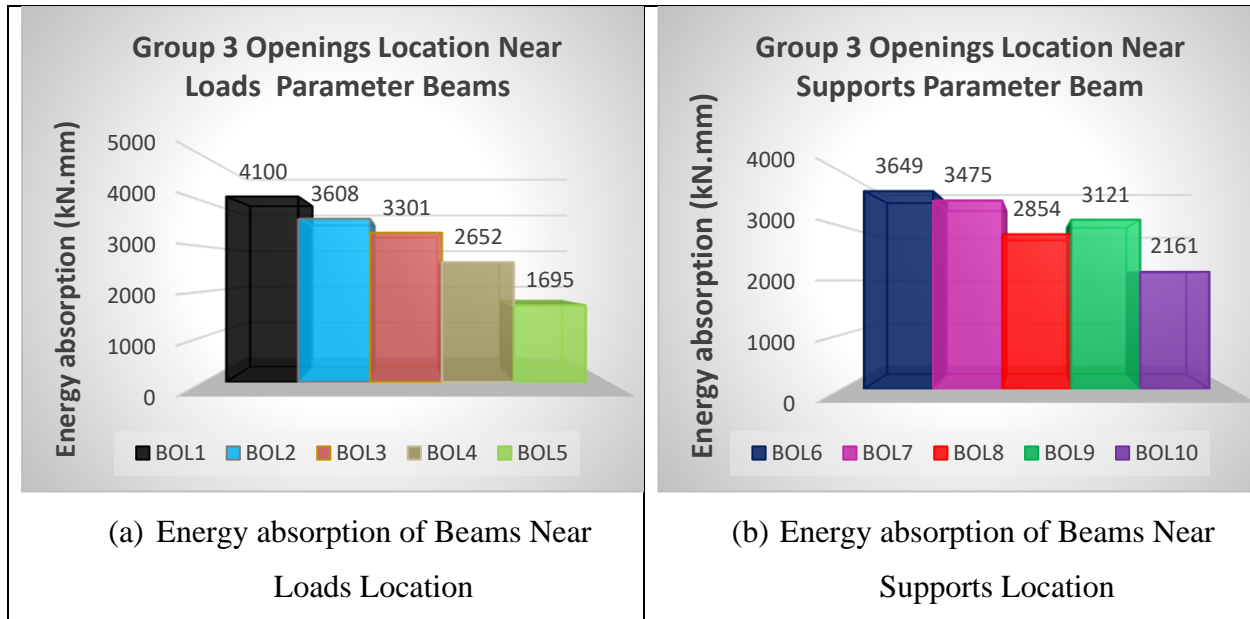


**Figure 4.37:** Energy absorption of Opening Location Parameter in Group 3.

## 4.11 Shear Span-to-Depth Ratio ( $a/d$ ) Parameter

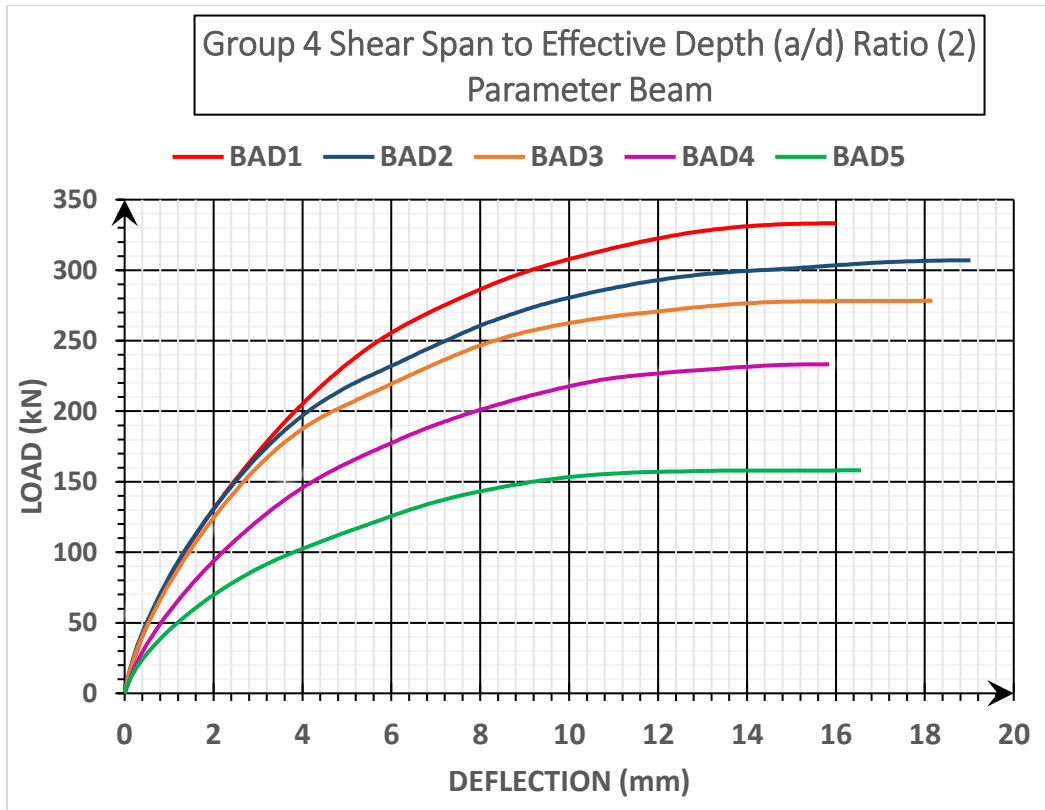
### 4.11.1 Effect of ( $a/d$ ) Ratio on Ultimate Shear Strength

Ten shear span-to-depth ratios ( $a/d$ ) of 2 and 2.8 were considered to inspect section shear resistance and understand various stress distribution modes. Specimens (BAD1, BAD2, BAD3, BAD4, and BAD5) with transverse openings (50\*50, 70\*70, 90\*90, 110\*110, and 136\*136 mm) had an ( $a/d$ ) ratio of 2, while specimens (BAD6, BAD7, BAD8, BAD9, and BAD10) with transverse openings (50\*50, 70\*70, 90\*90, 110\*110, and 136\*136 mm) had an ( $a/d$ ) ratio of 2.8. Table (4-2) provides the geometric descriptions of the adopted specimen sets, and Table (4-6) presents the related results analysis. The analysis in Table (4-6) indicates that varying the shear span alters the stress distribution modes, with ( $a/d$ ) ratios of 2, 2.4 and 2.8, respectively. Figures 4.38 show the load-deflection response for specimens with

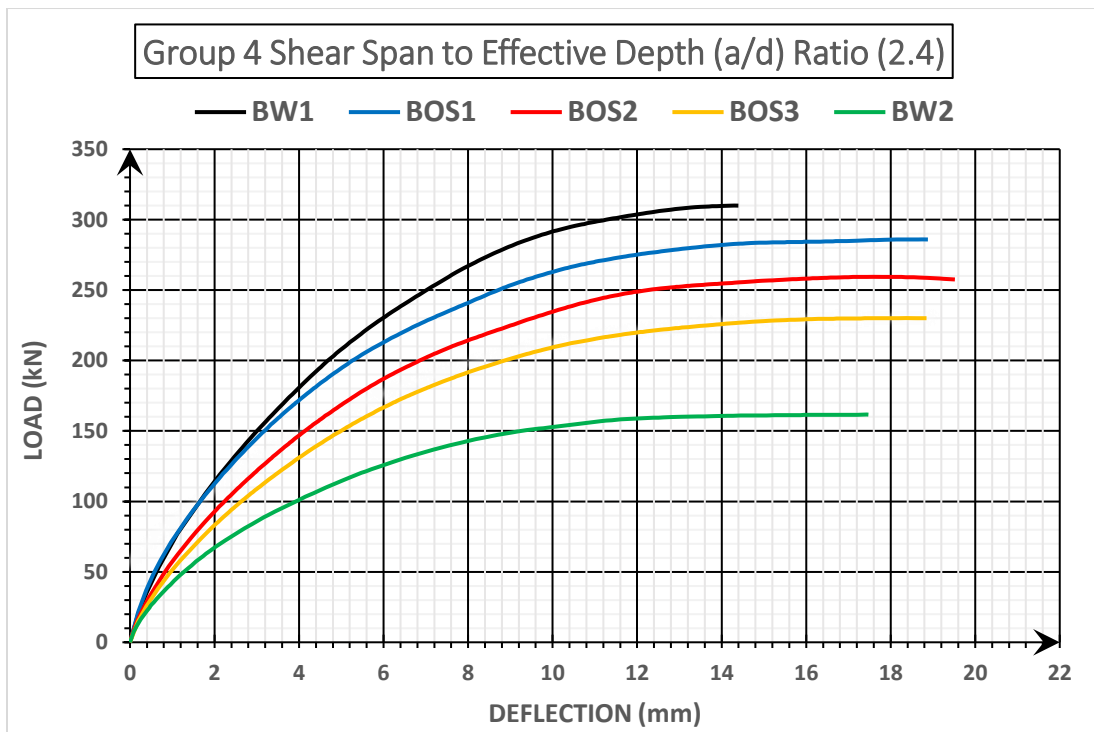
different shear spans. However, as the (a/d) ratio increases, the shear strength decreases.

**Table (4-6):** Model's Results for Group 4 of the composite beams.

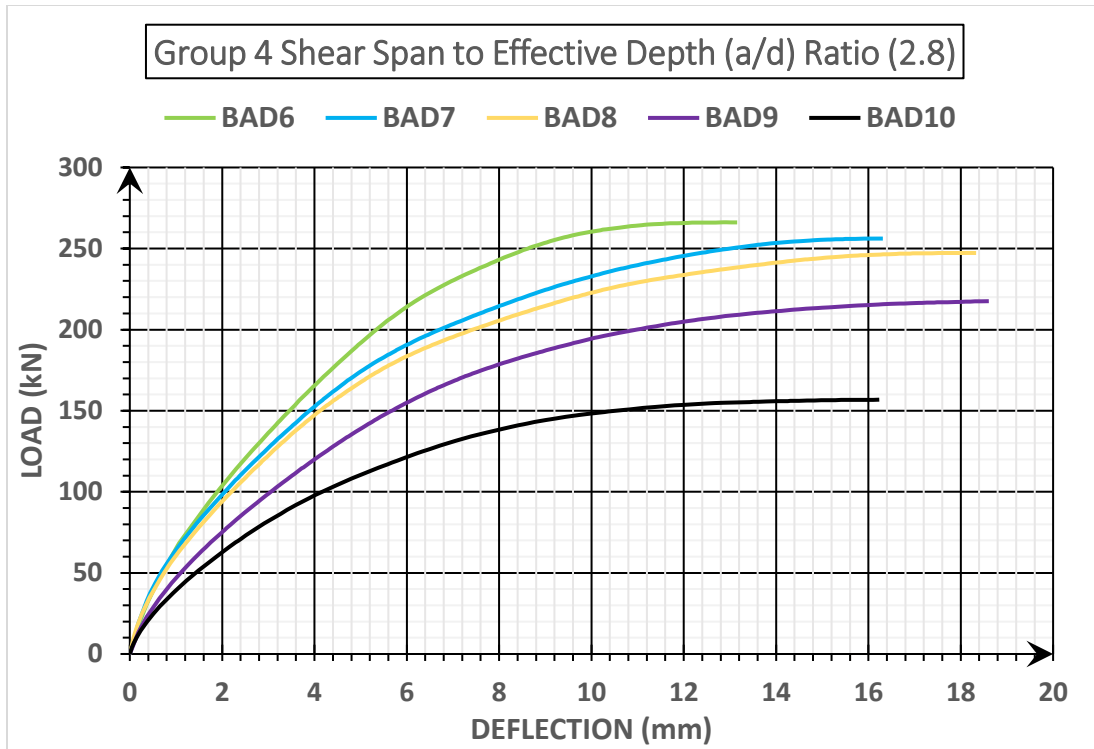
Beam with opening (mm)	Ultimate Shear Load (kN)	Yild Shear Load (kN)	Ultimate Deflection (mm)	Yild Deflection (mm)	Ductility Index	Initial Stiffness (kN/mm)	Energy Absorption (kN.mm)
<b>BAD1 (50x50)</b>	<b>333</b>	<b>210</b>	<b>16</b>	<b>4</b>	<b>4.0</b>	<b>53</b>	<b>4049</b>
<b>BAD2 (70x70)</b>	<b>307</b>	<b>185</b>	<b>19</b>	<b>3.6</b>	<b>5.3</b>	<b>51</b>	<b>4653</b>
<b>BAD3 (90x90)</b>	<b>278</b>	<b>150</b>	<b>18.2</b>	<b>2.8</b>	<b>6.5</b>	<b>54</b>	<b>4093</b>
<b>BAD4 (110x110)</b>	<b>233</b>	<b>140</b>	<b>15.85</b>	<b>3.6</b>	<b>4.4</b>	<b>39</b>	<b>2812</b>
<b>BAD5 (136x136)</b>	<b>158</b>	<b>80</b>	<b>16.6</b>	<b>2.4</b>	<b>6.9</b>	<b>33</b>	<b>2088</b>
<b>BW1 (50x50)</b>	<b>309</b>	<b>190</b>	<b>14.4</b>	<b>4.1</b>	<b>3.5</b>	<b>46</b>	<b>3239</b>
<b>BOS1 (70x70)</b>	<b>286</b>	<b>170</b>	<b>18.9</b>	<b>4</b>	<b>4.7</b>	<b>43</b>	<b>4258</b>
<b>BOS2 (90x90)</b>	<b>259.40</b>	<b>170</b>	<b>17.6</b>	<b>5</b>	<b>3.5</b>	<b>34</b>	<b>3452</b>
<b>BOS3 (110x110)</b>	<b>230.15</b>	<b>150</b>	<b>18.6</b>	<b>5</b>	<b>3.7</b>	<b>30</b>	<b>3306</b>
<b>BW2 (136x136)</b>	<b>161.60</b>	<b>90</b>	<b>17.5</b>	<b>3.1</b>	<b>5.6</b>	<b>29</b>	<b>2238</b>
<b>BAD6 (50x50)</b>	<b>266</b>	<b>165</b>	<b>13.2</b>	<b>4</b>	<b>3.3</b>	<b>41</b>	<b>2576</b>
<b>BAD7 (70x70)</b>	<b>256</b>	<b>140</b>	<b>16.3</b>	<b>3.6</b>	<b>4.5</b>	<b>39</b>	<b>3143</b>
<b>BAD8 (90x90)</b>	<b>247</b>	<b>125</b>	<b>18.35</b>	<b>3.25</b>	<b>5.6</b>	<b>38</b>	<b>3508</b>
<b>BAD9 (110x110)</b>	<b>218</b>	<b>110</b>	<b>18.6</b>	<b>3.6</b>	<b>5.2</b>	<b>31</b>	<b>3080</b>
<b>BAD10 (136x136)</b>	<b>157</b>	<b>75</b>	<b>16.25</b>	<b>2.8</b>	<b>5.8</b>	<b>27</b>	<b>1969</b>



(a) Load-Deflection Curves of Beams with Shear Span to Effective Depth (a/d) Ratio (2)



(b) Load-Deflection Curves of Beams with Shear Span to Effective Depth (a/d) Ratio (2.4)



(c) Load-Deflection Curves of Beams with Shear Span to Effective Depth ( $a/d$ ) Ratio (2.8)

**Figure 4.38:** Load Deflection Curve of Opening Shape Parameter in Group 4.

When beams have different shear span-to-depth ratios ( $a/d$ ) of 2, 2.4 and 2.8, analyses of the final shear load show that there is a decrease in shear capacity whenever the ( $a/d$ ) ratio is increased. For the case of beams with small transverse openings ( $50 \times 50$  mm), a rise from  $a/d=2$  to  $a/d=2.4$  causes about 7.21% decrease in ultimate shear loads indicating that longer shear spans greatly affect the resistance of beams against shear forces. For larger openings such as  $70 \times 70$  mm and  $90 \times 90$  mm openings, however, ultimate shear loads only decrease by 21% and 6.69% respectively when compared to the larger ratio for the same opening size.

Parallely, at last if the opening size is increased further up to about 110 on 110 mm, then it results into a little reduction of approximately 1.22% on ultimate shear load and 2.23% for 136 by 136 mm sizes. From this trend, we can say that an increase in ( $a/d$ ) ratio has less influence on shear strength as span length increases because size

of more significant voids will have already compromised stability of beams and therefore impacts due to span length would be negligible. Overall findings are true; narrow-beamed situations are more sensitive to span-depth changes leading to greater reductions when considering the greatest load-bearing capacities.

And for increasing the ratio from  $a/d=2.4$  to  $a/d=2.8$  for the case of beams with small transverse openings ( $50\times 50$  mm), the height causes a decrease in the ultimate shear loads by about 13.92%. For larger openings such as  $70\times 70$  mm and  $90\times 90$  mm openings, the ultimate shear loads are reduced by only 10.49% and 4.78% respectively, at last if the opening size is increased further up to about 110 on 110 mm, then it results into a reduction of approximately 5.28% on ultimate shear load and little reduction of 2.85% for  $136$  by  $136$  mm sizes when compared to the larger ratio for the same opening size.

Through an examination of how increased shear spans reduce stress on and cause failure in beams, we find the scientific rationale behind these outcomes. Furthermore, smaller openings increase stress concentration while being more influenced by alterations of  $(a/d)$  ratio; in contrast, larger ones have already affected inbuilt beam structure hence there is no change when span-length is raised.

#### **4.11.2 Effect of Shear Span to Effective Depth on Initial stiffness**

This parameter centers around shear span-to-depth ratio  $(a/d)$  force of composite beams on initial stiffness. Beams with multiple transverse openings such as  $50\times 50$  mm,  $70\times 70$  mm,  $90\times 90$  mm,  $110\times 110$  mm and  $136\times 136$  mm. were studied under two different ratios of  $a/d$ : 2 and 2.8. The experimental results showed that increase in  $(a/d)$  resulted in reduced initial stiffness. Thus when compared to those where  $a/d=2$ , beams having  $(a/d=2.8)$  had their stiffness decreased by 18.18% to 29.63%. For instance, BAD6 ( $a/d=2.8$ ) presented lower beam rigidity than BAD1

( $a/d=2$ ) by 22.64%, BAD7 declined stiffness against BAD2 by 23.53%, BAD8 on its part dropped it relative to BAD3 by 29.63%, BAD9 lost this property compared to BAD4 by 20.51% while on the other hand; BAD10 showed higher than this ratio about BAD5 by 18.18%. This consistent reduction in stiffness with a higher ( $a/d$ ) ratio suggests that increasing the shear span relative to the depth of the beam results in greater flexibility and reduced resistance to initial loads. The findings underscore the importance of considering the shear span-to-depth ratio in beam design, as a higher ratio can lead to decreased structural stiffness and performance. The Figures 4.39 shows the effect shear span to effective depth on initial stiffness. It can be concluded from the results that the transverse opening area increases by up to 324% while maintaining the same initial stiffness. Also, in large transverse openings, the initial stiffness value decreases by 60% compared to small openings.

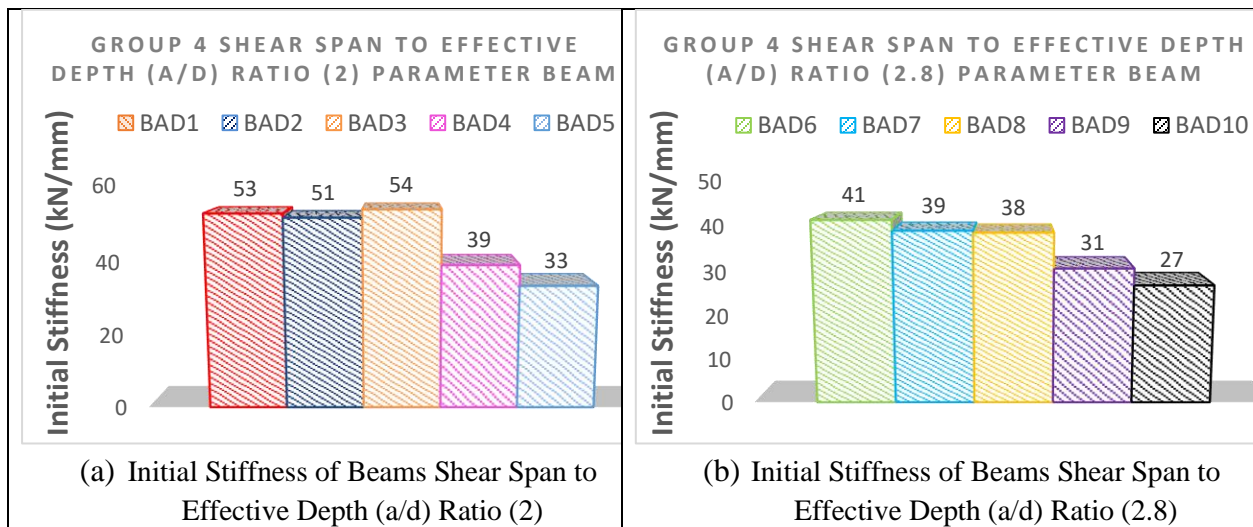


**Figure 4.39:** Initial Stiffness of Shear Span to Effective Depth Parameter in Group 4.

#### 4.8.4 Effect of Shear Span to Depth Ratio on Energy Absorption Capacity

Through this analysis, the role of shear span-to-depth ratios ( $a/d$ ) in the energy absorption for composite beams whose transverse openings differ has been examined. Two shear span-to-depth ratios were analyzed: 2 and 2.8. The two beam groups were compared according to their energy absorption capabilities; BAD1 to

BAD5 representing the beams with a ratio of 2 while BAD6 to BAD10 stands for those with 2.8 ratio. It can be observed that increase in shear span-to-depth ratio decreases energy absorption. In fact, for beams having a ratio of 2, energy absorption is higher than that of those having a ratio of 2.8. For example, Beam BAD1 ( $a/d$ ) = 2 absorbs 36.38% more energy than Beam BAD6 ( $a/d$ ) = 2.8 while Beam BAD2 shows a 32.45% increase compared to Beam BAD7. The downward trend in energy absorption is also seen in BAD3 which absorbs 14.29% more energy than BAD8, While BAD4 with an absorption that was 8.7% lower than BAD9's value respectively. The least decreasing between them is seen between BAD5 and BAD10 with just 5.7% decrease. These findings provide evidence that the shear span-to-depth ratio affects negatively on beams' ability to resist towards shear forces thereby impacting their structural performance, and the Figures 4.40 show the effect of Shear Span to Effective Depth Ratio on Energy Absorption Capacity.

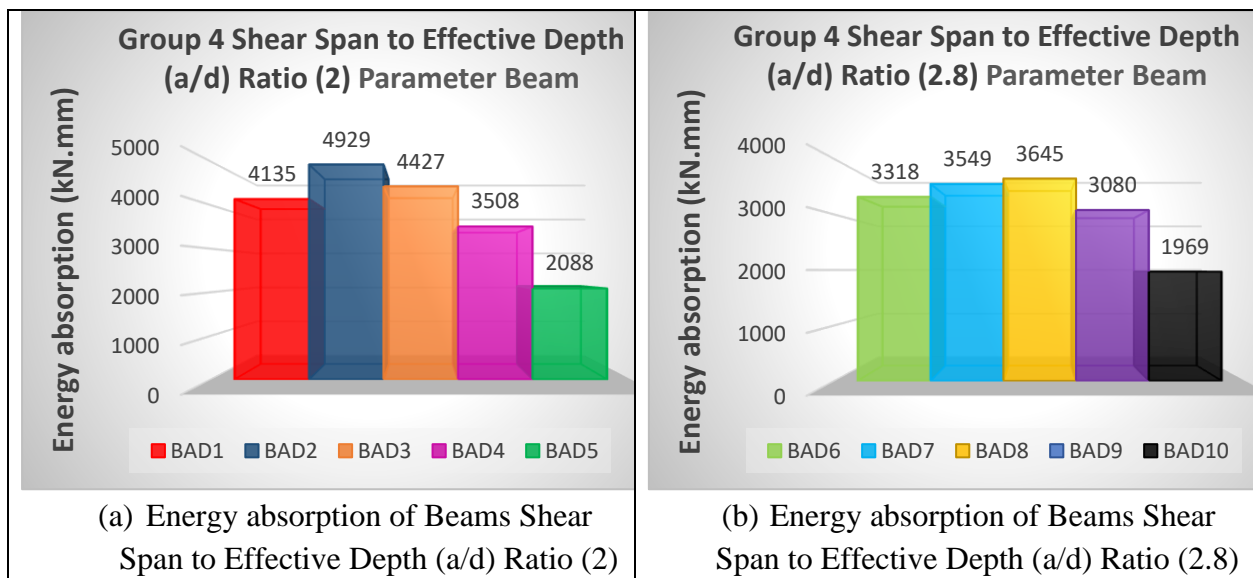


**Figure 4.40:** Energy absorption of Shear Span to Effective Depth Ratio Parameter in Group 4.

## 4.12 Compressive Strength of Concrete Parameter

### 4.12.1 Effect of Compressive Strength of Concrete on Ultimate Shear Strength

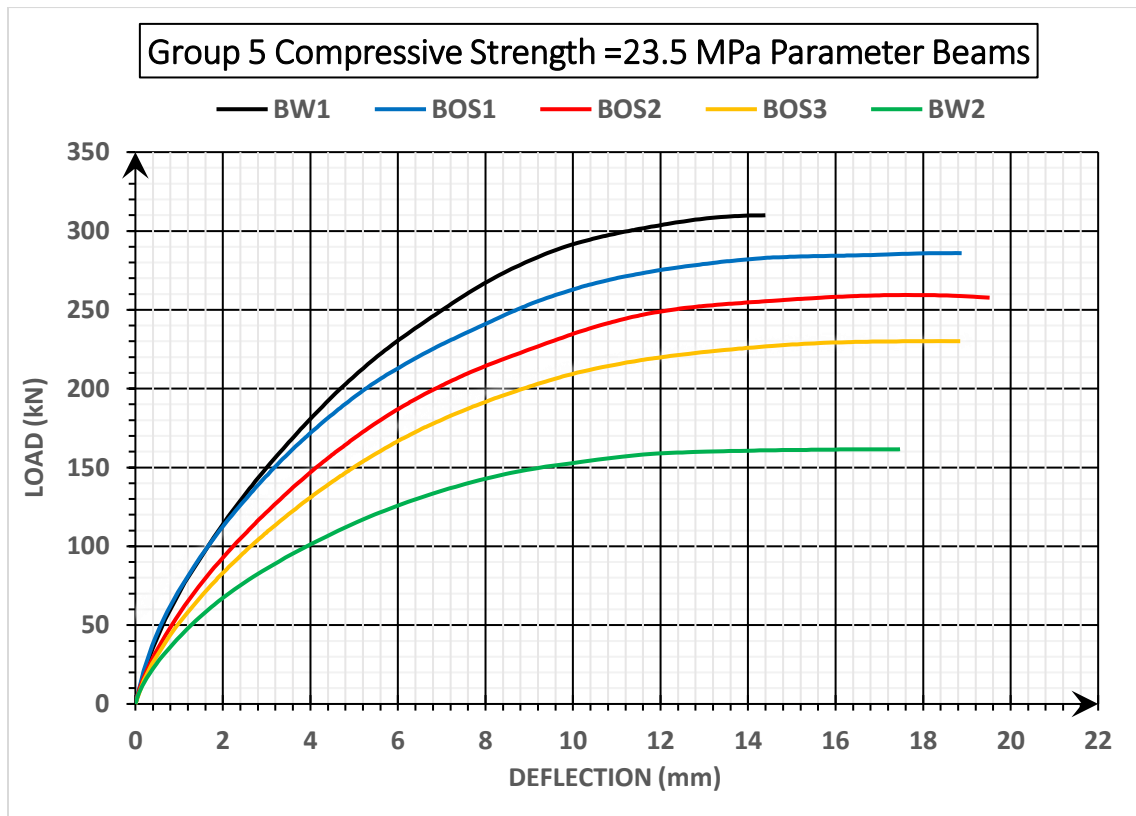
Different compressive strength of concrete condition is considered to inspect their effect on shear strength, ductility of the developed composite beam. Dimension, shape of openings and its location are geometry details of adopted specimens which are explained in the Table (4-2), Ten compressive strength of concrete ( $f'_c$ ) of 30 and 37.5 MPa were considered to inspect section shear resistance and understand various stress distribution modes. Specimens (BFC1, BFC2, BFC3, BFC4, and BFC5) with transverse openings (50\*50, 70\*70, 90\*90, 110\*110, and 136\*136 mm) had an ( $f'_c$ ) of 30 MPa, while specimens (BFC6, BFC7, BFC8, BFC9, and BFC10) with transverse openings (50\*50, 70\*70, 90\*90, 110\*110, and 136\*136 mm) had an ( $f'_c$ ) of 37.5 MPa, Specimens in the first group (BW1, BOS1, BOS2, BOS3, and BW2) with the same transverse opening dimensions and compressive strength of concrete ( $f'_c$ ) of 23.5 MPa were added for comparison. While Table (4-7) exhibits the related results. Figures 4.41 clearly depicts the various aspects of compressive strength of concrete on shear strength-deflection response.

**Table (4-7): Model's Results for Group 5 of the composite beams.**

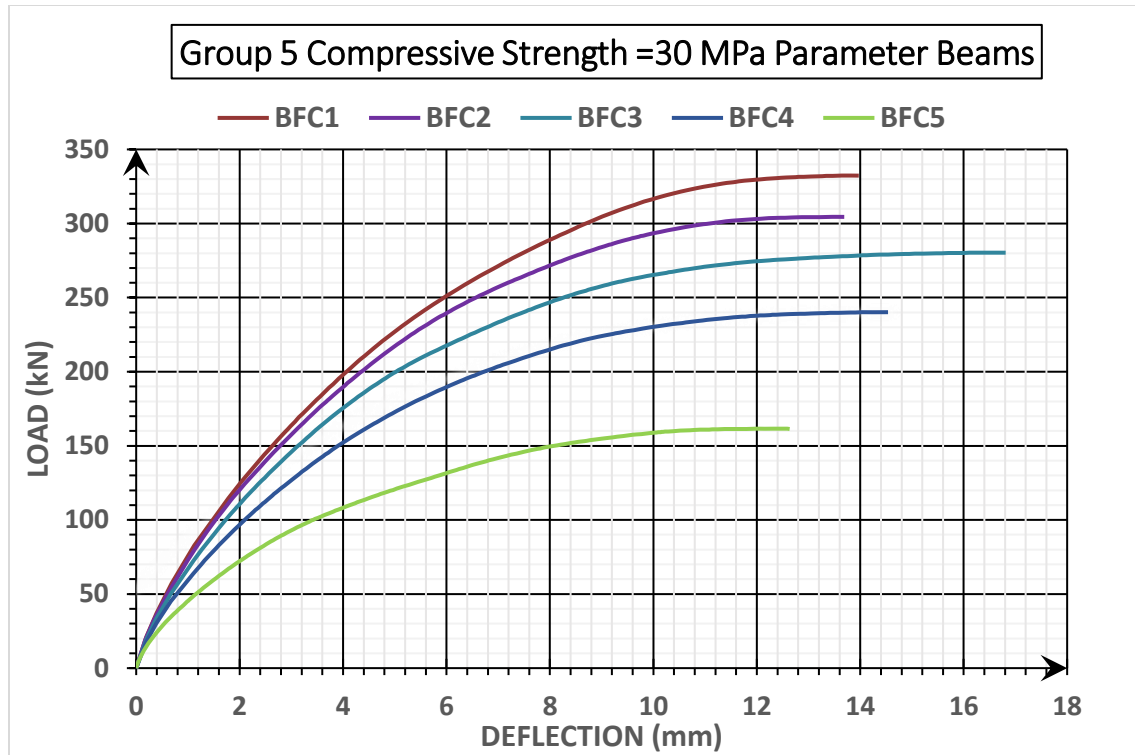
Beam with opening (mm)	Ultimate Shear Load (kN)	Yild Shear Load (kN)	Ultimate Deflection (mm)	Yild Deflection (mm)	Ductility Index	Initial Stiffness (kN/mm)	Energy Absorption (kN.mm)
<b>BW1 (50x50)</b>	<b>309</b>	<b>190</b>	<b>14.4</b>	<b>4.1</b>	<b>3.5</b>	<b>46</b>	<b>3239</b>
<b>BOS1 (70x70)</b>	<b>286</b>	<b>170</b>	<b>18.9</b>	<b>4</b>	<b>4.7</b>	<b>43</b>	<b>4258</b>
<b>BOS2 (90x90)</b>	<b>259.40</b>	<b>170</b>	<b>17.6</b>	<b>5</b>	<b>3.5</b>	<b>34</b>	<b>3452</b>
<b>BOS3 (110x110)</b>	<b>230.15</b>	<b>150</b>	<b>18.6</b>	<b>5</b>	<b>3.7</b>	<b>30</b>	<b>3306</b>
<b>BW2 (136x136)</b>	<b>161.60</b>	<b>90</b>	<b>17.5</b>	<b>3.1</b>	<b>5.6</b>	<b>29</b>	<b>2238</b>



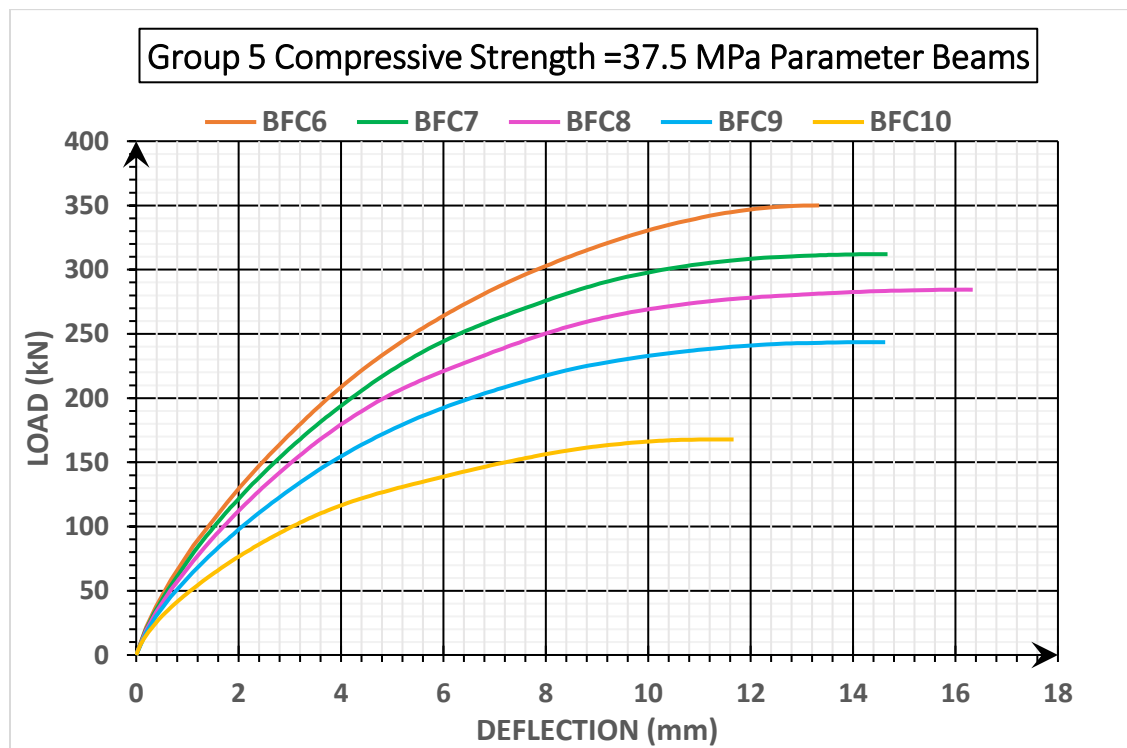
<b>BFC1 (50x50)</b>	<b>332</b>	<b>210</b>	<b>14</b>	<b>4.2</b>	<b>3.3</b>	<b>50</b>	<b>3374</b>
<b>BFC2 (70x70)</b>	<b>304</b>	<b>185</b>	<b>13.7</b>	<b>3.8</b>	<b>3.6</b>	<b>49</b>	<b>3078</b>
<b>BFC3 (90x90)</b>	<b>280</b>	<b>165</b>	<b>16.8</b>	<b>3.6</b>	<b>4.7</b>	<b>46</b>	<b>3676</b>
<b>BFC4 (110x110)</b>	<b>240</b>	<b>145</b>	<b>14.55</b>	<b>3.6</b>	<b>4.0</b>	<b>40</b>	<b>2639</b>
<b>BFC5 (136x136)</b>	<b>162</b>	<b>88</b>	<b>12.65</b>	<b>2.4</b>	<b>5.3</b>	<b>37</b>	<b>1527</b>
<b>BFC6 (50x50)</b>	<b>350</b>	<b>220</b>	<b>13.3</b>	<b>4.2</b>	<b>3.2</b>	<b>52</b>	<b>3317</b>
<b>BFC7 (70x70)</b>	<b>312</b>	<b>210</b>	<b>14.7</b>	<b>4.2</b>	<b>3.5</b>	<b>50</b>	<b>3437</b>
<b>BFC8 (90x90)</b>	<b>284</b>	<b>190</b>	<b>16.35</b>	<b>4.2</b>	<b>3.9</b>	<b>45</b>	<b>3596</b>
<b>BFC9 (110x110)</b>	<b>244</b>	<b>135</b>	<b>14.65</b>	<b>3.2</b>	<b>4.6</b>	<b>42</b>	<b>2696</b>
<b>BFC10 (136x136)</b>	<b>168</b>	<b>95</b>	<b>11.7</b>	<b>2.8</b>	<b>4.2</b>	<b>34</b>	<b>1444</b>



(a) Load-Deflection Curves of Beams with Compressive Strength =23.5 MPa



(b) Load-Deflection Curves of Beams with Compressive Strength =30 MPa



(c) Load-Deflection Curves of Beams with Compressive Strength =37.5 MPa

**Figure 4.41:** Load Deflection Curve of Opening Shape Parameter in Group 5.

The relationship between ultimate shear load and compressive strength of composite beams can be demonstrated when beams with 23.5 MPa concrete are compared with those with 30 MPa concrete. The results show an increase of about 6.93% in shear load for beams with 50 × 50 mm openings, while the shear capacity of beams with 70 × 70 mm openings increases by about 5.92%. Beams with 90 × 90 mm openings show a 7.36% improvement, while those with openings up to 110 × 110 mm increase by 4.10%. Even those with the largest possible openings (136 × 136 mm) will see a very slight increase in shear strength, estimated at about 0.25%.

While if beams with 23.5 MPa concrete are compared with those with 37.5 MPa concrete, there is an increase of about 11.7% in shear load for beams with 50 × 50 mm openings. The shear capacity of beams with 70 × 70 mm openings increases by about 8.33%. Beams with 90 × 90 mm openings show an improvement of 8.66%, while beams with openings up to 110 × 110 mm increase by 5.68%. Even beams with the largest possible openings (136 × 136 mm) will see a slight increase in shear strength, estimated at about 3.81%.

These increases can be attributed to greater material strength provided by higher compression concrete that enhances the beam's ability to resist shear forces acting upon it. Specifically, improved shear resistance results from superior strength and lower crack widths from use of high compressive strength concrete enabling better load distribution and consequently improved structural performance, as illustrated in Table (4-7). Also, the presence of the term  $(\sqrt{f'_c})$  in the  $V_c$  equation affects  $V_u$  and will increase with increasing compressive strength of concrete. It can be seen that taking into consideration all the variables that affect the ultimate shear strength, the shear strength of large openings is half the shear strength of large openings. Also, when changing the compressive strength of concrete from 23.5 MPa to 30 MPa, the shear strength is affected relatively little.

#### 4.12.2 Effect of Compressive Strength of Concrete on Initial stiffness

The aim of this parameter is to evaluate how the compressive strength of concrete affects the initial stiffness of composite beams. Two different compressive forces were applied in testing ten beams with different sizes of cross-sectional openings such as 50×50mm, 70×70mm, 90×90mm, 110×110mm and 136×136mm. The analysis revealed varying effects of compressive strength on the stiffness of the beam. When comparing 30 MPa beams (BFC1-BFC5) with 37.5 MPa beams (BFC6-BFC10), when it comes to the effect of concrete compressive strength on initial stiffness, the 37.5 MPa beams recorded an increase of 3.85% (BFC6 vs. BFC1) and 2% (BFC7 vs. BFC2) while there was a decrease of 2.17% (BFC8 vs. BFC3) and an increase of 4.76% (BFC9 vs. BFC4) and 8.11% (BFC10 vs. BFC5). It should be noted that although higher concrete compressive strength typically increases initial stiffness as shown in this experiment; it is important to note that this varies across different contexts. As shown in Figure 4.42. From results show that the initial stiffness is slightly affected by the compressive strength of the concrete.

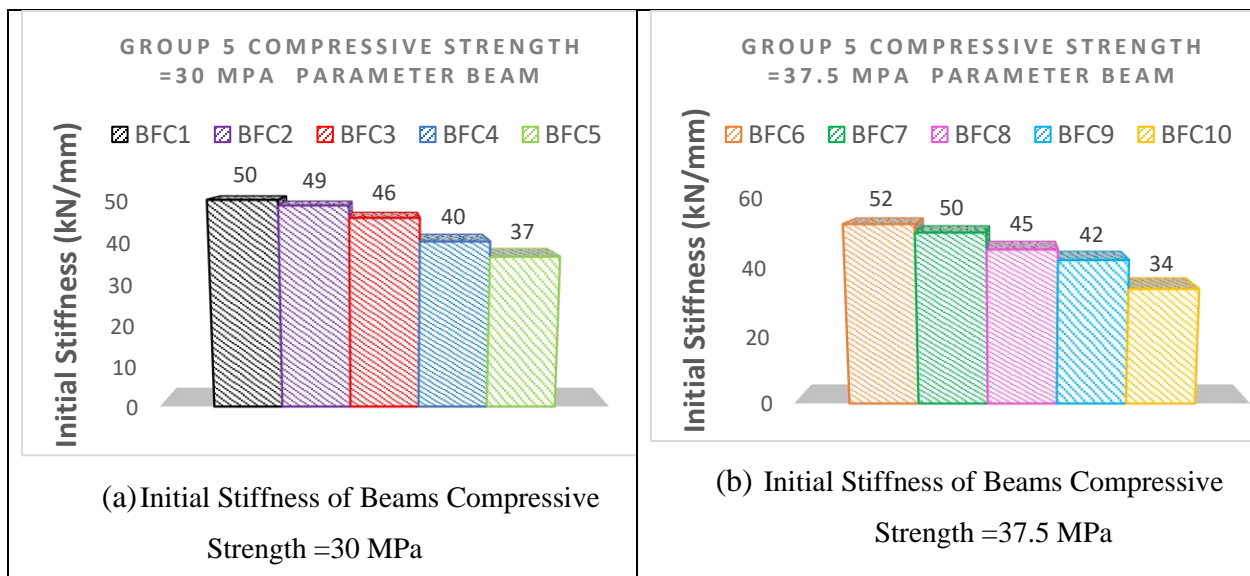


**Figure 4.42:** Initial Stiffness of Compressive Strength of Concrete Parameter in Group 5.

### **4.12.3 Effect of Compressive Strength of Concrete on Energy Absorption Capacity**

This parameter investigates how concrete compressive strength affects the energy absorption of composite beams with different transversal openings. Two levels of compressive strengths were examined: 30 MPa and 37.5 MPa. The values of energy absorption for beams having a strength of 30MPa (BFC1 to BFC5) were compared with those having a strength of 37.5 MPa (BFC6 to BFC10). The findings indicate that as the compressive strength increases, so does energy absorption. Specifically, beam BFC1 (37.5MPa) absorbs 1.69% more energy than beam BFC6 (30MPa) does; beam BFC7 has an increase over beam BFC2 by 10.45% while beam BFC3 is better than beam BFC8 by 2.18% in terms of energy absorption capacity. More significant variations are seen with two beams: BFC9 absorbs 2.11% additional powers than BFC4 does while BFC5 consumes 5.44% higher than the amount consumed by BFC 10 respectively. These findings imply that stronger concrete absorbs loads better than weaker ones which means less damage under loading conditions leading to increased lifespan, making it more attractive choice in civil engineering applications. As Shown in the Figures 4.43. And, from results show that the energy absorption is slightly affected by the compressive strength of the concrete.

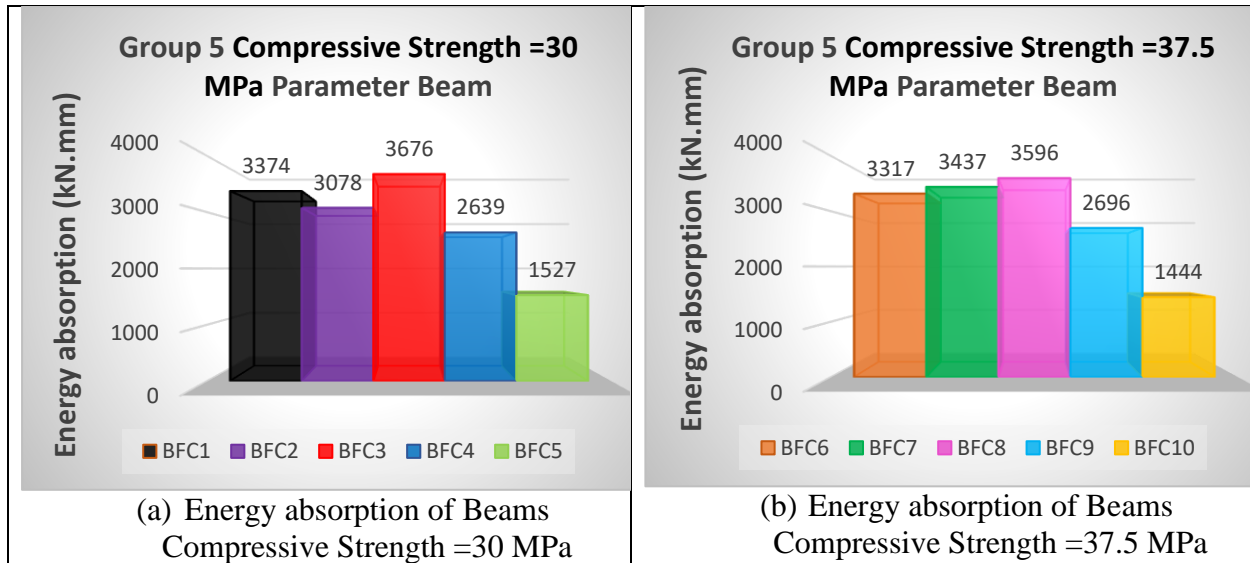


**Figure 4.43:** Energy absorption of Compressive Strength of Concrete Parameter in Group 5.

### 4.13 Tensile Reinforcement Parameter

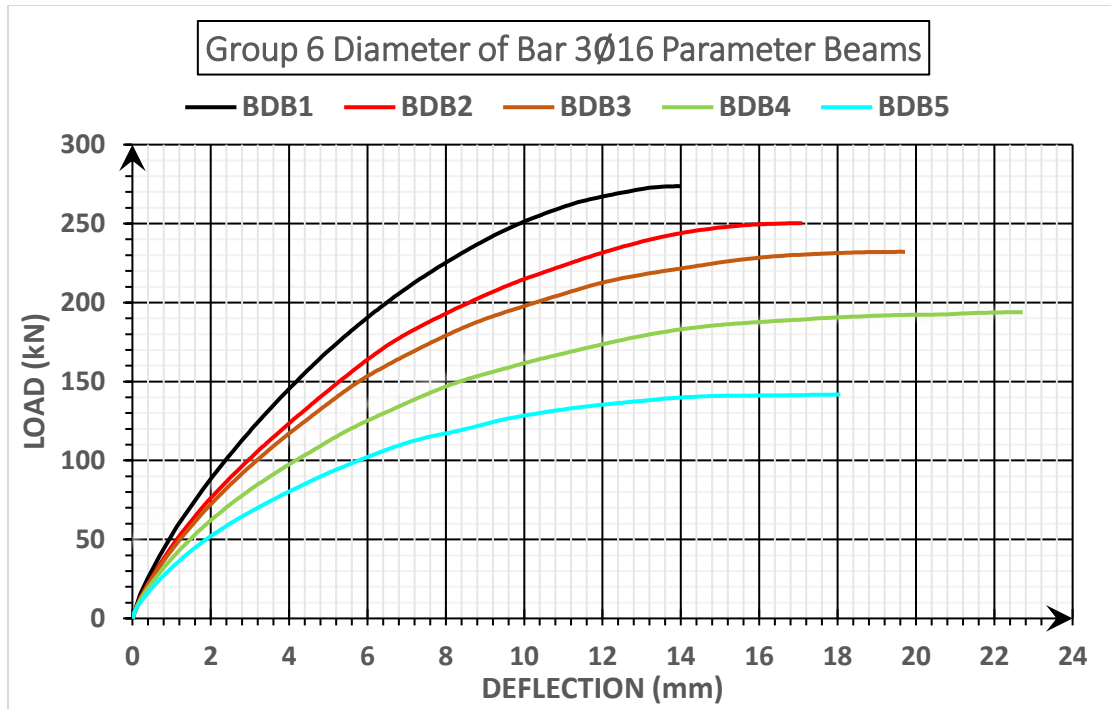
#### 4.13.1 Effect of Tensile Reinforcement on Ultimate Shear Strength

There are many mechanical effects of shear strength including: shear stress, dowel action, arch action, aggregate interlock, and residual tensile stress. In this study, the diameter of bars which its effect on dowel action behavior was the subject of interest in this section of the paper. Table (4-8) explains the related results, While the Table (4-2). Indicates the dimension, shape of openings and its location are geometry details of adopted specimens and explains shear span to effective depth ( $a/d$ ) and the compressive strength of concrete. Use two typers of longitudinal rebar reinforcement of ( $3\emptyset 16$ ,  $A_s=603 \text{ mm}^2$ ) and ( $2\emptyset 25\&2\emptyset 16$ ,  $A_s=1384 \text{ mm}^2$ ) were considered to inspect section shear resistance and understand various stress distribution modes. Specimens (BDB1, BDB2, BDB3, BDB4, and BDB5) with transverse openings ( $50*50$ ,  $70*70$ ,  $90*90$ ,  $110*110$ , and  $136*136 \text{ mm}$ ) had a longitudinal rebar reinforcement of ( $3\emptyset 16$ ,  $A_s=603 \text{ mm}^2$ ), while specimens (BDB6, BDB7, BDB8, BDB9, and BDB10) with transverse openings ( $50*50$ ,  $70*70$ ,  $90*90$ ,  $110*110$ , and

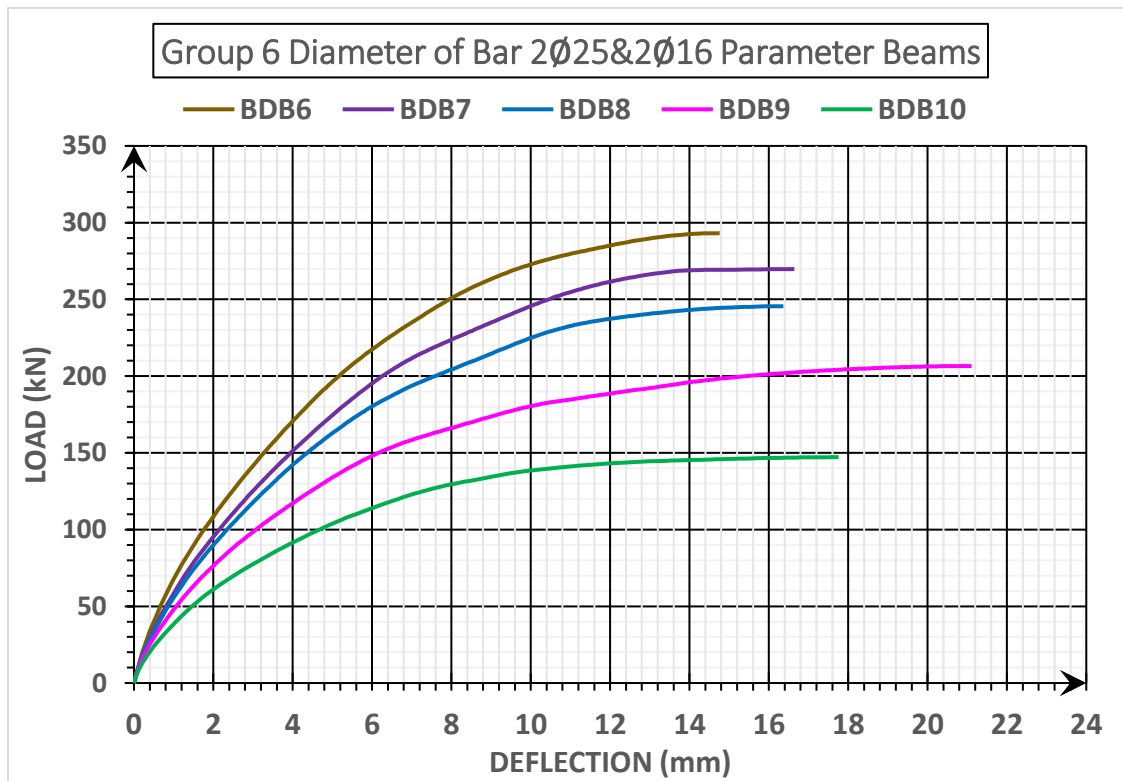
136\*136 mm) had a longitudinal rebar reinforcement of ( $2\phi 16&2\phi 25$ ,  $A_s=1384$  mm<sup>2</sup>). As shown in Figures 4.44, the various aspects of the longitudinal rebar reinforcement on shear strength-deflection response are evident.

**Table (4-8):** Model's Results for Group 6 of the composite beams.

Beam with opening (mm)	Ultimate Shear Load (kN)	Yild Shear Load (kN)	Ultimate Deflection (mm)	Yild Deflection (mm)	Ductility Index	Initial Stiffness (kN/mm)	Energy Absorption (kN.mm)
<b>BDB1 (50x50)</b>	<b>274</b>	<b>165</b>	<b>14</b>	<b>4.4</b>	<b>3.2</b>	<b>38</b>	<b>2627</b>
<b>BDB2 (70x70)</b>	<b>250</b>	<b>165</b>	<b>17.1</b>	<b>6</b>	<b>2.9</b>	<b>28</b>	<b>3037</b>
<b>BDB3 (90x90)</b>	<b>232</b>	<b>140</b>	<b>19.70</b>	<b>5.2</b>	<b>3.8</b>	<b>27</b>	<b>3413</b>
<b>BDB4 (110x110)</b>	<b>194</b>	<b>115</b>	<b>22.75</b>	<b>5.2</b>	<b>4.4</b>	<b>22</b>	<b>3391</b>
<b>BDB5 (136x136)</b>	<b>142</b>	<b>75</b>	<b>18.10</b>	<b>3.2</b>	<b>5.7</b>	<b>23</b>	<b>1960</b>
<b>BDB6 (50x50)</b>	<b>293</b>	<b>175</b>	<b>14.75</b>	<b>4.2</b>	<b>3.5</b>	<b>42</b>	<b>3156</b>
<b>BDB7 (70x70)</b>	<b>270</b>	<b>145</b>	<b>16.65</b>	<b>3.9</b>	<b>4.3</b>	<b>37</b>	<b>3352</b>
<b>BDB8 (90x90)</b>	<b>246</b>	<b>140</b>	<b>16.40</b>	<b>4</b>	<b>4.1</b>	<b>35</b>	<b>3004</b>
<b>BDB9 (110x110)</b>	<b>207</b>	<b>110</b>	<b>21.10</b>	<b>3.6</b>	<b>5.9</b>	<b>31</b>	<b>3414</b>
<b>BDB10 (136x136)</b>	<b>148</b>	<b>86</b>	<b>17.75</b>	<b>3.6</b>	<b>4.9</b>	<b>24</b>	<b>2069</b>



(a) Load-Deflection Curves of Beams with Diameter of Bar 3Ø16



(b) Load-Deflection Curves of Beams with Diameter of Bar 2Ø25&2Ø16

**Figure 4.44:** Load Deflection Curve of Opening Shape Parameter in Group 6.



Two types of longitudinal reinforcement bars ( $3\phi 16$ ) and ( $2\phi 25$  and  $2\phi 16$ ) were compared for ultimate shear loads in beams and it was observed that there is a steady rise with the latter configuration. For instance, beams strengthened by two 25 mm diameter reinforcing bars and two 16 mm diameter ones had their shear capacities increased remarkably for all sizes of transverse openings. In the case of beams with 50 mm openings, the shear load went up by approximately 6.48%. The increase in shear strength for beams with 70 mm openings was about 7.41%. Similarly, beams fitted to 90 mm wide openings had their shear force raised by 5.69% while those with 110 mm wide holes experienced an improvement of 6.28%. Even the biggest holes at 136 mm $\times$ 136 mm yielded a gain of around 4.17% more load resistance when examined through the lens of a traditional reinforcement scheme ( $2\phi 25$ & $2\phi 16$ ). This illustrates that more effective and larger longitudinal reinforcement provided by ( $2\phi 25$ & $2\phi 16$ ) improves load transfer leading to increased shear resistance which helps to mitigate the chances of shear failure.

The larger cross-sectional area of the reinforcement makes it more effective in transferring a load and capable of resisting greater shearing forces. It also reduces shear cracking and increases ductility as compared to the ( $2\phi 25$ & $2\phi 16$ ) type. This study hence shows that such reinforcement arrangements are significant for improving the shear behavior of composite beam designs, especially those with different shapes of cross sections.

#### **4.13.2 Effect of Tensile Reinforcement on Initial stiffness**

This parameter looks at the way different longitudinal rebar reinforcements affect composite beams' initial stiffness, which were tested through respective transverse openings of varying sizes on beams with two types of longitudinal reinforcement: ( $3\phi 16$ ) and ( $2\phi 16$  &  $2\phi 25$ ). Results show that BDB6 beam was stiffer than BDB1

beam by 9.52%, while BDB7 beam was stiffer than BDB2 by 24.32%. It was also observed that BDB8 beam was stiffer than BDB3 beam by 22.86%, and BDB9 was stiffer than BDB4 by 29.03%. The least stiff between them all was BDB10 as it had a percentage increase of 4.17% when compared to BDB5. These are indications that the greater amount and size of longitudinal reinforcement influence beams' stiffness, particularly for beams whose initial stiffness is lower; thus, selection of suitable configuration for reinforcement should be prioritized for achieving optimal structural performance. As shown in the Figures 4.45.

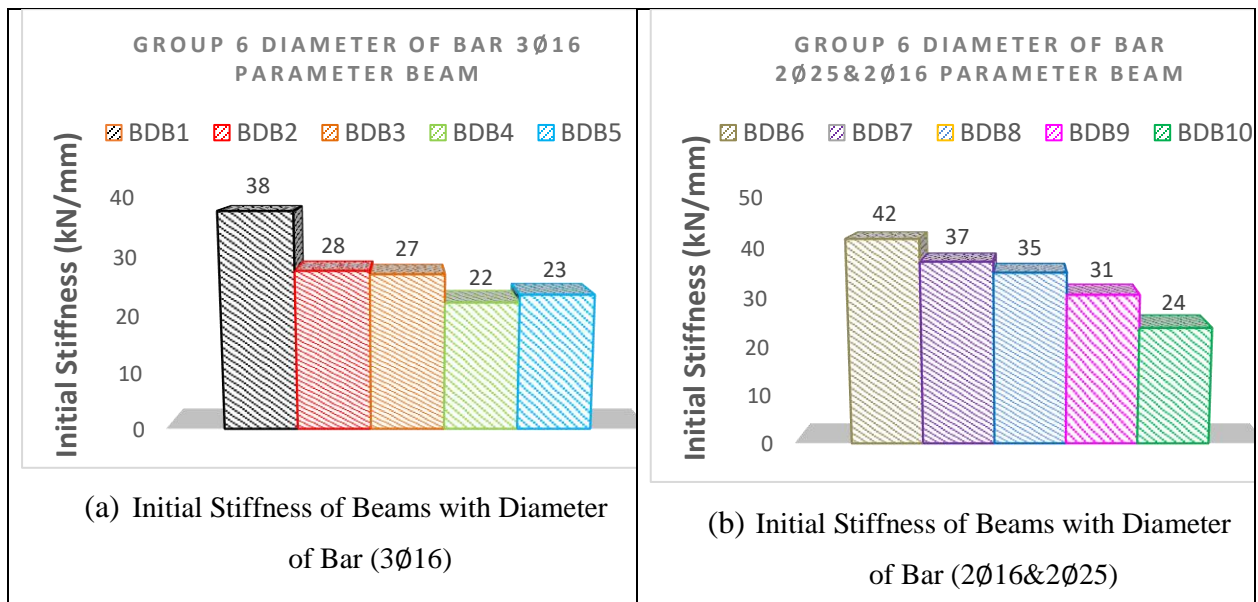


**Figure 4.45:** Initial Stiffness of Tensile Reinforcement Parameter in Group 6.

#### 4.13.3 Effect of Tensile Reinforcement on Energy Absorption Capacity

This parameter evaluates how longitudinal rebar reinforcement affects composite beam energy absorption having different transverse open spaces. Two types of reinforcement were studied: (3Ø16) and (2Ø25 & 2Ø16). The energies absorbed by beams having (3Ø16) reinforcements (BDB1 to BDB5) were compared with those of beams having (2Ø25 & 2Ø16) reinforcements (BDB6 to BDB10). The results

showed that beams with ( $2\phi 25$  &  $2\phi 16$ ) reinforcements usually have higher energy absorption. For example, Beam BDB6 that is fortified using ( $2\phi 25$  &  $2\phi 16$ ) absorbs 16.76% more energy than the one made up of ( $3\phi 16$ ) (BDB1). On the other hand, beam BDB7 shows an increase of 9.4% over beam BDB2 while beam BDB3 exhibits an improvement of 11.98% compared to beam BDB8. A slight rise was noted for beam BDB9 which absorbs 0.67% more energy than beam BDB4 and for beam BDB10 that has a percentage change of 5.27% against its counterpart BDB5. Lastly, these find out that larger and extra-long reinforcement significantly improves the capacity to absorb energy to facilitate better structural performance and resistance to shear forces. As shown in Figure 4.46.

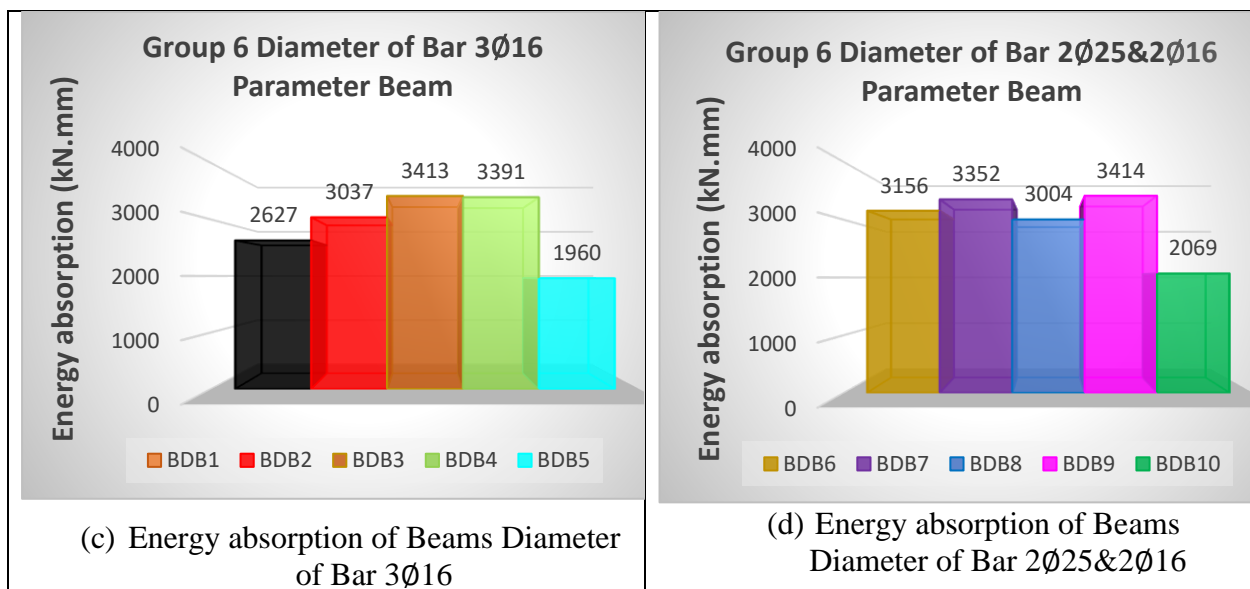


**Figure 4.46:** Energy absorption of Tensile Reinforcement Parameter in Group 6.

## CHAPTER FIVE: CONCLUSIONS AND RECOMENDATIONS

### 5.1 Conclusions

The current numerical study investigates the behavior of composite box steel-concrete beams using the Abaqus program for finite element analysis (FEM). By comparing the numerical results with previous experimental data, the structural behavior of the composite box steel-concrete beam models can be reasonably predicted. Several factors significantly influence the overall behavior of the beam at failure, and these effects can be summarized as follows:

#### 1. Effect of Opening Size on Shear Strength and Deflection

Increasing the size of transverse openings significantly reduces the shear strength and alters the deflection behavior. For beams with 50×50 mm openings, increasing the size to 70×70 mm resulted in a slight reduction in shear strength, while increasing to 90×90 mm caused a 16.1% decrease. A further increase to 110×110 mm led to a 25.5% reduction, and for 136×136 mm openings, the shear strength dropped by 47.7%. Additionally, smaller openings demonstrate approximately double the ultimate shear strength compared to larger openings.

#### 2. Effect of Opening Shape

The shape of the transverse openings effects the shear strength and stiffness. For square openings changed to circular openings, the shear strength slightly decreased for dimensions of 50 mm and 70 mm, while reductions of 12.8% and 12.4% were observed for openings of 90 mm and 110 mm, respectively. However, for 136 mm openings, circular openings increased shear strength by

13.25%. Circular openings also exhibit superior initial stiffness compared to square openings, but for energy absorption, square openings perform better, except in the case of large openings, where circular shapes provide an advantage.

### **3. Effect of Opening Location**

The location of transverse openings affects shear strength and deflection. Openings positioned closer to the applied loads (at  $a/5=126$  mm) result in a slight reduction in shear strength for openings of 50×50 mm, 70×70 mm, 90×90 mm, and 110×110 mm, with a more significant decrease of 15.9% for 136×136 mm openings. It can be concluded that openings located near the supports exhibit better shear strength performance compared to those positioned closer to the loads.

### **4. Effect of (a/d) Ratio on Shear Strength**

An increase in the (a/d) ratio corresponds to a decrease in shear strength. Specifically, the difference in shear strength between the highest and lowest (a/d) ratios is 20.1% for 50×50 mm openings, 16.6% for 70×70 mm openings, 11.15% for 90×90 mm openings, 6.45% for 110×110 mm openings, and only a slight reduction for 136×136 mm openings. When increasing the (a/d) ratio from 2 to 2.8, the shear strength decreases by 20% for small openings, while large openings remain unaffected by changes in the (a/d) ratio. For small openings, the transverse opening area can be increased by 324% without compromising initial stiffness. In contrast, large openings reduce initial stiffness by 60% compared to small openings.

### 5. Effect of Concrete Compressive Strength

Increasing the concrete compressive strength results in a slight improvement in shear strength. For beams with compressive strength of 30 MPa and square openings of 50×50 mm, shear strength slightly increased compared to beams with a compressive strength of 23.5 MPa. Raising the compressive strength to 37.5 MPa increased shear strength by 11.71% for 50×50 mm openings, with smaller increases for openings of 70×70 mm, 90×90 mm, 110×110 mm, and 136×136 mm. It can be concluded that the transverse opening area can be expanded by up to 200% while maintaining concrete compressive strength.

### 6. Effect of Reinforcement Bar Diameter on Shear Strength

The diameter of reinforcing bars has a limited effect on the shear strength of beams with large openings. For beams with square openings of 50×50 mm and reinforcement of 2Ø25+2Ø16 ( $A_s=1384 \text{ mm}^2$ ), shear strength is slightly higher than for beams with 3Ø16 ( $A_s=603 \text{ mm}^2$ ), regardless of opening size. For large openings, the shear strength is less dependent on longitudinal reinforcement. By increasing reinforcement steel by 230%, the transverse opening area can be increased by 100% without reducing shear strength. Additionally, for large openings, the initial stiffness does not depend on dowel action.

## 5.2 Recommendations

Here are points to be considered for making recommendations for future work:

1) The main aim of this study was to investigate a new structural element – composite encased steel-concrete beams with web openings in the shear zone – by

---

means of numerical analysis of its shear behavior. This new type of member should be examined in future research by using flexure tests on it (experimentally and numerically).

2) The tests were done using two-point loading during this investigation. Various loading conditions like distributed loads, cyclic loads and others must be investigated in the future studies (experimentally and numerically).

3) This work only dwelt on transverse square openings within the shear zone and then longitudinal opening through a hollow box made from steel. Other than these inside/outside stiffness designs can be adopted in later studies or research works with respect to composite encased steel-concrete beams that possess openings in their flexural zone or have multiple ones.

4) It is recommended that using different kinds of concrete including high-strength concrete as a way of advancing knowledge about their behavior may form part of future studies in the area.

## REFERENCES

- [1] Q. Q. Liang, M. Asce, B. Uy, M. A. Bradford, and H. R. Ronagh, “Strength Analysis of Steel-Concrete Composite Beams in Combined Bending and Shear,” 2005, doi: 10.1061/ASCE0733-94452005131:101593.
- [2] B. Aykac, S. Aykac, I. Kalkan, B. Dundar, and H. Can, “Flexural behavior and strength of reinforced concrete beams with multiple transverse openings,” *ACI Struct J*, vol. 111, no. 2, pp. 267–277, 2014, doi: 10.14359/51686442.
- [3] Ł. Zdanowicz and R. Wojdak, “STRUCTURAL ANALYSIS OF A FAILED RC BEAM WITH OPENINGS IN A BUILDING UNDER CONSTRUCTION ANALIZA STANU AWARYJNEGO BELKI ŻELBETOWEJ Z OTWORAMI W NOWO WZNOSZONYM BUDYNKU,” 2013.
- [4] G. G. Ahmed and V. F. Gerges, “Behavior of RC Beams with Openings Strengthened with CFRP Laminates,” 2020. [Online]. Available: <http://ijisd.journals.ekb.eg>
- [5] A. Y. Kamal, “Encased Beam with Variable Upper Steel Flange Position,” 2015. [Online]. Available: <https://www.researchgate.net/publication/279512191>
- [6] N. H. Tu’ma and M. R. Aziz, “Flexural Performance of Composite Ultra-High-Performance Concrete-Encased Steel Hollow Beams,” *Civil Engineering Journal (Iran)*, vol. 5, no. 6, pp. 1289–1304, Jun. 2019, doi: 10.28991/cej-2019-03091332.
- [7] P. K. RAGBIR SINGH, “EFFECTS OF OPENINGS IN RC BEAMS SUBJECTED TO STATIC AND CYCLIC LOADS,” 2011.
- [8] A. Ahmed, M. M. Fayyadh, S. Naganathan, and K. Nasharuddin, “Reinforced concrete beams with web openings: A state of the art review,” *Mater Des*, vol. 40, pp. 90–102, Sep. 2012, doi: 10.1016/j.matdes.2012.03.001.
- [9] K. Vedenoja, “The assessment of openings in existing load bearing concrete structures,” 2017.
- [10] Y. Yao, S. T. E. Tung, and B. Glisic, “Crack detection and characterization techniques - An overview,” Dec. 01, 2014, *John Wiley and Sons Ltd*. doi: 10.1002/stc.1655.
- [11] A. Siddika, M. A. Al Mamun, R. Alyousef, and Y. H. M. Amran, “Strengthening of reinforced concrete beams by using fiber-reinforced polymer composites: A review,” Sep. 01, 2019, *Elsevier Ltd*. doi: 10.1016/j.job.2019.100798.
- [12] OLA ADEL QASIM, “Behavior of reinforced reactive powder concrete slabs with openings,” 2013.
- [13] M. Meijs and U. Knaack, “Components and Connections Principles of Construction,” 2012.



- [14] J. Tanijaya, “Shear Stress Distribution in the Opening Chords of Hybrid R/C T-Beams with Opening,” in *MATEC Web of Conferences*, EDP Sciences, Jan. 2018. doi: 10.1051/mateconf/201814701005.
- [15] M. Sarcheshmehpour and H. E. Estekanchi, “Life cycle cost optimization of earthquake-resistant steel framed tube tall buildings,” *Structures*, vol. 30, pp. 585–601, Apr. 2021, doi: 10.1016/j.istruc.2021.01.038.
- [16] YEP KAR MUN, “STUDY ON BEHAVIOUR OF DIFFERENT SHAPES AND LOCATIONS OF OPENING ON REINFORCED CONCRETE BEAM BY USING ANSYS,” 2018.
- [17] M. A. Mansur and Kiang-Hwee Tan, “CONCRETE BEAMS with OPEN : Analysis and Design,” 1999.
- [18] K. D. Tsavdaridis and C. D’Mello, “Web buckling study of the behaviour and strength of perforated steel beams with different novel web opening shapes,” *J Constr Steel Res*, vol. 67, no. 10, pp. 1605–1620, Oct. 2011, doi: 10.1016/j.jcsr.2011.04.004.
- [19] F. De’Nan, C. K. Keong, and N. S. Hashim, “Shapes and sizes of web opening effects on bending behaviour of I-beam with web opening,” in *AIP Conference Proceedings*, American Institute of Physics Inc., Oct. 2017. doi: 10.1063/1.5005652.
- [20] J. A.-A. C. 426, *shear strength of reinforced concrete members (ACI 426R-74)*. 1973.
- [21] S. Amiri and R. Masoudnia, “Investigation of the Oppening Effects on the Behavior of Concrete Beams Without Additional Reinforcement in Opening Region Using Fem Method,” pp. 617–627, 2011, doi: 10.13140/RG.2.1.2108.1041.
- [22] N. F. Somes and W. G. Corley, “Circular openings in webs of continuous beams,” pp. 359–398, 1974.
- [23] J. Schlaich and K. Schäfer, “The design of structural concrete,” in *IABSE Workshop, New Delhi*, 1993.
- [24] J. Schlaich, K. Schaefer, and M. Jennewein, “TOWARD A CONSISTENT DESIGN OF STRUCTURAL CONCRETE.,” *PCI Journal*, vol. 32, no. 3, pp. 74–150, 1987, doi: 10.15554/pcij.05011987.74.150.
- [25] J. M. Hanson, “Square openings in webs of continuous joists,” *Portland Cement Assoc R & D Lab Bull*, 1969.
- [26] S. A. Salam, “Beams with openings under different stress conditions,” in *Conference on Our World in Concrete and Structures, Singapore*, pp. 25–26, 1977.
- [27] M. A. Mansur, “Effect of openings on the behaviour and strength of R/C beams in shear,” 1998.
- [28] A. C. I, “Building code requirements for reinforced concrete (ACI 318-63),” *American Concrete Institute*, 1963, Accessed: Apr. 11, 2024. [Online]. Available: <https://babel.hathitrust.org/cgi/pt?id=coo.31924003871732&seq=10>

- [29] A. A. and H. R. D. K. W. Nasser, "Behavior and design of large openings in reinforced concrete beams," pp. 25–33, 1967.
- [30] H. Du, X. Hu, D. Shi, and B. Fang, "Effect of reinforcement on the strength of the web opening in steel-concrete composite beam," *Eng Struct*, vol. 235, May 2021, doi: 10.1016/j.engstruct.2021.112038.
- [31] S. J. Hicks, "Design of Composite Beams with Large Web Openings: In Accordance with Eurocodes and the UK National Annexes," 2011, doi: 10.13140/RG.2.2.19276.62085.
- [32] D. Assi, "Verification and Parametric Analysis of Shear Behavior of Reinforced Concrete Beams using Non-linear Finite Element Analysis," *Journal of Engineering*, vol. 29, no. 11, pp. 184–202, Nov. 2023, doi: 10.31026/j.eng.2023.11.11.
- [33] A. Bashir, "Behaviour of Stainless Steel Composite Decking Under Combined Bending Moment and Concentrated Load," 2014, doi: 10.13140/2.1.2911.3920.
- [34] L. Librescu and O. Song, "Thin-Walled Composite Beams," 2005.
- [35] N. Gattesco, "Analytical modeling of nonlinear behavior of composite beams with deformable connection," 1999. [Online]. Available: [www.elsevier.com/locate/jcsr](http://www.elsevier.com/locate/jcsr)
- [36] W. M. Sebastian and R. E. Mcconnel, "NONLINEAR FE ANALYSIS OF STEEL-CONCRETE COMPOSITE STRUCTURES," 2000.
- [37] S. Bullo and R. Di Marco, "A simplified method for assessing the ductile behaviour of stud connectors in composite beams with high strength concrete slab," *J Constr Steel Res*, vol. 60, no. 9, pp. 1387–1408, Sep. 2004, doi: 10.1016/j.jcsr.2004.01.001.
- [38] E. J. Sapountzakis and J. T. Katsikadelis, "A new model for the analysis of composite steel - concrete slab and beam structures with deformable connection," *Comput Mech*, vol. 31, no. 3–4, pp. 340–349, 2003, doi: 10.1007/s00466-003-0436-1.
- [39] C. Faella, E. Martinelli, and E. Nigro, "Shear Connection Nonlinearity and Deflections of Steel-Concrete Composite Beams: A Simplified Method," pp. 12–20, 2003, doi: 10.1061/ASCE0733-94452003129:112.
- [40] B. U. M. A. B. and H. R. R. Q. Q. Liang, "Ultimate strength of continuous composite beams in combined bending and shear," pp. 1109–1128, 2004.
- [41] R. A. Barnes and G. C. Mays, "The transfer of stress through a steel to concrete adhesive bond," 2001.
- [42] E. Serrano, "A numerical study of the shear-strength-predicting capabilities of test specimens for wood-adhesive bonds," *Int J Adhes Adhes*, vol. 24, no. 1, pp. 23–35, Feb. 2004, doi: 10.1016/S0143-7496(03)00096-4.
- [43] B. K. Jang and T. Kishi, "Adhesive strength between TiNi fibers embedded in CFRP composites," *Mater Lett*, vol. 59, no. 11, pp. 1338–1341, May 2005, doi: 10.1016/j.matlet.2005.01.006.

- [44] G. Zhao and A. Li, “Numerical study of a bonded steel and concrete composite beam,” *Comput Struct*, vol. 86, no. 19–20, pp. 1830–1838, Oct. 2008, doi: 10.1016/j.compstruc.2008.04.002.
- [45] A. Murugesan and A. Narayanan, “Influence of a Longitudinal Circular Hole on Flexural Strength of Reinforced Concrete Beams,” 2016, doi: 10.1061/(ASCE).
- [46] A. F. Ashour and G. Rishi, “Tests of reinforced concrete continuous deep beams with web openings,” pp. 418–426, 2000.
- [47] M. A. Mansur, M. Asce, K. Hwee Tan, S.-L. Lee, and F. Asce, “COLLAPSE LOADS OF R/C BEAMS WITH LARGE OPENINGS,” 1984.
- [48] B. H. Osman, E. Wu, B. Ji, and S. S. Abdulhameed, “Shear behavior of Reinforced Concrete (RC) beams with circular web openings without additional shear reinforcement,” *KSCE Journal of Civil Engineering*, vol. 21, no. 1, pp. 296–306, Jan. 2017, doi: 10.1007/s12205-016-0387-7.
- [49] A. M. Sayed, “Numerical study using FE simulation on rectangular RC beams with vertical circular web openings in the shear zones,” *Eng Struct*, vol. 198, Nov. 2019, doi: 10.1016/j.engstruct.2019.109471.
- [50] A. A. Standard, “Building Code Requirements for Structural Concrete (ACI 318-05) and Commentary (ACI 318R-05),” 2005. [Online]. Available: [www.concrete.org](http://www.concrete.org)
- [51] Yuta Yamada, “Shear Load Carrying Mechanisms of RC Beams Without Stirrups Strengthened by Multiple Holes,” 2019.
- [52] Y. Yamada, “An analytical study on interactions of artificial cracks and holes contributing to increases in the shear strengths of RC beams,” *Journal of Advanced Concrete Technology*, vol. 17, no. 10, pp. 579–591, 2019, doi: 10.3151/jact.17.579.
- [53] Y. Yamada, “A study on construction of identifying method of hole positions contributing to change in shear strengths of RC beams without stirrups based on image analyses,” pp. 675–683, 2020.
- [54] N. Torunbalci, “Behaviour and design of large rectangular openings in reinforced concrete beams,” *Archit Sci Rev*, vol. 45, no. 2, pp. 91–96, Jun. 2002, doi: 10.1080/00038628.2002.9697497.
- [55] Y. O. Özkılıç *et al.*, “Shear and Bending Performances of Reinforced Concrete Beams with Different Sizes of Circular Openings,” *Buildings*, vol. 13, no. 8, Aug. 2023, doi: 10.3390/buildings13081989.
- [56] S. Mastan and S. S. Nachiar, “Numerical method and Validation using ANN of Composite Steel-Concrete Beam for Optimized Geometry and Emplacement of Web Opening,” 2023, doi: 10.21203/rs.3.rs-3190886/v1.
- [57] S. Q. Abdulridha, S. Z. Abeer, M. S. Nasr, and A. A. Waleed, “Numerical analysis of ultimate load and crack propagation in a concrete beam with longitudinal small hole,” in *Journal of*

*Physics: Conference Series*, IOP Publishing Ltd, Aug. 2021. doi: 10.1088/1742-6596/1973/1/012222.

- [58] D. N. Jabbar, A. Al-Rifaie, A. M. Hussein, A. A. Shubbar, M. S. Nasr, and Z. S. Al-Khafaji, "Shear behaviour of reinforced concrete beams with small web openings," in *Materials Today: Proceedings*, Elsevier Ltd, 2021, pp. 2713–2716. doi: 10.1016/j.matpr.2020.12.710.
- [59] Q. Q. Liang, S. Wales, B. Uy, M. A. Bradford, and H. R. Ronagh, "Strength Analysis of Steel-Concrete Composite Beams in Combined Strength Analysis of Steel-Concrete Composite Beams in Combined Bending and Shear Bending and Shear," 2005, doi: 10.1061/ASCE0733-94452005131:101593.
- [60] J. H. Ling, H. S. Tang, W. K. Leong, and H. T. Sia, "Behaviour of Reinforced Concrete Beams with Circular Transverse Openings under Static Loads," *JOURNAL OF SCIENCE AND APPLIED ENGINEERING (JSAE)*, vol. 3, no. 1, pp. 1–16, 2020.
- [61] A. A. G. Abu Altemen, A. A. K. Sharba, R. A. N. Al Ameri, M. K. Ibrahim, and M. Ozakca, "Effect of Laying Service longitudinal and Transverse Openings on Reinforced Concrete Hollow Beam Web under Flexural Loadings," *IOP Conf Ser Mater Sci Eng*, vol. 1076, no. 1, p. 012121, Feb. 2021, doi: 10.1088/1757-899x/1076/1/012121.
- [62] Ahmed S. Hamzah and Ammar Y. Ali, "SHEAR BEHAVIOR OF REINFORCED CONCRETE BEAMS WITH VERTICAL AND TRANSVERSE OPENINGS," 2020. [Online]. Available: <https://www.researchgate.net/publication/342241984>
- [63] A. Hamid Moatt and A. Hameed Aziz, "LOCALIZED TORSIONAL STRENGTHENING TECHNIQUE FOR RC BOX BEAMS WITH TRANSVERSE OPENINGS," *Journal of Engineering and Sustainable Development*, vol. 24, no. Special, pp. 341–358, Aug. 2020, doi: 10.31272/jeasd.conf.1.37.
- [64] R. V. R. Renjini, "NUMERICAL ANALYSIS OF RC BEAMS WITH OPENINGS STRENGTHENED USING CFRP UNDER IMPACT LOADING," *International Research Journal of Engineering and Technology*, 2018, [Online]. Available: [www.irjet.net](http://www.irjet.net)
- [65] Y. Gatia Abtan and H. Dhafer AbdulJabbar, "Experimental Study to Investigate the effect of Longitudinal and Transverse Openings on the Structural Behavior of High Strength Self Compacting Reinforced Concrete Beams," *Journal of Engineering and Sustainable Development*, vol. 2019, no. 01, pp. 66–79, Jan. 2019, doi: 10.31272/jeasd.23.1.5.
- [66] J. Suresh and R. A. Prabhavathy, "Behaviour of Steel Fibre Reinforced Concrete Beams with Duct Openings Strengthened by Steel Plates," 2014.
- [67] A. M. Morsy and A. M. Barima, "Behavior of R.C. Beams with Openings using Different Strengthening Techniques," *International Journal of Sciences: Basic and Applied Research (IJSBAR) International Journal of Sciences: Basic and Applied Research*, vol. 46, no. 1, pp. 195–219, 2019, [Online]. Available: <http://gssrr.org/index.php?journal=JournalOfBasicAndApplied>

- [68] mohamed kandil, gaylan el gadaa, and N. Meleka, "Flexural and Shear Strengthening of RC Beams with Large Openings by Steel or CFRP Plates," *ERJ. Engineering Research Journal*, vol. 43, no. 4, pp. 327–336, Oct. 2020, doi: 10.21608/erjm.2020.112799.
- [69] S. V Chaudhari and M. A. Chakrabarti, "Modeling of concrete for nonlinear analysis Using Finite Element Code ABAQUS," 2012.
- [70] V.-V. Dassault Systemes, "Abaqus/CAE User's Manual Abaqus 6.11 Abaqus/CAE User's Manual," 2009.
- [71] K. J. Bathe, "Finite Element Procedures in Engineering Analysis," 1996.
- [72] J. N. Reddy, "SOLUTIONS MANUAL for An Introduction to The Finite Element Method (Third Edition)," 2005.
- [73] R. D. , M. D. S. , & P. M. E. Cook, "Concepts and Applications of Finite Element Analysis," 2001.
- [74] O. C. Zienkiewicz, R. L. Taylor, and J. Z. Zhu, "The Finite Element Method: Its Basis and Fundamentals Sixth edition," 2005. [Online]. Available: [www.cimne.upc.es](http://www.cimne.upc.es)
- [75] Dassault Systèmes, "Analysis User's Guide Volume III," 2010.
- [76] P. Kmiecik and M. Kamiński, "Modelling of reinforced concrete structures and composite structures with concrete strength degradation taken into consideration," 2011.
- [77] R. G. Ray and A. Patel, "Elasto-plastic Analysis of Plate Using ABAQUS."
- [78] M. De Filippo, "Non-linear Static and Dynamic Finite Element Analyses of Reinforced Concrete Structures," 2016, doi: 10.13140/RG.2.2.17271.68004.
- [79] K. S. Hussein and N. H. Tu'ma, "Effect of using NSM CFRP and steel casing on the structural behavior of simply supported RC beams with transverse openings," *AIP Conf Proc*, vol. 2864, no. 1, p. 050002, Jan. 2024, doi: 10.1063/5.0186116.
- [80] M. Rakhshanimehr, M. R. Esfahani, M. R. Kianoush, B. A. Mohammadzadeh, and S. R. Mousavi, "Flexural ductility of reinforced concrete beams with lap-spliced bars," *Canadian Journal of Civil Engineering*, vol. 41, no. 7, pp. 594–604, 2014, doi: 10.1139/cjce-2013-0074.
- [81] T. J. Sullivan and G. M. Calvi, "INITIAL STIFFNESS VERSUS SECANT STIFFNESS IN DISPLACEMENT BASED DESIGN." [Online]. Available: <https://www.researchgate.net/publication/265097632>

## APPENDIX A

### Composite beam (solid beam)

**Table (A-1):** Information the composite beams.

Compressive Strength (MPa) ( $f_c'$ )	25	Effective Depth (mm) (d)	261.5
Beam Width (mm) ( b )	200	Yield Stress of Steel Bars (MPa) (fy)	414
Overall beam depth (mm) ( H )	300	Modulus of Elasticity of Steel Bars (MPa) (Es)	200000
Concrete Modulus of Elasticity (MPa) (Ec)	23500	Ultimate Concrete Strain ( $\epsilon_{cu}$ )	0.0035
0.85. $f_c'$	19.55	overhang length (m)	0.15
safety factor ( $\gamma_b$ )=	1.3	Load gap (m)	0.54
Span Length (m) (L) =	1.8	Shear span (m) (a)	0.63
Steel Density (KN/m <sup>3</sup> ) ( $\gamma_s$ )=	78.5	Concrete Density (KN/m <sup>3</sup> ) ( $\gamma_c$ )	24
depth flange concrete (mm) (t1)=	80	depth web concrete (hwc)	140
width web concrete (mm) (t3)=	75	diameter steel bar (mm) ( $\phi_r$ )	25
area of steel box (mm <sup>2</sup> ) (Asbox)=		diameter of the stirrups (mm) ( $\phi_s$ )	6
yield stress of steel box (Fybox)=	220	cover (mm)	20
width of flange steel box (mm) (b)	50	steel area (mm <sup>2</sup> ) (Asr)	
thickness of flange steel box (t)=	2	(3.14/4) ( $\pi/4$ )	0.785
depth of steel box (hbox)=	140	compressive bar (mm)	10
thickness of web steel box (tws)=	2	spacing between stirrups (mm) (s)	150
thickness steel box (tw)=	2	yield stress of stirrups (fy)	380
modulus elasticity box (Es)=	210000	buckling coefficient (kv)	5

$$d = h - \text{cover} - d_s - d_b/2 = 261.5$$

$$A_{\text{box}} = (b_{\text{box}} * t) * 2 + (h_{\text{box}} - t - t) * (tws) * 2$$

$$A_{\text{box}} = 744 \text{ mm}^2$$

Selection of tensile steel area ( $A_{sr}$ )

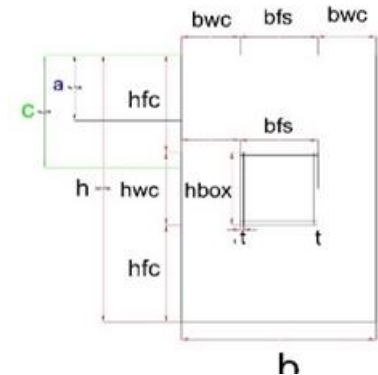
Select ( 3φ25 ) Mild steel bar

$$A_{sr} = 1471.875 \text{ mm}^2$$

From equilibrium we found depth of neutral axis

compressive forces = tensile forces

( Comp. force of concrete ) + ( Comp. force of steel box )  
 = ( tensile force of steel box )+ ( tensile force of steel  
 reinforcement )



$$( 0.85 f_c' b.a ) + ( A_{s_{box}} * F_{y_{box}} ) = ( A_{s_{box}} * F_{y_{box}} ) + ( A_{sr} * f_{yr} )$$

$$a = 143.3779412 \text{ mm}$$

$$C = a/\beta \quad , \beta = 0.85 \quad C = 168.6799308$$

$$C1 = 0.85 * f_c' * [b.t1 + 2 (c-t1).t3] = 622.6672794$$

$$\text{arm} = 128.6799308$$

$$Mn1 = C1 * \text{arm} = 80.12478242 \text{ kN.m} \quad (\text{from compressive force of concrete part})$$

$$C2 = A * f_{y_{box}} = [2.t.(c - t1) + b_{box}.t] * f_{y_{box}} = 100.0383391$$

$$\text{arm} = 44.3399654$$

$$Mn2 = C2 * \text{arm} = 4.435696494 \text{ kN.m} \quad (\text{from compressive force of steel box part})$$

$$T1 = A_s * f_y = 609.35625$$

$$Mn3 = T1 * (d - c) = 56.56048929 \text{ kN.m} \quad (\text{from tensile force due to steel bar})$$

$$T2 = A * f_{y_{box}} = [b * t + 2 \{ (h_{box} + t1) - c \} * t] * f_{y_{box}} = 133.1616609$$

$$\text{arm} = 25.6600346$$

$$Mn4 = T2 * \text{arm} = 3.416932826 \quad (\text{from tensile force due to steel box part})$$

$$M_n = M_{n1} + M_{n2} + M_{n3} + M_{n4} + M_{n5} = 153.4868212$$

Strength for dead load

$$W = [(A_c \cdot \gamma_c) + (A_{box} \cdot \gamma_s)], \quad W = 1.498404$$

$$M_{dead} = (W \cdot L^2) / 8 = 0.60685362 \text{ kN.m}$$

Area of 2  $\phi$  10 = 157 (Steel bars in compressive zone)

$$C_3 = A_s f_y = 64.998$$

$$\text{arm } C = (20 + 6 + 10/2) = 0.137679931$$

$$M_{n5} = C_4 \cdot \text{arm } C_4 = 8.948920142$$

$$M_{net} = 152.8799676 \text{ kN.m}$$

$$M_{net} = (P/2) \cdot 2 \quad (P/2) \cdot a \quad \rightarrow \quad P = (M_{net} \cdot 2) / a = 485.3332304 \text{ kN}$$

Shear strength

Shear strength for steel box

$$\text{clear span } h = h_{box} - (2 \cdot t_w) = 136$$

$$\text{area of box } A_w = 2 \cdot h \cdot t_w = A_w = 544$$

$$\text{if } h/t_w \leq 1.10 (k_v \cdot E / f_y)^{0.5}$$

$$68 \leq 75.99342077 \quad \text{so } c_v = 1$$

$$V_{box} = 0.6 \cdot f_{ish} \cdot A_w \cdot c_v = 71.808$$

shear strength for steel box

$$A_s (3\phi 25) \text{ mm}, \quad A_s = 1471.875$$



$$\rho_w = A_s / b d \quad \rho_w = 0.028142925$$

Shear strength for stirrups

$$\text{lever arm } z = 0.9 * d = 235.35$$

$$\text{area of stirrups} = A_v = 2 * (3.14 / 4) * (\phi_s)^2 = 56.52$$

$$V_s = (d/s) * (A_v) * (F_y), \quad V_s = 37.442616$$

Shear strength for concrete

$$(0.16 \sqrt{f_c'}) b w d = 41.84$$

$$V_c = \text{least of } \{ (0.16 \sqrt{f_c'} + 17 \rho_w) b w d = 66.861875$$

$$(0.16 \sqrt{f_c'} + 17 \rho_w) b w d = 75.835$$

$$V_n = V_c + V_s + V_{\text{box}} = 151.090616$$

$$V_u = V_n = 151.090616$$

$$V_u = P / 2$$

$$P = V_u * 2 = 302.181232 \text{ KN}$$

Comparison between P flexural and P shear

$$P \text{ flexural} = 485.3332304 \text{ kN}$$

$$P \text{ shear} = 302.181232 \text{ kN}$$

## الخلاصة

تستكشف هذه الرسالة الأداء الهيكلي للعتبات المركبة من الصلب والخرسانة التي تحتوي على فتحات عرضية، مع التركيز على تأثير حجم وشكل وموقع الفتحات على قوة القص والانحراف. يتناول البحث دراسة العتبات ذات الفتحات المربعة والدائرية بأحجام 50×50 ملم، 70×70 ملم، 90×90 ملم، 110×110 ملم، و136×136 ملم، ويحلل تأثير نسب طول القص إلى العمق (a/d)، ومقاومة الانضغاط للخرسانة، ومساحة التسليح الطولي في منطقة الشد.

تشير النتائج إلى أن زيادة حجم الفتحات العرضية تؤدي إلى انخفاض كبير في مقاومة القص وزيادة في الانحراف. على سبيل المثال، أدى تغيير حجم الفتحة من 50×50 ملم إلى 136×136 ملم إلى تقليل حمل القص بنسبة تصل إلى 47.7%. بالإضافة إلى ذلك، تقلل الفتحات الدائرية من مقاومة القص مقارنة بالفتحات المربعة للأحجام الصغيرة، ولكن بالنسبة للفتحات الكبيرة (136×136 ملم)، تزيد الفتحات الدائرية من حمل القص بنسبة 13.25%. كما أظهرت الدراسة أن العتبات التي تحتوي على فتحات قريبة من الدعامات تحقق أداءً أفضل من حيث مقاومة القص مقارنة بتلك التي تحتوي على فتحات قريبة من نقطة الحمل، خاصةً بالنسبة للفتحات الكبيرة، حيث انخفض حمل القص بنسبة تصل إلى 15.9%.

تلعب نسب طول القص إلى العمق (a/d) دورًا مهمًا في قوة القص، حيث يؤدي تقليل النسبة إلى زيادة في حمل القص. على سبيل المثال، أدى تقليل النسبة من 2.8 إلى 2 إلى زيادة حمل القص بنسبة تصل إلى 20% بالنسبة للفتحات الصغيرة. وعلى العكس، كانت الفتحات الكبيرة أقل تأثرًا بتغير النسبة (a/d) علاوة على ذلك، أدى زيادة قوة الضغط للخرسانة من 23.5 ميغا باسكال إلى 37.5 ميغا باسكال إلى تحسين طفيف في مقاومة القص، حيث زاد حمل القص بنسبة تصل إلى 11.71%.

أخيرًا، تُظهر الدراسة أن قطر قضبان التسليح يؤثر على قوة القص. فقد أظهرت العتبات التي تحتوي على مساحة تسليح أكبر، مثل تلك التي تحتوي على تسليح (16Ø2 & 25Ø2)، زيادة في قوة القص مقارنة بالعتبات ذات مساحة التسليح الأصغر. ومع ذلك، كان تأثير التسليح أقل وضوحًا بالنسبة للفتحات الكبيرة، حيث لم تتأثر سلوكيات العتبات بشكل كبير بتغير التسليح.

توفر هذه الدراسة رؤى قيمة حول تحسين تصميم العتبات المركبة من خلال تعديل حجم وشكل وموقع الفتحات، ونسبة (a/d)، وقوة الخرسانة، والتسليح لتحقيق قوة قص أعلى ومرونة هيكلية أفضل.

جمهورية العراق  
وزارة التعليم العالي والبحث العلمي  
كلية الهندسة/جامعة ميسان  
قسم الهندسة المدنية



دراسة عددية لمقاومة القص للعتبات المركبة من مقطع حديدي مجوف والخرسانة ذات  
الفتحات العرضية

من قبل

علي محسن عودة

رسالة

مقدمة الى كلية الهندسة جامعة ميسان

كجزء من متطلبات الحصول على درجة الماجستير في علوم الهندسة المدنية/الانشاءات

بأشراف

الأستاذ المساعد الدكتور: ناصر حكيم طعمة